Tesis Doctoral

Técnicas de escaneado móvil aplicadas a la digitalización y gestión en edificación

VNiVERSiDAD
D SALAMANCA

Departamento de Ingeniería Cartográfica y del Terreno

Rocío Mora Fernández de Córdoba

-- 2021 --

Dirigida por:

Diego González Aguilera

Susana Lagüela López

Luis Javier Sánchez Aparicio

Departamento de Ingeniería Cartográfica y del Terreno

Escuela Politécnica Superior de Ávila

Universidad de Salamanca

Autor:

Rocío Mora Fernández de Córdoba

Directores:

Dr. Diego González Aguilera

Dra. Susana Lagüela López

Dr. Luis Javier Sánchez Aparicio

2021

Título:

Técnicas de escaneado móvil aplicadas a la digitalización

y gestión en edificación

Programa de Doctorado:

Geotecnologías Aplicadas a la Construcción, Energía e Industria

(artículo 6 del R.D. 99/2011 de 28 de enero)

Universidad de Salamanca

Listado de Publicaciones

La presente Tesis Doctoral, realizada por compendio de artículos científicos publicados en revistas de impacto, consta de los cuatro artículos científicos que se enumeran a continuación:

1. **Use of a Wearable Mobile Laser System in Seamless Indoor 3D Mapping of a Complex Historical Site**

   Andrea di Filippo [1], Luis Javier Sánchez-Aparicio [2], Salvatore Barba [1], José Antonio Martín-Jiménez [2], Rocío Mora [2] and Diego González-Aguilera [2]

   [1] Department of Civil Engineering, University of Salerno, Via Giovanni Paolo II, 132, 84084 Fisciano (SA), Italy.

   [2] Department of Land and Cartographic Engineering. University of Salamanca, Higher Polytechnic School of Avila, Calle de los Hornos Caleros, 50, 05003 Avila, Spain;

   Remote Sensing, Noviembre 2018.
   DOI: 10.3390/rs10121897

2. **Automatic Point-Cloud Registration for Quality control in Building Works**

   Rocio Mora[1], Jose Antonio Martín-Jiménez[1], Susana Lagüela[1] and Diego González-Aguilera[1]

   [1] Department of Cartographic and Land Engineering, Higher Polytechnic School of Avila, University of Salamanca, Hornos Caleros 50, 05003 Ávila, Spain;

   Applied Sciences, Febrero 2021
   DOI: 10.3390/app11041465

3. **Integration of a wearable mobile mapping solution and advance numerical simulations for the structural analysis of historical constructions: A case of study in San Pedro church (Palencia, Spain)**

   Luis Javier Sánchez Aparicio[1,2], Rocío Mora[2], Borja Conde[3], Miguel Ángel Maté-González[2,4], María Sánchez-Aparicio[2] and Diego González-Aguilera[2]

[1] Department of Construction and Architectural Technology (DCTA). Escuela Técnica Superior de Arquitectura de Madrid (ETSAM), Universidad Politécnica de Madrid, Avda. Juan de Herrera 4, 28040, Madrid (Spain);

[2] Department of Cartographic and Land Engineering. University of Salamanca, High Polytechnic School of Ávila, Hornos Caleros, 50, 05003, Ávila (Spain);

[3] Department of Engineering Materials. School of Industrial Engineering, University of Vigo, Vigo (Spain);

[4] Department of Topographic and Cartography Engineering. Higher Technical School of Engineers in Topography, Geodesy and Cartography, Universidad Politécnica de Madrid, Mercator 2, 28031 Madrid, Spain;

Remote Sensing, Marzo 2021
DOI: 10.3390/rs13071252

4. An historical building information modelling approach for the preventive conservation of historical constructions: Application to the Historical Library of Salamanca

Rocío Mora [a], Luis Javier Sánchez-Aparicio [b], Miguel Ángel Maté-González [a,c,d], Joaquín García-Álvarez [e], María Sánchez-Aparicio [a], Diego González-Aguilera [a]

[a] Department of Cartographic and Land Engineering, University of Salamanca, Higher Polytechnic School of ´Avila, Hornos Caleros, Ávila, Spain

[b] Department of Construction and Technology in Architecture (DCTA), Escuela Técnica Superior de Arquitectura de Madrid (ETSAM), Universidad Politécnica de Madrid, Av. Juan de Herrera 4, 28040, Madrid, Spain

[c] Department of Environment, Land and Infrastructure Engineering, Politecnico di Torino, 10129 Torino, Italy

[d] Department of Topographic and Cartography Engineering, Higher Technical School of Engineers in Topography, Geodesy and Cartography, Technical University of Madrid, Mercator 2, 28031, Madrid, Spain

[e] Fundación Santa María la Real del Patrimonio Histórico, Aguilar de Campoo, Palencia, Spain

Automation in Construction, Octubre 2020.
DOI: 10.1016/j.autcon.2020.103449

Resumen

La aparición de los sistemas de escaneado láser dinámicos, capaces de capturar datos a medida que se avanza por la zona de interés, ha revolucionado la adquisición, agilizando y flexibilizando las tomas de datos y ofreciendo un abanico muy amplio de aplicaciones en el campo de la ingeniería y arquitectura, entre otros. Inicialmente, los sistemas de escaneado móvil comenzaron centrándose en la digitalización de grandes extensiones de terreno como carreteras o zonas forestales. Así, los equipos de escaneado se embarcan sobre vehículos terrestres o aéreos y se escanea a medida que se va recorriendo la zona. Este planteamiento no es aplicable a escenarios de interior, puesto que en estos espacios no hay recepción de los sistemas de posicionamiento global (GNSS) y además el equipamiento es muy grande y pesado como para utilizarlo en el interior de edificios o zonas pequeñas. La solución en estos casos de interior pasa por utilizar alguno de los siguientes planteamientos: i) empleo de sistemas "wearables" portables de escaneado móvil apoyados por técnicas SLAM (Simultaneous Location and Mapping), ii) empleo de drones terrestres que embarquen sistemas de escaneado láser y apliquen técnicas SLAM o Stop & Go.

Por todo ello, uno de los objetivos principales de esta Tesis Doctoral se centra en estudiar la viabilidad de diferentes sistemas portables de escaneado móvil para la digitalización en edificación, tanto histórica como de nueva construcción. Así pues, por un lado, se investigan los sistemas portables de escaneado móvil del tipo WMLS (Wearable Mobile Laser System) y por otro, se investiga la eficacia y viabilidad de utilizar escáner láser estáticos del tipo TLS (Terrestrial Laser Scanner) sobre plataformas móviles. Para estos últimos, se ha desarrollado un sistema híbrido, formado por un dron terrestre y un TLS, capaz de navegar de forma autónoma y digitalizar el entorno automáticamente. Ambos sistemas se han utilizado en diversos casos de estudio y se han analizado las precisiones, eficacia y viabilidad en diferentes ámbitos del conocimiento. Para ello, se han implementado diferentes algoritmos de reducción de ruido, como el novedoso filtro FSOR (Fast Statistical Outlier Removal), así como filtros anisotrópicos y de homogeneización. A continuación, se han realizado procesamientos básicos de cada nube de puntos, obteniendo cartografías y secciones resultantes. Finalmente, se han aplicado procesos más complejos a través del desarrollo de metodologías semiautomáticas para el modelado de elementos constructivos, utilizando superficies paramétricas de tipo RANSAC (RANdom SAmple Consensus), y superficies no paramétricas de tipo NURBs (Non-Uniform Rational B-spline). Los modelos CAD (Computer Aided Desing) as-built resultantes han permitido diseñar sistemas de conservación preventiva a través de enfoques HBIM (Heritage Building Information Modelling) y avanzar en el diagnóstico estructural actual y futuro de una construcción a través de simulaciones numéricas por el Método de Elementos Finitos (FEM).

Abstract

The recent appearance of dynamic laser scanning systems, with the ability to capture data while progressively moving the area of interest, has completely changed the different data acquisition techniques available. These systems speed up the data acquisition process, making data collection more flexible, and offering a very wide range of applications in the field of engineering and architecture, among others. Originally, mobile scanning systems began by focusing on recording large areas of land such as roads or forests. For this purpose, the scanning device is mounted onto a terrestrial or aerial vehicle, while the study area is digitized as the vehicle is in motion. This approach is not applicable to indoor scenarios, since insufficient reception is available for global positioning systems (GNSS), while most equipment is too large and heavy to be used inside buildings or small areas. The solution in these cases is to use one of the following approaches: i) use portable (wearable) mobile scanning systems supported by Simultaneous Location and Mapping (SLAM) techniques, ii) board terrestrial laser scanners on terrestrial drones of smaller dimensions that allow them to navigate indoors.

One of the main objectives of this Doctoral Thesis focuses on studying the viability of different portable mobile laser scanning systems for the digitization of indoor scenarios, both historical and new. From one perspective, portable mobile laser scanning systems, such as the WMLS (Wearable Mobile Laser System), are studied. Next, the efficacy and feasibility of using static laser scanners, such as TLS (Terrestrial Laser Scanner) mounted on mobile platforms, is also investigated. For this purpose, a hybrid system has been developed, consisting of a terrestrial drone and a TLS, able to navigate these scenarios autonomously while automatically digitizing the environment. Both systems have been used in several case studies, while their precision, efficacy and feasibility have been analysed in different areas of knowledge. Similarly, different noise reduction algorithms have been analysed, such as the novel FSOR (Fast Statistical Outlier Removal) filter, as well as anisotropic and homogenization filters. Following this, standard processing of each point cloud is performed, obtaining cartographies and cross-sections. Finally, more complex processes are applied. These processes involve the development of semi-automatic methodologies for the modelling of construction elements, using parametric surfaces of type RANSAC (RANdom SAmple Consensus), and non-parametric surfaces of type NURBs (Non-Uniform Rational B-spline). As a result, the as-built CAD (Computer Aided Design) models have been used to design preventive conservation systems through HBIM (Heritage Building Information Modelling) approaches and to advance towards the diagnosis of the current and future structural condition of a construction through numerical simulations by the Finite Element Method (FEM)

Agradecimientos

El desarrollo de la presente Tesis Doctoral ha sido posible gracias a la colaboración y ayuda de muchas personas que de una manera u otra han contribuido a que la investigación pudiera llegar a su fin. En esta sección me gustaría expresar mi agradecimiento a todas ellas.

En primer lugar, quiero agradecer a la Junta de Castilla y León y el Fondo Social Europeo, la financiación de esta Tesis Doctoral, a través del programa de ayudas para la contratación predoctoral de personal investigador (Orden: EDU/1100/2017).

En segundo lugar, agradecer a mis tutores y directores todo el trabajo, esfuerzo, interés y paciencia que han tenido a lo largo de estos años. Sin duda alguna, no habría sido posible llegar hasta aquí sin vosotros. Gracias por todo el conocimiento que me habéis aportado y por vuestra paciencia y temple en los momentos menos favorables.

También quiero agradecer a todos los compañeros del grupo de investigación TIDOP, quienes con su día a día en el laboratorio han contribuido al desarrollo de las diferentes investigaciones y han hecho posible que el trabajo fuera ameno y entretenido.

Por último, no puedo olvidar agradecer a todos mis amigos el apoyo que me han dado en todo momento y que en mayor o menor medida ha contribuido a que siguiera adelante. Gracias por vuestra paciencia infinita y por hacerme ver el aspecto positivo de las cosas cuando yo no lo veía.

Gracias a todos.

Índice de Contenidos

Capítulo I.

Introducción

1. Introducción

La digitalización y documentación de las nuevas construcciones y del patrimonio cultural y artístico es una tarea crucial tanto para que el legado histórico perdure como para que el mantenimiento y conservación se realicen de forma más eficiente. Por otro lado, para el caso de una nueva construcción, la fase proyectual, de concepción de espacios y decisión de materiales y técnicas constructivas, ha de estar en perfecta consonancia con lo realmente ejecutado. En muchos casos, el análisis de la evolución de la construcción se complica por falta de datos completos, referentes tanto a la realidad construida, en tres dimensiones (3D), como a la información semántica (ej. componentes constructivos, materiales empleados) [1]. Este enfoque difiere ligeramente del adoptado en construcciones históricas, que se basa en tres fases fundamentales [2]: i) análisis de sus valores tangibles e intangibles; ii) desarrollo de políticas de intervención basadas en diagnósticos multidisciplinares; y iii) gestión de la conservación tras la intervención del mismo. En las directrices para la conservación del patrimonio cultural, recogidas por primera vez en la Carta de Atenas [3] y posteriormente en la Carta de Venecia [4] y Cracovia [5], se hace especial hincapié en la necesidad de realizar enfoques multidisciplinares en cada intervención. Entender el objeto de estudio y disponer de datos del mismo es esencial en cualquier proyecto de conservación. En ambos casos, las tecnologías digitales de captura masiva de datos han alcanzado una enorme difusión, ya que agilizan considerablemente el registro de los datos y aseguran un resultado preciso y completo, así como la posibilidad de generar modelos útiles de análisis, simulación o interpretación [6]. Los modelos tridimensionales o modelos 3D generados con estas tecnologías se han posicionado como una herramienta versátil, precisa y completa tanto para trabajos de ingeniería [7], como para conservación del patrimonio [8, 9].

Las dos técnicas de digitalización y generación de nubes de puntos 3D más populares en la actualidad son la fotogrametría [10] y el escáner láser [11]. Por su lado, la fotogrametría permite reconstruir una escena en tres dimensiones a través de la orientación de una secuencia de imágenes digitales, haciendo uso para ello del Método General de la Fotogrametría [12]. Aunque su aplicación inicial comenzó en el campo de la cartografía, generando modelos del terreno, en las últimas décadas ha sido ampliamente utilizada en el campo del patrimonio cultural [13, 14] o de la edificación moderna [15-18]. Los avances en este campo han venido de la mano de las técnicas de Structure-from-Motion (SfM), que han permitido realizar la calibración y orientación de las imágenes de manera automática [19, 20], agilizando así el proceso. Pese a los buenos resultados que se obtienen de la fotogrametría, la facilidad de capturar los datos y su bajo coste (requiriendo únicamente de una cámara réflex convencional o un smartphone), esta metodología se ve muy limitada en escenarios muy complejos, donde se necesitan gran cantidad de imágenes para completar el modelo, lo que desemboca en una propagación de errores y una peor calidad del resultado [21]. Así mismo la fotogrametría se ve limitada en lugares con texturas muy similares o una iluminación irregular o escasa.

Por su parte, las técnicas de documentación con escáner láser terrestre (TLS) permiten obtener directamente nubes de puntos 3D de alta precisión utilizando sensores activos que capturan gran cantidad de información en muy poco tiempo [22, 23] sin depender de la iluminación de la escena o de la textura de los elementos. Las técnicas de documentación láser comenzaron en la década de los 80, y desde entonces han ido desarrollándose para ofrecer mejores resultados en

un tiempo menor [24] y en las últimas décadas se han utilizado en diversos campos como son la reconstrucción virtual de edificios [25], simulaciones numéricas [8] y detección de lesiones en edificación [9, 26], entre otras muchas aplicaciones.

No obstante, la digitalización mediante escáner láser de superficies extensas y complejas, con rangos cortos de visibilidad entre estancias, tales como los espacios interiores, conlleva la realización de un número elevado de estaciones para completar la toma de datos. Al igual que en el caso de la fotogrametría, esto se traduce en un alto coste computacional, una propagación de errores y un elevado tiempo del usuario en la toma de datos. Las soluciones como los Sistemas de Escaneado Láser Móvil (MLS-Mobile Laser Systems) han ido cobrando importancia en los últimos años hasta convertirse en sistemas aptos para la digitalización de escenarios interiores y exteriores [27, 28], minimizando la propagación de errores y ahorrando gran cantidad de tiempo en las tomas de datos. Dichas soluciones se basan en el uso conjunto de escáneres láser y unidades de posicionamiento y navegación capaces de registrar datos mientras se mueven por el escenario. Sin embargo, son todavía diversas las líneas de avance en el conocimiento dentro de este campo.

Este es el punto inicial de esta Tesis Doctoral, el estudio de diferentes técnicas de escaneado móvil aplicadas a la digitalización y gestión en edificación. Para tal fin se analizan diferentes metodologías de cartografiado móvil con sensores de diversas especificaciones y características, así como se analizan los resultados obtenidos y su aplicabilidad a la gestión y documentación de edificación, tanto histórica como de nueva construcción.

En este Capítulo se introducirá el trabajo de investigación realizado, comenzando por un estado del arte, que servirá de contextualización del tema, para posteriormente explicar las motivaciones y objetivos que se persiguen y se finalizará con la estructura de la Tesis Doctoral.

1.1 Estado del arte

1.1.1 Aplicaciones del escáner láser en ingeniería y arquitectura

El escáner láser es un sensor activo de captura masiva de datos que realiza mediciones en tiempo real, emitiendo de forma periódica un haz láser coherente que impacta con un determinado objeto, el que se quiere digitalizar, y posteriormente regresa al dispositivo en donde es calculada la distancia recorrida por el haz. El uso de estos dispositivos se ha ido popularizando a lo largo de la última década gracias a dos factores: i) la evolución de los escáneres láser, cada vez más ligeros y sencillos de manejar; y ii) los avances computacionales de los algoritmos y procesadores, que permiten trabajar eficientemente con grandes cantidades de datos. Así, el escáner láser se utiliza para monitorización de acantilados y glaciares [29-31], control y monitorización de grandes obras de ingeniería [6, 32-35], documentación del patrimonio cultural [36], inventariado de bosques [37, 38], modelado e inspección de edificios [39, 40], digitalización de ciudades (Smart-Cities) [41,42], o arqueología [43], entre otros. Este amplio abanico de aplicaciones tan diversas y con escenarios tan heterogéneos implica tener dispositivos que se adapten a las necesidades específicas de cada caso. En este sentido, de todos los principios de medición existentes, los dos más utilizados habitualmente por los escáneres

láser son: i) tiempo de vuelo; y ii) diferencia de fase. Los escáneres de tiempo de vuelo (ToF-Time of Flight) [44] miden el tiempo de transmisión del láser a partir del emisor, reflejándose este en el objeto escaneado, y retornando hasta el receptor. Esta técnica permite realizar mediciones a largas distancias (kilómetros) ya que el tiempo de retorno del láser puede ser controlado, y es posible almacenar varios retornos a partir de un único pulso. Por su parte, los escáneres de diferencia de fase [45] se basan en la emisión de una serie de ondas láser de diferente longitud de onda sobre el objeto medido, las cuales al ser reflejadas y recibidas de nuevo en el escáner permiten determinar la distancia al objeto, comparando la fase de las ondas emitidas con la de las ondas recibidas. Estos equipos son muy rápidos y altamente precisos, aunque con un alcance menor que los escáneres ToF [46].

Atendiendo al modo de captura de datos, los dispositivos de escaneado láser pueden clasificarse en estáticos y móviles (MLS). En el caso de los estáticos, el sensor se estaciona sobre un punto desde el cual se captura el área de interés que sea visible. A cada punto se le denomina escena o escaneo, y para cubrir todo el espacio puede ser necesario realizar varias escenas que posteriormente deben ser unidas analíticamente, con un solape mínimo del 30% entre ellas, para formar la nube de puntos 3D completa. En el caso de los dispositivos móviles, el sistema difiere ligeramente, pues se trata de sistemas integrados en plataformas que permiten el desplazamiento durante la medición. Por un lado, se dispone de un escáner, 3D o de línea, que puede complementarse con sistemas de posicionamiento tipo GNSSS (Global Navigation Satellite System) y/o IMU (Inertial Measurement Unit), además de odometría, en caso de ir montados en plataformas rodadas, para permitir el cálculo de la trayectoria recorrida durante la medición, y en consecuencia el alineamiento de la nube de puntos simultáneo o posterior a la adquisición, obteniéndose una única nube de puntos completa sin necesidad de registros posteriores.

Los sistemas estáticos proporcionan una densidad de puntos mayor y una precisión milimétrica, a la vez que son metodologías costosas en cuanto a tiempo de captura y procesamiento computacional se refiere. Su principal campo de actuación es la documentación de áreas reducidas tales como edificios [36], yacimientos arqueológicos [43] u obras de ingeniería [7, 34]. Por su parte, los sistemas móviles permiten registrar menos densidad de puntos [47, 48] y tienen precisión centimétrica, pero permiten realizar capturas de datos en muy poco tiempo. Estos sistemas comenzaron a desarrollarse para documentar grandes extensiones de terreno, utilizándose para documentación de grandes masas forestales [49] y zonas urbanas completas [50-52]. Así, se clasificaron los sistemas móviles, según el vehículo en el que fueran transportados, en aéreos (ALS) o terrestres (TLS), aunque también existen casos de sistemas marinos, en los que los sensores de medición se integran sobre barcos u otro tipo de plataforma marina [53]. Los sistemas aéreos (muchas veces asociados también al término LIDAR de Light Detection And Ranging) van embarcados en un avión, helicóptero o cualquier otro vehículo aéreo, mientras que los terrestres se embarcan en coches, furgonetas o vehículos terrestres. La comparativa entre diferentes sistemas de escaneado móvil realizada por Puente et al [54] determina que, independientemente de la plataforma en la que se embarque el sistema, los componentes principales que forman un sistema móvil de escaneado son cinco: i) la plataforma móvil; ii) sistemas de posicionamiento y navegación (GNNS, IMU, etc.); iii) escáner láser; iv) cámaras de video / foto (opcional); y v) sistema computacional de almacenamiento. La unidad de posicionamiento y navegación permite tener una referencia espacial, mientras que los

sensores de escaneado láser se encargan de adquirir los datos 3D/2D (puntos con coordenadas y/o imágenes respectivamente) [55]. Ambos sistemas (aéreos y terrestres) tienen similitudes no sólo en los componentes, sino también en que capturan nubes de puntos georreferenciadas, almacenan información del retorno del láser y el flujo de trabajo que se sigue con ambos es similar [56]. Las principales diferencias entre los sistemas aéreos y los terrestres, radican en la perspectiva y la densidad de puntos capturados [56]. Así, los ALS capturan datos cenitales, de modo que constituyen una buena alternativa para registrar superficies horizontales, cubiertas de edificios etc. pero no para superficies verticales, mientras que con los MLS pasa lo contrario, obteniendo una visión directa de las superficies verticales, pero no así de las partes superiores de los edificios. Por otro lado, los MLS capturan una densidad de puntos mayor (100 ptos/ m^2) que los ALS (entre 1 y 60 ptos/m^2) [56]. Por lo general los ALS se utilizan para generar modelos digitales del terreno de grandes extensiones [57, 58], caracterización de cuencas de ríos [59, 60] o de tejados [61], mientras que los TLS se utilizan para la digitalización de carreteras o vías de comunicación [62, 63]. La clave de cualquier MLS es el sistema de posicionamiento y navegación. A medida que las tecnologías satelitales y los sistemas inerciales fueron evolucionando, los sistemas MLS fueron mejorando los sistemas de referenciación, de manera que los vehículos se equipaban tanto con el sensor escáner láser como con receptores GNSS acoplados a unidades de medición inercial (IMU) y otras unidades de medida complementarias (ej. brújulas, odómetros) [55]. Este planteamiento resulta muy útil y versátil en escenarios de exterior donde la señal GNSS se recibe fácilmente y por tanto los datos resultantes están directamente georreferenciados. Sin embargo, estas condiciones no es posible adaptarlas a escenarios de interior, puesto que en ellos la señal GNSS no se recibe y puede haber limitaciones de accesibilidad. Teniendo esto en cuenta y que los sistemas MLS pueden ser significativamente más eficientes (número de puntos adquiridos por unidad de tiempo) que los TLS [64], surge una nueva línea de investigación centrada en conseguir sistemas de escaneado móvil para escenarios de interior y pequeñas superficies. Hasta el momento para documentar escenarios de interior y pequeñas extensiones los TLS estáticos habían sido los sistemas más utilizados.

1.1.2 Técnicas de escaneado láser móvil (MLS) aplicadas a interiores y/o extensiones pequeñas

Tal como ya se ha introducido en el apartado anterior, los escenarios de interior impiden, por sus características propias, el uso de sistemas GNSS para la georreferenciación. En este tipo de escenarios se hace uso de sistemas inerciales del tipo IMU junto con técnicas SLAM (Simultaneous Location and Mapping) [65] o con técnicas Stop & Go [66], para resolver el posicionamiento, la navegación y el mapeado del entorno. Las técnicas de SLAM comienzan a desarrollarse en el campo de la robótica como una estrategia de navegación autónoma de plataformas robóticas [67], tratando de resolver dos problemas en uno: i) la ubicación del dispositivo dentro del entorno en cada instante de tiempo; y ii) la creación de un mapa del entorno. Para ello se utilizan puntos característicos o reconocibles en la escena que cumplan las siguientes condiciones: i) ser claramente diferenciables, ii) ser redundantes en el entorno y iii) ser estáticos [68]. De esta forma, la trayectoria del sensor y la posición de las referencias se calculan simultáneamente y sin conocimientos previos, aplicando técnicas de cálculo probabilísticas. El flujo de trabajo consiste en aplicar recursivamente dos operaciones: (i)

primero se realiza una estimación tanto de la posición actual del sistema como del mapa actualizado del entorno, considerando los datos de navegación y trayectoria pasados y, (ii) posteriormente, la posición y mapa estimados se comprueban y corrigen con los datos actualizados de los sensores [55]. Existen dos alternativas tecnológicas para resolver este problema [69]: i) la alternativa *off-line* en la que se estiman a-posteriori toda la trayectoria seguida y el mapa completo resultante en base a todos los datos registrados; y ii) la alternativa *on-line*, en la que la posición actual y el mapa se van actualizando con los datos más recientes en cada instante. El coste computacional de la alternativa *off-line* hace que no sea adecuado para aplicaciones en tiempo real, pero permite alcanzar precisiones mayores en la nube final al ser posible el ajuste de la nube en su totalidad, mientras que la alternativa *on-line* permite ir generando el mapa y la trayectoria en tiempo real con un coste computacional no muy alto. Dependiendo de la alternativa con que se aborde el problema se utilizarán técnicas de estimación diferentes: así para las metodologías *on-line* se usan técnicas basadas en filtros [69] como el filtro de Kalman (KF) [70] y sus variantes [71,72], derivados del filtro Bayesiano, o el filtro FastSLAM [73] derivado del filtro de partículas; mientras que para las metodologías *off-line* se utilizan técnicas basadas en la optimización [55].

Sea cual sea el enfoque seguido en la técnica SLAM, es de interés establecer un itinerario cerrado, de forma que el punto de origen y fin de la trayectoria recorrida sea el mismo. De esta manera se minimiza la deriva acumulada por el SLAM en el tiempo y con ello se mejora la precisión de los resultados [74].

Por su parte, las técnicas de escaneado móvil mediante el método Stop & Go consisten en una aplicación particular de escaneado móvil en la que la captura de nubes de puntos se realiza cuando la plataforma móvil está parada, es decir, la plataforma móvil (generalmente drones terrestres) se mueve hasta el punto de escaneo, se para y cuando está detenida el escáner láser realiza el escaneo correspondiente. Cuando finaliza el escaneo, la plataforma móvil continúa hasta el siguiente punto y así sucesivamente [66]. Estas tecnologías surgieron con la idea de automatizar las capturas con TLS estático, mejorando su eficiencia y preservando su calidad [75-77], y después fueron evolucionando hacia el campo del escaneado móvil de manera que se pueden considerar como las predecesoras de los sistemas de cartografiado móvil con tecnología SLAM. En los casos del método Stop & Go la nube de puntos completa no se obtiene de manera automática, sino que se deben realizar tomas independientes que posteriormente se alinean en un mismo sistema de coordenadas de modo que formen un único escenario completo.

La brecha existente entre los sistemas de escaneado móvil Stop & Go y los sistemas de escaneado móvil SLAM radica principalmente en la relación entre el tiempo de captura y la precisión de los datos obtenidos. Con el acercamiento Stop & Go se suelen obtener datos con más precisión, pero son lentos a la hora de realizar la captura de datos, requiriendo además el uso de plataformas móviles. Por el contrario, con el acercamiento SLAM se suelen abarcar mayores extensiones en menos tiempo, siendo la densidad y precisión de la nube de puntos resultante menor.

A lo largo de esta Tesis Doctoral se abordan ambos enfoques de escaneado móvil, haciendo especial hincapié en los aspectos de interés anteriormente señalados como son el desarrollo de protocolos específicos para la captura con sistemas de escaneado móvil del tipo SLAM y Stop &

Go, así como el diseño de una plataforma robotizada (dron terrestre) que, basada en un planificador de rutas óptimo, sea capaz de digitalizar entornos complejos de manera automática.

Desde el punto de vista de los equipos de escaneado también existen diferencias entre los MLS de exterior y los de interior. Mientras que los MLS de exterior no están sometidos a limitaciones con respecto de su volumen o peso, dada la capacidad de las plataformas de portarlos, para el caso de escenarios interiores las plataformas móviles están limitadas para ser portadas, o empujadas, por el usuario: son más pequeñas y ligeras, lo que hace en muchos casos que sean menos robustas. De este modo, son portables por el propio usuario, bien en la mano o en una mochila debidamente equipada. Por lo tanto, los equipos han de ser manejables y cómodos de transportar. Actualmente existen tres tipos de MLS portables capaces de capturar datos mientras el usuario camina por el entorno [55]: i) sistemas de mochila (Backpack), en los que el usuario lleva el equipo montado en una mochila, ii) sistemas de mano (Handheld), en los que el usuario lleva el equipo en la mano y iii) sistemas de carrito (Trolley) en los que el equipo se monta sobre un carrito y se desplaza con el empuje por parte del usuario. De entre todas estas opciones disponibles a día de hoy, la primera de ellas, los MLS de mochila (también llamados en ocasiones WMMS del inglés Wearable Mobile Mapping System), ha sido objeto de estudio y análisis en esta Tesis Doctoral. En este tipo de sistemas, el sistema de posicionamiento (que puede incluir sensores GNSS y/o IMU), puede ser integrado en el propio láser, el cual, por sus dimensiones y peso, puede llevarse con una sola mano.

Finalmente, la forma más habitual de comprobar la calidad y precisión de los datos obtenidos con las técnicas SLAM, pasa por comparar las nubes de puntos generadas por sistemas más precisos como los TLS [78]. De acuerdo a estas comparaciones los sistemas de escaneado móvil apoyados por las técnicas SLAM ofrecen precisiones del rango del centímetro [24, 38] y tiempos de adquisición de datos muy por debajo de los que se necesitan con un TLS estático. Todo ello los hace soluciones eficientes y aptas para multitud de aplicaciones. Por su parte, la calidad de las técnicas Stop & Go se realiza comparando la nube de puntos con una red de control formada por puntos fijos obtenidos por procedimientos topográficos clásicos y con aparatos muy precisos (estación total) [79] y mediante análisis estadísticos basados en estimadores no paramétricos [80]. En esta Tesis Doctoral se investiga cómo estos dispositivos pueden ser utilizados en la documentación y conservación de edificios en construcción o históricos.

1.1.3 Procesado de nubes de puntos

Motivada la importancia e interés de los sistemas de escaneado láser móviles, la presente sección se centrará en desarrollar métodos de procesado de nubes de puntos adquiridas con estos sistemas. Los métodos de procesamiento de nubes de puntos desarrollados en esta Tesis Doctoral pueden clasificarse en dos grandes grupos: i) los métodos de filtrado y homogeneización de la nube de puntos; y ii) los métodos de alineamiento de nubes de puntos.

Filtrado y homogeneización

Sea cual sea la procedencia de la nube de puntos, será habitual la presencia de errores accidentales, sistemáticos y groseros (outliers) en forma de ruido, y la presencia de posibles artefactos no deseados, debido a las propias limitaciones del sensor, las condiciones de

iluminación o la naturaleza reflectante de las superficies escaneadas [81-83]. En el caso de las plataformas móviles, además, el propio movimiento del dron o del usuario que lo porta genera vibraciones y por tanto ruido en los datos [84]. Por lo tanto, antes de realizar ningún otro proceso sobre las nubes de puntos, estas deben filtrarse, para quedar limpias de todos aquellos puntos erróneos que puedan entorpecer procesados posteriores o incluso incrementar los tiempos de procesamiento. De acuerdo con Han et al [85], los métodos de filtrado de datos pueden clasificarse en seis grupos principales según las características que se utilicen para el cálculo. Así pues, se tienen métodos basados en: i) estadísticas; ii) vecindad de un punto; iii) proyección; iv) características del punto; v) ecuaciones diferenciales parciales (PDE); y vi) sistemas híbridos. De todos estos métodos, los basados en PDE y características del punto no son capaces de eliminar los llamados outliers, mientras que los métodos basados en estadísticas y vecindario de un punto sí que lo consiguen, además de filtrar el ruido y no modificar las características de los datos [85]. Por esta razón, esta Tesis Doctoral hará especial hincapié en los filtros basados en estadísticas y vecindario como herramienta fundamental para el procesado de bajo nivel de cualquier nube de puntos.

Los filtros basados en estadísticas analizan la homogeneidad de los datos con respecto al vecindario de cada punto. Los puntos que no están dentro de la homogeneidad de los datos son los llamados outliers o valores atípicos que no proporcionan una buena representación del entorno, indicando que están aislados y que no deben considerarse fiables. Al eliminar estos datos no sólo se consigue una representación más fiable de la realidad, sino que la eficiencia de cálculos posteriores se incrementa considerablemente y se reduce el error [84]. Zhang et al [86] fueron los primeros en desarrollar el conocido método de filtrado SOR (Statistical Outlier Removal) que posteriormente adaptaron Rusu et al [87] y que ha tenido diferentes variantes a lo largo de los años. En primera instancia, el filtro SOR efectúa un análisis de distancias entre uno de los puntos de la nube y sus vecinos más cercanos. Acto seguido, y asumiendo que la distancia entre un punto dado y sus vecinos sigue una distribución normal y que puede por tanto representarse a través de una media y una desviación estándar, el filtro elimina todos aquellos puntos que se encuentran fuera de una determinada desviación estándar [88]. Este método elimina los valores atípicos y deja las nubes de puntos limpias para los siguientes procesos, siendo robusto y fiable, aunque para grandes nubes de puntos el tiempo de cómputo aumenta considerablemente. Con el fin de mejorar su eficiencia, Balta et al [84] desarrollaron el FSOR (Fast Statistical Outlier Removal) que disminuye el tiempo de cálculo casi un 50% en grandes nubes de puntos.

Además de la limpieza de puntos atípicos y del ruido, se hace necesario ejecutar procesos de homogeneización de las nubes de puntos ya que los datos capturados por los sistemas escáner láser varían la densidad de puntos en función de la distancia, de manera que cuanto más lejano esté el objeto del láser, menor densidad de puntos se registra. La homogeneización de los datos permite tener una densidad uniforme en cada nube de puntos, así como poder combinar nubes de puntos procedentes de diferentes sensores o con diferentes características, tales como la densidad y cantidad de puntos [84]. La forma más eficiente de realizar tareas de homogeneizado es utilizar técnicas de Voxelizado [89, 90]. Estas técnicas consisten en hacer divisiones sucesivas del espacio 3D en partes o cubos de igual tamaño llamados vóxeles. Para cada vóxel se sustituyen los puntos contenidos en él por la aproximación a su centroide [84]. Así la nube de

puntos quedará filtrada con una densidad igual a lo largo de toda su extensión, lo que permite optimizar tiempos de cómputo de sucesivas tareas.

Atendiendo a ello, la presente Tesis Doctoral hará hincapié en el análisis y aplicación de dichas técnicas sobre nubes de puntos en sistemas de escaneado móvil, investigando, además, los resultados que se obtienen aplicando filtros anisotrópicos [91] para la reducción del ruido, más allá del ya citado filtro SOR (o su variante FSOR). Los filtros anisotrópicos se basan en eliminar el efecto aliasing o solapamiento de las señales y aplicándolos a las nubes de puntos mejoran la calidad de las texturas de las superficies, reduciendo la difuminación y manteniendo las características y los detalles.

Alineamiento de nubes de puntos

Alinear o llevar al mismo sistema de coordenadas las nubes de puntos ha sido una tarea inherente a cualquier proceso de captura de datos con escáner láser estático desde que su uso empezó a extenderse en la Comunidad Científica. Casi ningún escenario puede ser documentado con una única toma de datos, debido a la propia disposición geométrica del escenario, a las oclusiones que los objetos causan y a la limitación de distancia de alcance de los propios escáneres. Por tanto, será necesario realizar varios escaneos para cubrir toda la extensión. Cada escaneo se registra en su propio sistema de coordenadas local, requiriendo un proceso de alineamiento o registro de las tomas para poner todos los datos sobre un único sistema de coordenadas común que permita tener la reconstrucción completa del escenario. De igual forma, ese problema se repite para sistemas de escaneado móvil cuando se realiza el método Stop & Go o incluso cuando con los sistemas de escaneado móvil SLAM incorporan varias trayectorias para completar el escenario u objeto, teniendo que ser registradas en el mismo sistema de coordenadas. En ocasiones, las tareas de alineamiento pueden automatizarse a través de la colocación en el escenario de elementos de puntería artificiales, con tamaños y/o formas especiales (ej. esferas, planos o círculos entre otros) fácilmente reconocibles por programas de procesado. No obstante, la colocación de elementos artificiales no siempre es posible (ej. lugares inaccesibles) y requiere de mucho tiempo y planificación con el objetivo de conseguir una visibilidad de al menos tres elementos de puntería artificiales entre dos estaciones consecutivas. En una búsqueda de soluciones menos dependientes, han surgido métodos de alineamiento basados en características no artificiales, los cuales permiten resolver el problema basándose en características invariantes (detectores/descriptores) de las nubes de puntos, ya sean líneas, superficies o puntos. No es necesario añadir ningún elemento artificial en el escenario ya que los algoritmos se encargan de analizar los puntos y extraer características geométricas de los mismos. En ambos casos el registro de las nubes de puntos se realiza en dos pasos: (i) primero se realiza un alineamiento grosero o primera aproximación "*coarse-alignment*" y (ii) posteriormente se refina, "*fine-alignment*", esa transformación mediante métodos iterativos, hasta encontrar el mínimo de una función de coste (ej. distancia entre zonas de solape) [92, 93]. Ambos alineamientos hacen uso de transformaciones sólido-rígidas de seis parámetros (tres rotaciones y tres traslaciones) quedando definida dicha transformación a través de una matriz de traslación y rotación, también llamada matriz de transformación [93]. Así, una nube de puntos origen modifica su posición acorde a estos parámetros para acercarse a la nube de puntos de referencia. La forma de calcular dicha matriz de transformación pasa por

encontrar pares de puntos homólogos, comúnmente llamados correspondencias, entre las nubes de puntos. En el modo manual, los pares de puntos los marca el usuario, mientras que en el modo automático se encargan de ello los algoritmos detectores y descriptores 3D. Estos algoritmos analizan cada punto en relación con su entorno más cercano y son capaces de extraer características para determinar si dos puntos son potencialmente homólogos o no.

El alineamiento de nubes de puntos se apoya en un modelo estocástico no lineal que requiere de aproximaciones iniciales. Por ello, la estimación inicial del alineamiento (efectuada durante el *coarse-alignment*) juega un papel esencial en el resultado final, de manera que, si la estimación inicial no es lo suficientemente precisa, el resultado de la optimización (*fine-alignment*) no lo será [94]. Encontrar las correspondencias correctas es un paso determinante y por eso existen una gran variedad de detectores y descriptores que permiten adaptarse a cada caso. Los detectores 3D son los encargados de seleccionar un set de puntos potencialmente buenos para ser correspondidos. Se dividen en dos grupos: i) detectores de escala variable como el Local Surfaces Patches (LSP) [95] o el Intrinsic Shape Signatures (ISS) [96]; y ii) detectores de escala invariante como el Scale Invariant Feature Transform (SIFT) [97] o el Speed Up Robust Features (SURF) [98]. De igual modo existe un amplio abanico de descriptores 3D divididos en tres grupos: i) descriptores locales; ii) descriptores globales; y iii) descriptores híbridos. Los más utilizados son los descriptores locales, que analizan la vecindad de un punto. Ejemplos de este tipo de descriptores son el Intrinsic Shape Signatures (ISS) [96], el Point Feature Histogram (PFH) [99], el Signature of Histogram of Orientation (SHOT) [100] o el Fast Point Feature Histogram (FPFH) [101]. Por su parte, los descriptores globales en lugar de analizar cada punto individualmente, analizan y codifican la nube de puntos 3D completa [101]. Como consecuencia de ello, se generan menos descriptores, se agiliza el proceso y se consumen menos recursos. Ejemplos de descriptores globales son el Viewpoint Feature Histogram (VFH) [102] o el Global Structure Histogram (GSH) [103] muy utilizados en tareas de reconocimiento y segmentación de objetos. Los descriptores híbridos fusionan los principios de los descriptores locales y globales, para aprovechar al máximo las ventajas de cada descriptor y conseguir resultados óptimos [101]. Ejemplos de descriptores híbridos son el Local to Global Signature (LGS) [104] y el FPFH+VFH [105], que combina el descriptor local Fast Point Feature Histogram (FPFH) con el descriptor global Viewpoint Feature Histogram (VFH).

El último paso para conseguir el alineamiento completo de las nubes de puntos es refinar el resultado anterior hasta conseguir una matriz de transformación para la cual la distancia entre puntos, en las zonas comunes entre ambas nubes, sea mínima. El algoritmo por excelencia en este ámbito es el Iterative Closest Point (ICP), método de optimización matemática en el que la función de coste a minimizar es la distancia entre los puntos de las zonas de solape [106]. El ICP cuenta con multitud de variantes, siendo las más conocidas: i) point-to-point; y ii) point-to-plane. La primera de ellas minimiza la distancia entre puntos, por lo que el tiempo de cómputo es mayor, pero es muy robusto respecto al ruido Gaussiano. La segunda, por el contrario, minimiza la distancia entre el punto y el plano tangente a su punto correspondiente en la nube de puntos a registrar. Este método es más efectivo, pero menos resistente al ruido [106].

En la presente Tesis Doctoral se profundiza en el estudio de las combinaciones óptimas de detectores / descriptores 3D que optimizan el algoritmo ICP en tareas de digitalización de edificios.

1.1.4 Análisis estructural de edificios a través del Modelado por Elementos Finitos (FEM).

La vida útil de las construcciones determina en gran medida el éxito de estas. Dicho factor queda supeditado al buen diseño (correcta elección de materiales y sistemas constructivos) y al mantenimiento (análisis periódico) de las mismas. Para ambos casos, el cálculo analítico o mediante simulación numérica computacional [107, 108] constituye una pieza fundamental en el entendimiento de diferentes aspectos como pueden ser el energético [109-112], el comportamiento higrotérmico [113-115] o el estructural [116-118], entre otros. Centrándonos en el último de estos aspectos, el estructural, el interés científico-tecnológico pivota en torno a dos aspectos fundamentales: i) el análisis de nuevos materiales y soluciones constructivas; y ii) el entendimiento del comportamiento estructural del edificio ante diferentes casuísticas como pueden ser seísmos, asentamientos o la propia degradación del material constructivo [119 - 121]. Todo un abanico de posibilidades para las cuales el conocimiento adecuado del material, el sistema constructivo o una correcta digitalización (conocimiento exhaustivo de su geometría), son ingredientes necesarios para obtener resultados fidedignos. Centrando la mirada en el último de estos aspectos, el de la geometría, resulta innegable colocar en primera instancia a los sistemas TLS estáticos dada sus mayores prestaciones en términos de precisión y velocidad de captura de datos, permitiendo aspirar a la generación de modelos CAD de diferentes tipologías de infraestructuras y edificación [7, 122, 123]. En línea con este enfoque también podemos encontrar trabajos en los que se usa la fotogrametría SfM para dicha digitalización [19], y posterior obtención del modelo CAD, destacando la posibilidad de emplear drones para digitalizar lugares no accesibles desde tierra. En la actualidad, tres son los enfoques fundamentales para pasar dicha nube de puntos a un modelo CAD apto para posteriores simulaciones numéricas: i) la retopología de la malla propuesta por Gonizzi et al. [124]; ii) la voxelización de la nube de puntos propuesta por Castellazzi et al. [125]; iii) el uso de técnicas de ingeniería inversa a través de algoritmos para la creación de superficies paramétricas (tipo RANSAC Shape Detector) [126] o no paramétricas tipo NURBS [127].

Si bien el TLS o la fotogrametría SfM han sido los sensores más utilizados para estos trabajos [7, 19, 122, 123], son muy pocos los trabajos que integran las técnicas de escaneado móvil dentro de estos flujos de trabajo. Atendiendo a ello, en la presente Tesis Doctoral se profundiza en la viabilidad de utilizar los sistemas de escaneado móvil para la realización de análisis estructurales de edificios históricos donde la geometría real juega un papel muy relevante en los resultados obtenidos.

1.1.5 Gestión y conservación preventiva a través de los modelos BIM

Tal y como se señaló con anterioridad, la vida útil de una edificación exige en muchas ocasiones conocer diferentes aspectos de la misma, que varían desde cuestiones energéticas hasta de comportamiento estructural, demandando la intervención de diferentes expertos (ej. ingenieros, arquitectos, geólogos etc.) para lo cual resulta totalmente necesario el desarrollo de herramientas adecuadas para la gestión de toda la información disponible.

Con la aparición de los Building Information Modelling (BIM) [128] y toda la metodología asociada a estos modelos, el ciclo de vida de cualquier construcción puede ser documentada

desde sus inicios, durante todas sus fases constructivas hasta la fecha de su demolición, pasando por las diferentes etapas de vida y modificaciones que se vayan ejecutando. Los modelos BIM unifican en un mismo entorno de trabajo las características geométricas de los objetos con la información adicional de los mismos, ya sea información energética, de materiales, información de revisiones periódicas, propiedades mecánicas, resistencia, etc. De este modo los modelos BIM evolucionan los modelos geométricos (3D) añadiendo información de tiempo (4D), costes (5D), información ambiental (6D) e información de mantenimiento (7D). Además, la metodología BIM se basa en un trabajo colaborativo en el que todas las partes intervienen y trabajan sobre los mismos datos, lo que aumenta la productividad del trabajo en términos de costes, tiempo, coordinación y comunicación [129].

Si bien los modelos BIM permiten documentar exhaustivamente los edificios y todos los elementos contenidos en ellos, dicha metodología se desarrolló para aplicarse a edificios de nueva construcción. El modelado BIM se fundamenta en el uso de elementos paramétricos. Esto quiere decir que en lugar de modelarse instancias de los elementos (ej. una pared) se genera una familia con unas reglas y relaciones que controlan el comportamiento de los parámetros. Estas relaciones permiten que cada instancia de una clase varíe de acuerdo con sus propios ajustes de parámetros y relaciones contextuales [128]. En este contexto, prácticamente la totalidad de los elementos que se utilizan en nueva construcción son parametrizables (ej. perfiles normalizados, puertas o ventanas de dimensiones estandarizadas, etc.). Además, cuando se trata de nueva construcción se conocen de antemano todos y cada uno de los elementos que compondrán la estructura, sin importar si serán visibles o quedarán ocultos al finalizar la construcción. Sin embargo, no sucede lo mismo en edificios históricos. En gran parte de las ocasiones, no se tiene una información completa y exacta de los materiales utilizados, la composición de los mismos o las intervenciones realizadas, bien por falta de almacenamiento de esta información, o bien por falta de registro de datos en el momento de construcción [130]. Además, los elementos constructivos históricos no siempre son parametrizables, existiendo objetos únicos para cada construcción. Esta falta de información y de parametrización de los objetos añade un grado de dificultad extra a la hora de crear modelos BIM de edificios históricos. Es por ello que a estos modelos se les denomina HBIM (Historic Building Information Modelling). Trabajar con modelos HBIM implica definir de manera muy clara dos aspectos: (i) el nivel de detalle LoD (Level of Detail) y (ii) el nivel de información LoI (Level of Information). El LoD establece el grado de detalle de la geometría modelada, mientras que el LoI determina la información asociada al elemento. Dependiendo de la finalidad del HBIM serán necesarios unos LoD y LoI más altos o más bajos [131]. Por lo general, en los modelos HBIM, el LoI no tiene límites, permitiendo almacenar cualquier tipo de información necesaria y completar los modelos geométricos, independientemente del LoD con que se haya creado. Así, cualquier detalle no modelado queda contemplado en el LoI.

Disponer de modelos HBIM del patrimonio cultural facilita las tareas de monitorización y permite una gestión más eficiente de su conservación. En este sentido, se utilizan las nubes de puntos tridimensionales como elemento de partida para la generación de los modelos HBIM, realizando un proceso de ingeniería inversa, basada en modelado paramétrico. Una vez que el modelo HBIM se ha completado, mediante la integración de diferentes tecnologías, como el internet de las cosas (IoT), las bases de datos (BBDD) o la incorporación de datos específicos, se pueden realizar diversos análisis con diferentes aplicaciones externas. Así, por ejemplo, se

pueden utilizar módulos de cálculo térmico, análisis de diseño sostenible o estudios de eficiencia energética, entre otros.

En esta Tesis Doctoral se investiga de qué manera un modelo HBIM puede mejorar las tareas de conservación preventiva de edificios históricos, siendo este un enfoque de conservación en pleno desarrollo y capaz de ofrecer ahorros del 40-70% en comparación con los enfoques anteriores: la conservación correctiva [132]. La conservación preventiva responde al lema "*más vale prevenir que curar*", y consiste en analizar los riesgos a los que están sometidos los diferentes sistemas constructivos y bienes muebles de un edificio para así programar tareas de conservación periódicas que minimicen la aparición de daños en los mismos. Dicha programación de tareas exige conocer los riesgos, la vulnerabilidad de los elementos, así como controlar de forma periódica ciertos parámetros de carácter medioambiental (ej. la humedad, temperatura o luminosidad, entre otros) o de carácter estructural (ej. inclinaciones, aperturas, flechas, etc.). Parámetros para los cuales el uso de redes de sensores inteligentes resulta un paso necesario, requiriendo de una conexión entre el modelo físico y el virtual (generalmente sistemas HBIM o BIM) a través del uso de métodos basados en IoT. Así, mediante una red de sensores instalada en el edificio, es posible tener en el HBIM datos en tiempo real de los parámetros de conservación.

Considerando todo lo señalado con anterioridad, la investigación aquí presentada trata de ahondar en la definición de nuevas plataformas HBIM capaces de gestionar información de carácter multidisciplinar, conectarse con redes de sensores inteligentes sin olvidar la optimización en términos de coste a través de la integración de sistemas de escaneado móvil.

1.2 Objetivos

Teniendo en cuenta el contexto anteriormente mostrado, el **objetivo principal** de la presente Tesis Doctoral es avanzar en la **integración de los sistemas de escaneo móviles para la digitalización y creación de modelos CAD en edificación, tanto nueva como histórica**.

Derivado de este objetivo principal surgen una serie de **objetivos específicos**, que pasan a citarse a continuación:

- Estudiar los sistemas tradicionales de escaneado láser existentes, TLS, viendo las posibilidades que ofrecen, sus ventajas y desventajas, y sus precisiones, entre otras variables.
- Estudiar los sistemas de escaneado móvil del tipo SLAM, así como las precisiones que ofrecen, las comodidades, las limitaciones de distancias o la densidad de los datos.
- Desarrollar protocolos de captura de datos con sistemas de escaneo láser móviles, tipo SLAM y tipo Stop & Go, que optimicen el tiempo de captura y la calidad de los datos obtenidos.
- Desarrollar métodos de procesado de nubes de puntos (filtrado y homogeneización) que permitan mejorar la calidad de la nube de puntos obtenida, sin olvidar tampoco el desarrollo de métodos de alineamiento automático que agilicen el procesado de esta.
- Avanzar metodologías de ingeniería inversa que permitan pasar de las nubes de puntos capturadas por los sistemas de escaneado móvil a modelos CAD, FEM y BIM.

- Realizar análisis y gestión de los edificios en tiempo real, mediante la incorporación de tecnologías IoT en los modelos BIM generados a partir de las nubes de puntos.

1.3 Estructura de la Tesis Doctoral

La Tesis Doctoral aquí presentada se ha realizado por la modalidad de *compendio de artículos de acuerdo a la normativa reguladora de la Universidad de Salamanca.*

En total se presentan cuatro artículos publicados en revistas de impacto y que permiten avanzar en el estado del arte, así como abordar con éxito los objetivos anteriormente expuestos. Para ello el documento queda distribuido en un total de cinco capítulos:

- **Capítulo I:** Introducción
- **Capítulo II:** Digitalización de escenarios complejos
- **Capítulo III:** De la nube de puntos a los modelos FEM
- **Capítulo IV:** De la nube de puntos a los modelos BIM y la integración IoT
- **Capítulo V:** Conclusiones y trabajos futuros.

Capítulo I: Introducción. En este capítulo se da una visión general de los sistemas de escaneado láser móviles utilizados en esta Tesis Doctoral. Finalmente, en este capítulo se establecen los objetivos generales y específicos de la Tesis Doctoral y una breve estructura de la misma.

Capítulo II: Digitalización de escenarios complejos. En este capítulo se abordan diferentes técnicas de escaneado móvil de escenarios complejos y edificios. Por una parte, se aborda la digitalización mediante técnicas Stop & Go con un dron terrestre sobre el que se acopla un dispositivo TLS. Por otro lado, se estudian los equipos de escaneado móvil portable del tipo mochila basados en paradigmas SLAM. A lo largo de este capítulo se establece una guía de buenas prácticas para la correcta digitalización con los diferentes equipos y se analizan las ventajas e inconvenientes de cada una de las metodologías. Asimismo, se describe la metodología desarrollada para el procesamiento básico de las nubes de puntos, la cual ha sido empleada en todos los casos de estudio presentados en este documento.

Capítulo III: De la nube de puntos a los modelos FEM. Una vez establecida la guía de buenas prácticas de adquisición y el procesado básico de las nubes de puntos, en este capítulo se ahonda en los procesos de ingeniería inversa que permiten generar modelos CAD as-built (de la realidad construida) a partir de las nubes de puntos capturadas. Más concretamente, se propone una metodología de filtrado y creación de superficies paramétricas y no-paramétricas capaces de obtener la base geométrica adecuada para posteriores simulaciones numéricas. Dichas simulaciones hacen uso del método FEM, permitiendo conocer la respuesta estructural de un edificio ante diferentes escenarios (ej. carga gravitatoria o sismo, entre otros). Para validar dicha metodología se establece como caso de estudio la Iglesia de San Pedro situada en Becerril del Carpio, Palencia (España) en el que se utilizan los avances alcanzados en el Capítulo II tanto para la captura como para el posterior procesado.

Capítulo IV: De la nube de puntos a los modelos BIM y la integración de información IoT. Motivado por el auge de los modelos BIM y la necesidad de tener un proceso unificado a lo largo

de la vida de cualquier edificación, este capítulo hace hincapié en la creación de modelos BIM de edificios ya construidos a partir de la nube de puntos capturada con dispositivos de escaneado móviles. Se contempla en esta parte una introducción a los modelos BIM y su dinámica de trabajo, así como a la problemática existente en torno a la generación de modelos BIM de edificios históricos. Posteriormente, se muestra cómo los modelos BIM pueden ayudar a gestionar los edificios históricos mediante la utilización del IoT. En concreto se aborda el caso de estudio de la Biblioteca General Histórica de la Universidad de Salamanca, en la que se emplean sensores de temperatura, CO2, luminosidad y presencia humana. Estos sensores envían datos en tiempo real a un servidor, donde se incorporan al modelo BIM generado a partir de la nube de puntos, obteniendo así un sistema de monitorización en tiempo real que permite gestionar las ventilaciones, iluminaciones y entradas de personal de manera óptima para una correcta conservación del espacio y los bienes contenidos en el mismo.

Capítulo V. Conclusiones y trabajos futuros. Este es el capítulo final de la Tesis Doctoral en el que se establecen las conclusiones a las que se han llegado, así como una exposición de trabajos futuros que se pretenden realizar.

Capítulo II.

Guía de buenas prácticas y procesamiento básico de nubes de puntos

2. Guía de buenas prácticas y procesamiento básico de nubes de puntos

En este capítulo se abordan dos pilares fundamentales para la digitalización con sistemas de escaneado móvil: i) la guía de buenas prácticas de adquisición de datos; y ii) el procesado básico de las nubes de puntos obtenidas. El capítulo engloba dos de los cuatro artículos de la presente Tesis Doctoral, cada uno de ellos dedicado a una técnica diferente de escaneado móvil. Así pues, en primer artículo, titulado "*Use of a Wearable Mobile Laser System in Seamless Indoor 3D Mapping of a Complex Historical Site*" se profundiza en los sistemas de escaneado móvil del tipo mochila (WMLS- *Wearable Mobile Laser System*) mientras que, en el segundo artículo, titulado "*Automatic Point-Cloud Registration for Quality control in Building Works*" se investiga un sistema de escaneado móvil (técnica Stop & Go) formado por un dron terrestre y un láser escáner terrestre (TLS).

2.1 Sistema de escaneado móvil: WMLS

La presente sección tiene como objeto presentar el trabajo de investigación titulado "*Use of a Wearable Mobile Laser System in Seamless Indoor 3D Mapping of a Complex Historical Site*" y publicado en la revista científica *Remote Sensing* de MDPI en 2018.

Resumen

El artículo titulado "*Use of a Wearable Mobile Laser System in Seamless Indoor 3D Mapping of a Complex Historical Site*" investiga acerca de los mejores procedimientos y parámetros de procesado para digitalizar escenarios muy complejos con un escáner láser móvil del tipo mochila WMLS. El escenario objeto de estudio fue un Palacio del siglo XV en ruinas, en Segovia (España), edificio que se encontraba en avanzado estado de degradación con forjados colapsados, estancias muy angostas, rincones cubiertos de obstáculos, etc.

En este artículo se establece una guía de buenas prácticas de adquisición de datos y un protocolo de actuación para digitalizar escenarios muy complejos con el WMLS, de modo que para posteriores trabajos se pueda seguir esta guía y se optimice así el uso de estos dispositivos. Este artículo sirvió para sentar las bases de posteriores investigaciones, abriendo la puerta a la aplicación de sistemas de escaneo móviles para la digitalización de grandes superficies con dificultad de acceso y espacio.

Los objetivos de esta investigación son tres: i) comprobar la viabilidad del dispositivo WMLS para obtener modelos tridimensionales de escenarios muy complejos, haciendo especial hincapié en la precisión de los datos obtenidos y el ahorro de tiempo asociado a este dispositivo, ii) desarrollar un protocolo de toma de datos con estos dispositivos WMLS que optimice el tiempo de captura y la calidad de los datos y, iii) desarrollar métodos de procesado de datos que aumenten la calidad de los datos.

En el artículo se presentan, principalmente, tres contribuciones:

- Digitalización del interior y exterior del edificio con el WMLS: En esta parte, se presenta el dispositivo de escaneado móvil WMLS, así como la metodología seguida para realizar la digitalización del escenario en cuestión
- Filtrado y limpiado de los datos obtenidos: Una vez obtenidos los datos con el sistema WMLS, se muestra el proceso de limpieza y homogeneización de los datos obtenidos, de manera que se eliminan los datos erróneos y se obtiene una nube de puntos apta para posteriores procesos de cálculo.
- Comparativa de los resultados WMLS con el TLS: En esta sección se lleva a cabo un análisis comparativo de los resultados obtenidos con el sistema WMLS y el TLS, para conocer la precisión que el WMLS ofrece. La validación de la metodología se llevó a cabo de dos maneras diferentes: (i) validación local y (ii) validación global. Para la validación local se realizaron medidas entre planos opuestos (ej. techo y suelo). Cada medida se realizó cinco veces y se tomó como valor final la media aritmética de las cinco. Posteriormente se analizó estadísticamente la desviación de las medidas mediante los métodos introducidos por Nocerino et al. [24]. La validación global consistió en comparar los centroides de una red de esferas medidas por ambos sistemas. Además, se comprobó si con los datos obtenidos se podían extraer planos de planta y secciones aptas para los trabajos de restauración del edificio.

Las conclusiones que se obtuvieron de este artículo fueron varias: i) el sistema WMLS, más concretamente el sistema Zeb-Revo [133], es apto para digitalización de escenarios complejos, obteniéndose modelos con errores entre 1 y 3 cm, ii) con los datos obtenidos es posible generar planos de planta y secciones con la precisión suficiente como para acometer las tareas de restauración y reparación y, iii) este sistema aporta la gran ventaja de ser muy manejable y rápido, ahorrando mucho tiempo de toma de datos y pudiendo documentar espacios muy angostos y pequeños que con el TLS son muy difíciles de capturar.

remote sensing

MDPI

Technical Note

Use of a Wearable Mobile Laser System in Seamless Indoor 3D Mapping of a Complex Historical Site

Andrea di Filippo [1], Luis Javier Sánchez-Aparicio [2], Salvatore Barba [1], José Antonio Martín-Jiménez [2], Rocío Mora [2] and Diego González Aguilera [2,*]

1 Department of Civil Engineering, University of Salerno, Via Giovanni Paolo II, 132, 84084 Fisciano (SA), Italy; andrew89.adf@gmail.com (A.d.F.), sbarba@unisa.it (S.B.)
2 Department of Land and Cartographic Engineering. University of Salamanca, Higher Polytechnic School of Avila, Calle de los Hornos Caleros, 50, 05003 Avila, Spain; luisj@usal.es (L.J.S.-A.); joseabula@usal.es (J.A.M.-J.); rociomora@usal.es (R.M.)
* Correspondence: daguilera@usal.es

Received: 4 November 2018; Accepted: 26 November 2018; Published: 28 November 2018

Abstract: This paper presents an efficient solution, based on a wearable mobile laser system (WMLS), for the digitalization and modelling of a complex cultural heritage building. A procedural pipeline is formalized for the data acquisition, processing and generation of cartographic products over a XV century palace located in Segovia, Spain. The complexity, represented by an intricate interior space and by the presence of important structural problems, prevents the use of standard protocols such as those based on terrestrial photogrammetry or terrestrial laser scanning, making the WMLS the most suitable and powerful solution for the design of restoration actions. The results obtained corroborate with the robustness and accuracy of the digitalization strategy, allowing for the generation of 3D models and 2D cartographic products with the required level of quality and time needed to digitalize the area by a terrestrial laser scanner.

Keywords: cultural heritage; restoration; indoor mapping; laser scanning; wearable mobile laser system; 3D digitalization; SLAM

1. Introduction

The guidelines for the conservation and enhancement of cultural heritage, codified in the Athens Charter and repeatedly reiterated by subsequent documents up to the most recent Krakow Charter [1], underline the importance of multidisciplinary and scientific approaches for the management of interventions in cultural heritage sites [2].

Currently, the use of new technologies for the data acquisition in the architectural field has reached widespread diffusion, mainly due to the ability to digitalize artifacts with great precision and to the possibility of generating informative models useful for the analysis, simulation, and interpretation phases [3]. The most popular techniques, which have now become a reference standard, are modern photogrammetry [4] and laser scanning [5]. Photogrammetry acquires two-dimensional images that require mathematical processing to derive 3D information. Through precise formulations based on projective or perspective geometry [6], it transforms the data extracted from the images into three-dimensional metric coordinates and colors [7]. For its part, laser scanning is able to directly obtain the 3D point spatial position [8,9] with high accuracy and without lighting conditions, especially over homogeneous surfaces where photogrammetry cannot provide reliable results.

The main products obtained from both 3D point clouds and 2D orthoimages techniques have been used for the virtual reconstruction of cultural heritage sites [10], the analysis of rock-art

paintings [11,12], the creation of accurate numerical simulations [13], or even the analysis of pathological processes [14,15], among others.

Besides the wide range of advantages that these solutions can offer, the digitalization of large and complex areas, especially indoor scenarios, generally entails the use of a large amount of images (in the case of photogrammetry) or scan stations (in the case of the laser scanner), deriving in a time consuming fieldwork and thus in an important error propagation [16,17]. Hybrid solutions, such as mobile mapping systems (MMSs), have emerged with great capabilities and possibilities in the last few years, allowing the management of different sensors and the possibility to operate in complex outdoor and indoor scenarios [18–21], minimizing error propagation.

Since their early development in the late 1980s, MMSs have been progressively improved in order to provide increasingly more precise and denser data, acquired in a shorter amount of time [22]. Besides the progresses in optical sensors, one of the key advances in MMS is related to spatial referencing technology. While the very early applications were restricted to environments where the sensor positions were computed using ground control, advantages in satellite and inertial technology make spatial referencing possible in previously unknown and undiscovered places [23,24]. Furthermore, the miniaturization and cost reduction of components have played a fundamental role in the spread of MMS, allowing for more flexible, portable, and low-cost systems [22]. This attribute, within the capacity of generating 3D point clouds by means of a spatial referencing in previously unknown environments, has allowed the application of this technology in Unmanned Aerial Vehicles (UAV) [23,25,26], Unmanned Ground Vehicles (UGV) [27–29], or equipped in backs (e.g., the Leica Pegasus back-pack, the Heron MS-2 back-pack or the Kaarta Stencil) [22,24,30]. Meanwhile, the use of the two first platforms could reduce the problems associated with travelling speed during the data acquisition, as well as improving the time efficiency during the survey. Moreover, their application in indoor and narrow spaces (common in Cultural Heritage) could entail some problems. These limitations place the wearable mobile laser systems (WMLS) as a potential solution for mapping indoor environments, as it is possible to obtain a 3D point cloud of the environment with a centimeter's accuracy [22,24,30]. However, this accuracy could be strongly affected by the characteristics of the trajectory, such as the travelling speed or the path followed [22,31].

Under these assumptions, this paper evaluates the suitability of a wearable mobile laser system for the digitalization of a complex indoor environment belonging to a cultural heritage building, as well as for the generation of cartographic products required for its conservation and restoration. This wearable system combines laser scanning technology and an inertial measurement unit (IMU) in portable equipment that can be handled by an operator while walking through the cultural heritage site. This sensor acquires point clouds on the move, thanks to the Simultaneous Localization and Mapping algorithms (SLAM) [32,33], without needing the support of a global navigation satellite system (GNSS). During this evaluation, we took into account the different parameters that could influence the final quality of the 3D point cloud. These parameters are: (i) the identification of critical areas; (ii) the prevision for closing loops; (iii) the traveling speed; (iv) the time spent to obtain the 3D point cloud; and (v) the density of the point cloud.

2. Materials and Methods

2.1. Equipment

The WMLS tested in the case study was the ZEB-REVO, commercialized by GeoSLAM (Figure 1) [34], which consisted of a 2D time-of-flight laser scanner (Hokuyo UTM-30LX-F from Hokuyo Automatic Co., Osaka, Japan) rigidly coupled to an IMU mounted on a rotary engine. The motion of the scanning head on the motor drive was stored in a processing unit located in a small backpack and provided the third dimension to generate 3D information. This computer was equipped with batteries that fed the hand-held laser scanner through a special connection cable. A 3D SLAM algorithm was used to combine the 2D laser scan data with the IMU data, in order to return accurate

3D point clouds, following the full SLAM approach implemented in the robotic operative system (ROS) library [35]. With a 360° vertical field of view and 30 m of range in ideal indoor conditions (which was reduced to 15–20 m in real working circumstances), the operator moved through the indoor environment capturing more than 43,000 points per second. Regarding accuracy, the manufacturer declared that its value is 1–3 cm in relative terms and 1–30 cm in absolute positioning for a 10-min scan, with the closing of a single loop [34]. Table 1 shows further technical specifications.

Figure 1. Main components of the wearable mobile laser systems (WMLS) used for data acquisition.

Table 1. Technical specification of the Geo Simultaneous Localization and Mapping (SLAM) ZEB-REVO device.

Parameter	Value	Parameter	Value
Total device dimension (mm)	220 × 180 × 470	Laser measuring principle	Time of flight
Scanner dimension (mm)	86 × 112 × 287	Scanner resolution	0.625° H × 1.8° V
Total device weight (kg)	4.10	Wavelength (nm)	905
Scanner weight (kg)	1.00	Orientation system	MEMS IMU
Head rotation speed (Hz)	0.5	Camera	GoPro
Operating time (h)	4	Scan rate	100 lines/s 43,200 points/s
Field of view	270° (H) × 360° (V)	Points per scan line	432 (0.325° int)

2.2. Methodology

The formalization of a schematic procedural pipeline for data acquisition and management represents a fundamental step to test the effective possibility of using WMLS for tracking complex indoor environments.

In this regard, it is possible to identify a succession of methodological phases that characterize an inspection with this approach: (i) the survey design (planning of the path); (ii) the data acquisition (protocol and basic rules); (iii) the post-processing (SLAM algorithm to compute the sensor trajectory and map the environment); and (iv) the cartographic product generation (three-dimensional and two-dimensional digital models). Figure 2 outlines the main steps of the applied methodology.

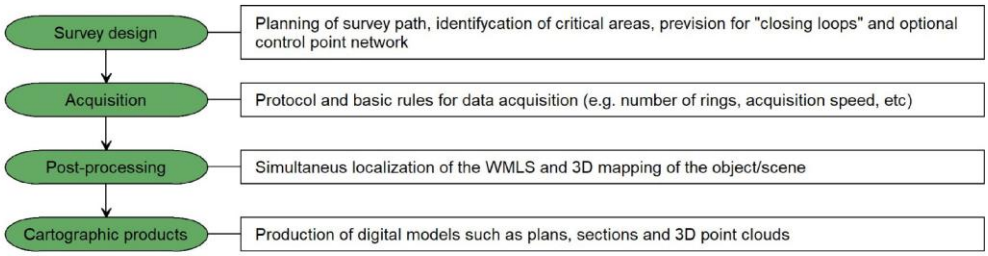

Figure 2. Methodological phases of the procedural pipeline for surveys with a WMLS.

2.2.1. Survey Design

Before conducting data acquisition, the user should plan the proposed survey path in order to identify potential problem areas, such as doorway transitions, stairwells, open spaces, and smooth walled passageways, generally with poor geometrical features. It should be noted that features are significant if the ratio of their size and their range is approximately 1:10 (e.g., a feature must be textgreater0.5 m in size for a distance of 5 m). In addition, if there are not sufficient features along the direction of travel, the SLAM algorithm cannot correctly determine forward motion. In these cases, the user can proceed in the following ways:

- Improve the background with additional references (e.g., boxes in a corridor or a parked vehicle in an open field);
- ensure that those limited features are scanned repeatedly as you move through the scene by pointing the WMLS in their direction. As a result, more measurement points will define the element, assuring its use as reference during the post-processing;
- avoid acquiring moving objects (e.g., passing pedestrians or vehicles) since the SLAM algorithm may support on them as static features.

The planning should also consider "closing loops" wherever possible. The approach used to transform the raw scan data into a point cloud uses a method analogous to the close traverse technique applied for surveys [36], in that a previously known position is used to determine its current location. The re-surveying of a known area allows the spreading of the compounded error around the loop and the improvement of the accuracy of the resulting point cloud. As a minimum, it is mandatory that the operator starts and ends the survey in the same position to ensure at least one loop closure (Figure 3).

In general, it is better to do circular loops rather than "there and back" loops where the path simply doubles back on itself [31]. This applies to horizontal and vertical rings—i.e., if possible enter and exit through different doors and move between floors via distinct stairwells. It is important to scan the closed loop regions carefully to ensure that the key features are scanned from a similar perspective. It may be necessary to turn around to return to a region from another direction. This is a crucial feature in poor environments.

Figure 3. Example of a survey design with the WMLS. The compensation of the accumulated error is possible thanks to the closure of the path following different track and acquiring the internal cloister area from different points of the route.

2.2.2. Acquisition

The process of scanning using WMLS is an important step since the collected data will inevitably influence the level of quality of the cartographic products. For these reasons, it is useful to define the following operative rules:

- Inspect the site of interest in advance in order to identify critical areas not detected during planning and remove any obstacles along the way;
- make easily accessible all the connections between different rooms and floors, such as doorways or stairs, so as to ensure safe passage of the operator and avoid moving objects during the scanning;
- walk slowly in order to have a good coverage and a high-resolution data. If the forward movement is too fast there may not be enough repeated features for the SLAM algorithm to transform the raw laser data into a point cloud;
- pay attention to the transition areas and tight curves that must be travelled slowly, guaranteeing a period when the scanner can display features on both sides. The same care is necessary when we change from a closed space (feature rich) to an open environment (feature poor);
- split large surveys into more than one scan mission. This is to avoid big file sizes as well as to reduce any drift effect and thus error propagation that might be created in the SLAM data. It is recommended that each scan mission is limited to 30 min [34].

2.2.3. Post-Processing: The Generation of the 3D Point Cloud

The post-processing approach adopted for the case study was the Simultaneous Localization and Mapping (SLAM) algorithm, which addressed the problem of positioning a mobile system in an unknown environment and provided its 3D mapping. Access to SLAM was justified in two ways: (i) placing the system within a space or environment (pose estimation or trajectory computation); (ii) 3D modelling of the environment (mapping or reconstruction).

A large variety of SLAM solutions are available; they can be classified either as filtering or smoothing [32]. Filtering approaches model the problem as an online state estimation, where the state of the system consists in the current instrument position and the map. The estimation is augmented and refined by incorporating new measurements as they become available. To highlight their incremental nature, filtering approaches are usually referred as online SLAM methods [37]. Conversely, smoothing approaches estimate the full trajectory of the instrument from the full set of measurements. They address the so-called full SLAM problem and typically rely on least-square error minimization techniques.

GeoSLAM algorithm is able to perform both an open-loop incremental solution for online SLAM and a closed-loop global registration for full SLAM (as in the case study). However, it is appropriate to introduce the general characteristics of the algorithm in order to understand its performance. For GeoSLAM formulation, the trajectory can describe the position of the sensor during data acquisition and can project raw laser measurements (2D laser profiles or segments) into a registered 3D point cloud when necessary. Data processing is an incremental (the segments are registered one-by-one) and iterative procedure following a framework similar to the iterative closest point (ICP) algorithm:

- The first step identified corresponding surface patches from the laser point cloud. The patches were determined by spatially decomposing the scene into a multiresolution voxel grid, controlled by the "voxel density" parameter; increasing it caused the algorithm to use smaller voxels. Clusters of laser points that were both spatially and temporally proximal were identified and used to compute surface properties based on the centralized second-order matrix of the point coordinates [33]. The surface normal was obtained from the eigenvector corresponding to the minimum eigenvalue of the second-order matrix. The surface planarity, computed from the ratio of the eigenvalues, was used to discard elements that were not approximately planar. These properties were used to establish a first registration of the segments. During this stage, the

following constrains were applied: (i) a filter for retaining only reciprocal correspondences and (ii) several boundary conditions that ensured continuity with the previous segment [33].

- In the second step, the estimated trajectory between two proximal surfaces was refined, minimizing the errors between matching surfaces and deviations from the measured IMU accelerations and rotational velocities. During this process, the following elements were considered into a cost-function (function to be minimized): (i) surface element match errors, (ii) IMU measurement deviations, and (iii) initial condition constraints. It is worth mentioning that the consideration of the IMU measurements ensured the estimated trajectory was smooth. The above terms of the cost-function were non-linear with respect to the rotational correction. Taking this into consideration, the algorithm used a linearization of the system by means of the Taylor expansion.

On the first iteration, the previously unprocessed trajectory segment was initialized by integrating the accelerometer and gyro measurements from the IMU. Since the processing window was advanced by a fraction of its length, the first section of the trajectory segment was already estimated from the previous time step; thus, the IMU data were only required to propagate the trajectory for the remainder of the window. As new data were acquired, the algorithm proceeded by processing a segment of the trajectory whose extremes were represented by positions occupied by the system in two well-defined moments. Next, it advanced the window by a fraction of its length from the previous time step. The dimension of segments was defined by the "window size" parameter. The number of iterations was controlled by the "convergence threshold" parameter; increasing it raised the maximum number of iterations for each processing step and reduced the convergence threshold during the online registration phase.

Considering that the previous process was an incremental procedure (also called open-loop solution) in which each segment was registered with respect to the previous segment, an error accumulation could be produced. In order to minimize the error accumulation, and considering that the data acquisition followed a close-loop path (Figure 3), the GeoSLAM algorithm applied a global registration procedure in which the close-loop restriction was taken into account. During this stage, the algorithm operated along the entire trajectory with one large window, instead of considering the trajectory in small segments (open-loop solution). Eventually, it was possible to give priority to flat surfaces in the search for feature correspondence. Moreover, it is worth mentioning that the laser scanner used by the tested WMLS was a line scanner (Figure 1) (Table 1). This laser was complemented with a rotational engine that allowed us to obtain a 2D profile in each period of time (segment of the scene). All of this was carried out by an operator. The movement of the operator along the scene guaranteed the acquisition of successive segments characterized by a certain overlap that the SLAM algorithm registered, allowing for the creation of the 3D point cloud.

2.2.4. Cartographic Products Generation

The generation of plants and sections required a vectorization of the 3D point cloud obtained from the fusion of the different paths. Thus, the following approach was carried out: (i) the extraction of sections from the 3D point cloud and (ii) the vectorization of the sections.

Regarding vectorization, the most efficient solutions are those that allow semi-automatic feature extraction from point clouds. The least-cost-path algorithms are particularly interesting [38] for our case study, since the automatic solutions are not able to recognize (and possibly not represent) the different objects in the scene and are influenced by the characteristic noise of the point clouds returned with a SLAM approach. Conceptually, a least-cost-path algorithm can be divided into two steps. In the first step, data points are linked with their nearest neighbors using a spherical search radius slightly larger than the point cloud resolution to produce a neighborhood network. A cost function, which represent the effort of moving along points in this network (hereafter referred to as "edges") is estimated. The second step derives the least-cost path between user-defined network points, providing

Remote Sens. **2018**, *10*, 1897

the estimated trace. Once a trace has been estimated, manual adjustments can be easily applied by adding intermediate waypoints and recalculating the relevant least-cost paths.

3. Results

3.1. Case Study: An XV Century Palace

With the aim of evaluating the potentialities and limitations of the WMLS technology, we selected a gothic palace in ruins, located in the urban center of Segovia (Castile and León, Spain), as a case study (Figure 4). The palace was erected in the 15th century as a consequence of the economic expansion experimented by the city, following the precepts of the civil plateresque architecture [39]. Its fronts are made of sandstone masonry and brick masonry. They stand out for their horizontality, showing a ratio height/width of 1/2. With respect to the inner composition, the construction shows the characteristic appearance of the palaces erected during this epoch, with two annular traces in the two first plans and an inner cloister in the center of the construction [39]. These elements are integrated on five levels: (i) basement; (ii) ground floor; (iii) mezzanine; (iv) first floor and; (v) gallery (maybe added during the XIX century), filling an area of about 3000 m^2 and holding more than 50 rooms. The internal courtyard is characterized by a front porch that transfers part of its weight to the masonry and partly to stone columns with granite base (Figure 5).

The construction is mainly made up of sandstone coming from the local quarries. In the lower part (foundations and basement) a masonry in stones connected with mortar prevails, to which a brick masonry and a half-timbered work are replaced, proceeding upwards (Figure 5).

Recent restoration measures have added structural elements in reinforced concrete, such as beams and pillars in order to avoid the collapse of the structure.

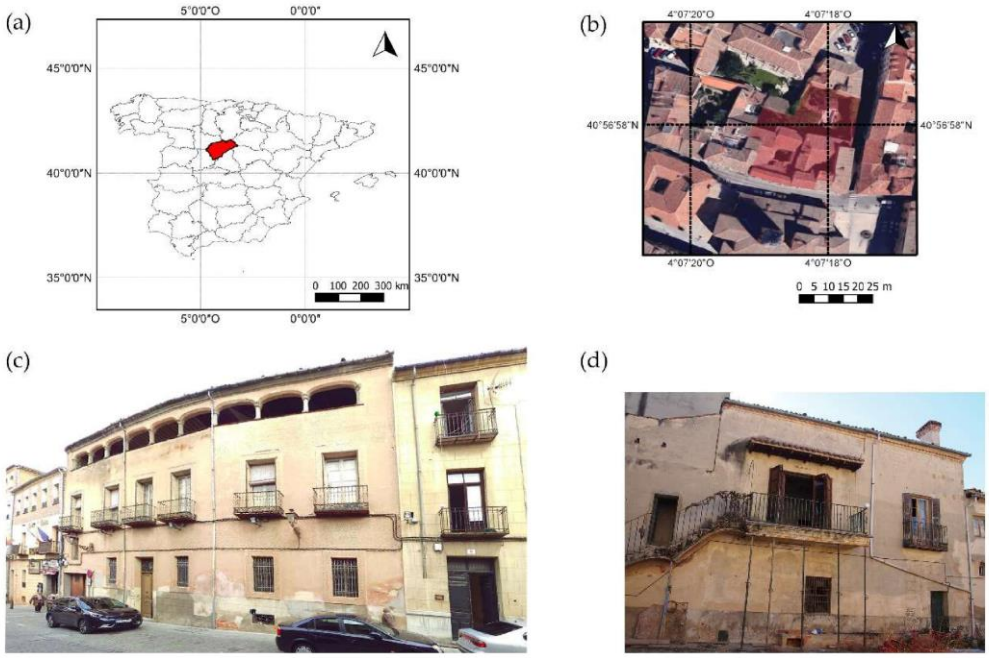

Figure 4. (**a**) Location of the province of Segovia; (**b**) the palace in Segovia; (**c**) main front facade of the palace; (**d**) back front facade of the palace.

Figure 5. Details of the internal cloister.

Timber slabs and open-node (Figure 6) trusses complement these masonry elements. The wooden floors are present both in the simple form, with single beams, and in the form composed of double row of beams and overlapping joists (Figure 7). The secondary frame is made up of a wooden plank in which a conglomerate jet has been made; it is composed of fine aggregates and mortar with a watering function and a thickness of a few centimeters. The finish provides the substrate and the relative flooring.

Figure 6. Gallery; detail of an open-node truss.

Figure 7. Internal cloister; detail of a wooden floor with a double row of beams and overlapping joists.

Nowadays, the state of conservation of the structure is deficient. The infiltration of water and the acid attack promoted by bird excrement have produced the rotting of the wooden elements with the consequent collapse of some floors (Figure 8). Rainfall has also caused the deterioration of sandstone masonry and the detachment of plasters in many environments. The capillary rising of moisture from the foundations has favored saline efflorescence and the appearance of mildew, phenomena accentuated by rainwater. These factors, along with the dust accumulated in the palace's many rooms, make the use of traditional digitalization techniques such as terrestrial photogrammetry or terrestrial laser scanning nearly impossible. These characteristics place the WMLS as the most suitable recording tool due to its flexibility, low weight, and capacity of recording large indoor areas without the support of any position global navigational satellite system (GNSS) [40].

Figure 8. Main cloister; detail of a collapsed wooden floor due to the rotting of the beams.

3.2. Mission Planning

Based on the guidelines previously defined (Sections 2.2.1 and 2.2.2), the surveyed palace was divided into four acquisition paths, each one with a different casuistic found during the digitalization of the heritage buildings (Figure 9):

- path 1 includes interior rooms, the main cloister, and a minimal part of the garden;
- path 2 includes interior rooms, the main cloister, and a part of the garden and a linear gallery;
- path 3 includes interior rooms, the main cloister, and the garden and the street front;
- path 4 includes interior rooms, the main cloister, and a smaller courtyard and the entire garden.

With these premises, the digitization of the internal areas took about 65 min (Table 2). Furthermore, using a terrestrial laser scanner (Faro Focus 3D) with the resolution at 1/5 and the quality at 3x, every scan of the interior took about two and a half minutes. Considering the time needed for the setup of the different stations, a total of 350 min was required for a survey of 70 stations (number compatible with the dimensions of the building), which was six times the period required with the WMLS.

Table 2. General information about the WMLS paths.

Path	Covered Floors	Walked Distance (m)	Acquisition Time (min)	Average Speed (m/s)
1	1	339.80	18.39	0.31
2	4	328.35	17.11	0.32
3	3	426.89	18.47	0.39
4	1	226.70	9.94	0.38

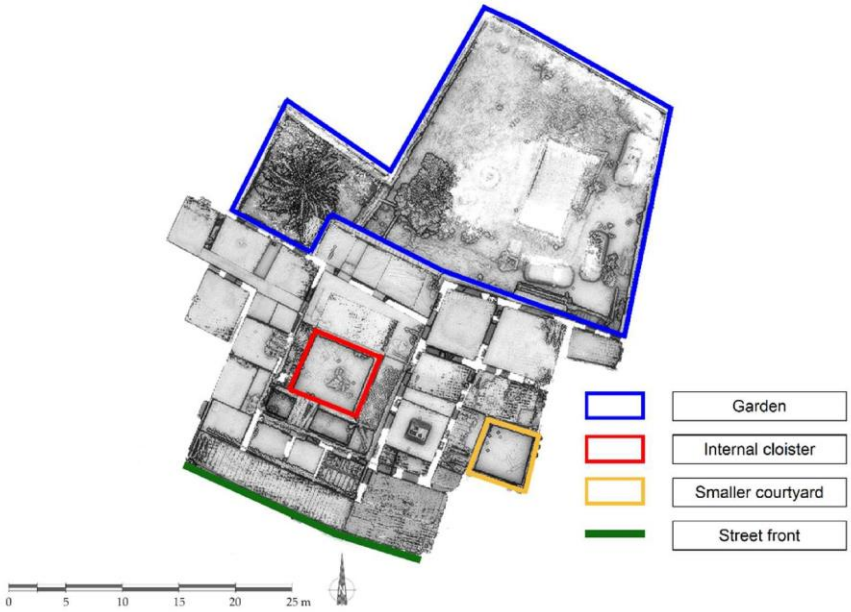

Figure 9. Plan view of the case study.

3.3. Data Processing and Registration

The GeoSLAM algorithm introduced in Section 2.2.3 was controlled by three fundamental parameters:

- The "convergence threshold," which increased or decreased the number of iterations for each processing step during the local and global registration phases. For the case study, a low value of the parameter was chosen, guarantying a quality of data that did not require a large number of iterations;
- the "window size," which defined the size of data samples processed by the algorithm. This helped to encompass the errors that occurred during the local registration phase. An intermediate value for this parameter was a perfect compromise between model quality and required hardware resources;
- the option "prioritize planar surfaces" was used for the case study and considered with very planar surfaces during the global registration phase. This helped to improve the global registration of very large data sets, common in the case of indoor mapping.

This setting guaranteed a processing time of the single path similar to the time required for the detection of the same (Table 3).

Table 3. Processing time of raw data with default setting of full SLAM parameters.

Default Algorithm Configuration		
Path	**Processing Time (min)**	**Difference between Processing and Acquisition time (%)**
1	23.18	≅20
2	23.76	≅21
3	25.31	≅25
4	12.42	≅22

It took approximately 83 min (about five times less time that was required to record the seventy stations needed by the terrestrial laser scanner) to solve the full SLAM problem in the four routes.

In order to perform the alignments between the different paths, a network of artificial targets (spheres) wa distributed around the cloister and on the internal and external facades (Figure 10)

Remote Sens. **2018**, *10*, 1897

(Figure 11). The use of spheres was not mandatory for the execution of the alignment, but this approach made it possible to analyze the registration error between the different paths. The centroids of homologous spheres, extracted by means of the RANSAC Shape Detector algorithm [41] were used as reference pairs. The error associated with the pairs was quantified through the discrepancy in the overall coordinate system between the spatial coordinates of the two homologous centroids (located in two different paths). The root mean square error (RMSE) of the whole registration was just over 3 cm for all the alignment processes achieved (a value perfectly compatible with the WMLS accuracy).

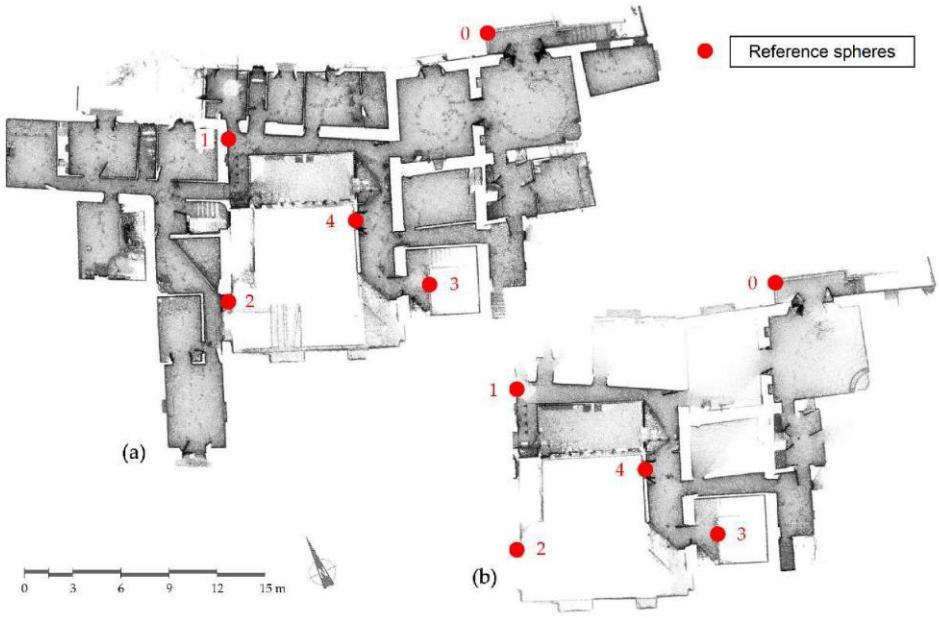

Figure 10. Reference sphere distribution on the first floor for the path 1 (**a**) and path 2 (**b**).

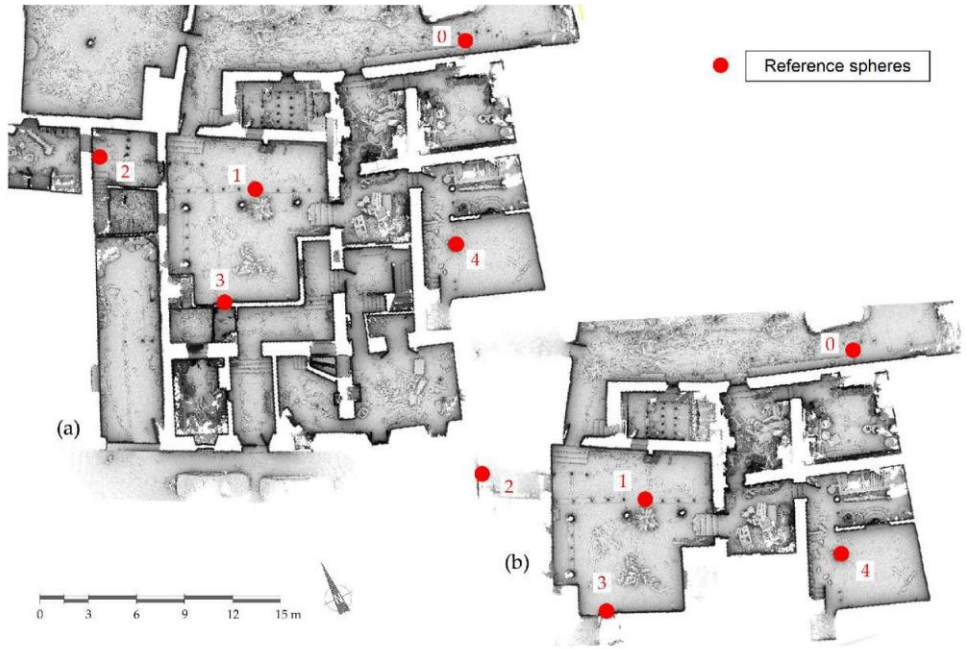

Figure 11. Reference sphere distribution on the ground floor for the path 3 (**a**) and path 4 (**b**).

3.4. System Validation

A further quality control of the acquired data was performed through a comparison with an outdoor network surveyed with a terrestrial laser scanner (Faro Focus 3D, employed for the detection of the front facade, the garden, and the internal cloister). The network consisted of 11 stations acquired with a resolution of 1/2 and a quality of 2x (Figure 12). The scans were aligned using the spherical targets and then an ICP algorithm, in order to create a ground truth.

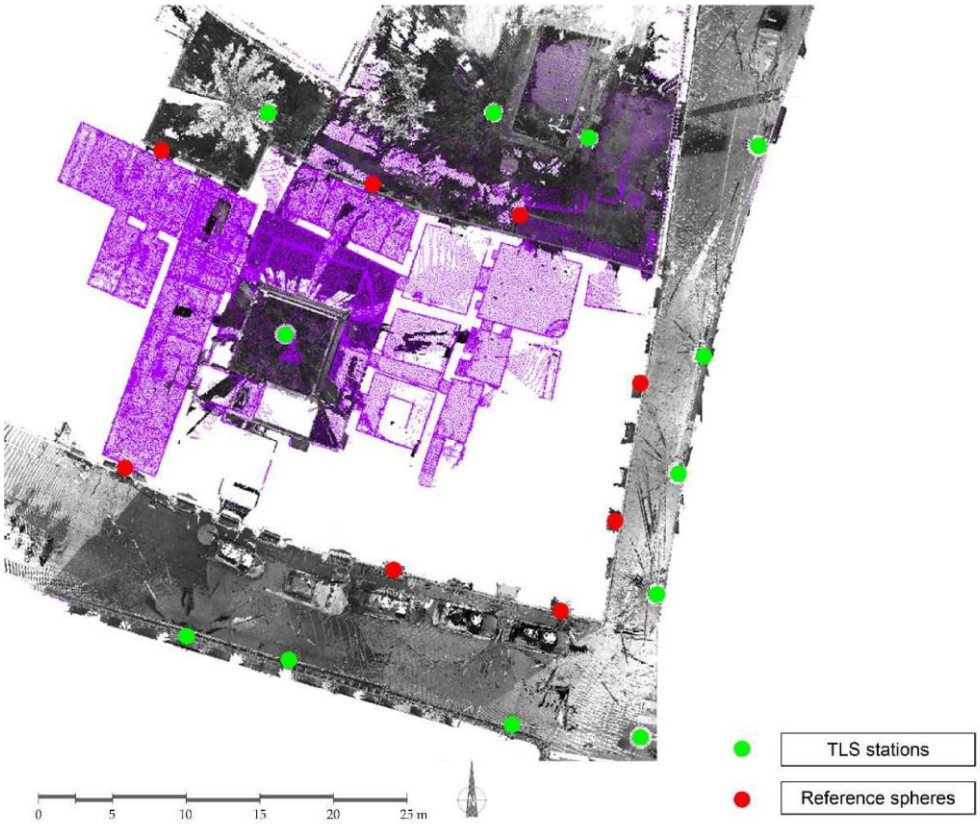

Figure 12. Reference sphere distribution on the first floor for the path 2 (red circles) and the outdoor TLS network (green circles). Scans coming from the terrestrial laser scanner are outlined in the grey color, whereas scans coming from the WMLS for the path 2 are represented in the purple color.

Considering the implemented cartographic products, the following validations were carried out: (i) a local validation and (ii) a global validation. The local validation was a comparison based on fitting flat geometric primitives on homologous point clouds. Some distance measurements were extracted, where each value was the mean of five distance measurements between two planes located on the opposite walls or between the floor and ceiling (Figure 13) (Figure 14). Starting from this data, the system was validated trough the indexes introduced by Nocerino et al. [22] (1) (2):

$$\mathrm{RLME} = \left(\frac{\mathrm{D_{Zm}} - \mathrm{D_{Fm}}}{\mathrm{D_{Fm}}}\right) \times 100 \tag{1}$$

$$\mathrm{RLMA} = 1 : \mathrm{ROUND}\left(\left|\frac{100}{\mathrm{RLME}}\right|\right) = 1 : \mathrm{ROUND}\left(\left|\frac{\mathrm{D_{Fm}}}{\mathrm{D_{Zm}} - \mathrm{D_{Fm}}}\right|\right) \tag{2}$$

The relative measurement error (RLME) was computed as the relative difference between measured distance $\mathrm{D_Z}$ for the GeoSLAM ZEB-REVO and the distance for the Faro Focus 3D, assumed

Remote Sens. **2018**, *10*, 1897

as reference length D_F. The relative length measurement accuracy (RLMA) was defined as the rounded absolute reciprocal value of the RLME times 100. Table 4 reports the results.

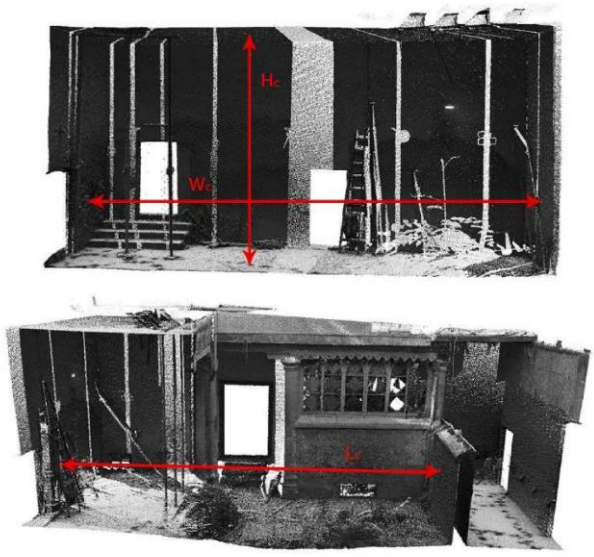

Figure 13. Distances measured for the accuracy evaluation.

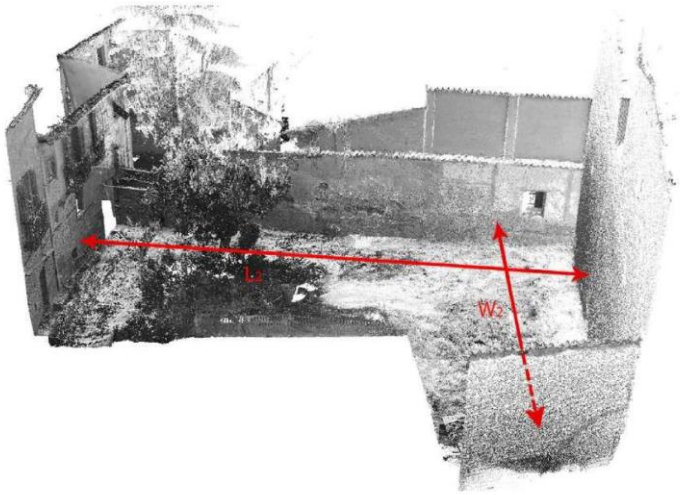

Figure 14. Distances measured for the accuracy evaluation.

Table 4. Measured distances with standard deviations (σ), relative length measurement errors (RMLE) and accuracies (RMLA).

		Faro Focus 3D		GeoSLAM ZEB-REVO			
		D_{Fm} (m)	σ (m)	D_{Zm} (m)	σ (m)	RLME	RLMA
Main cloister	L_1	10.279	0.008	10.268	0.010	−0.107	≈1:1000
	W_1	10.096	0.013	10.085	0.022	−0.109	≈1:600
	H_1	4.869	0.014	4.869	0.012	0.001	≈1:7000
Garden	L_2	22.730	0.012	22.756	0.011	0.114	≈1:800
	W_2	18.766	0.023	18.787	0.025	0.112	≈1:900

In the case of the main garden, the RLME assumed a slightly greater value than the main cloister. This was due to two factors: in the case of a SLAM system, the greater probability of error accumulation over longer distances (L_2 and W_2) and the decline in performance of the latter with outdoor acquisitions (being designed for indoor surveys). The global validation was carried out by comparing the centroids of the sphere network captured by both systems (Figure 12), with an approach similar to the one defined in Section 3.3. The RMSE obtained was around 3 cm, which was in line with the accuracy of the proposed method. In both the validation approaches, the accuracy of the WMLS was between 1 and 3 cm, which was compatible with the data provided by the manufacturer [34].

3.5. Plan and Section Restitution

The post-processing returns 3D point clouds, characterized by the number of points (and therefore of bytes required for its archiving), was not suited for the vectorization of two-dimensional products. Moreover, their density was not uniform, since it was related to the traveling speed along the paths and the overlapping of some parts of the clouds in the registration phase. Table 5 provides a schematic summary of the magnitude and mean surface density values for each point cloud. As can be seen from the comparison with Table 2, an increase in average speed corresponded to a decrease in the mean surface density.

Table 5. Point cloud features; the surface density is estimated by counting for each point the number of neighbors inside a sphere of three centimeters radius (R) and dividing this value by the sphere max section (πR^2).

Path	Number of Points	Mean Surface Density (points/m^2)	Number of Points after 1 cm Subsampling	Mean Surface Density after 1 cm Subsampling (points/m^2)
1	32,955,139	29,648	14,056,546	6140
2	30,059,713	28,399	14,032,348	5594
3	33,839,213	20,428	16,766,690	5348
4	16,720,282	18,488	9,210,536	4634

In order to generate plans and sections, a subsampling strategy based on distance (1 cm) was applied without producing any loss of detail that would compromise the quality of the products. As a result, a 3D point cloud with more than a 100 million points was obtained for the whole historical palace (Figure 15).

The final step involved tracing the two-dimensional products. To do this, several sections along the different floors of the building were extracted. Previously, in the application of the least-cost-path algorithm, a low pass filter was applied [42]. This strategy locally fit a plane around each point of the cloud and then removed those points far from the fitted plane (Figure 16a). For the present case study, the following parameters were used: (i) a neighbored search radius of 0.03 m and (ii) a relative error of 1 sigma for the exclusion of the points. Next, we applied the filtered point cloud using the least-cost-path algorithm, which allowed for the automatic vectorization of the plant (Figure 16b). Finally, some manual adjustments were conducted on the obtained vectorization data, allowing for the creation of plans in a quick and accurate way (Figure 17).

Remote Sens. **2018**, *10*, 1897

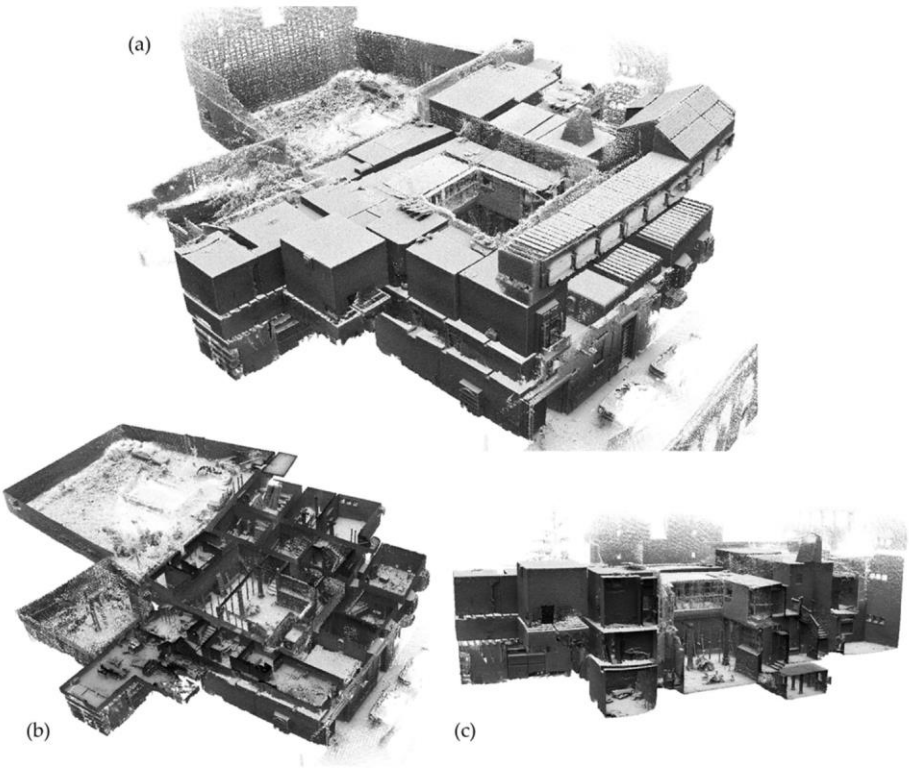

Figure 15. Final point cloud with more than a 100 million points: (**a**) perspective view; (**b**) horizontal section; (**c**) vertical section.

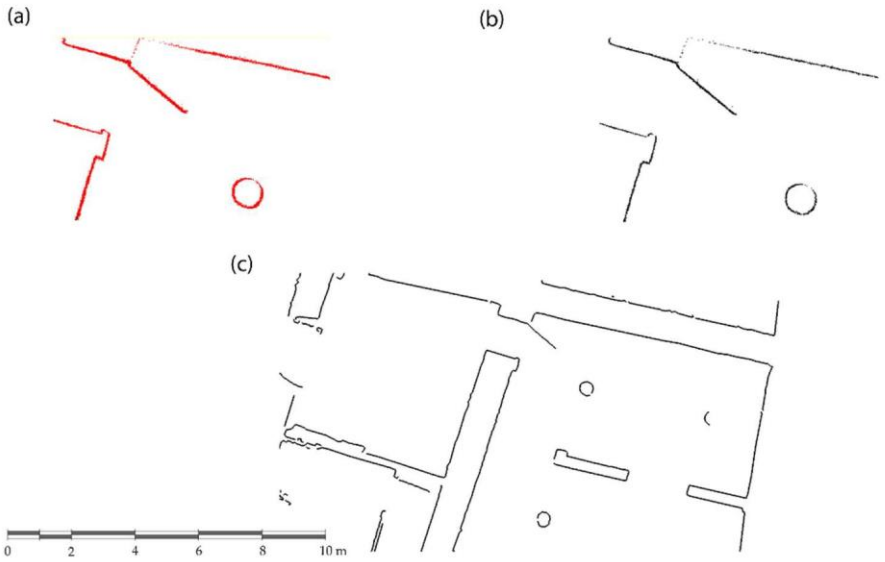

Figure 16. Detail of the vectorization process: (**a**) section extracted from the point cloud; (**b**) section filtered; (**c**) application of the least-cost-algorithm over the filtered section.

Figure 17. Ground floor plan and first floor plan.

4. Discussion

Based on the obtained results, as well as its proven its efficiency, accuracy, portability, and weight, it can be seen that the WMLS tested in our case study offers a potential solution for mapping complex cultural heritage sites.

Regarding the efficiency, the WMLS needed just 63 min to capture the data (distributed in a total of four paths) and 83 min to solve the SLAM problem. In both cases, the system outperformed the time estimated for a terrestrial laser scanner to digitalize the same construction (around 70 scan stations). In comparison with other state-of-the-art MMS, such as the Leica Pegasus back-pack or the Heron MS-2 back-pack, the proposed WMLS solution had a lower data acquisition rate (43,000 points per second against 600,000 points per second captured by the Leica Pegasus back-pack and 700,000 points per second captured by the Heron system). The WMLS capture rate is suitable in terms of its density, capacity to detect geometrical features, and for its ability to map indoor cultural heritage environments.

Regarding the accuracy, the point cloud returned by the WMLS guaranteed an accuracy within a centimeter in relation to the point cloud obtained by a terrestrial laser scanner. These values were similar to those obtained by Nocerino et al. [22] for indoor environments and those obtained by Cabo et al. [43] in an outdoor environment with many geometrical features. This accuracy seems to be linked with the number of geometrical features present in the scene, as well as the planning of the data acquisition using several close-loops.

Concerning the portability, the tested sensor had approximately 4 kg of weight and small dimensions (220 × 180 × 470 mm) (Table 1) in comparison with other MMS, such as the Leica Pegasus backpack, with an estimated weight of 12 kg and dimensions of 310 mm × 270 mm × 730 mm, the Heron MS-2 back-pack mapping solution, with a total weight of 11 kg, and the NavVIS 3D system, which requires a cart to support its sensors [22,24,44]. These characteristics are especially relevant for the digitalization of the palace, since this building shows narrow areas (Figure 8) in which the other MMS would have problems.

5. Conclusions

In this paper, a wearable mobile laser system (WMLS) has been presented and tested for the digitalization of a complex cultural heritage building. This device highlights for its lightweight,

flexibility in comparison with other traditional techniques, such as terrestrial photogrammetry or terrestrial laser scanning. The combination of this instrument, mainly composed by a 2D Hokuyo laser scanner and an Inertial Measurement Unit, together with the Simultaneous Location and Mapping approach, allows the acquisition of indoor environments dynamically without the necessity of stations or the use of global navigation satellite systems.

Investigation results estimate that the WMLS requires the complete digitalization of the entire structure, with around 3000 m^2, in about 65 min. A quick comparison demonstrates how the acquisition time of the wearable system is approximately equal to the sixth part of the time required by the terrestrial laser scanner (Faro Focus 3D), providing the correct accuracy and density of data for the creation of sections and plans for restoration projects. The post-processing phase itself is around five times shorter than the corresponding registration of the laser scans.

The process of registering the different paths, which uses spherical target centroids as control points, returns a RMSE of about 3 cm, compatible with the accuracy of the analyzed system, and is able to offer excellent results in complex environments, such as the one described in this paper. These potentialities are also confirmed by the comparison with an external network generated by a terrestrial laser scanner. During this stage, the accuracy of the system has been evaluated at two different scales: (i) at the local scale using the relative length measurement error (RLME) and the relative length measurement accuracy (RLMA), and (ii) at the global scale, where the root mean square error (RMSE) between the centroids detected by each system, WMLS and laser scanner, have been confronted. In both cases the accuracy of the system is estimated between 1 and 3 cm.

Future investigations could concern the integration of the point clouds generated by the WMLS into building information modelling (BIM) systems. Another future development could concern the process of coloring automatically the point cloud of WMLS by synchronizing the acquisition path with video captured by GoPro and the subsequent projection of the frames on the cloud itself.

Author Contributions: All authors conceived and designed the experimental campaign; A.d.F., L.J.S.-A., and D.G.A. performed the experimental campaign; A.d.F., L.J.S.-A., J.A.M.-J., and R.M. performed the pre-processing and post-processing steps; A.d.F., L.J.S.-A., and S.B. wrote the article and all authors read and approved the final version.

Funding: The authors wish to thank HERGONSA S.L. for the access and the economic support to develop this case study.

Acknowledgments: Authors wish to thank the V SUDOE INTERREG for providing the framework of the HeritageCARE project, Ref. SOE1/P5/P0258. This work has also been framed in the research project Patrimonio 5.0 by Junta of Castilla y León, Ref SA075P17.

Conflicts of Interest: the authors declare no conflict of interest.

References

1. Krakow Charter 2000: Principles for Conservation and Restoration of Built Heritage. Available online: http://hdl.handle.net/1854/LU-128776 (accessed on 20 September 2018).
2. Torres-Martínez, J.A.; Seddaiu, M.; Rodríguez-Gonzálvez, P.; Hernández-López, D.; González-Aguilera, D. A multi-data source and multi-sensor approach for the 3D reconstruction and web visualization of a complex archaelogical site: The case study of "Tolmo De Minateda". *Remote Sens.* **2016**, *8*, 550. [CrossRef]
3. Garcia-Gago, J.; Gomez-Lahoz, J.; Rodríguez-Méndez, J.; González-Aguilera, D. Historical single image-based modeling: The case of Gobierna Tower, Zamora (Spain). *Remote Sens.* **2014**, *6*, 1085–1101. [CrossRef]
4. Waldhäusl, P.; Ogleby, C. 3 × 3 rules for simple photogrammetric documentation of architecture. In *International Archives of Photogrammetry and Remote Sensing, Proceedings of the Close Range Techniques and Machine Vision, Melbourne, Australia, 1–4 March 1994*; Australian Photogrammetric and Remote Sensing Society: Melbourne, VIC, Australia, 1994.
5. Barber, D.; Mills, J. *3D Laser Scanning for Heritage: Advice and Guidance to Users on Laser Scanning in Archaeology and Architecture*; Historic England: Swindon, UK, 2007, ISBN 978-1848025219.
6. Kraus, K.; Waldhäusl, P. *Photogrammetry: Fundamentals and Standard Processes*; Dümmler Köln: Munich, Germany, 1993, ISBN 978-3427786849.

7. Fabio, R.; Sabry, E.H. Image-based 3D Modelling: A Review. *Photogramm. Rec.* **2006**, *21*, 269–291. [CrossRef]
8. Blais, F. Review of 20 years of range sensor development. *J. Electron. Imaging* **2004**, *1*, 13. [CrossRef]
9. Guidi, G.; Russo, M.; Beraldin, J.-A. *Acquisizione 3D e Modellazione Poligonale*; McGraw-Hill: New York, NY, USA, 2010, ISBN 978-8838665318.
10. Kalay, Y.; Kvan, T.; Affleck, J. *New Heritage: New Media and Cultural Heritage*, 1st ed.; Routledge: London, UK, 2007, ISBN 978-0415773560.
11. Torres-Martínez, J.A.; Sánchez-Aparicio, L.J.; Hernández-López, D.; González-Aguilera, D. Combining geometrical and radiometrical features in the evaluation of rock art paintings. *Digital Appl. Archaeol. Cult. Herit.* **2017**, *5*, 10–20. [CrossRef]
12. Gonzalez-Aguilera, D.; Muñoz-Nieto, A.; Rodriguez-Gonzalvez, P.; Menéndez, M. New tools for rock art modelling: Automated sensor integration in Pindal Cave. *J. Archaeol. Sci.* **2011**, *38*, 120–128. [CrossRef]
13. Sánchez-Aparicio, L.J.; Riveiro, B.; Gonzalez-Aguilera, D.; Ramos, L.F. The combination of geomatic approaches and operational modal analysis to improve calibration of finite element models: A case of study in Saint Torcato Church (Guimarães, Portugal). *Constr. Build. Mater.* **2014**, *70*, 118–129. [CrossRef]
14. Sánchez-Aparicio, L.J.; Del Pozo, S.; Ramos, L.F.; Arce, A.; Fernandes, F.M. Heritage site preservation with combined radiometric and geometric analysis of TLS data. *Autom. Constr.* **2018**, *85*, 24–39. [CrossRef]
15. Del Pozo, S.; Herrero-Pascual, J.; Felipe-García, B.; Hernández-López, D.; Rodríguez-Gonzálvez, P.; González-Aguilera, D. Multispectral radiometric analysis of façades to detect pathologies from active and passive remote sensing. *Remote Sens.* **2016**, *8*, 80. [CrossRef]
16. Guidi, G.; Beraldin, J.-A.; Ciofi, S.; Atzeni, C. Fusion of range camera and photogrammetry: A systematic procedure for improving 3-D models metric accuracy. *IEEE Trans. Syst. Man Cybern. B* **2003**, *33*, 667–676. [CrossRef] [PubMed]
17. Stumpfel, J.; Tchou, C.; Yun, N.; Martinez, P.; Hawkins, T.; Jones, A.; Emerson, B.; Debevec, P.E. Digital Reunification of the Parthenon and its Sculptures. In Proceedings of the VAST, Brighton, UK, 5–7 November 2003; pp. 41–50.
18. Paparoditis, N.; Papelard, J.-P.; Cannelle, B.; Devaux, A.; Soheilian, B.; David, N.; Houzay, E. Stereopolis II: A multi-purpose and multi-sensor 3D mobile mapping system for street visualisation and 3D metrology. *Rev. Fr. Photogramm. Teledetec.* **2012**, *200*, 69–79.
19. Remondino, F.; Toschi, I.; Orlandini, S. Mobyle Mapping Systems: Recenti sviluppi e caso applicativo. *GEOmedia* **2015**, *19*, 6–10.
20. Al-Hamad, A.; El-Sheimy, N. Smartphones based mobile mapping systems. *Int. Arch. Photogramm. Remote Sens. Spat. Inf. Sci.* **2014**, *40*, 29. [CrossRef]
21. Piras, M.; Di Pietra, V.; Visintini, D. 3D modeling of industrial heritage building using COTSs system: Test, limits and performances. *Int. Arch. Photogramm. Remote Sens. Spat. Inf. Sci.* **2017**, *42*, 281. [CrossRef]
22. Nocerino, E.; Menna, F.; Remondino, F.; Toschi, I.; Rodríguez-Gonzálvez, P. Investigation of indoor and outdoor performance of two portable mobile mapping systems. In *Videometrics, Range Imaging, and Applications XIV*; International Society for Optics and Photonics: Munich, Germany, 2017.
23. Kumar, G.A.; Patil, A.K.; Patil, R.; Park, S.S.; Chai, Y.H. A lidar and imu integrated indoor navigation system for uavs and its application in real-time pipeline classification. *Sensors* **2017**, *17*, 1268. [CrossRef] [PubMed]
24. Lehtola, V.V.; Kaartinen, H.; Nüchter, A.; Kaijaluoto, R.; Kukko, A.; Litkey, P.; Honkavaara, E.; Rosnell, T.; Vaaja, M.T.; Virtanen, J.-P. Comparison of the selected state-of-the-art 3d indoor scanning and point cloud generation methods. *Remote Sens.* **2017**, *9*, 796. [CrossRef]
25. Flener, C.; Vaaja, M.; Jaakkola, A.; Krooks, A.; Kaartinen, H.; Kukko, A.; Kasvi, E.; Hyyppä, H.; Hyyppä, J.; Alho, P. Seamless mapping of river channels at high resolution using mobile lidar and uav-photography. *Remote Sens.* **2013**, *5*, 6382–6407. [CrossRef]
26. Opromolla, R.; Fasano, G.; Rufino, G.; Grassi, M.; Savvaris, A. LiDAR-inertial integration of UAV localization and mapping in complex enviroments. In Proceedings of the 2016 International Conference on Unmanned Aircraft Systems (ICUAS), Arlington, VA, USA, 7–10 June 2016.
27. Niu, X.; Yu, T.; Tang, J.; Chang, L. An online solution of lidar scan matching aided inertial navigation system for indoor mobile mapping. *Mob. Inf. Syst.* **2017**, *2017*, 4802159. [CrossRef]
28. Shamseldin, T.; Manerikar, A.; Elbahnasawy, M.; Habib, A. SLAM-based Pseudo-GNSS/INS Localization System for Indoor LiDAR Mobile Mapping Systems. In Proceedings of the IEEE/OIN PLANS 2018, Monterey, CA, USA, 23–26 April 2018.

29. Pierzchała, M.; Giguère, P.; Astrup, R. Mapping forests using an unmanned ground vehicle with 3D LIDAR and graph-SLAM. *Comput. Electron. Agric.* **2018**, *145*, 217–225. [CrossRef]
30. Lagüela, S.; Dorado, I.; Gesto, M.; Arias, P.; González-Aguilera, D.; Lorenzo, H. Behavior analysis of novel wearable indoor mapping system based on 3d-slam. *Sensors* **2018**, *18*, 766. [CrossRef] [PubMed]
31. Farella, E. 3d mapping of underground environments with a hand-held laser scanner. In Proceedings of the SIFET Annual Conference, Lecce, Italy, 8–10 June 2016.
32. Thrun, S. Simultaneous localization and mapping. In *Robotics and Cognitive Approaches to Spatial Mapping*; Jefferies, M.E., Yeap, W., Eds.; Springer: Luxembourg, 2008; pp. 13–41, ISBN 978-3-540-75388-9.
33. Bosse, M.; Zlot, R.; Flick, P. Zebedee: Design of a spring-mounted 3-d range sensor with application to mobile mapping. *IEEE Trans. Robot.* **2012**, *28*, 1104–1119. [CrossRef]
34. GeoSLAM Technology, ZEB-REVO Solution Brochure. Available online: https://gpserv.com/wp-content/uploads/2017/01/ZEB-REVO-Brochure-v1.0.3.pdf (accessed on 15 August 2018).
35. Quigley, M.; Conley, K.; Gerkey, B.; Faust, J.; Foote, T.; Leibs, J.; Wheeler, R.; Ng, A.Y. ROS: An open-source Robot Operating System. In Proceedings of the ICRA Workshop on Open Source Software, Kobe, Japan, 12–17 May 2009; p. 5.
36. Kavanagh, B.F. *Surveying Principles and Applications*, 7th ed.; Pearson Education: Upper Saddle River, NJ, USA, 2006, ISBN 978-0137009404.
37. Grisetti, G.; Kummerle, R.; Stachniss, C.; Burgard, W. A tutorial on graph-based SLAM. *IEEE Intell. Transp. Syst. Mag.* **2010**, *2*, 31–43. [CrossRef]
38. Thiele, S.T.; Grose, L.; Samsu, A.; Micklethwaite, S.; Vollgger, S.A.; Cruden, A.R. Rapid, semi-automatic fracture and contact mapping for point clouds, images and geophysical data. *Solid Earth* **2017**, *8*, 1241. [CrossRef]
39. Navarro, P.C. The Royal Country Estates around the Monastery of El Escorial: Medieval Tradition and Flemish Influence. *Rev. EGA* **2014**, 46–53. [CrossRef]
40. Misra, P.; Enge, P. *Global Positioning System: Signals, Measurements and Performance*, 2nd ed.; Ganga-Jamuna Press: Lincoln, MA, USA, 2010, ISBN 9780970954428.
41. Schnabel, R.; Wahl, R.; Klein, R. Efficient RANSAC for point-cloud shape detection. In *Computer Graphics Forum*; Blackwell Publishing Ltd.: Oxford, UK, 2007; pp. 214–226.
42. Han, X.-F.; Jin, J.S.; Wang, M.-J.; Jiang, W.; Gao, L.; Xiao, L. A review of algorithms for filtering the 3D point cloud. *Signal Process. Image Commun.* **2017**, *57*, 103–112. [CrossRef]
43. Cabo, C.; Del Pozo, S.; Rodríguez-Gonzálvez, P.; Ordóñez, C.; González-Aguilera, D. Comparing Terrestrial Laser Scanning (TLS) and Wearable Laser Scanning (WLS) for individual Tree Modeling at Plot Level. *Remote Sens.* **2018**, *10*, 540. [CrossRef]
44. Heron Wearable Mobile Mapping. Available online: https://gexcel.it/en/solutions/heron-mobile-mapping (accessed on 18 November 2018).

2.2. Sistema de escaneado móvil: dron terrestre con TLS

En esta sección se exponen los resultados de investigación alcanzados en el artículo titulado "*Automatic Point-Cloud Registration for Quality control in Building Works*" publicado en la revista científica *Applied Sciences* de MDPI en 2021.

Resumen

Si bien en el primer artículo se vio que los sistemas de escaneado móvil portables como el WMLS son soluciones aptas, cómodas y rápidas para el modelado y posterior parametrización de edificios, la densidad y precisión de los datos arrojados es inferior a la ofrecida por los TLS estáticos. Con el objetivo de superar esta limitación, se opta por desarrollar una plataforma y metodología intermedia, entre los TLS estáticos y los sistemas WMLS: un sistema Stop & Go. Para tal fin se integra un TLS estático en un dron terrestre, complementado con un planificador de rutas que permite que el dron opere sin supervisión. La captura de datos se realiza mediante técnicas Stop & Go, es decir el láser comienza a funcionar cuando el dron está parado en un punto de estación y cuando el escaneo termina el láser se apaga y el dron continúa hasta el siguiente punto de estación. La validación de esta metodología se realizó en un edificio en construcción en Badalona, Barcelona (España). Dicho edificio se encontraba en diferentes estados constructivos y se realizaron capturas de datos en varias plantas del mismo, con el fin de comprobar la viabilidad del sistema para realizar tareas de control de diferentes elementos constructivos.

Los objetivos de esta investigación son cuatro: i) comprobar la viabilidad del uso de sistemas TLS como sistemas de escaneado móvil, combinando las tecnologías de escaneado láser con los drones, ii) desarrollar un protocolo de captura de datos óptimo para estos dispositivos, iii) desarrollar una metodología de tratamiento de los datos que optimice los resultados y los tiempos computacionales, y iv) comprobar la calidad de los modelos obtenidos y su aplicabilidad a control de obras.

El trabajo se desarrolla en las diferentes fases que se exponen a continuación:

- Digitalización del escenario mediante el uso del sistema de escaneado móvil compuesto de TLS y dron terrestre. En esta fase se explica el sistema de captura de datos y sus diferentes componentes, prestando una atención especial al planificador de rutas, pues es el elemento que hace posible que todo el sistema opere de manera autónoma, sin necesidad de un usuario. Dicho planificador toma como dato de entrada el plano en planta de la superficie a escanear junto con los parámetros de calidad exigidos, generando de forma automática la ruta óptima teórica a seguir por el dron, así como el número de estaciones de escaneo. Además, el sistema cuenta con sensores de detección de huecos y obstáculos incorporados, lo que permite evitar colisiones y accidentes en tiempo real. Así, el planificador de rutas es capaz de actualizar la ruta calculada si los sensores detectan un obstáculo en ella.
- Procesado de los datos obtenidos. Una vez que se tienen los datos adquiridos, se aborda su tratamiento, centrándose en dos procesos: (i) el filtrado de puntos no necesarios y (ii) el alineamiento automático de todas las tomas realizadas. El filtrado de puntos se

realiza mediante dos técnicas: primero se aplica el algoritmo FSOR que elimina el ruido y los puntos erróneos de manera eficaz, y posteriormente se aplica un filtro passthrough basado en el histograma de la nube de puntos. Con ello se consigue aislar los puntos no pertenecientes a la zona de estudio y eliminar aquellos puntos lejanos que pudieran haberse medido por estar al alcance el láser. El alineamiento automático de las nubes de puntos se basa en la aplicación de detectores y descriptores 3D junto con una solución iterativa del tipo ICP. En el trabajo se hace un repaso del estado del arte de los diferentes algoritmos y combinaciones de algoritmos que se utilizan más habitualmente y se presenta la metodología desarrollada, consistente en utilizar el detector Harris 3D y el descriptor PFH para calcular la aproximación inicial y luego realizar el alineamiento fino mediante el algoritmo ICP. Esta combinación aporta los mejores resultados y es apta para escenarios de interior o exterior, no necesitando elementos de puntería artificiales en la escena ni intervención alguna por parte del usuario.

- Validación del sistema y método propuestos: En esta parte se exponen los métodos utilizados para validar la metodología y comprobar la calidad de los datos obtenidos. Dicha validación se llevó a cabo de dos maneras: i) realizando una comparativa del modelo completo alineado con el modelo BIM que se toma como referencia, y ii) realizando medidas de elementos constructivos, como los pilares, sobre la nube TLS generada y comparando con los valores teóricos. Para la primera forma de validación, se colocaron la nube de puntos TLS y el modelo BIM en el mismo sistema de coordenadas y se utilizaron estimadores no paramétricos (ej. mediana y la desviación absoluta de la mediana normalizada, NMAD) para comprobar los errores entre ambos modelos, resultando que el error estaba por debajo del centímetro. Para el segundo control de calidad, se escogieron varios pilares de la obra y se realizaron medidas del ancho y el largo de los mismos (cada medida se repitió cinco veces y se consideró como medida final, la media aritmética de esas cinco medidas). Estas medidas se compararon con las medidas teóricas y se realizaron estimaciones robustas con estimadores no paramétricos (mediana y NMAD), con los que se concluyó que el error de todas las medidas estaba por debajo del centímetro, siendo errores admisibles para realizar controles de calidad en obras.

Como resultado de esta investigación se obtuvieron varias conclusiones: i) el método desarrollado es válido para realizar control de calidad de obras, en especial en aquellas fases que requieren una precisión milimétrica, ii) el método de procesado básico desarrollado consistente en el filtrado, homogeneización y alineamiento de las nubes de puntos, proporciona resultados fiables y precisos y iii) el sistema desarrollado proporciona un marco de trabajo y una guía de buenas prácticas para la digitalización de escenarios con un sistema de escaneo TLS embarcado en un dron terrestre, siempre que esté provisto de un planificador de rutas y opere con el método Stop & Go.

applied sciences

MDPI

Article

Automatic Point-Cloud Registration for Quality Control in Building Works

Rocio Mora, Jose Antonio Martín-Jiménez, Susana Lagüela and Diego González-Aguilera *

Department of Cartographic and Land Engineering, Higher Polytechnic School of Avila, University of Salamanca, Hornos Caleros 50, 05003 Ávila, Spain; rociomora@usal.es (R.M.); joseabula@usal.es (J.A.M.-J.); sulaguela@usal.es (S.L.)

* Correspondence: daguilera@usal.es; Tel.: +34-920353505 (ext. 3820)

Abstract: Total and automatic digitalization of indoor spaces in 3D implies a great advance in building maintenance and construction tasks, which currently require visits and manual works. Terrestrial laser scanners (TLS) have been widely used for these tasks, although the acquisition methodology with TLS systems is time consuming, and each point cloud is acquired in a different coordinate system, so the user has to post-process the data to clean and get a unique point cloud of the whole scenario. This paper presents a solution for the automatic data acquisition and registration of point clouds from indoor scenes, designed for point clouds acquired with a terrestrial laser scanner (TLS) mounted on an unmanned ground vehicle (UGV). The methodology developed allows the generation of one complete dense 3D point cloud consisting of the acquired point clouds registered in the same coordinate system, reaching an accuracy below 1 cm in section dimensions and below 1.5 cm in walls thickness, which makes it valid for quality control in building works. Two different study cases corresponding to building works were chosen for the validation of the method, showing the applicability of the methodology developed for tasks related to the control of the evolution of the construction.

Keywords: unmanned ground vehicle; terrestrial laser scanner; point cloud registration; indoor mapping; as-built models; building works; quality control; software development

Citation: Mora, R.; Martín-Jiménez, J.A.; Lagüela, S.; González-Aguilera, D. Automatic Point-Cloud Registration for Quality Control in Building Works. *Appl. Sci.* **2021**, *11*, 1465. https://doi.org/10.3390/app11041465

Academic Editor: Paraskevi Nomikou
Received: 24 December 2020
Accepted: 3 February 2021
Published: 5 February 2021

1. Introduction

The demand for 3D models of building interiors has grown in the recent years due to (1) the need to have as-built 3D models available for tasks related to planning and maintenance in buildings and (2) the proliferation of the building information modelling (BIM) standard [1–4]. The most common techniques for the generation of 3D models have been photogrammetry [5–7] and laser scanning [8,9]. Regarding the first, evolution has come with advances in computer vision and structure-from-motion techniques. These made possible the computation of the orientation and self-calibration parameters of a high number of images regardless the a priori knowledge of position and orientation. However, aspects such as presence of homogeneous surfaces (i.e., textureless), changes in illumination, the need to scale the model and the computational cost have been the main drawbacks when generating quality 3D models in indoor scenes with photogrammetry. With respect to the second technique, terrestrial laser scanners (TLS) allow the generation of high-precision 3D models [10–13], but the acquisition requires meticulous planning, together with a high number of acquisition sets, and the application of an efficient registration technique to join all the point clouds acquired in the same point cloud, within a unique coordinate system. This issue has been studied several times in the last years and several solutions have been developed. Table 1 shows a comparison between different approaches attending to five different aspects: (i) the need of artificial targets, (ii) the need of RGB images, (iii) the number of point clouds that can be aligned with each method (i.e., only two point clouds or several point clouds), (iv) the minimum overlap between scans and v) the sensitivity to

noise. For example, [14] developed a fully automatic registration method of point clouds using special targets attached to the objects. The algorithm searches the specific templates of these targets using radiometric and geometric information (shape, size and planarity) and evaluates invariant parameters between each scan to calculate the registration. Although this method works, it depends on the placement of artificial targets in the scene. Placing targets is not always possible, and it requires previous works and detailed studies of the environment. Other studies have evaluated the registration using shape patterns between scans, such as planes [15]. This way, two point clouds are coarsely aligned using plane extraction to find tie points. This method is time-consuming and works only for pairs of point clouds, not being directly applicable to a set of scans. [16] implemented a registration method between scans based on linear and planar shapes to find homologous points and apply a coarse alignment. In [17], 2D images were used in combination with 3D models to improve point clouds registration. Two-dimensional images are used to add texture to the point clouds and to provide information about common features through their search with the SURF descriptor. With this, the matrix transformation is created and refined with different strategies such as RANSAC. This method reaches sufficient results only when the overlap between scans is good. To solve this problem, [18] presented a novel methodology to register outdoor and indoor point clouds using a two-step process: first, they extracted common features using the RGB information acquired by a digital camera and then they refined the alignment using iterative closest points (ICP) or planes matching techniques, that work properly even when the overlap between scans is poor. Both methods are robust and suitable for indoor and outdoor scenarios, but a hybrid calibrated system composed by an RGB camera and a laser scanner is mandatory. Moreover, both methods are based on the use of RGB images and textures, so it is not applicable for scans without that information. A fully image-based methodology was proposed by [19]. In this work, a four-step process is performed: (1) creation of a scan network; (2) coarse alignment; (3) filtering outliers and (4) fine alignment based on the minimum loop expansion (MLE) method. The authors use panoramic images associated to each scan to identify common features between them, so it is not possible to use this methodology for scans without these images or textures. In a similar line, [20] proposed a methodology to organise the scans in a network based on the correspondences detected between pairs of scans. Once the scans are connected, a coarse registration is applied and finally a fine registration performs the alignment process. Although the process is effective, the accuracies achieved are between 9 and 32 mm, values similar to those currently achieved with mobile laser scanner (MLS) systems.

Table 1. Comparison between different registration approaches, including our proposed method.

	Target Based [14]	Plane Based [15,16]	Image Based [17]	Image Based + Network [18–20]	Proposed Method
Target Need	X				
Image Need			X	X	
Only Pairwise Registration		X	X		
Minimum Overlap Required	X	X	X	X	X
Noise Sensitive	X	X	X	X	X

MLS allow the generation of 3D models in a unique acquisition, with the direct result of a single point cloud, consequently with one coordinate system [21,22]. However, the guarantee of metric quality of the 3D models depends on the knowledge of the trajectory of the MLS, which is a complicated task in indoor scenes due to the low coverage of the GNSS signal. Simultaneous localization and mapping (SLAM) techniques are an efficient alternative for the computation of the trajectory but do not guarantee the precision required in applications such as quality control during construction works. The reason is that most MLS systems are equipped with low-cost and lower performance laser devices in order to cope with the weight requirements [23], such as Velodyne HDL-32 or Hokuyo UTM in Zeb-Revo system, that present maximum nominal precision between 2 and 3 cm [24], not

comparable with the millimetre-precision of TLS systems [25]. Di Filippo et al. [21] use a MLS to create the 3D models of existing buildings in a short time. However, the errors are between 1–3 cm, which is not acceptable for control tasks in building works, where the maximum deviation allowed for transversal sections in columns [26] is ±10 mm.

Providing the highest precision of TLS compared to some MLS, TLS has been used for quality control of built environments in repeated occasions, in combination with artificial referencing systems such as artificial targets for the semi-automatic registration of the different point clouds acquired [22]. This requires the intervention of the user in some tasks, especially in the planning of the acquisition and the registration of point clouds into the same coordinate system.

Regarding user intervention with MLS, the systems in the market that are adequate for indoor mapping require to be pushed or carried by the user [23]. Thus, their use is limited in scenarios with elements of risk such as obstacles and hanging pieces, as well as in difficult-access areas. This limits their use in most "under construction" scenarios.

Trying to minimize the user intervention and achieve better results with SLAM techniques and high-quality point clouds, [27] presented a SLAM solution for robotic indoor mapping registration in which static and dynamic scans are used together to achieve optimal results. Static scans provide high quality point clouds, and dynamic scans provide the trajectory and the 3D point clouds of hidden areas between static scans. This technique allows us to generate high-quality point clouds in an automatic way using SLAM algorithms, but the global accuracy of the process is between 25 and 50 mm, exceeding the limits allowed for quality control of works in construction [26]. This global accuracy is formed by around 3 mm error from the nominal accuracy of the LiDAR used (SICK 2D laser scanner), and consequently, it can be deduced that more than a 20 mm error is introduced by the data processing.

Thus, the generation of quality and complete 3D point clouds from building interiors requires the use of TLS because of their high precision and the dynamic performance of the measurements in order to cover all the scenes. However, the methodology that exploits the advantages of this combination has not been established yet. For this reason, this paper is focused on two main goals: (i) minimizing the user interaction during the infield works and the processing tasks and (ii) establishing an automatic workflow to register all the scans without any target on the scene and without user intervention. Taking this into account, this paper presents a new methodology for the automatic registration of point clouds acquired with an unmanned ground vehicle (UGV). Nevertheless, this approach is applicable to point clouds coming from other photogrammetric or laser scanning sensors. The results are subjected to their use in the quality control of the different phases of a construction work.

Regarding point cloud registration, different approaches have been developed in the scientific community.

The pre-alignment of point clouds is usually performed based on detectors and descriptors, that is, algorithms that detect points of interest on 3D and describe them according to their geometric or radiometric characteristics. There are several 3D detectors and descriptors, focusing on different special characteristics [28,29]. Thus, the optimal detectors and descriptors depend on the particularities of each case [30], and their selection affects the result.

The detector scale invariant feature transform (SIFT) [31] has been widely used in automatic registration tasks, since it is not affected by the scale. Although it was initially developed to work with 2D information from images, it was adapted by [32] to operate in 3D using the principal curvature of the points in the role of the intensity of the pixels. [33] used the SIFT detector to automatically register 3D point clouds without artificial targets, but the test was performed in a single building without surroundings. [34] developed a methodology in which the 3D point cloud and the associated RGB /intensity images were used together to compute the registration. Their method was highly sensitive to the size of the overlapping area and depended on the acquisition of images associated to

the scans. Moreover, the SIFT detector requires a lot of time to complete the processing, and its performance is optimal for the registration of two point clouds [30] but does not perform correctly for registering a higher number of point clouds, as is the case in this study. Similar results are obtained with the normal aligned radial feature (NARF) detector, which takes advantage of the key points in the borders and significant geometric structures [30]. The set of resultant key points is poor, so it works for the alignment of pairs of point clouds individually.

The Harris 3D detector detects corners and edges through the analysis of the relation of each point with its neighbours. A set of point rings is generated for each group of points, and their centroid is determined. A paraboloid is adjusted to the neighbour points in each centroid, and PCA is applied to compute the mean square surface of the paraboloid. Finally, the evaluation of the changes in the surface is performed through the analysis of the derivatives of the surface, in combination with a continuous Gaussian function [35,36]. The Harris 3D detector is invariant to rotation, scale, variations in luminosity and presence of noise.

Once the feature points have been detected, a describing process is performed to extract the corresponding points between the point clouds. The description process analyses each point in relation to its neighbours, focusing on its geometric or radiometric properties. Thus, the signature of histograms of orientations (SHOT) descriptor [37,38] splits into several bins a sphere that is centred at a feature point and collects the histogram of normal angles in each bin to build the descriptor. Other descriptors such as USC or 3DSC [39] also consider a sphere superimposed on the feature point and divides it into smaller segments. In these cases, the number of points contained is computed at each segment and weighted inversely by the segment density. These descriptors are not robust enough in environments with presence of noise [39]. Ref [40] developed the point feature histogram (PFH) descriptor, which besides searching the correspondences between points, classifies them in primitive groups such as corners, edges or planes [29].

It should be highlighted that the scenarios of construction works present similarities and repetitive patterns, especially in the early stages of the works where the predominant elements are pillars, walls, doors and windows, all presenting similar shapes. Moreover, the scans of these scenarios are affected by illumination changes. All these factors complicate the process of detection and characterization of corresponding points between point clouds, provided that two different points from different point clouds can be assigned very similar descriptions and be incorrectly considered as corresponding due to their similar characteristics. In order to avoid all the previous drawbacks and to develop a methodology that is easy to use, the detector selected was Harris 3D [41,42] in combination with the point feature histogram (PFH) descriptor.

The paper is structured as follows: after the Introduction, Section 2 presents the methodology developed and the technology used; Section 3 shows the results obtained after the application of the methodology to the quality control of the construction works based on statistical analysis with robust estimators. Section 4 describes the conclusions extracted during the work.

2. Materials and Methods

2.1. Materials

Unnamed Ground Vehicle (UGV) and Terrestrial Laser Scanner (TLS)

Data acquisition for this work was performed with a TLS, Faro Focus 3D 330, mounted on a UGV controlled by an automatic route planner [43]. The path planner uses a 2D drawing of the building as input data, being able to calculate the number of stations needed and the positions of each scan point according to the overlap and the accuracy established [43]. Using this approach, the UGV can work autonomously, without supervision, following the path planned and operating at night to avoid interruptions during the building tasks. The TLS Faro Focus 3D 330 (Figure 1) is used as a static scanning system through a Stop&Go process. In the Stop&Go mode [44], the TLS captures data when the UGV is stopped, mak-

ing a conventional static TLS measurement. Once the scan is finished, the UGV continues its route to the next target point, where another scan is performed. Thus, the TLS is fully autonomous and acquires data with a precision of ±2 mm at 10 m.

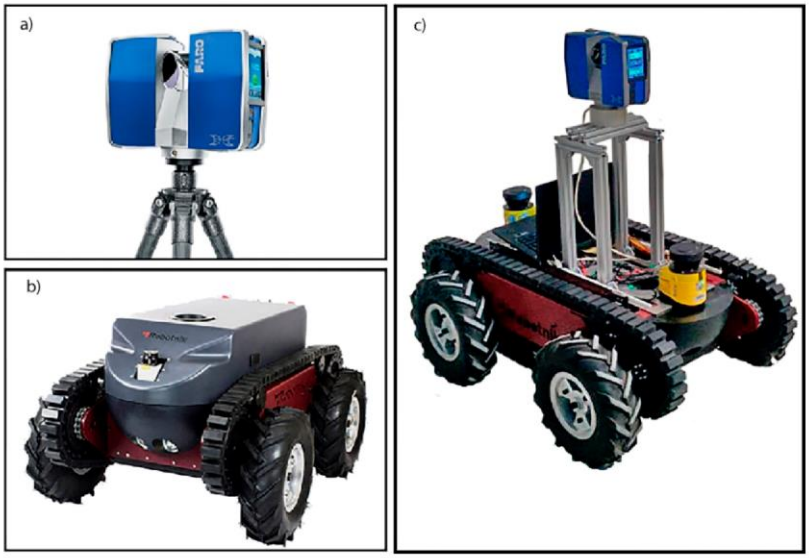

Figure 1. System used for data acquisition: (**a**) terrestrial laser scanner FARO 3D × 330. (**b**) Unnamed ground vehicle guardian from Robotnik. (**c**) Hybrid system: terrestrial laser scanner (TLS) on unnamed ground vehicle

The Faro Focus 3D 330 consists of an infrared laser scanner that measures coordinates directly using the phase difference of the laser ray in the range of 0.60–330 m in a wavelength of 1550 nm. The field of view covers 300° vertically and 360° horizontally, with a resolution of 0.009° and a measurement rate of 122,000–976,000 points per second, also registering radiometric information for each point. The nominal precision of the TLS is ±2 mm at 10 m distance in normal illumination conditions to a 90% reflective surface, with a ray divergence of 0.19 mrad. All these characteristics ensure that the quality standards in construction can be achieved and determine its selection as the scanning system. The Faro Focus system has been mounted on an UGV, Guardian Robotnik, with a payload of 100 kg, speed of 3 m/s, autonomy between 3 and 10 h in normal performance and capacity to detect occlusions and obstacles using two laser scanner SICK S300 Expert integrated at the front and the back of the UGV. Additionally, the path planning developed by [43] was incorporated to give the UGV full autonomy in the acquisition tasks.

2.2. Method

The method developed for the automatic registration follows an execution line structured in different steps (Figure 2). The laser data acquired with the robotic system (Step 1) are subjected to an automatic pre-processing of the laser data (Step 2). The pre-processing consists of a coarse noise filtering based on the analysis of the coordinate histogram, followed by a homogenization of the resolution of the resultant point clouds through voxelization [45] and a filtering process. Then, the registration strategy developed is applied (Steps 3 and 4): (i) coarse registration of each point cloud based on 3D detectors and descriptors (Step 3) [46], (ii) fine registration with iterative closest point (ICP) technique (Step 4) [47]. The result is one 3D point cloud joining all the point clouds acquired into one unique coordinate system, obtained with no user interaction. The last step of the methodology

is the quality control of the construction works focused on certain constructive elements (Step 4).

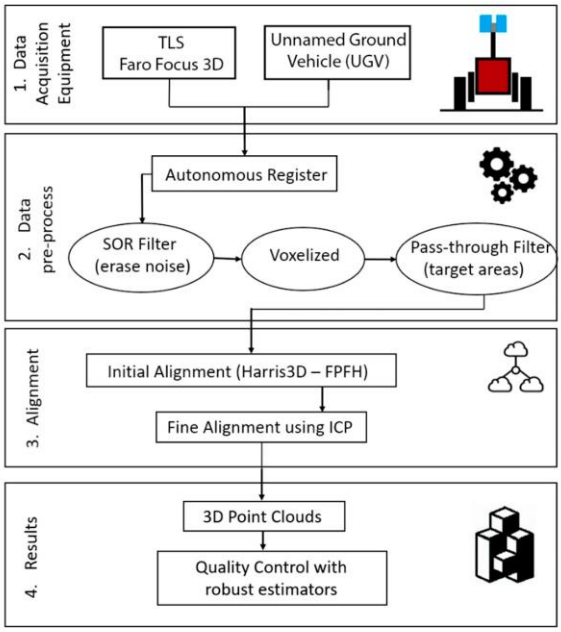

Figure 2. Methodology proposed for automatic registration of point clouds.

2.2.1. Path Planning

The UGV is equipped with an automatic path planner able to calculate the optimal route for the data acquisition. The workflow of the route planner [43] is shown in Figure 3.

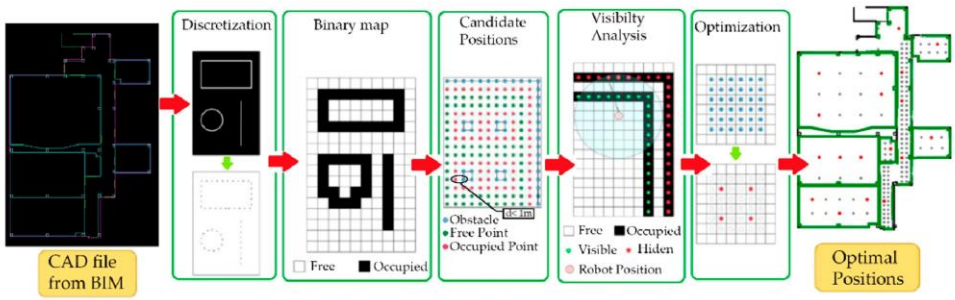

Figure 3. Path-planning workflow.

This planner takes the 2D CAD files of each floor extracted from the BIM model as input data. Constructive elements, such as walls, columns or floors are grouped in layers. Then, each layer is discretized into points with the same resolution (configurable parameter), and a binary occupancy map is performed. A classification of elements based on its non-navigable position (e.g., holes and constructive elements) and navigable position is performed. Next step estimates the candidate positions where the scanner device can make a scan by performing a grid distribution. The dimensions of the UGV are taken in consideration in this step leaving a security margin of 1 m near each building element.

The output of this step is a map with candidate positions, construction element points and no candidate positions. Before designing the optimal route, a visibility analysis on each candidate position is performed in order to know the theoretical area of building elements that would be captured. The visibility analysis is made by a ray-tracing algorithm in combination with the maximum scanner range. The scanner range is a criterion to ensure good density and quality of the acquisition data and is used as the limit of each candidate position analysis. For the study case, the maximum scanner range was 10 m. Finally, an optimization of candidate positions is performed by using the back-tracking algorithm [48]. This algorithm minimizes the scan points ensuring the minimum coverage of the elements selected. For the study case, the minimum coverage was 90%. Once the positions have been optimized, the optimal route is created using the travelling salesman problem followed by the ant colony optimization algorithm [49]. The optimal route is the path with the minimum number of scans that can cover the whole scenario with the setup parameters defined.

During the execution of the route, the path planner is constantly working for ensuring the good performance of the route. In fact, if any scan point is not reachable due to an obstacle (very common in building works) the path planner re-calculates an alternative scan point and thus the resulting route. The calculation of this alternative trajectory is carried out on the fly immediately when the impossibility of reaching a scan point is detected. As a result, the UGV can automatically acquire the data, guaranteeing the setup parameters conditions without user interaction.

2.2.2. Pre-Processing

Commonly, the point clouds acquired by 3D laser scans contain noise. The noise is composed by points measured with positional errors. These errors are due to vibrations, reflections, far points or moving elements during the scan works, so it is important to filter them to prevent their influence in the rest of the calculus.

The first operation is an automatic noise elimination using statistical outlier removal (SOR) filter [50]. The SOR filter automatically eliminates the noise present in the point clouds by performing a proximity analysis for each point with the neighbour points (Figure 4). For this case, the fast statistical outlier removal (FSOR) proposed by Balta et al. [51] was used to minimize the processing time and optimize resources.

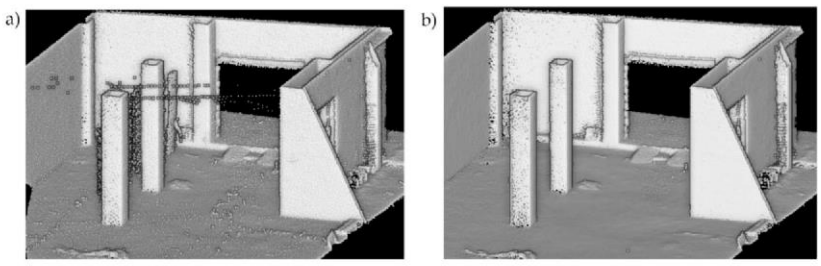

Figure 4. Fast statistical outlier removal (FSOR) filter applied over the point cloud. (**a**) Detail of raw point cloud with noise; (**b**) result after applying FSOR filter.

After cleaning the point cloud, a passthrough filter [52,53] based on the coordinate histogram of the point clouds is applied. Because the Faro Focus captures data in the range 0.60–330 m, the system measures points that are too far from the scan station and consequently useless for the application (Figure 5a,c). The first automatic filter applied removes the farthest points computing the coordinates distribution along the different axis (x, y, z). For each axis, the coordinates are converted to scalar field, and its histogram of distribution is filtered according to the position with highest accumulation of points in

each case. This procedure was applied in the three directions obtaining a first filtered point cloud (Figure 5b,d).

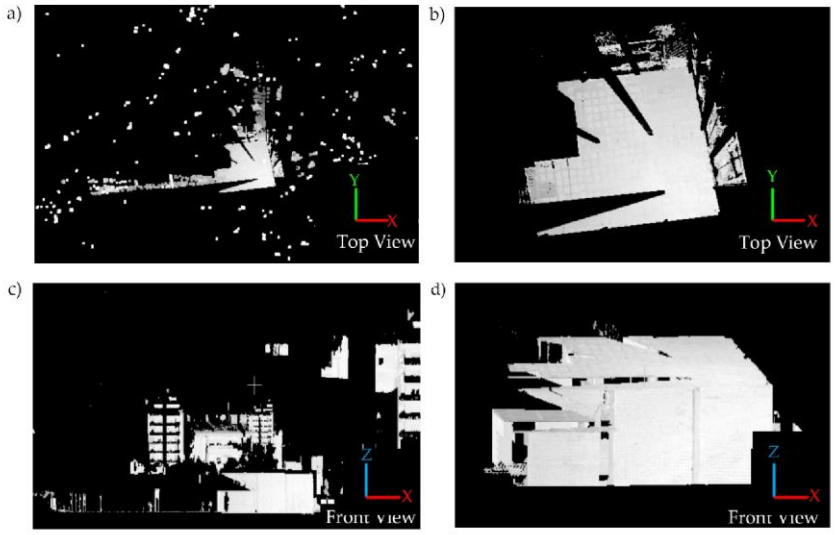

Figure 5. Passthrough filter based on the coordinate histograms. (**a**) Top view of raw scanned data with scatter. (**b**) Top view of scanned data after filter by *X*-coordinates histogram (**c**) Front view of raw scanned data with scatter. (**d**) Result after coordinates histogram filter.

Finally, a homogenization of the point cloud is performed. It is well known that 3D point clouds acquired with a laser scanner present heterogeneous point density. The further away from the station point, the lower point density. The voxel-grid filter [53,54] allows the generation of a uniform dataset by dividing the space in cubes of custom size and replacing the points on each cube by the centroid of that set of points. The voxelization [45] is performed in an automatic way: the size of the voxel depends on the density of the point cloud, which is calculated through the study of the mean distance of each point to its closest neighbours. In this way, the process is completely automated, as well as adaptative to the data of each scenario.

2.2.3. Alignment

Once the point clouds are pre-processed, their pre-alignment is performed based on detectors and descriptors. In the proposed methodology, the detector selected was Harris 3D [41,42] in combination with the point feature histogram (PFH) descriptor. Finally, an ICP alignment was applied.

The Harris 3D detector presents good results in construction scenarios, since its characteristics are optimal for the identification of points in pillars, vertical walls and ceilings, by its corners and edges. It is also fast and detects large sets of interest points with a good correspondence [55]. The Harris 3D detector allows for several variations depending on the evaluation of the trace and the determinant (det) of the covariance matrix (Cov) [41]. In all the variations, the response of the key points $r(x, y, z)$ is estimated, but different criteria are applied in each case. The original Harris 3D detector is performed using Equation (1), while Harris 3D Lowe follows Equation (2) and the variant Harris 3D Noble (Figure 6) applies Equation (3), where the trace of the covariance matrix is not squared.

$$r(x,y,z) = \det(Cov(x,y,z) - k(trace(Cov(x,y,z)))^2 \quad (1)$$

$$r(x,y,z) = \frac{\det(Cov(x,y,z))}{trace(Cov(x,y,z))^2} \quad (2)$$

$$r(x,y,z) = \frac{\det(Cov(x,y,z))}{trace(Cov(x,y,z))} \quad (3)$$

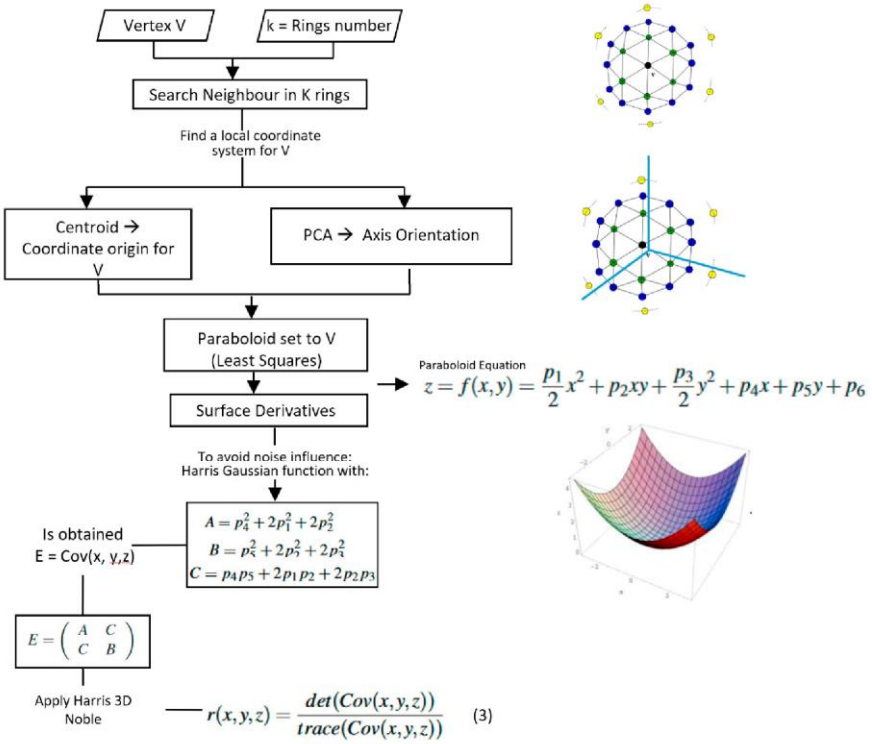

Figure 6. Harris 3D Noble detector: performance mode.

These changes among Harris 3D variants modify the evaluation of the relation between the determinant and the trace of the covariance matrix, which affects in the result of the point detection [42]. The Harris 3D method includes a constant k that depends on the point cloud data, while Harris 3D Lowe and Harris 3D Noble do not consider this factor, being independent of the input data [56]. This fact led to the selection of Harris 3D Noble as an optimal point detector in the methodology developed.

Since the detector used (Harris 3D) focuses mainly on detecting corners and edges, and because the PFH descriptor is more robust against changes in the viewpoints and delivers reliable information between the point clouds [30,41], the latter was chosen for this work, since it is common to have different points of view, illumination changes and good overlap between scans.

The 3D PFH descriptor describes each point with its neighbours generalizing the normal vectors (n) and the mean curvature (α, ϕ, θ), and representing these values in a histogram. The histogram will have a unique and invariant signature for each point. Providing two points, p and q, a reference system can be created consisting of three unit vectors (u, v, w) [57]. Thus, the difference between normal vectors in points p (n_p) and q

(n_q) is determined with three angular variables (Equations (4)–(6)) where d represents the distance between p and q.

$$\alpha = arc\cos(v \cdot n_q) \tag{4}$$

$$\varnothing = arc\cos\left(u \cdot \frac{p-q}{d}\right) \tag{5}$$

$$\theta = arc\tan(w \cdot n_p,\ u \cdot n_p) \tag{6}$$

Being:
u the surface normal at p
$v = u \times \frac{p-q}{d}$
$w = u \times v$
$d = \| p - q \|_2$

The three angles are coded with distance, and together they form the final descriptor, with the concatenation of the histograms of the four variables.

The 3D PFH descriptor is applied to all points identified as feature points with the Harris 3D Noble detector, in such way that each point is associated with a description, and the coincidence of descriptions is used for the determination of correspondences between points from different point clouds. The identification of corresponding points allows the computation of the transformation between point clouds to the same coordinate reference system. In addition, the description of each point allows its classification into the different primitives such as edges, corners or planes.

The invariance to rotation, scale, variations in luminosity and presence of noise is the reason for the selection of the couple Harris 3D–PFH for the study of indoor building scenes. This results in the efficient detection of points of interest in corners and borders and the assignment of correspondences between feature points of different point clouds. However, for those cases with repetitive elements such as pillars, some erroneous correspondences can appear. In order to minimize this effect, the methodology proposed includes a restriction of maximum distance between corresponding points. This restriction avoids the determination of erroneous points correspondences produced by the similarity between different zones.

The filter that discriminates according to the distance between points is graphically explained in Figure 7a. Its performance is as follows: Corresponding points for each point of interest are searched within a distance threshold. This search, together with the initial results of the detector/descriptor combination, allows us to refine the registration between point clouds, thus improving the results. This step is reiterated until the root mean square error (RMSE) is below a threshold established according to the criteria for quality control in the works. The purpose of this study is to check and validate sections of the building based on variations and translations of the built elements. For the first case, the tolerances allowed are $\pm$10 mm and for the second case $\pm$24 mm [26]. To ensure that all the data meet these tolerances, the quality threshold is set to 5 mm.

Once the Harris 3D detector and PFH descriptor have been computed and a first coarse alignment based on features has been applied to all the point clouds, some of them are correctly aligned, but some others are not. This is due to the similarity between scans, which can cause imperfections in the final alignment. However, the point clouds are approximated to their real positions and the generation of one unique 3D point cloud formed by all the point clouds can be completed with the final adjustment of the registration, which eliminates the errors. The final adjustment is performed using the ICP algorithm [58]. ICP consists of an iterative process in which the distance error between point clouds is minimized until the point clouds are perfectly aligned. Each iteration consists of three steps: (i) finding pairs of corresponding points; (ii) estimation of the transformation that minimizes the distance between corresponding points; (iii) application of the transformation to the point clouds. Since ICP is an iterative algorithm, it is mandatory to have a good initial

transformation to make its convergence possible [59]. This initial estimation comes from the coarse alignment, which already makes a good estimation of the point clouds positions.

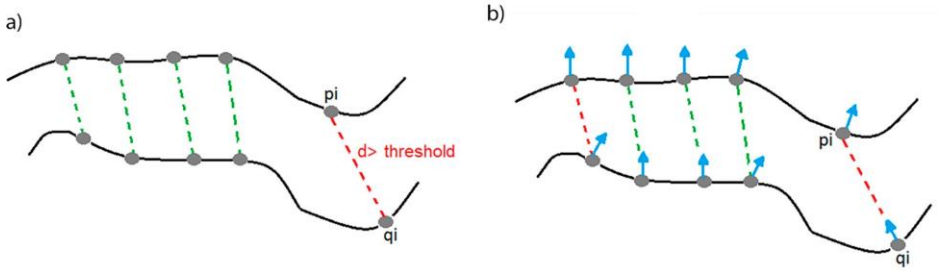

Figure 7. Method for filtering correspondences with ICP algorithm: (**a**) method based on distance; (**b**) method based on normal vectors, which application was discarded.

It should be highlighted that the registration method based on the compatibility between normal vectors (Figure 7b) is not applicable in these scenarios, due to the presence of repetitive structures with similar characteristics (squared pillars, vertical walls, doors, among others) that resulted in similar descriptions based on the normal vector in spite of their difference. This invalidity of the normal vector method was analysed through its application to the cases of study and shown through the lack of convergence regarding the ICP algorithm.

The ICP algorithm can be applied in a point-to-point or in a point-to-plane mode. The first performs the adjustment between point clouds by minimizing the distance between one point in the point cloud of reference and its corresponding point in the point cloud to register. The second adjusts the point cloud through the minimization of the distance between the point in the point cloud of reference and the tangent plane to its corresponding point in the point cloud to register. Studies shown that the validity of point-to-point ICP is more robust to Gaussian noise than point-to-plane ICP [60]. However, the latter undergoes fewer iterations, and it is more effective [60]. Since the point clouds are cleaned and filtered from noise before starting the registration process, the point-to-point ICP method was chosen for this work.

The main advantage of the double step Harris 3D/PFH and point-to-point ICP registration is that there is no need of user interaction, and there is no need to place any targets in the scene to serve as points of interest, because the points of interest in the method proposed are naturally present in the scene.

3. Results and Discussion

3.1. Case Study

The validation of the methodology proposed is performed through its application to two different scenarios of a residential building located in Badalona (Spain). The building has asymmetric U-shaped floor plan (Figure 8a). In the moment of the acquisition, the building was being constructed with a life expectation of 50 years. The plan is 25,000 m^2 and is vertically distributed in two basements dedicated to parking, one base floor dedicated to commercial offices and the upper floors destined to housing. The building is divided in two blocks, north and south, with 14 and 13 floors, respectively.

The foundations of the building are constructed with a rectangular base, 200 × 45 cm and 260 × 45 cm size, individually or in groups of two elements with capped piles for load transmission. Retaining walls are made of concrete with temporary anchoring.

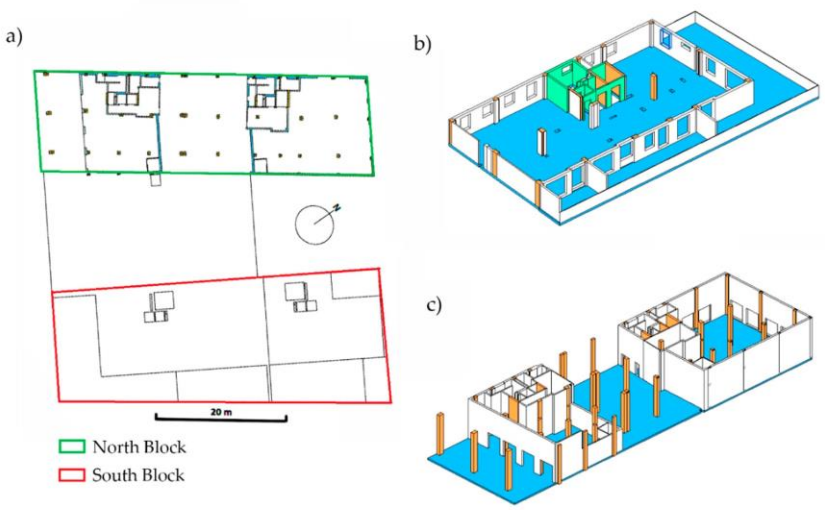

Figure 8. Building selected as case study: (**a**) 2D planes of the buildings. (**b**) Building information modelling (BIM) model of the first floor in the north block selected as the first study case. (**c**) BIM model of the ground floor in the south block selected for the second study case.

In the moment of data acquisition, the building was under different periods of construction, allowing for the testing of the methodology proposed in different environments and complexities of construction works. Two floors were selected for the data acquisition: (i) Floor 1 in the north block, which presents 810 m^2 (Figure 8b) and (ii) the ground floor in the south block, with 845 m^2 (Figure 8c). These floors were selected due to their condition of construction and geometrical complexity, which can be considered as representative for construction works. During acquisition, there were walls, pillars, holes (for the lift and drainpipes), floors and ceilings present in the scenes, as well as construction materials such as scaffolds and boards.

3.2. Data Acquisition

Data acquisition was performed with the UGV described in Section 2.1. For the first study case, seven stations were needed, in the Stop&Go strategy, for the complete acquisition (Figure 9b). For the second study case, a total of 11 stations were needed to cover all the spaces (Figure 9d). In the second study case, more stations were necessary, since this floor was in a more advanced state of construction and there were more occlusions between elements. The position of the stations was optimized by the path planning programmed in the UGV [43] in order to minimize the trajectories (Figure 9a,c), acquiring all the information required. Since both floors were in the construction phase (Figure 9b), the trajectory had the requirement of including all the pillars in the data acquisition. Resolution and quality of the data acquired were adjusted in a compromise to obtain all the information needed and to minimize acquisition time and quantity of data generated. Thus, 60% overlap between stops was established, together with a scanning resolution of 4 mm at 20 m. The overlap percentage was selected towards the optimization of the automatic registration process in terms of precision and reliability. In addition, providing the minimum acquisition range of the TLS (0.6 m), all points at a distance below 0.8 m from the TLS were discarded from the acquisition (Table 2)

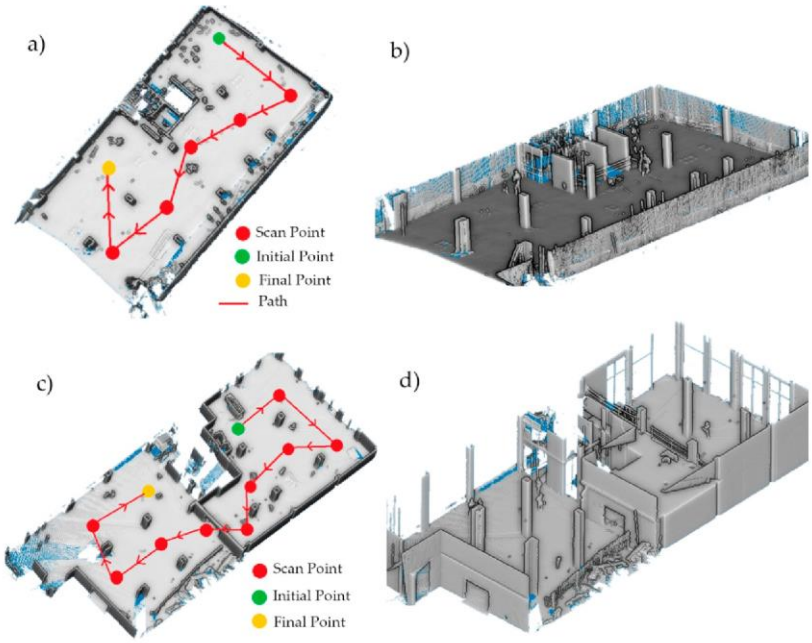

Figure 9. Optimal route followed by the unmanned ground vehicle (UGV) for data acquisition; (**a**) optimal route and scan points in the first study case; (**b**) resulting Faro point cloud of the first study case; (**c**) optimal route and scan points of the second study case; (**d**) resulting Faro point cloud of the second study case.

Table 2. Scanning parameters for the acquisition with TLS.

Parameter	Value
Mean laser range (m)	8
Security distance (m)	0.8
% Scanning overlap	60%
Scanning resolution	4 mm at 20 m

The time required per scan position was approximately 3 min. This value should be added to the time required in the trajectory between stops, for a total acquisition time of 25 and 45 min for the first and second study cases, respectively.

For the first and second study cases, the result of the acquisition was six and eleven point clouds with 24 million points each, respectively. To have a homogeneous and clean point cloud in the next steps, the raw point clouds were filtered as described in Section 2.2. In this application, the voxel size was established at 0.5 cm, resulting in point clouds about 7 million points each and with homogeneous data distribution. The UGV can operate at night and can go over piles of rubble as well as muddy and wet surfaces thanks to its caterpillar wheels.

3.3. Automatic Registration

The automatic registration procedure described in Section 2.2 was applied to the six and eleven TLS point clouds acquired for each study case, after the application of the filtering procedure. That is, (i) one coarse registration based on the Harris 3D Noble detector and the PFH descriptor with which the point clouds are positioned close to their real position (Figure 10b) in the shared coordinate system; (ii) one fine registration procedure based on ICP for the positioning of the point clouds with millimetre precision

(Figure 10c). The final 3D point clouds, after removing duplicated points, are formed by 44 million points and 73 million points for the first and second study cases, respectively.

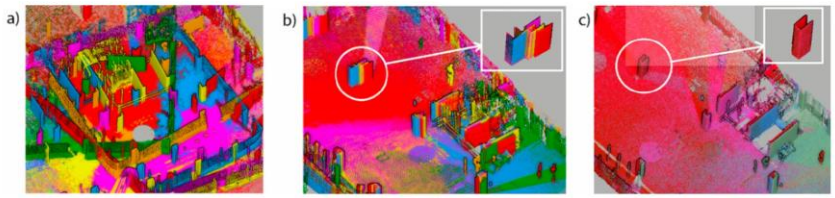

Figure 10. Automatic registration procedure: (**a**) initial state of the point clouds (all referenced to the (0,0,0), with relative coordinates regarding the position of the TLS in each acquisition); (**b**) state of the point clouds after the initial registration based on Harris 3D Noble–PFH, with a detail of the pillars where the error in registration is noticeable; (**c**) final result of the ICP registration, with a detail of the pillar shown in (**b**), which was correctly registered during this last step. Each colour represents a different point cloud.

Regarding processing time, the total time for the automatic procedure required 23 and 48 min for the first and second study cases, respectively, in a PC Mountain Studio3D i5 Ivy with Intel Core i5-3570K processor and 32 Gb RAM with operating system Windows 10 64 bits, and no need for interaction by the user.

3.4. Quality Control

The BIM models (Figure 8b,c) were used as reference for the quality control. More precisely, the registration of the BIM and point clouds was done manually using a local data established by the company, which corresponds with the definition of a local origin and the direction of X and Y axes. The Z axis was always considered along the vertical. After that, two different approaches were performed for analysing the quality: (i) the models were compared with the designed building information model (BIM) to find visual discrepancies between as-built and BIM models; (ii) the accuracy of the point clouds was checked comparing against the BIM models. In particular, the accuracy of the point clouds was checked using two different dimensional analysis: (i) dimensional control of the pillars, (ii) distance between construction elements. For the dimensional control, the dimensions obtained from the as-built model, automatically registered, were compared to the dimensions measured in the reference BIM.

The reference BIM provides a theoretical model very close to the final result expected for the construction, and it is updated over the time. This contributes to making the quality control during the whole process. The BIM reflects the geometry, metrical properties, material properties and construction phases of each element, together with the final layout of the building [61]. This way, the BIM is considered as a theoretical model in this case and provides the reference measurements for the structural elements chosen to validate the methodology in each phase.

However, the point clouds registered with the automatic procedure proposed contain a high amount of information, and their statistical distribution is often non-normal [62]. Thus, the statistical analysis performed was based on nonparametric estimators of the median, m, such as the normalized median absolute deviation ($NMAD$) (Equation (7)) and the bi-weight mid-variance ($BWMV$) (Equation (8)). These parameters allow us to perform a comparison and, consequently, a more precise and reliable quality control.

$$NMAD = 14,826 \cdot MAD \tag{7}$$

$$BWMV = \frac{n \cdot \sum_{i=1}^{n} a_i \cdot (x_i - m)^2 \cdot (1 - U_i^2)^4}{\left(\sum_{i=1}^{n} a_i \cdot (1 - U_i^2) \cdot (1 - 5U_i^2)\right)^2} \tag{8}$$

where:

$$a_i = \begin{cases} 1, \; if \mid U_i \mid < 1 \\ 0, \; if \mid U_i \mid \geq 1 \end{cases} \tag{9}$$

$$U = \frac{x_i - m}{9 \cdot MAD} \tag{10}$$

being the median absolute deviation (MAD) defined by Equation (11) and described as the median (m) of the absolute deviation of the median of the data (m_x) and x_i the measurements performed on the registered point cloud.

$$MAD = m \cdot (\mid x_i - m_x \mid) \tag{11}$$

Table 3 shows the results of bias and dispersion for the discrepancies of TLS vs. BIM for the two study cases.

Table 3. Bias and dispersion results of the TLS vs. BIM for the two study cases.

	Bias	**Dispersion**	
	Median (m)	**NMAD (m)**	**(BWMV) (m)**
Study Case 1	0.007	±0.007	±0.00005
Study Case 2	0.008	±0.008	±0.00007

Considering that the approach developed provides values admissible for quality control tasks, a comparison of measurements on the point cloud registered with the method and on the reference BIM measurements was performed. The elements where the errors in registration are most evident are pillars. Table 4 shows the admissible tolerances within the most relevant structural elements in a building according to [26].

Table 4. Tolerances in the different structural elements according to [26]. "*D*" represents the transversal dimension of the elements.

Tolerances in Construction Elements	
Cross Section ($D < 30$)	+10–8 mm
Cross Section ($30 < D < 100$)	+12–10 mm
Cross Section ($100 < D$)	+24–20 mm
Vertical deviation outer edges columns	±6 mm
Wall Thickness < 25 cm	+12–10 mm
Wall Thickness > 25 cm	+16–10 mm

The validation focuses on the dimensions and the cross sections of the pillars. These elements are predefined, making them adequate as control elements. Seven pillars of the first study case and seven pillars of the second study case were subjected to measurements of their width at three different heights: low height at 0.20 m, medium height at 1.20 m and high height at 2.50 m from the floor. Each measurement is performed five times, and robust statistical estimators are calculated from these measurements. Table 5 shows the theoretical measurements (performed on the BIM) in each pillar and the measurements performed on the as-built model resulting from our methodology. Table 6 shows the results of the robust statistical parameters calculated from the dimensional analysis (median and BWMV). Provided that the tolerance for pillar section control is established at 8–10 mm (Table 4), the results obtained with the methodology proposed are applicable in this type of scenario.

Table 5. Results of the control measurements performed in the different pillars, seven for the first study case and seven for the second study case.

	Element	BIM Width (mm)	As-Built Width (mm)
Study Case 1	Pillar 1	500	500
	Pillar 2	450	450
	Pillar 3	350	351
	Pillar 5	450	449
	Pillar 6	450	450
	Pillar 7	350	348
	Pillar 8	600	600
Study Case 2	Pillar 1	600	597
	Pillar 2	450	452
	Pillar 3	450	451
	Pillar 4	450	448
	Pillar 5	450	448
	Pillar 6	400	398
	Pillar 7	500	498

Table 6. Bias and dispersion data for the analysed data in both study cases.

		Bias	Dispersion	
		Median (mm)	NMAD (mm)	(BWMV) (mm)
Study Case 1	Pillar 1	503	±1.5	±0.5
	Pillar 2	450	±4.4	±9.6
	Pillar 3	352	±3.0	±9.0
	Pillar 5	449	±3.0	±9.8
	Pillar 6	451	±1.5	±7.6
	Pillar 7	348	±1.5	±3.3
	Pillar 8	600	±1.5	±2.3
Study Case 2	Pillar 1	597	±1.5	±2.9
	Pillar 2	452	±1.5	±1.6
	Pillar 3	451	±1.5	±1.8
	Pillar 4	447	±1.5	±1.6
	Pillar 5	448	±2.9	±4.4
	Pillar 6	398	±2.9	±7.7
	Pillar 7	497	±1.5	±3.0

An additional test of the dimensions of one pillar on each study case is performed by adjusting planes to each face of the pillars (Figure 11). This test is performed as an evaluation method of the quality of the results. This additional evaluation is necessary, because the point cloud is formed by discrete points, and the punctual measurements can present non-robust results, since they depend on the points used for the measurements.

The metrical verification in the planar case consists in computing the size of the pillars by measuring the distance between opposite sides of the pillars and comparing the distances measured with the real dimensions of the pillars (Table 7). Thus, the width of the pillar is denoted as *d1* (distance between planes 3 and 4), and the length of the pillar is *d2* (distance between planes 1 and 2), as shown in Figure 11c.

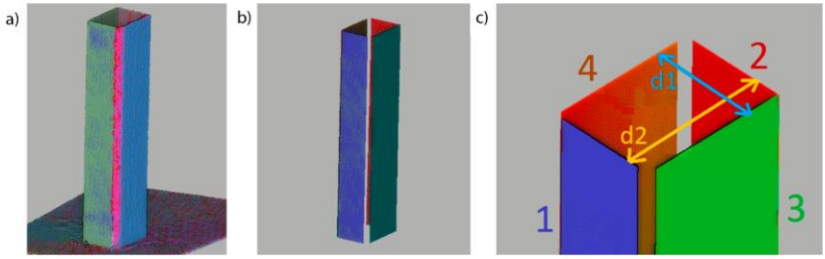

Figure 11. (**a**) Point cloud of a pillar obtained after the automatic registration proposed; (**b**) plane adjustment for each pillar face; (**c**) control measurements performed on the pillar.

Table 7. Result of the control measurements performed on pillar 3 (study case 1) and on the pillar 9 (study case 2). The measurements performed correspond to distances between opposite sides of the pillar (Figure 11).

Id	BIM Model		As Built Model		Errors	
	Width (mm)	Length (mm)	Width–*d1* (mm)	Length–*d2* (mm)	Width (mm)	Length (mm)
Pillar 3 (Study Case 1)	350.0	500.0	350.9	490.6	0.9	0.4
Pillar 9 (Study Case 2)	360.0	500.0	360.1	500.2	0.1	0.2

Provided that the pillars are the elements more influenced by the results of the registration, and given the results obtained for them, the automatic registration methodology proposed presents adequate quality and precision for its application in quality control of construction works: the methodology allows for the measurement of the pillars with an error below 10 mm and the performance of any additional measurement from the point cloud.

4. Conclusions

This paper presents a new methodology for the automatic acquisition and registration of point clouds for indoor scenarios in construction works. The main contributions of the presented approach are two-fold: (i) the possibility of automatically capturing point clouds based on the Stop&Go method and using an UGV; (ii) a methodology of point cloud registration fully automatic that works with any photogrammetric or laser scanning point clouds.

The methodology proposed presents an automatic data acquisition with an UGV equipped with a TLS and an automatic route planner able to calculate the best route and producing no interferences during the construction works. The different point clouds acquired are automatically registered using a combination of detector/descriptor. The integral methodology can be completely autonomous and automatic, with no need of artificial elements that disturb the construction scenario and no need of user interaction. The precision obtained in the automatic registration was evaluated through metric verifications on the resulting point cloud. The errors are below 1 cm in all measurements performed. This precision validates the use of the methodology in quality control scenarios in construction works for the identification and control of construction elements.

The methodology presented for point cloud registration consists of three steps: (i) pre-processing of the data filtering and homogenizing of the point clouds, (ii) a coarse registration and (iii) a fine registration. The data were acquired with an autonomous unnamed ground vehicle with the Faro laser scan mounted on it and applying the Stop&Go method. The UGV can operate at night and with no user intervention thanks to the path

planner. The resultant point cloud has enough quality, density and precision for quality control in building works (less than 1 cm in section dimensions and less than 1.5 cm in wall thickness).

For the coarse registration, a combination of Harris 3D detector and PFH descriptor was used, since this combination allows the best detection of feature points on corners, edges and planes. These parametric forms are the most common in building scenarios and provide robust results. The detector/descriptor method allows to be applied on any set of point clouds, captured with any laser scan system, using a UGV or not.

In addition, the chosen detector/descriptor-based method uses only geometric information to compute the coarse alignment. This means that it is not necessary to have radiometric information (RGB colour), making the methodology more scalable and suitable for many more study cases. In this line, the Harris 3D/PFH combination was chosen, because it does not need images to perform the calculations, as other detectors and descriptors do, such as SIFT or SURF. Being independent of image capturing makes the methodology scalable an accessible for many more situations.

Despite the independence of the laser scan system, the equipment used has some limitations. For example, it has not been designed to be able to climb stairs, although it can go through small bumps such as planks. In addition to the TLS for data acquisition, the UGV is equipped with two laser scanners SICK S300 Expert integrated at the front and the back of the UGV that allow to detect objects and holes. The combination of this system with the path planning makes it totally autonomous. The path planning incorporates an algorithm to recalculate the optimal route in those cases where the target point is inaccessible. This occurs frequently in building construction environments where materials or debris can appear unexpectedly. In order to minimize the traffic of personnel, the data acquisition can be carried out at night, since the laser system is an active system and does not need light to operate.

Regarding future works, the first research line will improve the coarse registration for those cases with a considerable number of outliers. Furthermore, the recognition of artificial targets could be included to improve those cases where the coarse registration is not good enough. The second research line will focus on the automatic extraction of the semantics of the different construction elements from the point cloud and either the classification of the elements or the conversion of the as-built model to a surface 3D model or a BIM. The use of BIM as a reference was possible for this work, but usually the BIM model is not available, in such way that the natural evolution of the as-built model generated automatically with the methodology proposed is the generation of the BIM.

Author Contributions: Conceptualization, D.G.-A. and R.M.; methodology, D.G.-A., S.L. and R.M.; software, R.M. and J.A.M.-J.; validation, S.L., D.G.-A. and R.M.; formal analysis, J.A.M.-J. and S.L.; writing—original draft preparation, S.L. and D.G.-A.; all the authors contributed to writing—review and editing; visualization. All authors have read and agreed to the published version of the manuscript.

Funding: Authors would like to thank the Junta de Castilla y León and the Fondo Social Europeo for the financial support given through programs for human resources (EDU/1100/2017).

Institutional Review Board Statement: Not applicable.

Informed Consent Statement: Not applicable.

Data Availability Statement: The data presented in this study are available on request from the corresponding author.

Acknowledgments: Special thanks to the Cátedra Iberdrola VIII Centenario–University of Salamanca for funding given to personnel resources, and the Ministerio de Economia, Industria y Competitividad–Gobierno de España (RTC-2016-5257-7).

Conflicts of Interest: The authors declare no conflict of interest.

References

1. Azhar, S.; Khalfan, M.; Maqsood, T. Building information modelling (BIM): Now and beyond. *Constr. Econ. Build.* **2012**, *12*, 15–28. [CrossRef]
2. Real Decreto 1515/2018, de 28 de diciembre, por el que se crea la Comisión interministerial para la incorporación de la metodología BIM en la contratación pública. Available online: https://www.boe.es/eli/es/rd/2018/12/28/1515 (accessed on 28 December 2020).
3. Jung, W.; Lee, G. The status of BIM adoption on six continents. *Int. J. Civ. Environ. Struct. Constr. Archit. Eng.* **2015**, *9*, 444–448.
4. Kreider, R.G.; Messner, J.I. *The Uses of BIM: Classifying and Selecting BIM Uses*; State College Pennsylvania: State College, PA, USA, 2013; p. 22.
5. Remondino, F.; Guarnieri, A.; Vettore, A. 3D modeling of close-range objects: Photogrammetry or laser scanning? In *Videometrics VIII*; International Society for Optics and Photonics: San José, CA, USA, 2005; Volume 5665, p. 56650M.
6. Alidoost, F.; Arefi, H. An image-based technique for 3D building reconstruction using multi-view UAV images. *Int. Arch. Photogramm. Remote Sens. Spat. Inf. Sci.* **2015**, *40*, 43. [CrossRef]
7. Guarnieri, A.; Vettore, A.; Remondino, F.; Church, O.P. Photogrammetry and Ground-Based Laser Scanning: Assessment of Metric Accuracy of the 3D Model of Pozzoveggiani Church. 2004. Available online: https://www.fig.net/resources/proceedings/fig_proceedings/athens/papers/ts26/TS26_4_Guarnieri_et_al.pdf (accessed on 5 February 2021).
8. Bernat, M.; Janowski, A.; Rzepa, S.; Sobieraj, A.; Szulwic, J. Studies on the use of terrestrial laser scanning in the maintenance of buildings belonging to the cultural heritage. In Proceedings of the 14th Geoconference on Informatics, Geoinformatics and Remote Sensing, SGEM, Albena, Bulgaria, 17–26 June 2014; Volume 3, pp. 307–318.
9. Pritchard, D.; Sperner, J.; Hoepner, S.; Tenschert, R. Terrestrial laser scanning for heritage conservation: The Cologne Cathedral documentation project. *ISPRS Ann. Photogramm. Remote Sens. Spat. Inf. Sci.* **2017**, *4*, 213–220. [CrossRef]
10. Sánchez-Aparicio, L.J.; Del Pozo, S.; Ramos, L.F.; Arce, A.; Fernandes, F.M. Heritage site preservation with combined radiometric and geometric analysis of TLS data. *Autom. Constr.* **2018**, *85*, 24–39. [CrossRef]
11. Sánchez-Aparicio, L.J.; Bautista-De Castro, Á.; Conde, B.; Carrasco, P.; Ramos, L.F. Non-destructive means and methods for structural diagnosis of masonry arch bridges. *Autom. Constr.* **2019**, *104*, 360–382. [CrossRef]
12. Del Pozo, S.; Herrero-Pascual, J.; Felipe-García, B.; Hernández-López, D.; Rodríguez-Gonzálvez, P.; González-Aguilera, D. Multispectral radiometric analysis of façades to detect pathologies from active and passive remote sensing. *Remote Sens.* **2016**, *8*, 80. [CrossRef]
13. Cabo, C.; Del Pozo, S.; Rodríguez-Gonzálvez, P.; Ordóñez, C.; González-Aguilera, D. Comparing terrestrial laser scanning (TLS) and wearable laser scanning (WLS) for individual tree modeling at plot level. *Remote Sens.* **2018**, *10*, 540. [CrossRef]
14. Akca, D. *Full Automatic Registration of Laser Scanner Point Clouds*; ETH Zurich: Zurich, Switzerland, 2003.
15. Theiler, P.W.; Schindler, K. Automatic registration of terrestrial laser scanner point clouds using natural planar surfaces. *ISPRS Ann. Photogramm. Remote Sens. Spat. Inf. Sci.* **2012**, *3*, 173–178. [CrossRef]
16. Chen, S.; Nan, L.; Xia, R.; Zhao, J.; Wonka, P. PLADE: A Plane-Based Descriptor for Point Cloud Registration with Small Overlap. *IEEE Trans. Geosci. Remote Sens.* **2019**, *58*, 2530–2540. [CrossRef]
17. Gai, M.; Cho, Y.K.; Xu, Q. Target-free automatic point clouds registration using 2D images. In Proceedings of the ASCE International Workshop on Computing in Civil Engineering, Los Angeles, California, 23–25 June 2013; pp. 865–872.
18. Kim, P.; Chen, J.; Cho, Y.K. Automated point cloud registration using visual and planar features for construction environments. *J. Comput. Civ. Eng.* **2018**, *32*, 04017076. [CrossRef]
19. Ge, X.; Hu, H.; Wu, B. Image-Guided Registration of Unordered Terrestrial Laser Scanning Point Clouds for Urban Scenes. *IEEE Trans. Geosci. Remote Sens.* **2019**, *57*, 9264–9276. [CrossRef]
20. Weinmann, M.; Jutzi, B. Fully automatic image-based registrationof unorganised TLS data. *Int. Arch. Photogramm. Remote Sens. Spat. Inf. Sci.* **2011**, *38*, W12.
21. Di Filippo, A.; Sánchez-Aparicio, L.; Barba, S.; Martín-Jiménez, J.; Mora, R.; González Aguilera, D. Use of a Wearable Mobile Laser System in Seamless Indoor 3D Mapping of a Complex Historical Site. *Remote Sens.* **2018**, *10*, 1897. [CrossRef]
22. Sánchez-Aparicio, L.J.; Conde, B.; Maté-González, M.A.; Mora, R.; Sánchez-Aparicio, M.; García-Álvarez, J.; González-Aguilera, D. A Comparative Study between WMMS and TLS for the Stability Analysis of the San Pedro Church Barrel Vault by Means of the Finite Element Method. *Int. Arch. Photogramm. Remote Sens. Spat. Inf. Sci.* **2019**, *4215*, 1047–1054. [CrossRef]
23. Otero, R.; Lagüela, S.; Garrido, I.; Arias, P. Mobile indoor mapping technologies: A review. *Autom. Constr.* **2020**, *120*, 103399. [CrossRef]
24. Geo-SLAM Zeb-Revo. Available online: http://geoslam.com/hardware-products/zeb-revo/ (accessed on 5 February 2021).
25. Faro Focus 3D. Features, Benefits & Technical Specifications. Available online: https://knowledge.faro.com/Hardware/3D_Scanners/Focus/Technical_Specification_Sheet_for_the_Laser_Scanner_Focus_3D (accessed on 5 February 2021).
26. EHE-08. *Instrucción de Hormigón Estructural Secretaría General Técnica*; Ministerio de Fomento: Madrid, España, 2008.
27. Kim, P.; Chen, J.; Cho, Y.K. SLAM-driven robotic mapping and registration of 3D point clouds. *Autom. Constr.* **2018**, *89*, 38–48. [CrossRef]
28. Tombari, F.; Salti, S.; Di Stefano, L. Performance evaluation of 3D keypoint detectors. *Int. J. Comput. Vis.* **2013**, *102*, 198–220. [CrossRef]

29. Chen, Z.; Czarnuch, S.; Smith, A.; Shehata, M. Performance evaluation of 3D keypoints and descriptors. In *International Symposium on Visual Computing*; Springer: Cham, Switzerland, 2016; pp. 410–420.
30. Hänsch, R.; Weber, T.; Hellwich, O. Comparison of 3D interest point detectors and descriptors for point cloud fusion. *ISPRS Ann. Photogramm. Remote Sens. Spat. Inf. Sci.* **2014**, *2*, 57. [CrossRef]
31. Lowe, G. SIFT-the scale invariant feature transform. *Int. J.* **2004**, *2*, 91–110.
32. Rusu, R.B.; Cousins, S. 3D is here: Point cloud library (PCL). In Proceedings of the 2011 IEEE International Conference on Robotics and Automation, Shanghai, China, 9–13 May 2011; pp. 1–4.
33. Böhm, J.; Becker, S. Automatic marker-free registration of terrestrial laser scans using reflectance. In Proceedings of the 8th Conference on Optical 3D Measurement Techniques, Zurich, Switzerland, 9–12 July 2007; pp. 9–12.
34. Moussa, W.; Abdel-Wahab, M.; Fritsch, D. An automatic procedure for combining digital images and laser scanner data. *Int. Arch. Photogramm. Remote Sens. Spat. Inf. Sci.* **2012**, *39*, B5. [CrossRef]
35. Sipiran, I.; Bustos, B. Harris 3D: A robust extension of the Harris operator for interest point detection on 3D meshes. *Vis. Comput.* **2011**, *27*, 963. [CrossRef]
36. Pratikakis, I.; Spagnuolo, M.; Theoharis, T.; Veltkamp, R. A robust 3D interest points detector based on Harris operator. In *Eurographics Workshop on 3D Object Retrieval*; 2010; Volume 5, Available online: https://users.dcc.uchile.cl/~{}isipiran/papers/SB10b.pdf (accessed on 4 February 2021).
37. Tombari, F.; Salti, S.; Di Stefano, L. A combined texture-shape descriptor for enhanced 3D feature matching. In Proceedings of the 2011 18th IEEE International Conference on Image Processing, Brussels, Belgium, 11–14 September 2011; pp. 809–812.
38. Aldoma, A.; Marton, Z.C.; Tombari, F.; Wohlkinger, W.; Potthast, C.; Zeisl, B.; Rusu, R.B.; Gedikli, S.; Vincze, M. Tutorial: Point cloud library: Three-dimensional object recognition and 6 DOF pose estimation. *IEEE Robot. Autom. Mag.* **2012**, *19*, 80–91. [CrossRef]
39. Salih, Y.; Malik, A.S.; Walter, N.; Sidibé, D.; Saad, N.; Meriaudeau, F. Noise robustness analysis of point cloud descriptors. In *International Conference on Advanced Concepts for Intelligent Vision Systems*; Springer: Cham, Switzerland, 2013; pp. 68–79.
40. Rusu, R.B.; Blodow, N.; Marton, Z.C.; Beetz, M. Aligning point cloud views using persistent feature histograms. In Proceedings of the 2008 IEEE/RSJ International Conference on Intelligent Robots and Systems, Nice, France, 22–26 September 2008; pp. 3384–3391.
41. Filipe, S.; Alexandre, L.A. A comparative evaluation of 3D keypoint detectors in a RGB-D object dataset. In Proceedings of the 2014 International Conference on Computer Vision Theory and Applications (VISAPP), Lisbon, Porgutal, 5–8 January 2014; Volume 1, pp. 476–483.
42. Orts-Escolano, S.; Morell, V.; García-Rodríguez, J.; Cazorla, M. Point cloud data filtering and downsampling using growing neural gas. In Proceedings of the 2013 International Joint Conference on Neural Networks (IJCNN), Dallas, TX, USA, 4–9 August 2013; pp. 1–8.
43. Díaz-Vilariño, L.; Frías, E.; Balado, J.; González-Jorge, H. Scan planning and route optimization for control of execution of as-designed BIM. *Int. Arch. Photogramm. Remote Sens. Spatial Inf. Sci.* **2018**, *XLII-4*, 143–148. [CrossRef]
44. Heikkilä, R.; Kivimäki, T.; Mikkonen, M.; Lasky, T.A. Stop & Go Scanning for Highways—3D Calibration Method for a Mobile Laser Scanning System. In Proceedings of the 27th International Symposium on Automation and Robotics in Construction, Bratislava, Slovakia, 25–27 June 2010; pp. 40–48.
45. Vo, A.V.; Truong-Hong, L.; Laefer, D.F.; Bertolotto, M. Octree-based region growing for point cloud segmentation. *ISPRS J. Photogramm. Remote Sens.* **2015**, *104*, 88–100. [CrossRef]
46. Gesto-Diaz, M.; Tombari, F.; Gonzalez-Aguilera, D.; Lopez-Fernandez, L.; Rodriguez-Gonzalvez, P. Feature matching evaluation for multimodal correspondence. *ISPRS J. Photogramm. Remote Sens.* **2017**, *129*, 179–188. [CrossRef]
47. Holz, D.; Ichim, A.E.; Tombari, F.; Rusu, R.B.; Behnke, S. Registration with the point cloud library: A modular framework for aligning in 3-D. *IEEE Robot. Autom. Mag.* **2015**, *22*, 110–124. [CrossRef]
48. Golomb, S.W.; Baumert, L.D. Backtrack programming. *J. ACM* **1965**, *12*, 516–524. [CrossRef]
49. Dorigo, D. *Ant Colonies for the Traveling Salesman Problem*; Université Libre de Bruxelles: Brussels, Belgium, 1997; Volume 1, pp. 53–66.
50. Han, X.F.; Jin, J.S.; Wang, M.J.; Jiang, W.; Gao, L.; Xiao, L. A review of algorithms for filtering the 3D point cloud. *Signal Process. Image Commun.* **2017**, *57*, 103–112. [CrossRef]
51. Balta, H.; Velagic, J.; Bosschaerts, W.; De Cubber, G.; Siciliano, B. Fast statistical outlier removal-based method for large 3D point clouds of outdoor environments. *IFAC Pap. OnLine* **2018**, *51*, 348–353. [CrossRef]
52. Miknis, M.; Davies, R.; Plassmann, P.; Ware, A. Near real-time point cloud processing using the PCL. In Proceedings of the 2015 International Conference on Systems, Signals and Image Processing (IWSSIP), London, UK, 10–12 September 2015; pp. 153–156.
53. Miknis, M.; Davies, R.; Plassmann, P.; Ware, A. Efficient point cloud pre-processing using the point cloud library. *Int. J. Image Process.* **2016**, *10*, 63–72.
54. Ximin, Z.; Xiaoging, Y.; Wanggen, W.; Junxing, M.; Qingmin, L.; Libing, L. The Simplification of 3D Color Point Cloud Based on Voxel. In Proceedings of the IET International Conference on Smart and Sustainable City 2013 (ICSSC 2013), Shanghai, China, 19–20 August 2013.
55. Yu, T.H.; Woodford, O.J.; Cipolla, R. A performance evaluation of volumetric 3D interest point detectors. *Int. J. Comput. Vis.* **2013**, *102*, 180–197. [CrossRef]

56. Liu, J.; Jakas, A.; Al-Obaidi, A.; Liu, Y. A comparative study of different corner detection methods. In Proceedings of the 2009 IEEE International Symposium on Computational Intelligence in Robotics and Automation-(CIRA), Daejeon, Korea, 15–18 December 2009; pp. 509–514.
57. Alexandre, L.A. 3D descriptors for object and category recognition: A comparative evaluation. In Proceedings of the Workshop on Color-Depth Camera Fusion in Robotics at the IEEE/RSJ International Conference on Intelligent Robots and Systems (IROS), Vilamoura, Portugal, 7 October 2012; Volume 20, p. 7.
58. Besl, P.J.; McKay, N.D. Method for registration of 3-D shapes. In *Sensor Fusion IV: Control Paradigms and Data Structures*; International Society for Optics and Photonics: Bellingham, WA, USA, 1992; Volume 1611, pp. 586–606.
59. Sharp, G.C.; Lee, S.W.; Wehe, D.K. ICP registration using invariant features. *IEEE Trans. Pattern Anal. Mach. Intell.* **2002**, *24*, 90–102. [CrossRef]
60. Li, P.; Wang, R.; Wang, Y.; Tao, W. Evaluation of the ICP Algorithm in 3D Point Cloud Registration. *IEEE Access* **2020**, *8*, 68030–68048. [CrossRef]
61. Barnes, P.; Davies, N. *BIM in Principle and in Practice*; ICE Publishing: London, UK, 2015.
62. Rodríguez-Gonzálvez, P.; Garcia-Gago, J.; Gomez-Lahoz, J.; González-Aguilera, D. Confronting passive and active sensors with non-gaussian statistics. *Sensors* **2014**, *14*, 13759–13777. [CrossRef] [PubMed]

Capítulo III.

De la nube de puntos a los modelos FEM

3. De la nube de puntos a los modelos FEM

En este capítulo se exponen los resultados del artículo científico "*Integration of a wearable mobile mapping solution and advance numerical simulations for the structural analysis of historical constructions: A case of study in San Pedro church (Palencia, Spain)*", publicado en la revista científica *Remote Sensing* de MDPI en 2021.

Resumen

Si bien el uso de sistemas WMLS está teniendo un gran auge en patrimonio, su uso se restringe fundamentalmente a la obtención de la nube de puntos para la valorización o creación de cartografías básicas de dichas edificaciones, no existiendo investigaciones centradas en su explotación dentro del campo del diagnóstico y la conservación preventiva. Eco de ello, el artículo aquí presentado plantea el uso de los sistemas de escaneado móvil del tipo WMLS para generar modelos aptos con los que ejecutar simulaciones numéricas avanzadas utilizando el método FEM que sirvan para el diagnóstico de estas construcciones.

La metodología se comprobó en la Iglesia de San Pedro situada en Becerril del Carpio (Palencia). Esta iglesia sufrió un asentamiento en la parte norte de la nave central provocando la aparición de diferentes lesiones de carácter geométrico (deformaciones y grietas). El trabajo de restauración llevado a cabo para estabilizar el edificio consistió en recalzar la cimentación del lado norte y reforzar el extradós de la bóveda con un mortero con fibras de basalto. El método presentado en este artículo abre un nuevo abanico de posibilidades para la utilización de sistemas WMLS en el diagnóstico de construcciones históricas, que a día de hoy no se ha explorado.

Los objetivos de partida de la investigación son dos: i) utilizar los sistemas WMLS en edificación histórica para obtener modelos 3D aptos para análisis estructurales y ii) entender el comportamiento estructural de nuevas soluciones de restauración, basadas en morteros reforzados con fibras, utilizando para ello simulaciones numéricas del tipo FEM.

El artículo, tras una introducción y una descripción del edificio objeto de estudio en el que se incluye su estado de conservación y las diferentes intervenciones previas a las que fue sometido, consta de cuatro fases, que pasan a describirse a continuación:

- Captura de datos: la digitalización de la iglesia se realizó utilizando el sistema de escaneado móvil del tipo WMLS, que como ya se demostró en artículos anteriores permite digitalizar de manera rápida escenarios complejos y angostos con una precisión de entre 1-3 cm. La metodología seguida fue la propuesta en Capítulo I: Guía de buenas prácticas. Se realizó un único recorrido con una duración de 18 minutos y obteniendo una nube de puntos de 27 millones de puntos, incluyendo el interior y el exterior de la iglesia.
- Procesado de la nube de puntos: La nube de puntos obtenida contiene ruido debido al propio láser y a la deriva de la estimación de la técnica SLAM. Para mejorar la calidad de la nube de puntos y los resultados posteriores, se realizó un filtrado de ruido, utilizando un filtro anisotrópico [91] que es capaz de eliminar el ruido manteniendo los detalles y bordes originales sin necesidad de definir ninguna variable para su ejecución. Dicho

filtro viene a mejorar los resultados que se obtienen con la aplicación de un filtro tipo FSOR (analizado en el Capítulo II). La mejora otorgada por el filtro fue analizada a través de un estudio estadístico con estimadores robustos no paramétricos [134]. En este caso se tomó como "verdad terreno" la nube de puntos capturada con un TLS en trabajos previos. Los resultados de aplicar este filtro demuestran que dicho procesado básico es capaz de reducir el error de la nube de puntos WMLS.

- Generación del modelo CAD As-Built: la creación del modelo CAD se llevó a cabo de manera semiautomática utilizando principalmente formas paramétricas a través del algoritmo RANSAC Shape Detector y de estrategias no paramétricas tipo NURBS. Los muros verticales sin deformaciones no-lineales complejas se modelaron de manera automática con el algoritmo RANSAC Shape Detector, que ajusta el mejor plano a los puntos candidatos. Aquellos muros con deformaciones complejas fuera del plano se ajustaron mediante el uso de NURBS. Asimismo, la bóveda de cañón se modeló mediante NURBS dada su complejidad geométrica. Finalmente, para los arcos se extrajo su sección y se aplicó una extrusión. Como resultado se obtiene un modelo CAD completo, con discrepancias menores al centímetro, respecto a la nube de puntos filtrada anteriormente. Dichas discrepancias se obtuvieron aplicando una comparativa (cloud-to-mesh) entre la nube de puntos y el modelo CAD generado, y obteniendo la máxima distancia entre ambos.
- Análisis estructurales: El análisis estructural se llevó a cabo utilizando la estrategia FEM, para evaluar desde un punto de vista estático y dinámico la influencia del mortero reforzado con fibras, añadido al extradós de las bóvedas en las actuaciones previas. Dicho análisis tuvo como principal objetivo ver el impacto de este tipo de actuaciones, que son altamente intrusivas en el comportamiento global de la iglesia. Para ello se siguió una metodología de tres pasos: i) se generó una malla numérica a partir del modelo CAD, ii) se definieron los modelos constitutivos de los materiales, y iii) se realizaron los diferentes análisis numéricos para evaluar el comportamiento estructural frente a cargas verticales (gravedad) y horizontales (sísmicas). Dado que se quería comprobar la contribución que las capas de mortero aportan al edificio, se realizaron dos tipos de simulaciones: una sin considerar el mortero y otra considerando el mortero, de manera que pudieran analizarse las diferencias. En ambos casos se aumentó la carga hasta el colapso del edificio.

Los resultados obtenidos en este artículo demuestran que, en ausencia de problemas de suelo, la iglesia estudiada es segura y capaz de soportar una gran carga gravitacional, sin que el mortero de refuerzo tenga una influencia especial; es decir, tanto con el mortero como sin él, la estructura es segura. El factor de seguridad es de 8.86 sin la capa de refuerzo y de 9.03 con la misma, es decir que sin la capa de refuerzo el edificio es capaz de soportar 8.86 veces su peso y con la capa de refuerzo la resistencia aumenta hasta 9.03 veces su propio peso. Con respecto a las cargas sísmicas, el edificio es seguro y se encuentra dentro de los límites establecidos, pero en este caso se ha comprobado que las capas de mortero aumentan la capacidad sísmica del edificio en casi un 115%.

Las conclusiones que se obtienen de este artículo son varias: i) los equipos de escaneado móvil del tipo WMLS son aptos para digitalizar edificios muy complejos y utilizar los datos obtenidos en análisis estructural, ii) los sistemas WMLS tienen una aplicabilidad muy flexible y un gran rendimiento (con tiempos para obtener la nube de puntos del orden de la décima parte que con el TLS), principalmente gracias a su portabilidad, iii) los datos obtenidos han de ser procesados para eliminar el ruido y homogeneizar los puntos, iv) el filtro anisotrópico es capaz de filtrar el

ruido de estos dispositivos eficazmente sin que se pierda la geometría, v) la digitalización con WMLS permite poder pasar de las nubes de puntos a modelos CAD as-built de manera semi automática utilizando formas paramétricas y no paramétricas, disminuyendo considerablemente el trabajo de modelado y obteniendo modelos precisos, con discrepancias inferiores a un centímetro y, vi) en relación con los análisis de estructuras ejecutados, se concluye que las capas de mortero aumentan la capacidad sísmica de la estructura estudiada, mientras que para cargas verticales las capas mortero no cambian el comportamiento del edificio.

remote sensing

MDPI

Article

Integration of a Wearable Mobile Mapping Solution and Advance Numerical Simulations for the Structural Analysis of Historical Constructions: A Case of Study in San Pedro Church (Palencia, Spain)

Luis Javier Sánchez-Aparicio [1,2,*], Rocío Mora [2], Borja Conde [3], Miguel Ángel Maté-González [2,4,5], María Sánchez-Aparicio [2] and Diego González-Aguilera [2]

[1] Department of Construction and Architectural Technology (DCTA), Escuela Técnica Superior de Arquitectura de Madrid (ETSAM), Universidad Politécnica de Madrid, Avda. Juan de Herrera 4, 28040 Madrid, Spain
[2] Department of Cartographic and Land Engineering, University of Salamanca, High Polytechnic School of Ávila, Hornos Caleros, 50, 05003 Ávila, Spain; rociomora@usal.es (R.M.); miguelangel.mate@upm.es (M.Á.M.-G.); mar_sanchez1410@usal.es (M.S.-A.); daguilera@usal.es (D.G.-A.)
[3] Department of Engineering Materials, School of Industrial Engineering, University of Vigo, 36208 Vigo, Spain; bconde@uvigo.es
[4] Department of Topographic and Cartography Engineering, Higher Technical School of Engineers in Topography, Geodesy and Cartography, Universidad Politécnica de Madrid, Mercator 2, 28031 Madrid, Spain
[5] Department of Environment, Land and Infrastructure Engineering, Politecnico di Torino, 10129 Torino, Italy
* Correspondence: lj.sanchez@upm.es; Tel: +91-336-65-14

Citation: Sánchez-Aparicio, L.J; Mora, R.; Conde, B.; Maté-González, M.Á.; Sánchez-Aparicio, M.; González-Aguilera, D. Integration of a Wearable Mobile Mapping Solution and Advance Numerical Simulations for the Structural Analysis of Historical Constructions: A Case of Study in San Pedro Church (Palencia, Spain). *Remote Sens.* **2021**, *13*, 1252. https://doi.org/10.3390/rs13071252

Academic Editors: Francesca Cigna and Nicola Masini

Received: 30 January 2021
Accepted: 22 March 2021
Published: 25 March 2021

Publisher's Note: MDPI stays neutral with regard to jurisdictional claims in published maps and institutional affiliations.

Abstract: This work aims at enhancing the current methodologies used for generating as-built CAD models suitable for advanced numerical simulations. To this end, this paper proposes the use of a wearable mobile mapping system that allows one to improve the digitalization stage in terms of flexibility and time required. The noise showed by the resulting point cloud, based on the simultaneous location and mapping (SLAM) solution, demands a post-processing stage that introduces the use of a parameter-free noise reduction filter. This filter improves the quality of the point cloud, allowing for the adjustment of surfaces by means of parametric and non-parametric shapes. These shapes are created by using reverse engineering procedures. The results showed during this investigation highlight a novel application of this sensor: the creation of as-built CAD models for advanced numerical simulations. The results of this investigation are complemented by a valuable contribution with respect to the use of an advanced restoration solution, by means of textile reinforced mortar. To this end, the CAD model is used as the geometrical base for several numerical simulations by means of the finite element method. All this procedure is applied in a construction with structural problems.

Keywords: geoinformatics; wearable mobile mapping; historical construction; masonry; finite element method; pushover analysis

1. Introduction

The modern concept of the restoration and conservation of historical constructions demands the use of multidisciplinary and scientifically proved approaches able to study the building from different points of view. Inside this context, the analysis of the structural stability of the building plays an essential role in the design of a proper restoration action or conservation plan. Nowadays, there are plenty of applications able to simulate the structural stability of historical constructions, from classical approaches based on the limit

analysis theory to modern computational strategies that use the discrete or the finite element method (FEM) [1]. FEM could be considered as one of the most powerful and versatile strategies, able to simulate different scenarios such as material losses, construction stages, seismic events or settlements among others [2–4]. Within this context, there are several investigations that highlight the necessity of having rigorous structural mapping and the consequent numerical implementation, especially against seismic events on which the construction could suffer redundant structural damages [5–8]. According to this, a proper survey and building mapping is required for an adequate numerical simulation, demanding the proper integration of different approaches coming from the geoinformatics. This discipline is able to provide a set of remote sensing approaches, such as static terrestrial laser scanning or photogrammetry (especially by means of the structure from motion approach), that can create as-built CAD models [2,3,9–11]. These methods allow one to digitalize historical structures in form of point clouds. Then, these point clouds are post-processed to adapt it to further numerical evaluations. One of the most recent methods to pass from the point cloud to the numerical model is the Cloud2FEM method developed by Castellazzi et al.[12]. This method transforms the point cloud into a solid model by means of voxel elements. Another recent method is the approach proposed by Gonizzi et al. [13]. This approach is based on the use of a retopologization of the mesh, allowing to create as-built CAE models. Both strategies require a point cloud with the absence of holes, not controlling the level of detail introduced in the numerical simulation as well as requiring further post-processing in the case of introducing different types of materials or even construction joints. In contrast to this, it is possible to find alternatives in the literature based on the use of the latest advances in reverse engineering procedures [3,14]. This approach is able to manage the level of detail of the final model as well as to represent the construction imperfections [14] or even complex deformation by means of non-uniform rational basis splines (NURBS) surfaces with great accuracy [3], making it possible to manage incomplete point clouds. These types of surfaces are mathematical models based on the use of basis splines (B-splines) curves that allow one to model complex non-parametric surfaces with great accuracy. To this end, the NURBS surface uses a set of control points with different weights, as well as a set of B-splines on orthogonal directions which can be defined by a bi-variable local coordinate system made up by *U* and *V* axes. Large values of control points along its local direction (*U* or *V)* imply higher computational costs but more accurate results in this direction [15]. In all the cases previously showed, the digitalization of the structure is required by means of remote sensing strategies.

Since its early development in 1980, hybrid solutions such as the mobile mapping system (MMSs) have emerged as a potential alternative to structure from motion (SfM) and static laser scanning approaches [16]. These devices combine the spatial referencing provided by a position unit with the geometrical data captured by a mapping sensor (laser scanner head or a digital camera) [16] through the use of the so-called simultaneous location and mapping approach (SLAM) [17]. This combination places this approach as the most effective digitalization strategy, especially in complex scenarios on which a large number of scan stations, or even a complex photogrammetric network are required [16,18]. The studies carried out by Fillipo et al. [19]; Barba at al. [20] or Sánchez-Aparicio et al. [21] highlights its efficiency, making it possible to minimize in around 10 times the effort required for digitalizing this scenario by means of a static laser scanner. Inside the different MMSs available nowadays, the wearable mobile mapping solutions (WMMS) are one of the most used. Basically, these devices are adapted to be easily carried by a person, making it possible to digitalize a scenario simply by walking. Its flexibility allows one to digitalize a wide variety of Cultural Heritage (CH) scenarios, which are commonly characterized by the presence of complex and narrow spaces [20–23], or even large surfaces [18,19]. Barba et al. [20] present a work on which a WMMS is used in the inner part of the Chapel of the Holy Shroud with the presence of narrow spaces. Nocerino et al. [22] use this solution to digitalize an underground Word War fortress. It is worth

mentioning that the main application of the point cloud obtained by this type of sensor is mainly focused on the extraction of basic cartographic products, such as plants or sections [19,21], as well as for the dissemination and valorisation of CH scenarios [22]. Its use within the diagnosis of historical constructions, i.e., for the creation of advanced numerical simulations, is an open issue nowadays without research works focused on this. In this sense, Sánchez-Aparicio et al. [21] make a comparison, from the structural point of view, between a WMMS and a high precision static laser scanner. To this end, two different 2D finite element simulations were created and simulated. One was based on the data captured by a WMMS and another one based on the terrestrial laser scanner (TLS) point cloud. The results obtained highlights the potentialities of this approach in contrast with the traditional ones, obtaining a discrepancy of about 3% in terms of safety factor and showing the same collapse mechanism [21].

Another relevant issue for the restoration of historical constructions concerns the use of suitable retrofitting techniques. These types of interventions demand the development of extensive experimental campaigns, monitoring tasks as well as numerical analysis that allows one to have a complete knowledge of the construction and its history [24]. Nowadays there are plenty of applications that allow one to restore historical constructions depending on the symptoms showed. Within this complex context, the use of textile reinforced mortars (TRMs) has gained remarkable attention over the last few years [25]. This type of solution is a composite material made up by fibre roving embedded in an inorganic matrix, improving the mechanical behaviour of masonry structures against axial loads, in-plane shear/flexure and out-of-plane flexure. Several studies can be found in the most recent literature highlighting its suitability and efficiency in historic masonry structures, especially in the case of strengthening against seismic actions [26–28], demanding the use of experimental campaign as well as the development of proper numerical models able to simulate its particular mechanical behaviour against different events [26].

Under the basis previously exposed, this work aims at improving the current methodologies for generating as-built CAD models for advanced 3D numerical simulations. To this end, the proposed approach investigates the use of a WMMS solution with the aim of minimizing the time invested for creating 3D CAD models by means of reverse engineering approaches. Additionally, this paper evaluates the use of a parameter-free noise reduction filter. These types of filters are not commonly used due to the robustness of the static approaches [3,10]. However, investigations carried out by Nocerino et al. [16], Fillipo et al. [19] and Barba et al. [20] highlight the presence of a certain noise in the MMS's point clouds that could hinder the creation of surfaces required for reverse engineering. With respect to the previous work carried out by the authors [21], this work proposes a methodology for using the WMMS point cloud as a geometrical base for 3D CAD models. This methodology includes the use of several automatic segmentation approaches based on the random sample consensus (RANSAC) method, the use of NURBS approaches as well as the use of an anisotropic filter in order to enhance the quality of the 3D point cloud obtained by the WMMS.

Apart from contributing to the improvement of creating as-built CAD models, this work advances in the knowledge of the structural behaviour of novel constructive solutions, more specifically TRM retrofitting techniques. To this end, a retrofitted masonry construction was analysed: the Romanesque church of San Pedro in Becerril del Carpio (Palencia, Spain), allowing one to obtain conclusions about the efficiency of this type of solution against vertical and horizontal loads.

After the Introduction, Section 2 describes the study case used as well as its current conservation status. Section 3 presents the methodology used for generating an advanced numerical simulation using a WMMS. Section 4 shows the numerical simulations carried out, confronting the structural performance of the church with and without TRM layers on the extrados of its vaults. In Section 5, the discussions and conclusions are drawn.

2. The Romanesque Church of San Pedro (Becerril del Carpio, Palencia, Spain)

2.1. Description of the Structure

The Catholic church of San Pedro is located at the municipality of Becerril del Carpio in the province of Palencia (Castilla y León, Spain) (Figure 1). The construction of the church started in 1262, showing some elements, such as the apse, in the Late-Gothic style.

Figure 1. Location of the Romanesque church of San Pedro (Becerril del Carpio, Spain).

The church has a unique nave with a length of 23.71 m and a width of about 8.78 m. This nave shows a Late-Romanesque barrel vault with around 0.31 m thickness and an eight ribbed vault in the apse and a tower at its beginning [21] (Figure 2). Between the barrel and the ribbed vault, is possible to observe a triumphal arch supported by two columns with Gothic capitals. Both constructive elements were built with a regular sandstone masonry. The vertical walls that support the vaults respond to a typical three leaf masonry wall made up by two faces of regular sandstone and an infill core. The north-east wall has an average width of 0.87 m with a total of four buttresses made up with regular sandstone. On the other hand, the south-east wall has an average width of 1.43 m without the presence of buttresses (Figure 2b). The tower was built with a regular limestone masonry, showing in the east part of it a space made up by regular sandstone and brick masonry. The body annexed to the main nave serves nowadays as sacristy and is covered by an eight-side ribbed vault (Figure 2c).

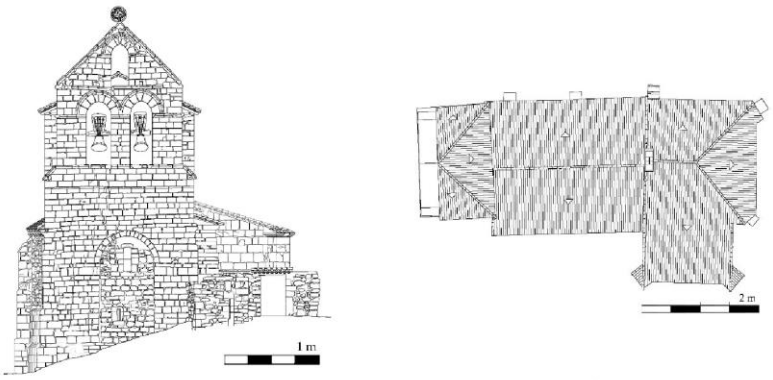

(**a**) (**b**)

(**c**) (**d**)

Figure 2. Planimetry of the church: (**a**) main elevation; (**b**) top view; (**c**) longitudinal section and (**d**) transversal section.

2.2. Intervention Works Carried Out during 2011

In 2007, the conservation status of the church was considered deficient. This status was promoted by the lack of conservation actions, such as the presence of biological colonies, moistures as well as garbage. All these elements were accelerating the degradation of the different assets placed within the church. Additionally, a modification of the soil properties promoted the presence of a settlement on the north part of the church. In response of this soil modification, the main nave of the church suffered a large movement to adapt its shape to the new boundary conditions. Several cracks appeared along the tower and the annexed body as well as out-of-plane movement in the north part of the main nave within the presence of several plastic hinges along the vaults (Figure 3).

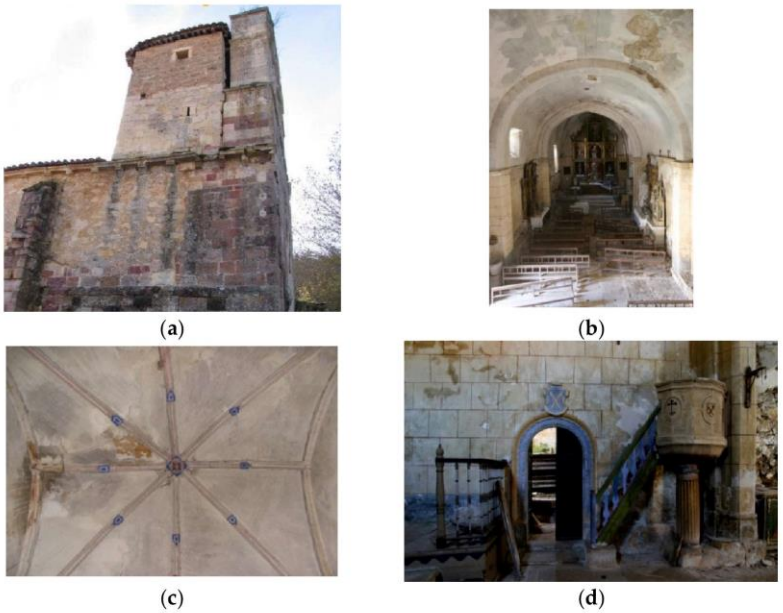

(**a**) (**b**)

(**c**) (**d**)

Figure 3. Conservation status before the intervention: (**a**) structural movement of the tower; (**b**) large deformation in the main nave; (**c**) cracks, moisture and detachment on the ribbed vault and (**d**) presence of moisture, erosions, detachment and garbage at the entrance of the annexed body.

According to this condition, a diagnosis work was carried out with the aim of investigating the origin of the different damages observed. In line with the result obtained during the diagnosis phase, a restoration project was carried out in 2011 acting in different parts of the church: (i) the assets and (ii) the structure. The latter was retrofitted by adding an armoured concrete solution made up by a concrete HA-25 (equivalent to a C25/30 in the Eurocode 2) as well as a steel B-500S (equivalent to a S500 in the Eurocode 2) (Figure 4a) [29]. Complementary to this action, the extrados of the vaults was retrofitted with a TRM solution. This composite solution was made up by a lime matrix with carbon fibres, adding a total of three layers, each one with an average thickness of 10 mm (Figure 4b,c). The original roof of the church, made up by an infill layer until the tiles, was replaced by a timber solution with cross-laminated beams supported at both side of the nave and covered by a waterproof solution and ceramic tiles (Figure 2c,d) (Figure 4d).

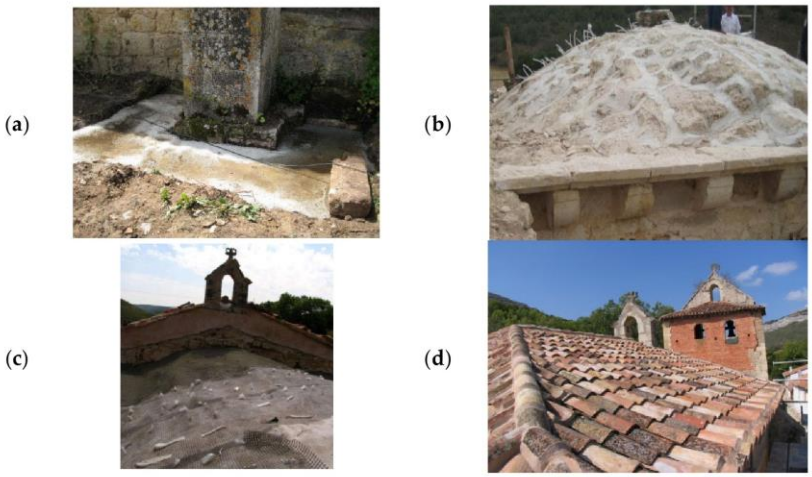

Figure 4. Restoration works at structural level: (**a**) addition of armoured concrete to one of the buttresses of the main nave; (**b**) preparation of the extrados surface of the ribbed vault for the application of the textile reinforced mortar (TRM) layers; (**c**) application of the TRM solution and (**d**) final appearance of the roof.

3. From the Point Cloud to the As-Built CAD Model

As it was stated in Section 2, the structure of the church has suffered large deformations as a result of a soil settlement. This situation has promoted the presence of complex out-of-plane deformations at the south part of the nave, the tower, as well as the ribbed vaults of the main nave (Figure 3). All of this demands the use of remote sensing methodologies able to create, in an efficient way, an as-built CAD model for further numerical simulations. According to this, a three-fold workflow was proposed as follows: (i) 3D digitalization of the heritage site by using a WMMS system equipped in a small backpack; (ii) point cloud post-processing by applying noise reduction filters and (iii) CAD modelling through the use of parametric and NURBS surfaces. All these stages are described in detail in the following sections.

3.1. Wearable Mobile Mapping System (WMMS)

The WMMS used for the present work was the ZEB-REVO mobile mapping system [30]. This device is commercialized by the company GeoSLAM [31] and it is made up by a 2D rotating laser scanner head, Hokuyo UTM-30LX-F (Hokuyo Automatic Co., Ltd. Osaka, Japan) rigidly coupled to an Inertial Measurement Unit (IMU) on a rotary engine. The data captured by both sensors is stored in a processing unit located in a small

backpack (Figure 5). All these devices are carried by an operator, whose movement provides the third dimension required to generate the 3D point cloud. The 3D point cloud is generated by combining the information coming from the scanning head and the IMU sensor, using to this end the full SLAM approach of the robotic operative system (ROS) library [32]. It must be taken into consideration that the previous process is an incremental procedure, in which each segment is aligned with respect to the previous one. The error accumulation derived from the incremental procedure is minimized by a global registration on the basis that the starting and ending points are the same (closed-loop solution).

(**a**) (**b**)

Figure 5. Wearable mobile mapping system used: (**a**) main components and (**b**) photo taken during the data acquisition.

This sensor has a default range of 0.60–30 m for indoors environments and 0.60 to 15 m for outdoors, capturing 40,000 points per second. This device is also equipped with a GoPro camera that allows one to record a video while the laser is capturing the scene. The manufacturer ensures an accuracy of 1–3 cm for a 10-min scan, with the closing of a single loop [30]. Table 1 shows further technical specifications.

Table 1. Technical specifications of the wearable mobile mapping solution (WMMS) used.

WMLS Zeb REVO	
Measuring principle	Time of flight
Operating time	4 h
Field of view	270° (H) × 360° (V)
Wavelength (nm)	905
Scanner resolution (°)	0.625 H × 1.8 V
Orientations system	MEMS IMU
Scanner dimensions (mm)	86 × 113 × 287
Total weight (kg)	4.10
Scanner weight (kg)	1.00
Dimensions (mm)	220 × 180 × 470
Working range (m)	0.60–30 m indoors 0.60–15 outdoors
Measurement rate	40,000 points per second
Accuracy (cm)	1–3

3.2. Digitalization of the Structure

The WMMS device previously described was used for digitalizing the church. Prior to the data acquisition with the WMMS device, an on-site inspection was carried out with the aim of designing the most appropriate data acquisition protocol, taking into account the suggestions proposed by di-Filippo et al. [19], with the following statements standing out: (i) ensuring the accessibility to all the areas; (ii) removing obstacles along the way and, (iii) planning a closed-loop in order to compensate for the error accumulation. During the data acquisition, a closed-loop path was followed with the aim of compensating the drift of the system (Figure 6). In order to ensure a homogenous density of the point cloud, the walking speed was constant, paying a special attention to transition areas such as corners or entrances.

According to these considerations, a unique loop was necessary to digitalize the outdoors as well as the indoors of the church, investing a total of 16 min. Then, a full SLAM approach was applied, allowing one to fuse the data captured by the IMU and the line scanner. To this end, the ROS library was used [32] by applying the parameters suggested by di Filippo et al. [19]. This stage required a total of 18 min to be completed, allowing one to obtain a complete digitalization of the church made up by 27 million points (Figure 7). The absolute error of this 3D point cloud in comparison with a TLS one was of 0.007 m [21].

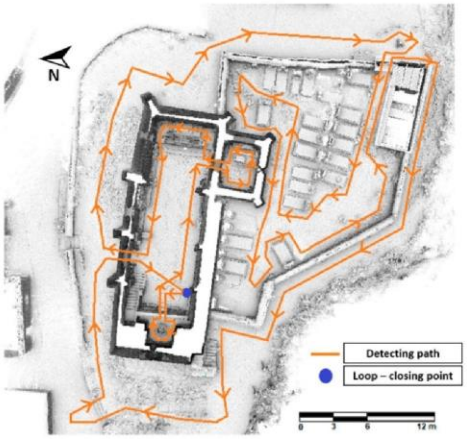

Figure 6. Path followed during the data acquisition.

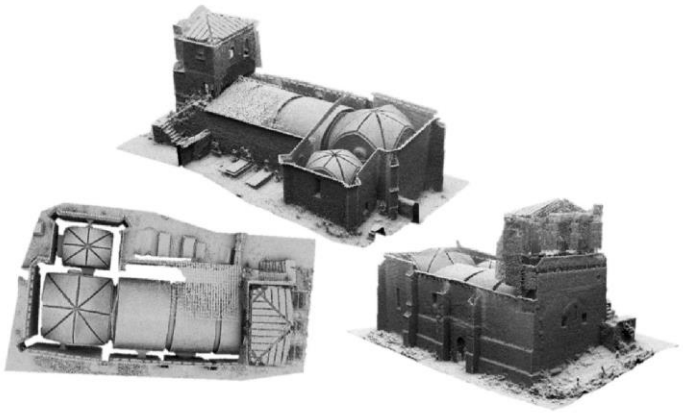

Figure 7. General view of the point cloud obtained.

3.3. Point Cloud Post-Processing

Considering the product derived from the previous stage, a noise filtering stage was performed with the aim of improving the quality of the point cloud for the subsequent stages. In the case of the WMMS point cloud, the noise is dependent on the laser scanner as well as of the drift that appears during the pose estimation carried out by the SLAM algorithm. In this case, it was decided to split the whole point cloud of the church in nine different test areas, considering that in each area the SLAM drift could be neglected (Figure 8). Each of these test areas were aligned with respect to its homologous TLS point cloud. The TLS point cloud used was the point cloud captured during the experimental works carried out by Sánchez-Aparicio et al. [21]. After the proper alignment, a segmentation phase was carried out with the aim of deleting the non-overlapped areas between the WMMS and the TLS point cloud.

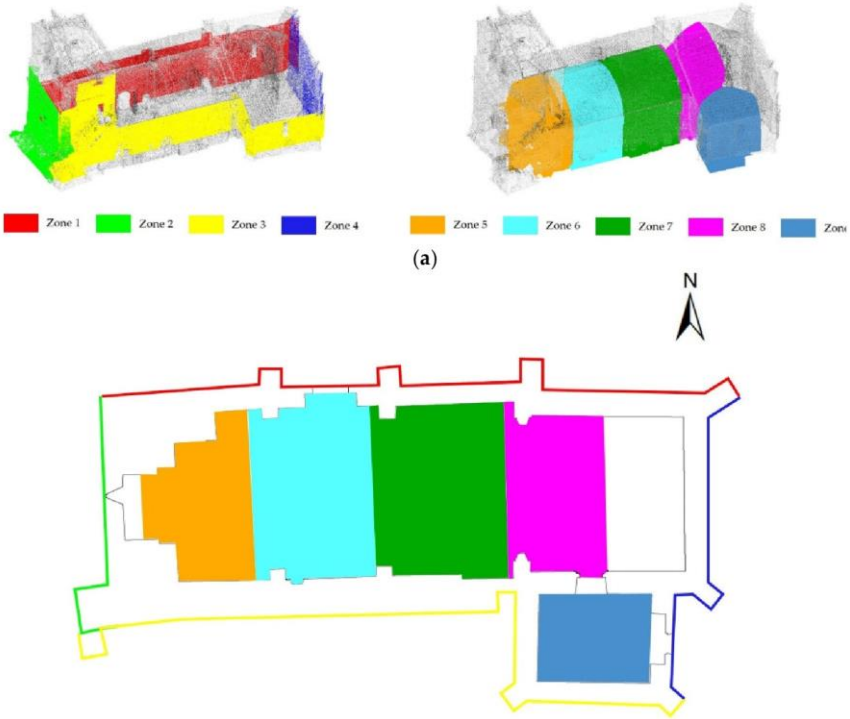

Figure 8. Test zones considered for evaluating the performance of the noise reduction filter: (**a**) 3D view and (**b**) plant view.

Nowadays, there are plenty of filters that attempt to reduce the noise of point clouds. An example of this variety of filters is the fast cluster statistical outlier removal (FCSOR) [33]. This filter improves the traditional statistical outlier removal (SOR) filter by getting a homogeneous point cloud and performing the statistical analysis over different voxelized parts at the same time. The process is faster, obtaining better results than the traditional SOR filter. Within the emerging field of deep learning there are some filters such as PCPNET [34] and PointCleanNet [35] which estimate local shape properties from

noisy and outlier-ridden point sets. Both methods, based on PointNet library [36], compare the noisy point clouds with the clean point cloud in order to train a convolutional neural network that allows one to reduce the noise. For this work, it was decided to use the algorithm proposed by Xu and Foi [37]. This denoising strategy is based on aggregation of multiple polynomial surfaces computed on directional neighbourhoods. These neighbourhoods are locally adapted in accordance with the shape of the point cloud by using the local polynomial approximation-intersection of confidence intervals strategy over each point of the point cloud. Finally, a dense aggregation of moving least squares is applied to denoise the point cloud. As suggested by Xu and Foi [37], this algorithm is able to reduce the noise while preserving fine features as well as sharp edges. It is worth mentioning that the TLS point cloud obtained by Sánchez-Aparicio et al. [21] in this church was considered with the aim of evaluating the performance of this algorithm. Thus, the discrepancies of the WMMS point cloud and the TLS point cloud could be considered a valid metric for evaluating the quality of the denoised WMMS point cloud. These discrepancies, before and after the application of the filter, were obtained by using the cloud-to-cloud comparison available in the open-source software CloudCompare® [38]. Before applying the filter (Figure 9a) the maximum discrepancies between clouds is 3 cm and 78% of the points have an error below 1 cm. After applying the filter (Figure 9b), the maximum discrepancies are 2 cm and 95% of the points have less than 1 cm of difference.

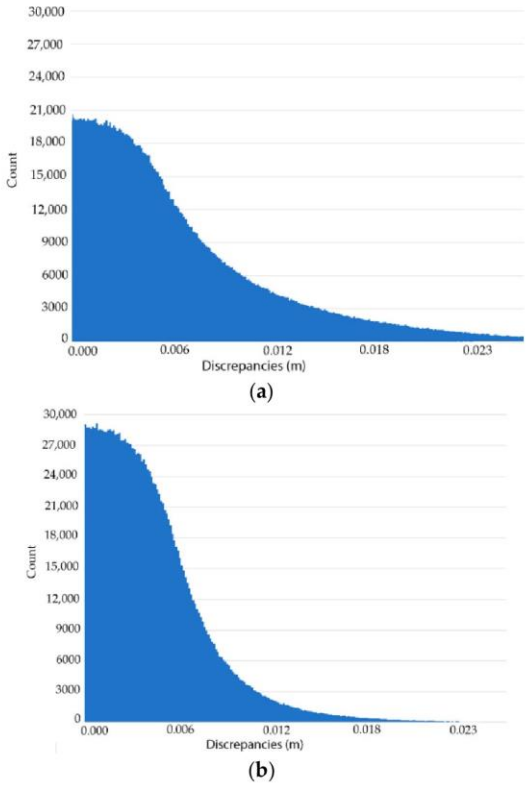

Figure 9. Histograms of the relative discrepancies between the terrestrial laser scanner (TLS) and the WMMS in the test zone 3: (**a**) before applying the filter, the maximum error is 3 cm and around 80% of the data are below 1 cm of error and (**b**) after the application of the noise reduction filter, the maximum error is 2 cm and 95% of the data are below 1 cm of difference.

As highlighted by Rodriguez-González et al. [39]; the use of Gaussian estimators (i.e., mean and standard deviation) would be not appropriate to evaluate the discrepancies between two point clouds. According to this, the normality of the samples was evaluated by means of the QQ-plot. The results obtained by the application of the QQ-plots showed that the discrepancies do not follow a normal distribution (Figure 10), requiring to use non-parametric indexes such as the median (m) and the NMAD values (Equations (1) and (2)).

$$NMAD = 1.4826 \cdot MAD, \quad (1)$$

$$MAD = m \cdot (|x_i - m_x|), \quad (2)$$

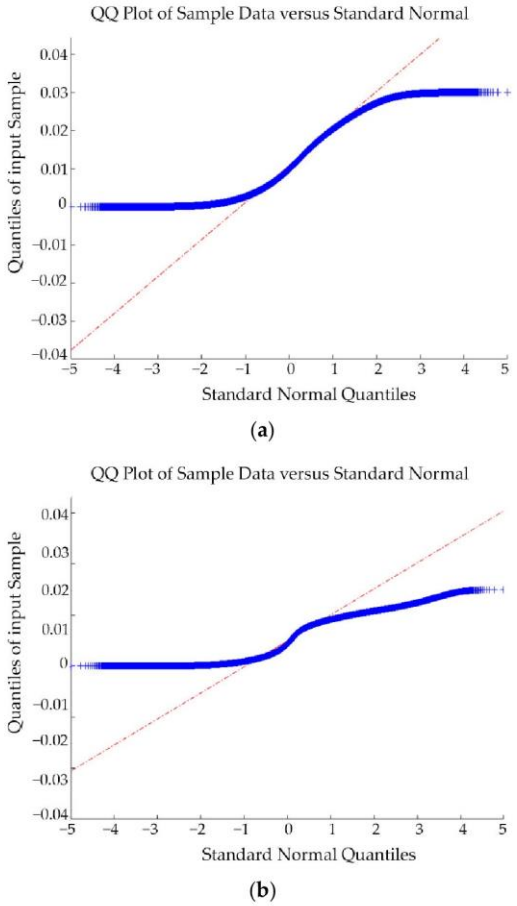

(**a**)

(**b**)

Figure 10. QQ-plots of the relative discrepancies between the TLS and the WMMS in the test zone 3: (**a**) before and (**b**) after the application of the noise reduction filter. In blue, the deviation of the quantiles position of the sample in comparison with expected quantiles for a normal distribution. In red, the trend line for a perfect Gaussian population.

Table 2 shows the statistical results obtained in the different test areas. As it was expected, the median value obtained was low due to the decision to evaluate small areas which were registered by means of the ICP algorithm. The NMAD values before noise reduction were in accordance with the expected errors of the WMMS point cloud. Both

estimators, median and NMAD, improve with the application of the anisotropic filter. This improvement is also visible from a qualitative point of view (Figure 11).

Table 2. Statistical results over different zones of the point clouds. On the left, it is shown the results before applying the anisotropic filter and on the right, the results after the filter has been applied.

Cases	Without Noise Reduction		With Noise Reduction	
	Bias	Dispersion	Bias	Dispersion
	Median (m)	NMAD (m)	Median (m)	NMAD (m)
Case 1	0.005	±0.004	0.003	±0.002
Case 2	0.005	±0.004	0.003	±0.003
Case 3	0.005	±0.004	0.004	±0.003
Case 4	0.005	±0.005	0.004	±0.003
Case 5	0.005	±0.005	0.003	±0.003
Case 6	0.005	±0.005	0.002	±0.002
Case 7	0.010	±0.009	0.008	±0.005
Case 8	0.007	±0.007	0.005	±0.005
Case 9	0.014	±0.011	0.010	±0.009

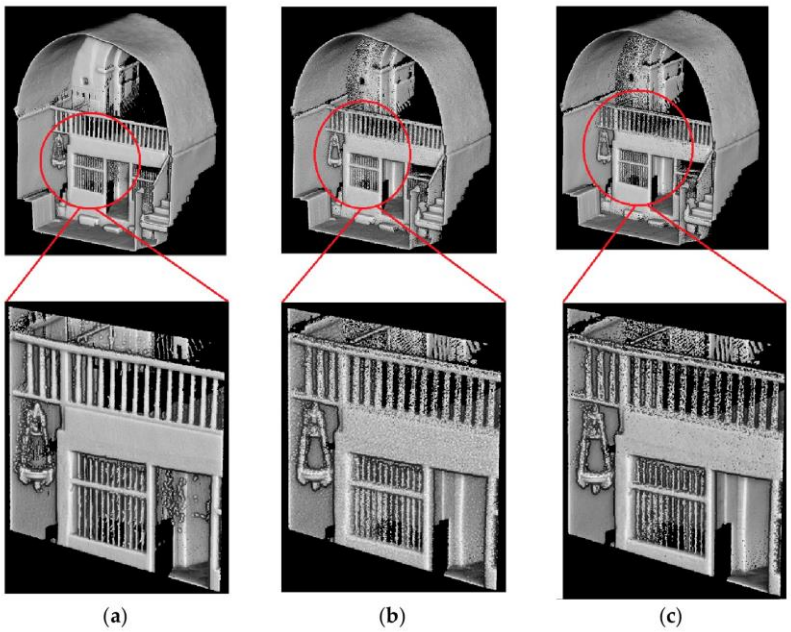

(**a**) (**b**) (**c**)

Figure 11. Noise reduction stage within the test zone 5: (**a**) reference point cloud coming from the TLS campaign; (**b**) original WMMS point cloud and (**c**) filtered WMMS point cloud.

3.4. Reverse Engineering

The current section shows the semi-automatic reverse engineering procedure used to obtain the as-built CAD model from the WMMS point cloud (Figure 12).

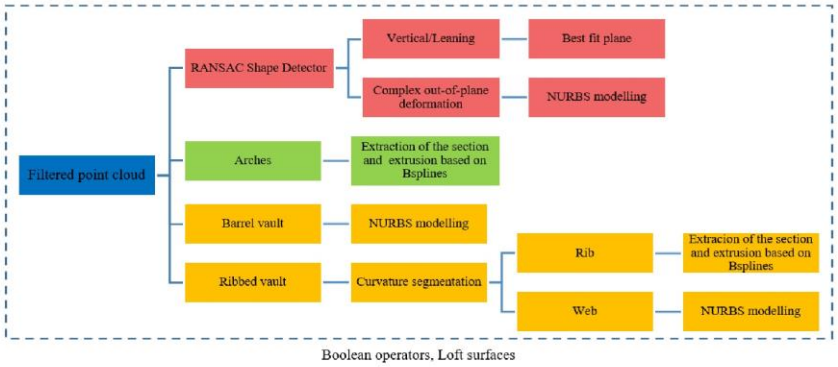

Figure 12. Graphical workflow proposed for creating the as-built CAD model. The red rectangles are those stages used for modelling the masonry wall. The green and orange rectangles include the strategies for modelling the arches and the vaults, respectively. RANSAC: random sample consensus.

In a first stage, the procedure defined by Sánchez-Aparicio et al. [40] for extracting and evaluating the deformation of vertical walls was applied. The results allow us to classify the walls into two groups (Figure 13): (i) vertical/leaning walls and (ii) walls with complex out-of-plane deformations. The vertical/leaning walls were modelled by adjusting its points to the best-fit plane. The parameters of this plane are those obtained by the random sample consensus (RANSAC) shape detector algorithm [41]. On the other hand, the walls with complex out-of-plane deformations were modelled by using the surface deformation approach suggested by Barrazzetti et al. [15]. This approach allows one to model complex surfaces, i.e., organic shapes, vaults or deformed constructive elements, by a progressive modification of a seed surface, transforming it into a NURBS surface that follows the point cloud closely. The modification of this surface is carried out by varying the weights, control points and knot vectors of the NURBS surface until the adjustment is reached. To this end, a planar seed surface with a total of 32 subdivisions along the U and V axis was considered. These parameters allow one to model the north walls with great accuracy (Figure 13).

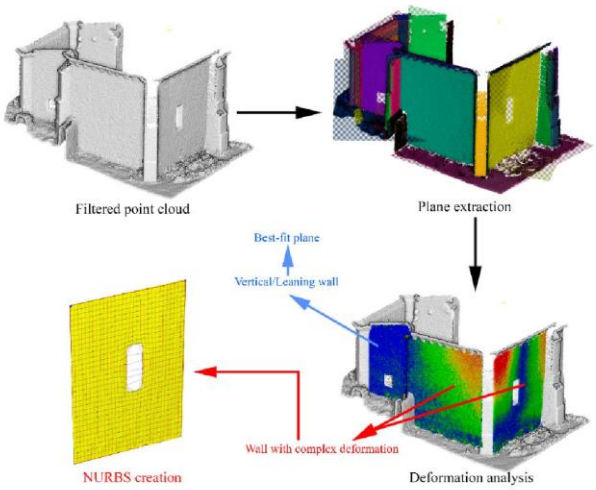

Figure 13. Workflow used for modelling walls.

The different arches of the main nave were modelled as follows: (i) the extraction and vectorization of a transversal and longitudinal section at the middle of the arch by using b-splines and (ii) the extrusion of the transversal section along the longitudinal one. On the contrary, the vaults were modelled by using the surface deformation approach previously defined. On the one hand the barrel vault was modelled directly, meanwhile the ribbed vaults were modelled by using a three-fold approach. Firstly, a segmentation based on curvature was applied, allowing one to split the ribs from the webs. Then, the ribs were modelled in a similar way to the arches, simplifying its original shape to a rectangular one with the same inertial values. Finally, the different webs of the vault were modelled using the surface deformation approach. Both approaches allow to one obtain an accurate CAD representation able to represent the different irregularities of the vaults. As Figure 14 shows, around 75% of the points could by represented with a total agreement in comparison with the original point cloud. The major discrepancies are about 1 cm, appearing on areas with strong curvature variation. These discrepancies are in line with other research works [15] and could be improved by using a higher number of subdivisions. It is worth mentioning that the extrados of the vaults, which were not captured by the WMMS, were modelled by applying the offset operator proposed by Barattezzi et al. [15], using to this end the values extracted in Sánchez-Aparicio et al. [21]. The infill of the vaults was modelled manually by assuming the criteria adopted in the previous work [21].

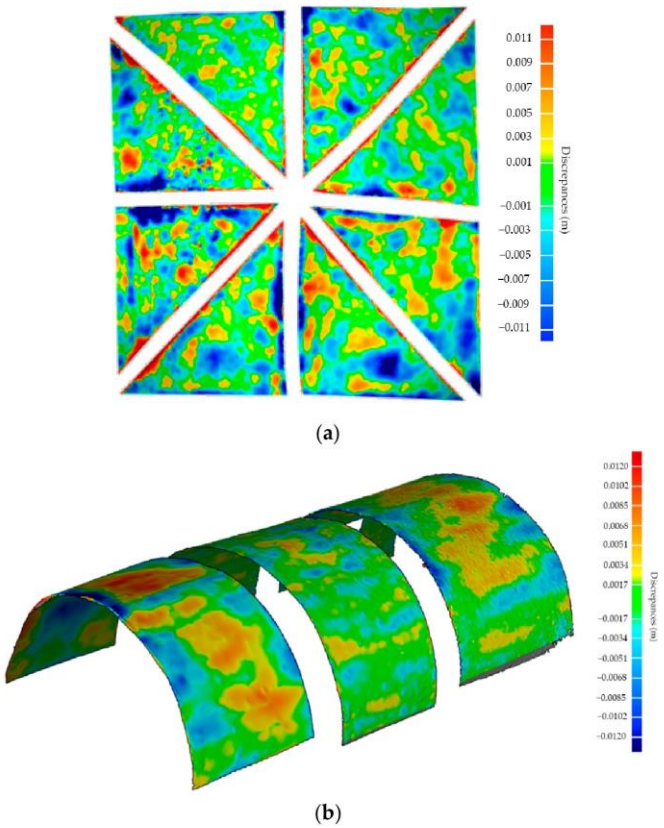

Figure 14. Discrepancies between the point cloud and the as-built CAD model: (**a**) barrel vault and (**b**) ribbed vault.

All the constructive elements and materials were integrated in a unique CAD model by using different Boolean operators as well as different Loft surfaces. As a result, it was possible to create an as-built CAD model able to capture the complex deformations of the church for further numerical simulations (Figure 15).

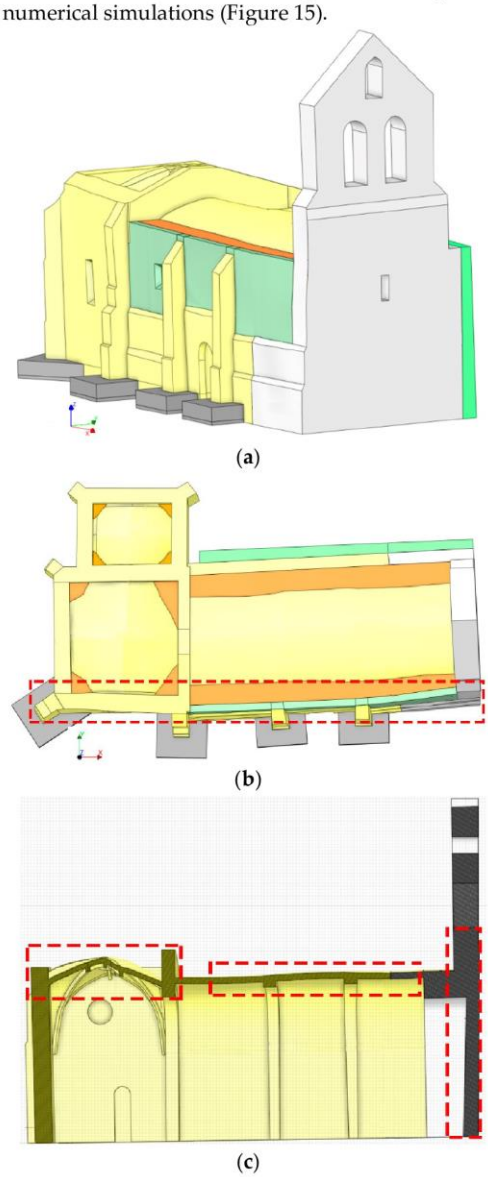

Figure 15. As-built CAD model: (**a**) general view; (**b**) plant view and (**c**) transversal section. In red it is highlighted some areas of the church with complex deformations properly modelled by the proposed approach. In yellow, grey and green the different masonries identified, in orange the infill of the vaults.

4. Structural Analysis

This section outlines the different considerations and results obtained during the structural analysis of the church. In this case, it was decided to use the FEM strategy for

evaluating the influence of the TRM solution from a static and a dynamic point of view. Firstly, a numerical mesh was generated by using the as-built CAD model previously generated. Then, the different materials were considered by defining specific constitutive models. Finally, several numerical analyses were carried out with the aim of evaluating the structural performance of the church against vertical and horizontal loading. All these stages were performed in the commercial FEM package TNO Diana® [42].

4.1. Numerical Mesh

Due to the complexity of the model, it was decided to create a fine mesh based on linear elements according with the recommendations exposed by Lourenço and Pereira [43]. Taking this into consideration, the average size of the element was about 0.15 m, ensuring at least three elements along the thickness of the vertical walls. Concerning the vaults, and taking into consideration the non-linear areas that will appear during the different numerical simulations, the average size of the element was reduced to 0.10 m. In both cases, solid tetrahedral elements were used. The TRM layers were modelled by using a set of curved shell elements for defining the matrix in which the textile is embedded as an equivalent grid without the possibility of slippage [26]. This modelling strategy was also used for defining the armoured concrete placed at the foundation level. As a result of these considerations, the numerical model was made up by a total of 507,595 elements (Figure 16): (i) 17,028 shell elements for simulating the TRM layers and (ii) 490,567 solid elements for simulating the masonry, concrete and infill layers of the church. On the one hand, the shell elements chosen were three-node triangular isoperimetric curved shell elements with a total of five integration points along its thickness. This assumption is in line with the suggestions made by Oliveira et al. [26]. Regarding the solid elements, it was decided to use four-node, three-side isoparametric solid pyramid elements with linear interpolation and numerical integration as suggested by Lourenço and Pereira [43]. This combination of elements, shell and solid, is common when real-scale historical structures are simulated [44,45]. Finally, a set of control nodes were chosen with the aim of evaluating the displacements suffered on key parts of the church (Figure 16).

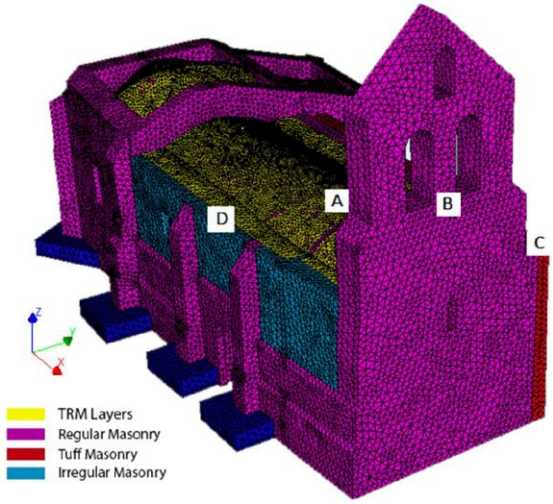

Figure 16. General view of the numerical mesh. The point A refers to the control node placed at the intrados of the barrel vault. Point B refers to the control node used for the pushover analysis in the +*X* direction. The control node placed at the same height but at the intrados of the tower was used for the analysis in the –*X* direction. Points C, D refer to the nodes used for the pushover analysis in the direction +*Y* and –*Y*, respectively.

4.2. Constitutive Models and Material Properties

The mechanical behaviour of the masonry elements was defined by using a macromodelling approach. More specifically, the total strain crack model implemented was used in the non-linear FEM package TNO Diana®. In this case, a post-peak exponential softening law was used for the tensile regime. Meanwhile, the compressive behaviour was simulated by using a post-peak parabolic and exponential softening. The Young modulus, density and compressive strength of the masonries were determined in accordance with Table C8A.2.2 of the Italian standard NTC 2008 [46]. Due to the absence of specific mechanical tests, a knowledge level of LC1 was assumed. Thus, the compressive strength of the masonry was reduced by 1.35. The Poisson ratio for all the masonries was established as 0.2, meanwhile the non-linear properties of these elements were obtained from the following considerations [47]: (i) a ductility index of 1.6 mm and (ii) a tensile strength comprised between 0.2 and 0.1 N/mm^2 with a mode I fracture energy of 0.05 N/mm. The infill of the vaults was modelled by assuming the properties of the irregular masonry showed within Table C8A.2.2. Table 3 shows the numerical values of the properties considered.

Table 3. Mechanical properties of the different materials used during the numerical simulation.

Parameter	Regular Masonry (Limestone) with Infill Core	Irregular Masonry (Sandstone and Tuff) with Infill Core	Tuff Masonry (Vaults)
Young modulus (Gpa)	1.44	1.02	1.08
Poisson ration (-)	0.20	0.20	0.20
Density (kg/m^3)	2000	2000	1600
Tensile strength (N/mm^2)	0.10	0.10	0.10
Fracture energy in tensile regime (N·mm)	0.05	0.05	0.05
Compressive strength (N/mm^2)	2.22	1.48	1.41
Fracture energy in compressive regime (N·mm)	3.55	2.45	2.34

The concrete was simulated by following the total strain crack model, using to this end the properties suggested by the Eurocode for a concrete type C-25/30 and a steel S500 [29]. On the other hand, the TRM layers were simulated by using a macromodelling strategy, as suggested by Oliveira et al. [23]. The mechanical properties of each part of this composite solution, matrix and fibre were obtained from the manufacturer (Table 4) as well as the experimental results obtained in similar works [48]. For the mortar, a total strain crack model with a plateau and parabolic function was assumed for the tensile and compressive regime, respectively. On the contrary, the fibre was simulated as a perfect brittle material.

Table 4. Mechanical properties of the matrix and fibre materials used in the TRM layers.

Properties		Value
Mortar	Young modulus (GPa)	4.00
	Poisson ratio (-)	0.20
	Thickness (m)	0.03
	Density (kg/m^3)	1850
	Compressive strength (MPa)	2.50
	Fracture energy (N/mm)	3.44
	Tensile strength (MPa)	0.55
	Plateau and strain	0.0016
	Power c	0.6
Carbon fibre	Young modulus (GPa)	160
	Poisson ratio (-)	0.20
	Reinforcement ratio (mm^2/m)	44
	Density (kg/m^3)	1780
	Tensile strength (Mpa)	4300

4.3. Structural Impact of the TRM Layers

This section has the aim of evaluating the impact of the retrofitted solution in the response of the structure. To this end, several non-linear analyses were carried out, namely: (i) gravitational analysis for evaluating the performance of the TRM layers against vertical loading and (ii) seismic analysis for checking the contribution of these layers to the horizontal capacity of the church. The regular Newton–Rapson method in combination with the arc-length control and the line-search technique were used as algorithms for solving the non-linear problem. The convergence criteria established was based on energy, using a threshold of 0.001. It is worth mentioning that the roof of the church was represented by means of a superficial load, assuming the load used in Sánchez-Aparicio et al.[21].

4.3.1. Results Obtained from the Static Non-Linear Analysis

This section is devoted to showing the numerical results obtained during the non-linear static analysis. In this case, two different numerical simulations were carried out with the aim of evaluating the contribution of the TRM layers to the vertical capacity of the church: (i) a simulation considering only the armoured concrete and (ii) an analysis considering the armoured concrete as well as the TRM layers. In both cases, the load increases until the collapse of the structure.

To evaluate the structural performance of the church against vertical loading, a non-linear static analysis increasing gravitational loading until failure was carried out. The control node selected for displacement monitoring corresponds to point A indicated in Figure 16, which is located at the intrados of the barrel vault. As a result of these analyses, it was possible to estimate the safety factor of the structure in terms of a load factor with respect to the self-weight considering both scenarios, without strengthening and with the retrofitting based on the TRM composite solution.

Figures 17–19 shows the results of these analysis. As it was expected, the church can stand a large gravitational load before collapsing, suggesting that in the absence of a soil problem the structure is safe (including or not the TRM layers). In the absence of the TRM layers, the church has a safety factor of 8.86. Meanwhile, the presence of this composite solution slightly increases the safety factor to 9.03, also incrementing the stiffness of the structure (Figure 17). The collapse in both cases is similar, appearing with the inclination of the north wall as well as the formation of plastic hinges in tensile and compressive regimes at the vault of the main nave (Figure 18) (Figure 19). In the case of considering the TRM

layer, the cracks at the extrados appears at the beginning of the vault, more specifically in the frontier between the vault retrofitted and the vault without TRM (Figure 19).

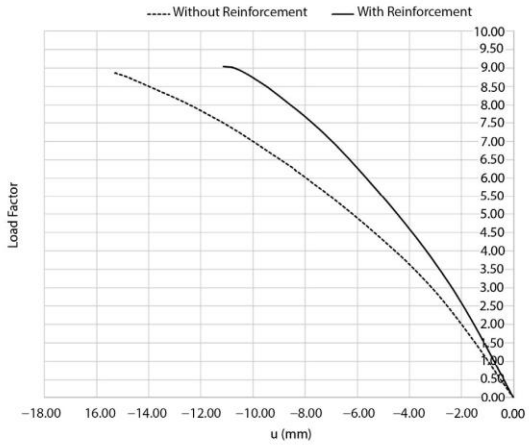

Figure 17. Load–displacement curves obtained during the static non-linear analysis. The dash line represents the structure with the TRM layers.

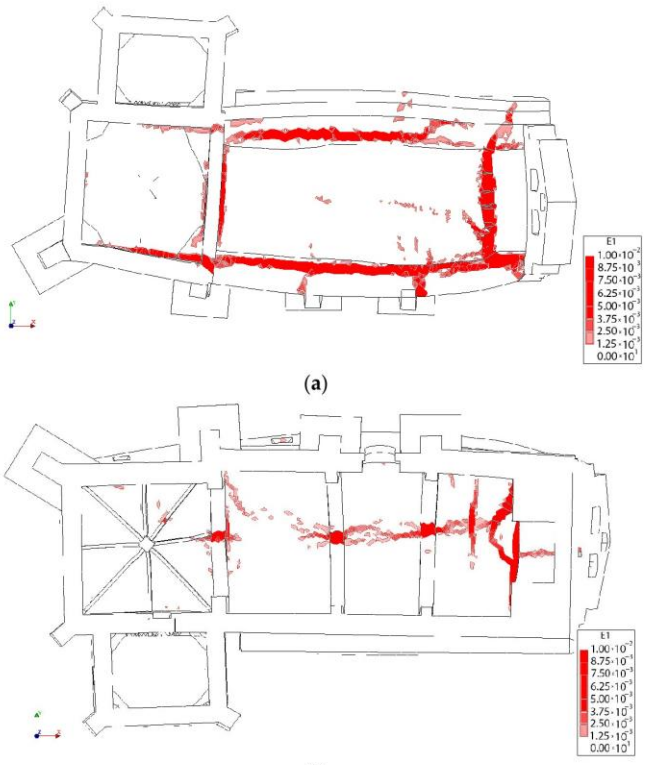

Figure 18. First principal strains at the moment of collapse in absence of TRM layers: (**a**) view from the extrados of the vault and (**b**) view from the intrados of the vault.

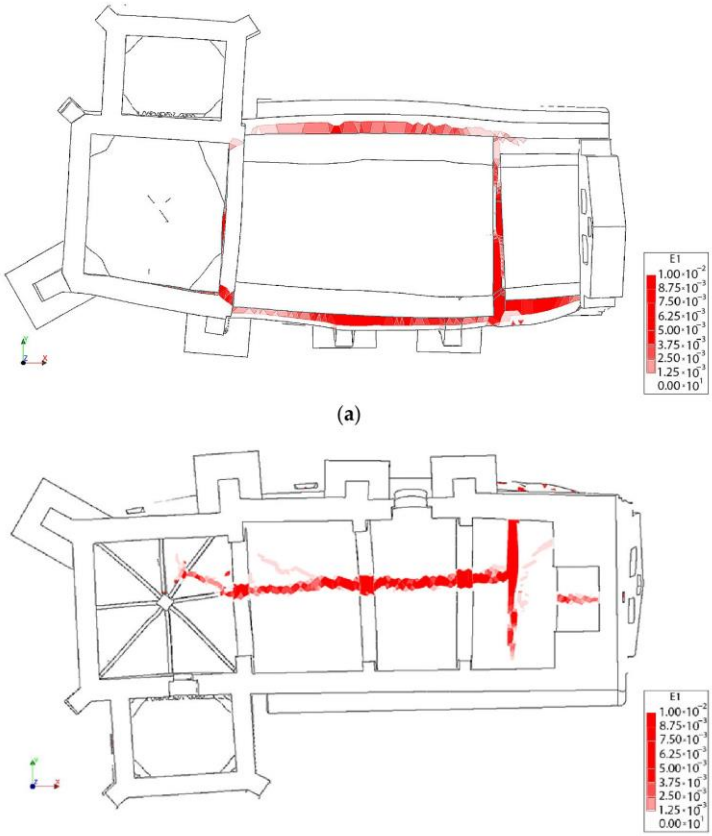

Figure 19. First principal strains at the moment of collapse in presence of TRM layers: (**a**) view from the extrados of the vault and (**b**) view from the intrados of the vault.

4.3.2. Results Obtained from the Seismic Analysis

As several authors have highlighted [26–28], the use of TRM layers have a large impact on the seismic performance of historical constructions. According to this, further numerical evaluations were carried out with the aim of evaluating the contribution of the TRM layers of the church, as well as to know the maximum allowable acceleration. From the different non-linear numerical strategies able to simulate the seismic performance of masonry constructions, the current work uses the pushover analysis.

The non-linear static (pushover) analysis is a numerical method proposed by many standards such as Eurocode 8 for estimating the seismic performance of a structure. This method is well documented in the existing literature [43,49]. During this stage, the structure is subjected to gravity loading as well as a monotonic lateral loading pattern that represents the inertial forces acting on the structure during a seismic event. In this work, a total of four analyses using transversal lateral forces proportional to the mass were carried out to evaluate the seismic performance of the church in the longitudinal (+X, −X) and transversal directions (+*Y*, −*Y*) (Figure 16). The results of these analyses are given in terms of the so-called capacity curves, describing the displacement at some predefined control nodes (Figure 16) against the base shear factor, i.e., the ratio between the horizontal forces acting at the base of the structure and its total self-weight. It is worth mentioning that the control

points considered during this analysis were placed on critical areas (Figure 16): (i) at the top of the tower for the pushover at the direction *X* and (ii) a point at the top of the walls placed at the middle of the nave for the pushover analysis carried out at the direction *Y*.

As in the previous section, the regular Newton–Raphson method, combined with the arc-length control and the line-search technique, was adopted to obtain the solution of the arising non-linear equations system. This method allows one to predict the deformations and damage as well as the weak areas of the church. It is worth mentioning that the equilibrium of the equation system is guaranteed by using the same criterions as those exposed in the previous section.

The result of the pushover analysis highlights the influence of the TRM layer in the seismic performance of the structure, especially in the lateral direction (+*Y*, −*Y*). In this situation, the maximum load factor of the church increases from a value of 0.55 and 0.52 to 0.64 and 0.59 (Figure 20). The asymmetric values obtained from the different evaluations are in line with the asymmetric arrangement of the structure (Figures 20–24). In both cases, the presence of TRM layers allows one to prevent the creation of diagonal cracks along the main barrel vault. In this situation, the damage is focused on the vicinities of the main nave (Figures 22 and 24).

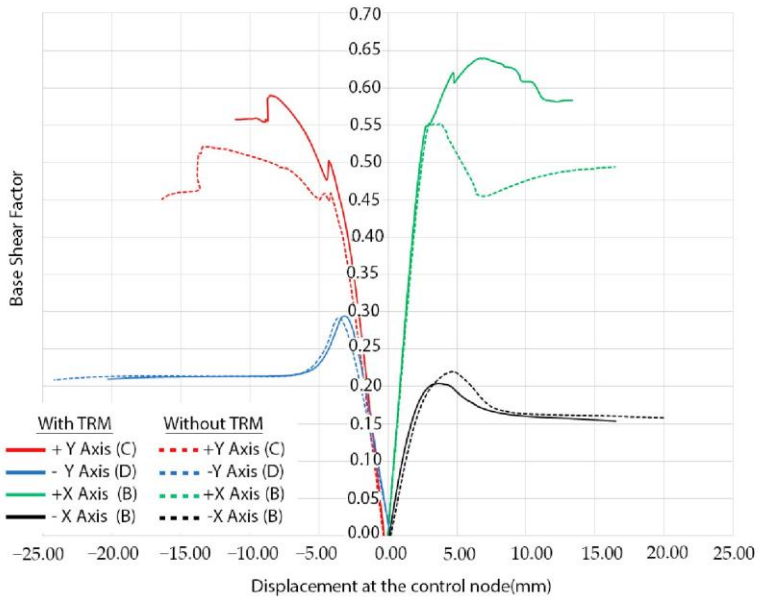

Figure 20. Mass-proportional pushover capacity curves in the four main directions (red colour for the +*Y*, green colour for +*X*, blue for the −*Y* and black for the −*X*). Dash lines represent the behaviour of the structure without the TRM layer. The control points used for each curve has been placed between markers.

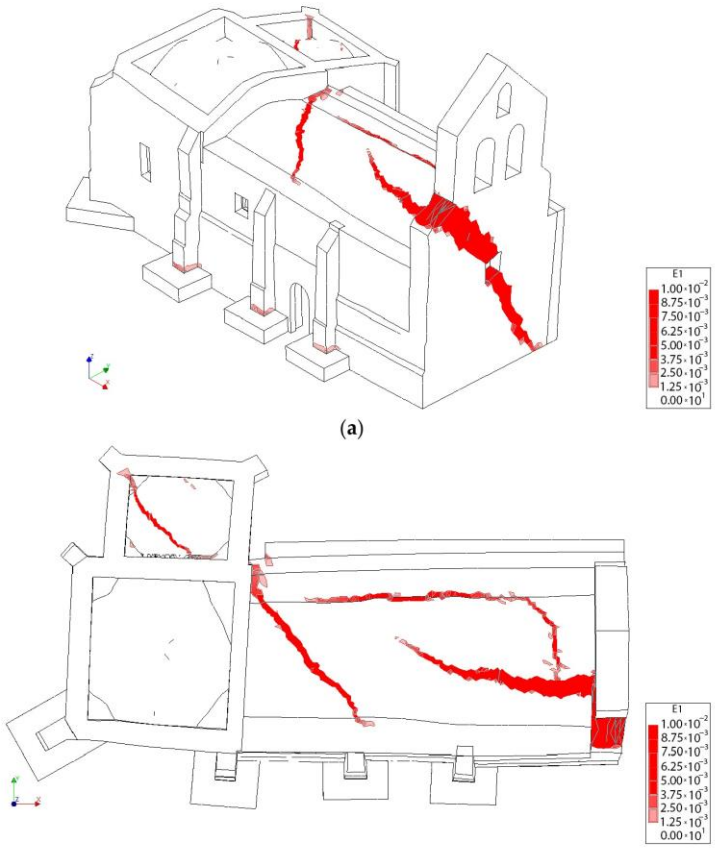

Figure 21. Distribution of the first principal strains at the collapse point in the transversal direction +*Y* without considering the TRM layers: (**a**) 3D view and (**b**) plant view.

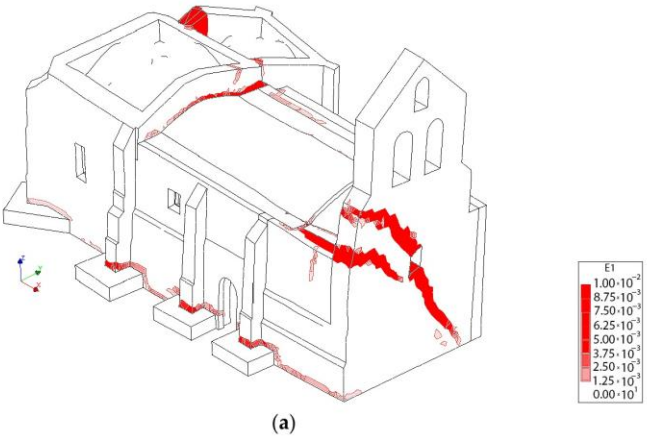

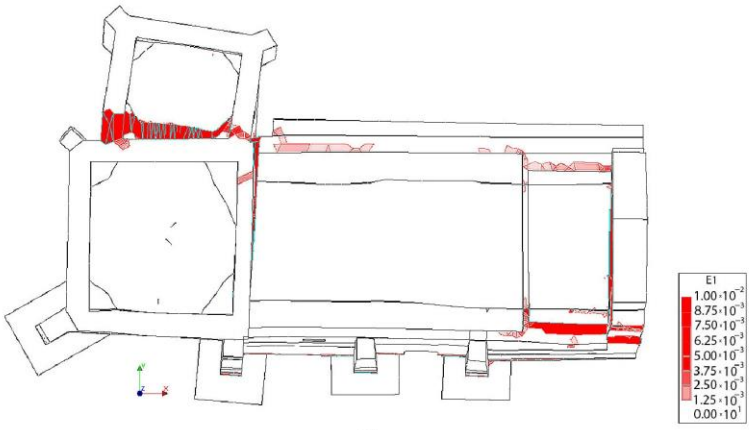

(**b**)

Figure 22. Distribution of the first principal strains at the collapse point in the transversal direction +*Y*, considering the TRM layers: (**a**) 3D view and (**b**) plant view.

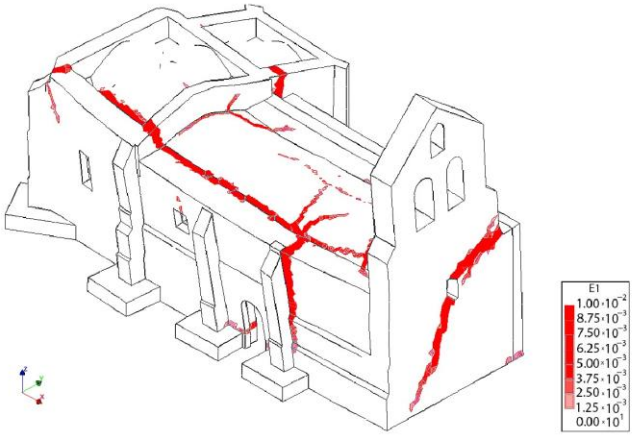

(**a**)

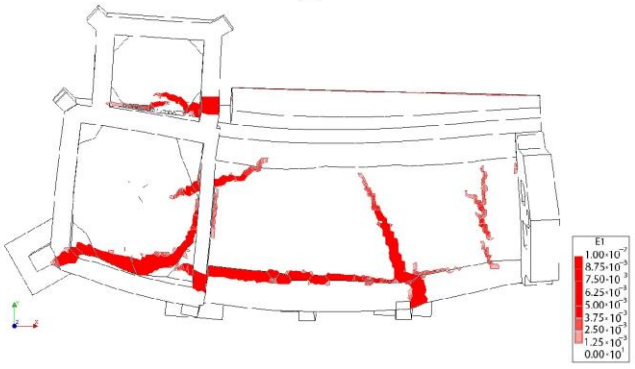

(**b**)

Figure 23. Distribution of the first principal strains at the collapse point in the transversal direction −*Y* without considering the TRM layers: (**a**) 3D view and (**b**) plant view.

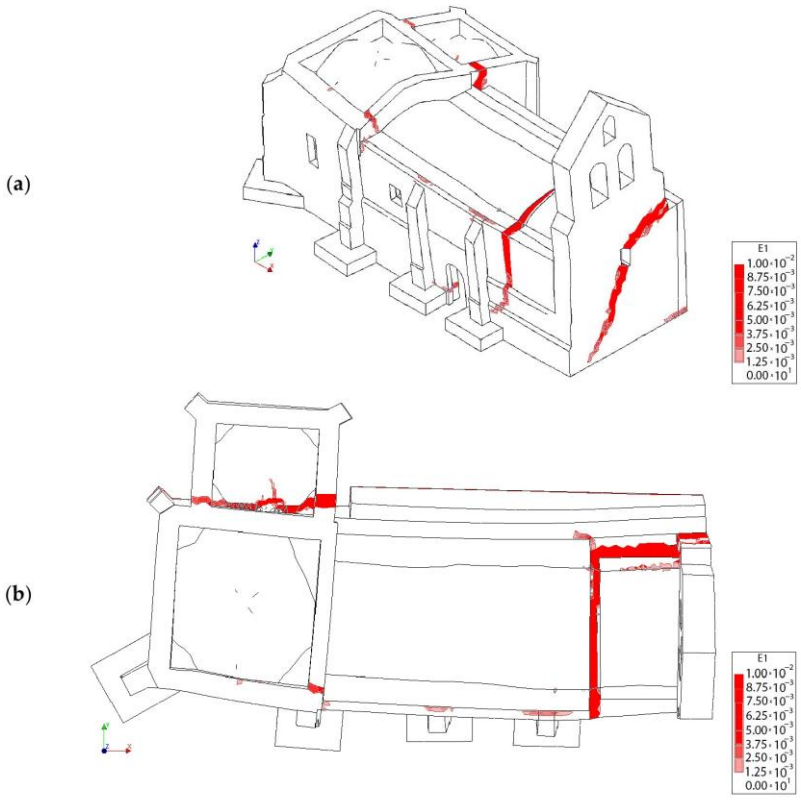

Figure 24. Distribution of the first principal strains at the collapse point in the transversal direction −*Y*, considering the TRM layers: (**a**) 3D view and (**b**) plant view.

With regard to the longitudinal direction, it is possible to observe that the TRM layers do not have a considerable influence on the seismic performance of the church. In both cases, the collapse is produced by the overturning of the main façade of the tower (Figure 25), which is a local failure mode. This point clearly reflects that pushover analysis, although being a very useful and powerful tool for seismic performance assessment, sometimes might present some limitations, especially with respect to a more comprehensive non-linear time history analysis. This direction represents the most vulnerable direction of the church with a maximum capacity of 0.29 (Figure 20).

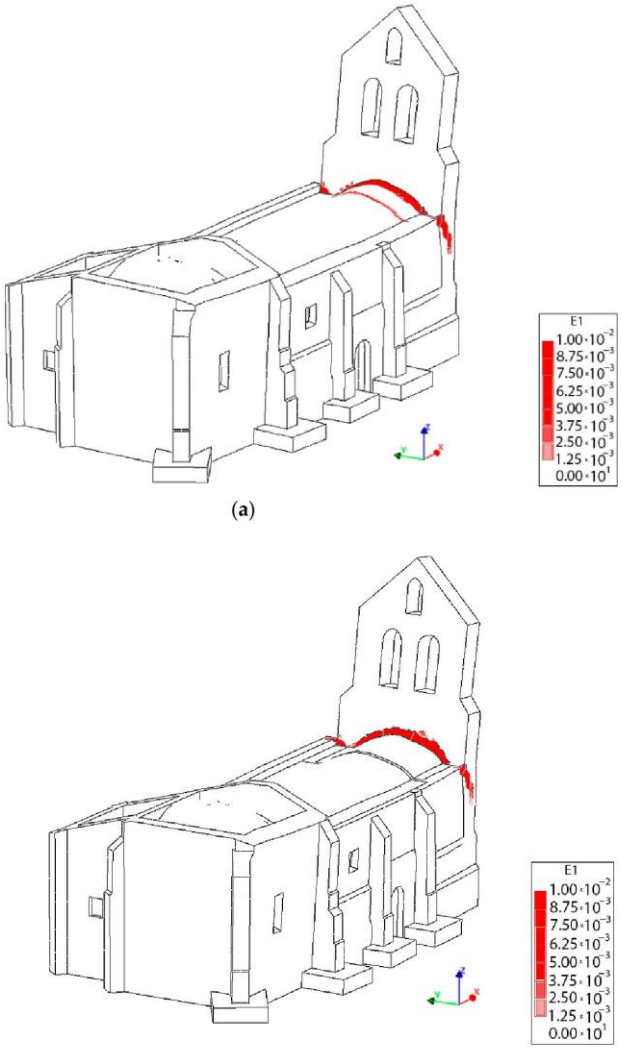

Figure 25. 3D view at the moment of the collapse: (**a**) without TRM layers and (**b**) with TRM layers.

The verification of the structural safety for the seismic action was carried out following the Spanish seismic code [50]. In particular, the assigned peak ground acceleration value for this area is lower than 0.04 g. Adopting a force-based seismic assessment criterion [43], it can be concluded that the church meets the requirements in all the situations, being the minimum capacity obtained for the positive X direction (0.20 g). Thus, pushover analysis, besides bringing invaluable results regarding the seismic safety level of the structure, was also used in this study to judge the effectiveness of the TRM-based retrofitting strategy as well as to evaluate the overall mechanical performance in terms of damage progression and the identification of potential vulnerabilities or weak areas.

5. Conclusions

From this study, it was possible to extract different conclusions with respect to the WMMS sensor as well as the use of composite solution for retrofitting masonry structures. On the one hand, the use of WMMS devices show several advantages, such as the great performance or the flexibility of it. Regarding the first one, the time invested for digitalizing the church was reduced by about 7.5 times in comparison with traditional techniques. With respect to the second one, the great portability makes it possible to digitalize complex and narrow spaces. However, the data provided shows noise which hinders the creation of a CAD model and requires the use of noise reduction filters. Regarding this, we propose the use of a parameter-free noise reduction filter that increases the quality of the point cloud, minimizing its discrepancies with respect to a TLS point cloud by about 37%, with some areas in which the decrease is about 60% (Table 2). This improvement is lower in the inner zones due to the presence of ornamental parts. Additionally, it is possible to observe an increase in the quality from a visual point of view, that makes the reverse engineering stage easier (Figure 11). The time required for this stage could be considered acceptable, investing a total of 50 min for filtering a point cloud of 27 million points. This stage was carried out in a PC Mountain Studio3D i5 Ivy with Intel Core i5-3570K processor and 32 Gb RAM with operating system Windows 10 64 bits. The use of this filter, which is parameter-free, allows one to improve the application of reverse engineering procedures by any person who is not an expert in the field.

Regarding the reverse engineering strategy, the use of RANSAC approaches with curvature segmentation strategies and NURBS-based approaches allows one to properly model the deformations of a structure, increasing the automation of the process. However, the presence of shadows in the original point cloud as well as the necessity of splitting the different materials requires the intervention of the user in order to obtain a reliable CAD model for further numerical evaluations.

Finally, from this work it is possible to conclude that the use of TRM solutions, which are invasive solutions, increase the lateral capacity of the structure evaluated by about 115% in contrast with an increment of 102% for the vertical loading. This system seems to be efficient in seismic areas.

Future works will be focused on the use of complementary modelling strategies such as the retopologization of the mesh. This approach will allow one to reduce the amount of user intervention during the CAD modelling stage which contains several steps that are performed in a manual way, requiring the investment of large amount of time. Additionally, an extensive experimental campaign will be planned, devoted to obtaining more data about the mechanical behaviour of the masonries by means of sonic testing or even the use of operational modal analysis for updating the numerical model. This data will be complemented by additional structural analysis (e.g., 3D limit analysis) in order to double-check the results obtained. Finally, it is planned to develop a 3D numerical model with the TLS data. This model will be used to compare the numerical results obtained with a 3D FEM model generated with the WMMS and the TLS point cloud.

Author Contributions: Conceptualization, L.J.S.-A., B.C., M.Á.M.-G., R.M. and M.S.-A.; methodology, L.J.S.-A., B.C., R.M.; formal analysis, L.J.S.-A., M.Á.M.-G. and D.G.-A.; writing—original draft preparation, L.J.S.A., M.Á.M.-G., R.M., M.S.-A. and D.G.-A.; writing—review and editing, L.J.S.-A., B.C., M.Á.M.-G., R.M., M.S.-A. and D.G.-A. All authors have read and agreed to the published version of the manuscript.

Funding: This research was partially funded by ERDF funds through the V SUDOE INTERREG program within the framework of the HeritageCARE project, Ref. SOE1/P5/P0258 and the research project Patrimonio 5.0 funded by Junta of Castilla y León, Ref. SA075P17.

Data Availability Statement: not applicable

Acknowledgments: The authors would like to thank Santa Maria la Real Foundation for providing part of the data necessary for this study. Special thanks to the architects Juan Carlos Prieto Vielba

and Jesús Castillo Oli. These architects designed the restoration action carried out on the church whose project title was "Proyecto básico y de ejecución de restauración. Iglesia de San Pedro. Becerril del Carpio. Palencia". The authors also want to thank the Junta de Castilla y León and the Fondo Social Europeo for the financial support given through programs for human resources (EDU/1100/2017) to the corresponding author of this paper (R.M.), and to the European Union for providing a post-doctoral Grant to another of the authors within the actions Marie Skłodowska-Curie Individual Fellowships, H2020-MSCA-IF-2019 (Grant agreement ID: 679 894785; AVATAR project) (M.A.M.G.).

Conflicts of Interest: The authors declare no conflict of interest.

References

1. Roca, P.; Cervera, M.; Gariup, G.; Pela', L. Structural analysis of masonry historical constructions. Classical and advanced approaches. *Arch. Comput. Methods Eng.* **2010**, *17*, 299–325, doi:10.1007/s11831-010-9046-1.
2. Aguilar, R.; Noel, M.F.; Ramos, L.F. Integration of reverse engineering and non-linear numerical analysis for the seismic assessment of historical adobe buildings. *Autom. Constr.* **2019**, *98*, 1–15, doi:10.1016/j.autcon.2018.11.010.
3. Sánchez-Aparicio, L.J.; Bautista-De Castro, Á.; Conde, B.; Carrasco, P.; Ramos, L.F. Non-destructive means and methods for structural diagnosis of masonry arch bridges. *Autom. Constr.* **2019**, *104*, 360–382, doi:10.1016/j.autcon.2019.04.021.
4. Masciotta, M.G.; Pellegrini, D.; Brigante, D.; Barontini, A.; Lourenço, P.B.; Girandi, M.; Padovani, C.; Fabbrocino, G. Dynamic characterization of progressively damaged segmental masonry arches with one settled support: Experimental and numerical analyses. *Frat. ed Integrità Strutt.* **2019**, *14*, 423–441, doi:10.3221/IGF-ESIS.51.31.
5. Lagomarsino, S. Damage assessment of churches after L'Aquila earthquake (2009). *Bull. Earthq. Eng.* **2012**, *10*, 73–92, doi:10.1007/s10518-011-9307-x.
6. Fuentes, D.D.; Baquedano Julià, P.A.; D'Amato, M.; Laterza, M. Preliminary seismic damage assessment of mexican churches after september 2017 earthquakes. *Int. J. Archit. Herit.* **2019**, doi:10.1080/15583058.2019.1628323.
7. Clementi, F. Failure analysis of apennine masonry churches severely damaged during the 2016 central Italy seismic sequence. *Buildings* **2021**, *11*, 58, doi:10.3390/buildings11020058.
8. Yurdakul, M.; Yılmaz, F.; Artar, M.; Can, Ö.; Öner, E.; Daloğlu, A.T. Investigation of time-history response of a historical masonry minaret under seismic loads. *Structures* **2021**, *30*, 265–276, doi:10.1016/j.istruc.2021.01.008.
9. Kassotakis, N.; Sarhosis, V.; Riveiro, B.; Conde, B.; D'Altri, A.M.; Mills, J.; Milani, G.; de Miranda, S.; Castellazzi, G. Three-dimensional discrete element modelling of rubble masonry structures from dense point clouds. *Autom. Constr.* **2020**, *119*, 103365, doi:10.1016/j.autcon.2020.103365.
10. Pepe, M.; Costantino, D.; Restuccia Garofalo, A. An Efficient pipeline to obtain 3D model for HBIM and structural analysis purposes from 3D point clouds. *Appl. Sci.* **2020**, *10*, 1235, doi:10.3390/app10041235.
11. Bassoli, E.; Vincenzi, L.; D'Altri, A.M.; de Miranda, S.; Forghieri, M.; Castellazzi, G. Ambient vibration-based finite element model updating of an earthquake-damaged masonry tower. *Struct. Control Health Monit.* **2018**, *25*, e2150, doi:10.1002/stc.2150.
12. Castellazzi, G.; D'Altri, A.M.; de Miranda, S.; Ubertini, F. An innovative numerical modeling strategy for the structural analysis of historical monumental buildings. *Eng. Struct.* **2017**, *132*, 229–248, doi:10.1016/j.engstruct.2016.11.032.
13. Gonizzi, S.; Politecnico, B.; Milano, D.; Guidi, G.; Di Milano, P.; Gonizzi Barsanti, S.; Guidi, G. A geometric processing workflow for transforming reality-based 3D models in volumetric meshes suitable for FEA. *Int. Arch. Photogramm. Remote Sens. Spat. Inf. Sci.* **2017**, *XLII-2/W3*, 331–338, doi:10.5194/isprs-archives-XLII-2-W3-331-2017.
14. Bautista-De Castro, Á.; Sánchez-Aparicio, L.J.; Ramos, L.F.; Sena-Cruz, J.; González-Aguilera, D. Integrating geomatic approaches, Operational Modal Analysis, advanced numerical and updating methods to evaluate the current safety conditions of the historical Bôco Bridge. *Constr. Build. Mater.* **2018**, *158*, 961–984, doi:10.1016/j.conbuildmat.2017.10.084.
15. Barazzetti, L.; Banfi, F.; Brumana, R.; Previtali, M. Creation of parametric BIM objects from point clouds using nurbs. *Photogramm. Rec.* **2015**, *30*, 339–362, doi:10.1111/phor.12122.
16. Nocerino, E.; Pablo, R.-G.; Menna, F. *Introduction to Mobile Mapping with Portable Systems*; CRC Press: Boca Raton, FL, USA, 2019; ISBN 9781351018869.
17. Durrant-Whyte, H.; Bailey, T. Simultaneous localization and mapping: Part I. *IEEE Robot. Autom. Mag.* **2006**, *13*, 99–108, doi:10.1109/MRA.2006.1638022.
18. Nocerino, E.; Menna, F.; Kessler, F.B.; Fondazione, F.R.; Kessler, B.; Remondino, F.; Toschi, I.; Rodríguez-Gonzálvez, P. Investigation of indoor and outdoor performance of two portable mobile mapping systems. *SPIE Opt. Metrol.* **2017**, doi:10.1117/12.2270761.
19. di Filippo, A.; Sánchez-Aparicio, L.J.; Barba, S.; Martín-Jiménez, J.A.; Mora, R.; Aguilera, D.G. Use of a wearable mobile laser system in seamless indoor 3D mapping of a complex historical site. *Remote Sens.* **2018**, *10*, 1897, doi:10.3390/rs10121897.
20. Barba, S.; di Filippo, A.; Limongiello, M.; Messina, B. Integration of active sensors for geometric analysis of the Chapel of the Holy Shroud. In Proceedings of the 27th CIPA International Symposium "Documenting the Past for a Better Future", Ávila, Spain, 1–5 September 2019; Volume XLII-2/W15, pp. 149–156.
21. Sánchez-Aparicio, L.; Conde, B.; Maté-González, M.A.; Mora, R.; Sánchez-Aparicio, M.; García-Álvarez, J.; González-Aguilera, D. A comparative study between WMMS and TLS for the stability analysis of the San Pedro Church Barrel vault by means of

the finite element method. In Proceedings of the 27th CIPA International Symposium "Documenting the Past for a Better Future", Ávila, Spain, 1–5 September 2019; Volume XLII-2/W15, pp. 1047–1054.
22. Nocerino, E.; Menna, F.; Toschi, I.; Morabito, D.; Remondino, F.; Rodríguez-Gonzálvez, P. Valorisation of history and landscape for promoting the memory of WWI. *J. Cult. Herit.* **2018**, *29*, 113–122, doi:10.1016/j.culher.2017.07.007.
23. Maté-González, M.Á.; Sánchez-Aparicio, L.J.; Sáez Blázquez, C.; Carrasco García, P.; Álvarez-Alonso, D.; de Andrés-Herrero, M.; García-Davalillo, J.C.; González-Aguilera, D.; Hernández Ruiz, M.; Jordá Bordehore, L.; et al. On the combination of remote sensing and geophysical methods for the digitalization of the san lázaro middle paleolithic rock shelter (Segovia, Central Iberia, Spain). *Remote Sens.* **2019**, *11*, 2035, doi:10.3390/rs11172035.
24. Roca, P.; Lourenço, P.B.; Gaetani, A. *Historic Construction and Conservation. Materials, Systems and Damage*; Publisher: Routledge: London, England, 2019; ISBN 978-0-429-05276-7.
25. Kouris, L.A.S.; Triantafillou, T.C. State-of-the-art on strengthening of masonry structures with textile reinforced mortar (TRM). *Constr. Build. Mater.* **2018**, *188*, 1221–1233, doi:10.1016/j.conbuildmat.2018.08.039.
26. Oliveira, D.V.; Ghiassi, B.; Allahvirdizadeh, R.; Wang, X.; Mininno, G.; Silva, R.A. Macromodeling approach for pushover analysis of textile-reinforced mortar-strengthened masonry. In *Numerical Modeling of Masonry and Historical Structures: From Theory to Application*; Elsevier: Amsterdam, The Netherlands, 2019; pp. 745–778, ISBN 9780081024393.
27. Gunes, B.; Cosgun, T.; Sayin, B.; Ceylan, O. Structural rehabilitation of a Middle Byzantine ruin and the masonry building constructed above the ruin. Part I: The ruin. *Eng. Fail. Anal.* **2019**, *105*, 503–517, doi:10.1016/j.engfailanal.2019.06.065.
28. Bru, D.; Ivorra, S.; Baeza, F.J. Seismic behavior of a masonry chimney retrofitted with composite materials: A preliminary aproach. *Int. J. Saf. Secur. Eng.* **2017**, *7*, 486–497, doi:10.2495/SAFE-V7-N4-486-497.
29. Europan Committee for Standardization. *Eurocode 2: Design of Concrete Strucures*; Publisher: Europan Committee for Standardization, 1992.
30. GeoSLAM A Survey REVOlution. Introducing the ZEB-REVO Mobile Indoor Mapping System. Available online: https://gpserv.com/wp-content/uploads/2017/01/ZEB-REVO-Brochure-v1.0.3.pdf (accessed on 15 December 2020).
31. GeoSLAM ZEB Go—GeoSLAM. Available online: https://geoslam.com/solutions/zeb-go/ (accessed on 1 September 2020).
32. Quigley, M.; Gerkey, B.; Conley, K.; Faust, J.; Foote, T.; Leibs, J.; Berger, E.; Wheeler, R.; Ng, A. ROS: An open-source robot operating system. *ICRA Work. Open Source Softw.* **2009**, *3*, 5.
33. Balta, H.; Velagic, J.; Bosschaerts, W.; De Cubber, G.; Siciliano, B. Fast statistical outlier removal based method for large 3D Point clouds of outdoor environments. *IFAC-PapersOnLine* **2018**, *51*, 348–353, doi:10.1016/j.ifacol.2018.11.566.
34. Guerrero, P.; Kleiman, Y.; Ovsjanikov, M.; Mitra, N.J. PCPNet learning local shape properties from raw point clouds. *Comput. Graph. Forum* **2018**, *37*, 75–85, doi:10.1111/cgf.13343.
35. Rakotosaona, M.; La Barbera, V.; Guerrero, P.; Mitra, N.J.; Ovsjanikov, M. PointCleanNet: Learning to denoise and remove outliers from dense point clouds. *Comput. Graph. Forum* **2020**, *39*, 185–203, doi:10.1111/cgf.13753.
36. Qi, C.R.; Su, H.; Mo, K.; Guibas, L.J. PointNet: Deep learning on point sets for 3D classification and segmentation. **2017**, *6*, 652–660.
37. Xu, Z.; Foi, A. Anisotropic denoising of 3D point clouds by aggregation of multiple surface-adaptive estimates. *IEEE Trans. Vis. Comput. Graph.* **2019**, doi:10.1109/tvcg.2019.2959761.
38. CloudCompare: 3D point cloud and mesh processing software Open Source Project. Available online: http://www.cloudcompare.org/ (accessed on 15 December 2020).
39. Rodríguez-Gonzálvez, P.; Jiménez Fernández-Palacios, B.; Muñoz-Nieto, Á.; Arias-Sanchez, P.; Gonzalez-Aguilera, D. Mobile LiDAR system: New possibilities for the documentation and dissemination of large cultural heritage sites. *Remote Sens.* **2017**, *9*, 189, doi:10.3390/rs9030189.
40. Sánchez-Aparicio, L.J.; Del Pozo, S.; Ramos, L.F.; Arce, A.; Fernandes, F.M. Heritage site preservation with combined radiometric and geometric analysis of TLS data. *Autom. Constr.* **2018**, *85*, 24–39, doi:10.1016/j.autcon.2017.09.023.
41. Schnabel, R.; Wahl, R.; Klein, R. Efficient RANSAC for point-cloud shape detection. *Comput. Graph. Forum* **2007**, *26*, 214–226, doi:10.1111/j.1467-8659.2007.01016.x.
42. TNO DIANA BV DIANA—Finite Element Analysis. User's Manual. Available online: https://dianafea.com/diana-manuals (accessed on 10 November 2020).
43. Lourenço, P.B.; Greco, F.; Barontini, A.; Pia Ciocci, M.; Karanikoloudis, G. *Seismic Retrofitting Project: Modeling of Prototype Buildings*; Publisher: The Getty Conservation Institute: Los Angeles, USA, 2019.
44. Ciocci, M.P.; Sharma, S.; Lourenço, P.B. Engineering simulations of a super-complex cultural heritage building: Ica Cathedral in Peru. *Meccanica* **2018**, *53*, 1931–1958, doi:10.1007/s11012-017-0720-3.
45. Illampas, R.; Ioannou, I.; Lourenço, P.B. Seismic appraisal of heritage ruins: The case study of the St. mary of carmel church in cyprus. *Eng. Struct.* **2020**, *224*, 111209, doi:10.1016/j.engstruct.2020.111209.
46. Norme tecniche per le costruzioni (NTC-08). http://www.ingegneriasoft.com/pdf/Norme_Tecniche_Costruzioni_2008_cap1-12.pdf (accessed on 10 November 2020).
47. Lourenço, P.B. Structural Masonry Analysis : Recent Developments and Prospects. In 14th International Brick and Block Masonry Conference, Sydney, Australia 17-20 February 2008.
48. Kariou, F.A.; Triantafyllou, S.P.; Bournas, D.A.; Koutas, L.N. Out-of-plane behaviour of TRM strengthened masonry walls. In Proceedings of the SMAR 2017-Fourth Conference on Smart Monitoring Assessment and Rehabilitation of Civil Structures, Zurich, Switzerland, 13-15 September 2017.

49. O'Hearne, N.; Mendes, N.; Lourenço, P.B. Seismic analysis of the San Sebastian Basilica (Philippines). In Proceedings of the Proceedings of the 40th IABSE Symposium: Tomorrow's Megastructures, Nantes, France, 19–21 September 2018.
50. Seismic Standards Standing Committee Seismic construction standard: General and building (NCSE-02). https://www.mitma.gob.es/recursos_mfom/0820200.pdf (accessed on 10 November 2020).

Capítulo IV.

De la nube de puntos a los modelos BIM

4. De la nube de puntos a los modelos BIM

En esta sección se aborda el último artículo que compone la Tesis Doctoral, titulado "*An historical building information modelling approach for the preventive conservation of historical constructions: Application to the Historical Library of Salamanca*" y publicado en la revista científica *Automation in Construction* de Elsevier en 2021

Resumen

Tal y como se señaló en la anterior sección, el uso de sistemas WMLS es una cuestión abierta, no solo en el campo del diagnóstico, sino también en el campo de la conservación preventiva. Por ello, en el artículo aquí presentado se desarrolla un sistema de conservación preventiva de edificios históricos a través de la integración de sistemas de escaneado móvil tipo WMLS, modelos de gestión HBIM y redes de sensores IoT de monitoreo. El primero de estos enfoques permite crear un esqueleto geométrico adecuado sobre el cual verter todo el conocimiento experto y el big-data procedente de la red de monitoreo, mientras que el segundo de los enfoques permite la integración adecuada de dichos datos. Con todo ello es posible conocer el estado de conservación del edificio y sus elementos, y es posible utilizar indicadores KPI (Key Performance Indicators) para establecer las condiciones ambientales de cada uno de los bienes contenidos en el edificio.

Los objetivos de este artículo son tres: i) comprobar si los sistemas WMLS son viables para generar modelos BIM de edificios históricos, ii) utilizar la tecnología IoT a través de una red de sensores para conectar el edificio real con el modelo BIM, y iii) utilizar indicadores KPI para conocer el estado de conservación del edificio en tiempo real y optimizar así las actuaciones necesarias. El sistema fue validado en la Biblioteca General Histórica de la Universidad de Salamanca (España).

En el artículo se presentan 4 fases de trabajo:

- Digitalización del escenario: en esta parte del artículo se presenta la digitalización de la Biblioteca General Histórica de la Universidad de Salamanca con un sistema de escaneo móvil del tipo WMLS, evaluado y validado en el Capítulo I y III. Se siguieron las técnicas de digitalización establecidas en la guía de buenas prácticas del primer artículo (Capítulo I) obteniendo una nube de puntos de 15 millones de puntos en un recorrido de 8 minutos y un tiempo de procesado de 6 minutos.
- Generación del modelo HBIM: mediante metodologías de ingeniería inversa se genera un modelo CAD intermedio, que de manera fidedigna plasma todas las características del edificio. Con el modelo CAD, y previamente a la generación del modelo HBIM, se realiza un análisis del nivel de detalle (LoD) y el nivel de Información (LoI) necesarios para el trabajo en cuestión. Este punto se presenta como algo fundamental antes de abordar la generación de cualquier BIM. El LoD da cuenta de la geometría de los elementos, la posición y la orientación. En los modelos HBIM, los objetos tienen gran cantidad de detalles difíciles de modelar con formas paramétricas, especialmente en todas las partes ornamentales de los elementos. Además, a diferencia de los BIM tradicionales, en los HBIM cada elemento es único, no siguiendo un patrón repetitivo,

por lo que el modelado se complica considerablemente si se intenta llegar a un LoD muy elevado. Es por ello que se hace fundamental en trabajos HBIM determinar el mínimo LOD necesario. La pregunta que se plantea para los trabajos de conservación preventiva desarrollados en este trabajo es: *¿es realmente relevante el modelado de los aditamentos ornamentales de los objetos*? La respuesta es no, y es un punto fundamental tratado en el artículo. Lo importante es tener las geometrías de los objetos de manera que el tamaño de éstos sea acorde a la realidad y, sobre todo, tener la posición exacta de los elementos dentro del HBIM, no siendo tan relevante digitalizar los detalles. La posición de los bienes es fundamental porque para el análisis del estado de conservación, cada objeto se monitoriza en base al sensor instalado más cercano.

Por su parte el LoI almacena información relevante de los objetos, pero que nada tiene que ver con la geometría. Así el LoI almacena datos de los sensores, fechas de inspección, información de materiales, intervenciones realizadas o imágenes de detalle. En definitiva, con el LoI se tiene una ficha personalizada de cada objeto, donde se puede añadir toda la información necesaria para cada caso. Así, en el artículo se decidió utilizar un nivel de detalle (LoD) bajo y un nivel de información (LoI) muy alto.

Con esta configuración en mente se realizó el modelo BIM mediante la utilización de cuatro familias principales: (i) elementos constructivos, (ii) bienes, (iii) nodos o sensores, y (iv) daños.

Los elementos constructivos, considerando que se modeló únicamente el interior de la Biblioteca General Histórica, se engloban en cuatro tipos de familias: (i) muros de mampostería, (ii) bóvedas o arcos, (iii) ventanas, y (iv) suelo. A cada una de estas familias se les asignó información particular acorde a sus propiedades constructivas como son los materiales o las capas, y también a todas ellas se les asignó información relativa a su estado de conservación.

Por su parte, los daños se representaron geométricamente como parches de tamaño variable, acorde a su extensión, adheridos siempre a otro objeto. Su LoI es exhaustivo acorde con el atlas de daños específico desarrollado [135, 136]. Además, a los daños se les añadió información del estado de riesgo del elemento, la urgencia de realizar acciones y la condición de estado en que se encuentra dicho elemento. De igual forma la red de monitorización se representó mediante dispositivos que se acoplan a los elementos constructivos o bienes muebles. En su nivel de información se establecieron los 27 parámetros incluyendo parámetros bioclimáticos (ej. temperatura, luminosidad, CO2), biológicos y estructurales entre otros, así como información específica del fabricante y protocolos de mantenimiento.

Finalmente, los bienes muebles se representaron con diferentes familias, adaptadas a la geometría específica de cada tipo de bien. A todos los bienes muebles se les asignó una parte de información común: los parámetros de conservación preventiva. De esta manera todos los elementos son tratados igual a la hora de inspeccionar su estado.

- Red de sensores e integración IoT: con el HBIM generado, lo siguiente es conectar el modelo HBIM con el edificio real, para tener datos actualizados de los parámetros de conservación. Para ello se hace uso del IoT mediante la red de monitorización instalada en la Biblioteca. Esta red consta de 39 nodos (23 para monitorizar temperatura y humedad ambiente, 1 para la detección de presencia humana, 8 para medir la luminosidad, 2 para CO2, 2 para la radiación solar y 1 para la presencia de xilófagos). Estos sensores están conectados a un servidor al que periódicamente mandan los datos de los parámetros que miden y se almacenan en una base de datos relacional, MySQL, alojada en el propio servidor. Desde el modelo HBIM cada bien inventariado recupera

de esta base de datos los parámetros actualizados del sensor más cercano, almacenando cada parámetro en el nivel de información asignado.

Comprobación del estado de conservación: con los datos actualizados en cada momento se realiza el cálculo del indicador KPI propuesto por Corgnati et al. [137]. Este KPI permite conocer, de una manera sencilla, el estado bioclimático de los elementos considerando todos los parámetros monitorizados.

Para una visualización sencilla por parte del usuario final se añadió una codificación de colores a los bienes, según su KPI, así como una etiqueta llamada "*Status Risk*" que hace alusión al riesgo que corre el elemento según sus condiciones ambientales. Así, un riesgo bajo indica buenas condiciones de conservación, y se le asigna el color verde; un riesgo medio indica que algo no está del todo bien y debe revisarse, asignándose un color amarillo al bien y un riesgo alto indica que es necesaria una actuación inmediata para evitar el deterioro del elemento, asignándose un color rojo. En el caso de elementos compuestos por más de un material, en la visualización del riesgo se estableció al material más desfavorable para prevenir problemas mayores.

Finalmente, en el artículo se aborda el plugin desarrollado, que permite visualizar el estado de conservación y los parámetros climáticos según las exigencias del usuario. Así pues, se puede visualizar un histórico de datos de un determinado sensor en unas fechas establecidas por el usuario, se pueden hacer análisis de todo el espacio interior en función de un único parámetro, por ejemplo, la temperatura, o se puede visualizar el modelo según la urgencia de riesgo de los diferentes bienes. En definitiva, se puede monitorizar el modelo completo con datos monitorizados en tiempo real y actuar de forma rápida para que los elementos no sufran deterioros.

Las conclusiones que se obtuvieron de este artículo son varias: i) se concluye que los sistemas WMLS son aptos para la digitalización de edificios históricos y permiten el paso a modelos HBIM con la precisión adecuada, además de ahorrar mucho tiempo en la toma de datos y permitir la documentación de espacios muy complejos, ii) se ha demostrado que se pueden realizar modelos HBIM con un nivel de detalle bajo (LoD) pero un nivel de información (LoI) muy alto y que con ellos se pueden acometer tareas de conservación preventiva de manera exitosa y exhaustiva, permitiendo incluso prevenir problemas mayores. Además, con esta investigación se ha visto la gran utilidad que en este tipo de escenarios tiene el IoT, puesto que permite conectar el modelo HBIM generado con el edificio real. De este modo se tienen datos reales en el modelo HBIM y se pueden realizar los cálculos necesarios y entender el estado de conservación del edificio de un vistazo. De esta manera, si algo no está dentro de las tolerancias será fácil de detectarlo (estará en rojo o amarillo) y rápidamente se podrá actuar para corregirlo. Finalmente, y no menos importante, se concluye que el uso de los indicadores KPI es una forma eficiente de monitorizar el estado bioclimático de los edificios sin desestimar ningún parámetro, pues todos son tenidos en cuenta para establecer el estado de conservación.

Automation in Construction 121 (2021) 103449

Contents lists available at ScienceDirect

Automation in Construction

journal homepage: www.elsevier.com/locate/autcon

An historical building information modelling approach for the preventive conservation of historical constructions: Application to the Historical Library of Salamanca

Rocío Mora [a,*], Luis Javier Sánchez-Aparicio [b], Miguel Ángel Maté-González [a,c,d], Joaquín García-Álvarez [e], María Sánchez-Aparicio [a], Diego González-Aguilera [a]

[a] Department of Cartographic and Land Engineering, University of Salamanca, Higher Polytechnic School of Ávila, Hornos Caleros, Ávila, Spain
[b] Department of Construction and Technology in Architecture (DCTA), Escuela Técnica Superior de Arquitectura de Madrid (ETSAM), Universidad Politécnica de Madrid, Av. Juan de Herrera 4, 28040, Madrid, Spain
[c] Department of Environment, Land and Infrastructure Engineering, Politecnico di Torino, 10129 Torino, Italy
[d] Department of Topographic and Cartography Engineering, Higher Technical School of Engineers in Topography, Geodesy and Cartography, Technical University of Madrd, Mercator 2, 28031, Madrid, Spain
[e] Fundación Santa María la Real del Patrimonio Histórico, Aguilar de Campoo, Palencia, Spain

ARTICLE INFO

Keywords:
Cultural heritage
Preventive conservation
Historical building information modelling
Internet of things
Monitoring network
Wearable mobile mapping system

ABSTRACT

This work presents an approach for the preventive conservation of historical constructions by means of Historical Building Information Modelling (HBIM) strategies. To this end, the methodology exploits the latest advances in inspection protocols, digitalization tools -by means of the novel back-pack mapping systems- as well as wireless monitoring networks. All this information is integrated in the HBIM environment by using ad-hoc families and interoperable communication protocols that allow obtaining a complete knowledge of the conservation status of the site. Additionally, the approach uses key performance indicators in order to evaluate the environmental conditions of the different assets presented in the site. All these features have been validated in one of the most representative heritage buildings in Spain: The General Historical Library of the University of Salamanca.

1. Introduction

Nowadays preventive conservation could be considered the most effective preservation approach for heritage buildings. This strategy is able to safe around 40–70% of the total maintenance costs in contrast with traditional remedial approaches by avoiding major interventions and promoting the use of monitoring networks as well as periodic inspections [1]. However, there are several challenges that turn difficult its effective implementation, requiring the development of standardized and integrated protocols for documenting and managing all the information needed to preserve the site. In this context, BIM-based strategies have been placed in as one of the most promising technologies. These approaches aim at improving the building life-cycle process by introducing the concept of interoperability, increasing cost- and time-effectiveness as well as improving the communication between agents [2]. In the context of built cultural heritage, this approach is commonly named as HBIM (Historic Building Information Modelling). It is emerging as a new management system, focused on digitalizing historic structures by creating full physical models populated with meaningful attributes, namely the construction system, constituent materials, existing damages, monitored quantities or maintenance costs among others [3–6]. This approach offers several advantages compared to traditional methods, such as: i) centralization of information; ii) analysis of the different interventions carried out and; iii) fluid communication between agents. This set of advantages makes possible the use of HBIM approaches for structural analysis [7,8], damage assessment [4–6,9], restoration [6], documentation [10] and digital representation [11], requiring all the appropriate definition of the different elements. This definition needs of establishing a set of rules, which could be grouped in: i) the Level of Detail (LoD) and; ii) the Level of Information (LoI).

The first level of definition demands the 3D modelling of the elements. In this context Murphy et al. [12] propose using remote sensing approaches to capture the data, enabling to create accurate digital replicas of the building and its assets. This issue is especially important

* Corresponding author.
E-mail address: rociomora@usal.es (R. Mora).

https://doi.org/10.1016/j.autcon.2020.103449
Received 29 May 2020; Received in revised form 1 October 2020; Accepted 9 October 2020

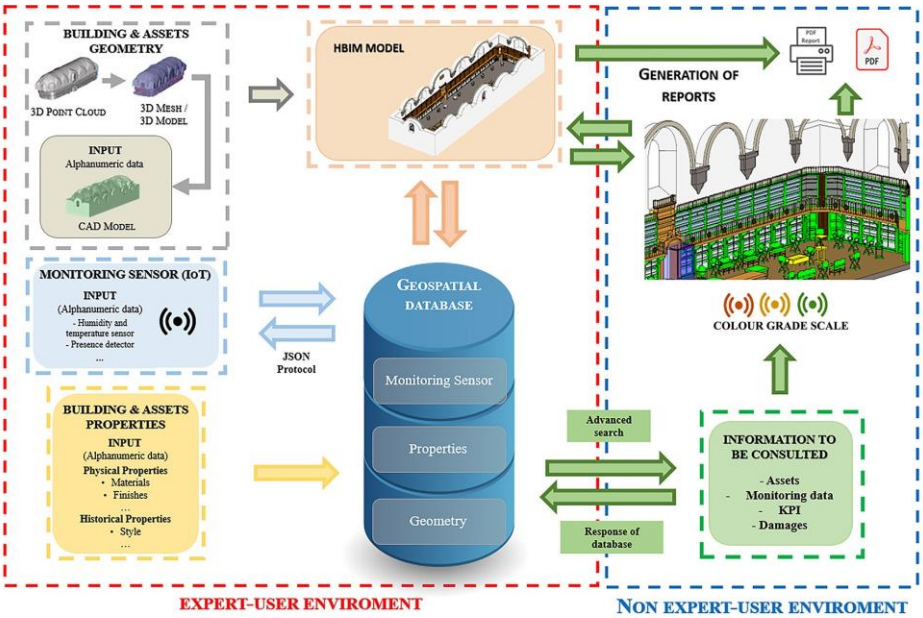

Fig. 1. Graphical representation of the HBIM methodology implemented.

in historical constructions since these elements -construction or not- are often unique pieces with specific geometrical features. Within this context, it is possible to find plenty of applications on which the laser scanning and photogrammetric approaches are used to digitalize historical sites for HBIM applications [10,12,13]. Besides the aforementioned advantages of these solutions, digitalizing heritage sites usually requires the use of a large number of images or scan stations, turning time consuming and involving a possible error accumulation along the network [14]. To cope with these limitations, hybrid solutions, such as the mobile mapping systems (MMSs), have emerged in the last few years. Among the MMSs systems available nowadays, the wearable mobile laser systems (WMLS) have been placed in a privilege position for capturing cultural heritage scenarios [14,15]. This solution combines a 2D laser scanning technology and an inertial measurement unit (IMU) in a portable device which could be handled by a unique operator. The system acquires information while the operator is walking around the heritage site. Then, the 3D point cloud is created by applying the Simultaneous Location and Mapping algorithm (SLAM) [16]. According to di-Filippo et al. [14] and Sánchez-Aparicio et al. [17], this system is ten time faster than laser scanning procedures, providing accuracies that range from 1 to 3 cm.

As stated by Diara and Rinaudo (2019) [18], HBIM models extend the possibilities of CAD models by adding semantic relations between the 3D objects and information. This relation could be understood as the LoI of the object, demanding the proper definition of materials or degradation processes among others. For example, Brumana et al. [19] uses custom properties in the objects to map the damages presented in the building, increasing the objects' LoI by adding historical information. Quattrini et al. [20] proposes the use of shared parameters to establish the same LoI for different HBIM elements. According to Azenha et al. [21], external sources, such as 360 images and laser-scanning data, could be used in this group to complement the geometrical definition of the objects.

Complementary to these considerations, the diagnosis and preventive conservation of cultural heritage sites require the use of monitoring networks to evaluate relevant parameters along the time. These analysis allow to understand the interferences between the assets and their environment [2] or even to evaluate the structural condition of the building, including the possible relation between these parameters and the environmental ones [22]. The first of these aspects is especially relevant in museums and libraries due to the use of active building conditioning systems that control critical variables for the conservation of assets such as the temperature, humidity or luminosity among others [23]. However, the great amount of data generated could be hardly interpreted by non-expert users [24]. To cope with this limitation, several authors propose the application of the so-called Key Performance Indicators (KPI). These indexes are commonly used for a quick and easily readable assessment of heritage structures [22] as well as for evaluating the bioclimatic conditions in museums and libraries [25,26].

Under the previously exposed basis, this work shows an HBIM methodology for the preventive conservation of heritage sites. This methodology integrates geometrical data coming from a WMMS and the information derived from a monitoring network with the standardized inspection protocols developed by the European initiative HeritageCare [27,28]. This initiative attempts to implement standardized protocols for preventive conservation. These protocols are articulated in a total of three complementary levels: i) the Service Level 1 that aim at providing a rapid condition screening of the heritage site; ii) the Service Level 2 that use Web-GIS tool for providing an extended knowledge of the site and its assets and; iii) the Service Level 3 that integrated all the data in a HBIM environment. For more details about these Service Levels reader refers to Masciotta et al. [27]. More specifically, this work will show the results obtained during the implementation of the third service level in one of the Spanish pilot cases: The Historical Library of the University of Salamanca. This implementation gives a step-forward in the current preventive conservation policies of the Library based on the work carried out by Sánchez-Aparicio et al. 2020 [29]. In this work a new Web-GIS platform, based on the use of 360° images and a geospatial database, is developed, corresponding with the second service level of conservation. This platform is mainly focused to the manager of the site, plotting

Fig. 2. WMMS used: a) user working with the wearable laser scan (Zeb-Revo). b) Zeb-Revo equipment.

the essential information for the preventive conservation of the site by means of easy-readable reports as well as the use of KPI based on a unique tolerance defined by the guideline PAS 198:2012 [30]. The main novelties of this work in comparison with this one are: i) the use of HBIM approaches instead of GIS methods for the management of information related with the constructions elements and the assets placed within the Library; ii) an improvement in the use of KPI for preventive conservation by exploiting the data coming from the BIM families as well as a set of tolerances in accordance with the type of material presented; iii) the capacity of filtering the assets with respect to the type of damage presented or its conservation risk and; iv) the possibility of downloading technical information related with the monitoring network.

According to this, the paper is structured as follows: after this initial Introduction, Section 2 describes the materials and methods used for the implementation of the preventive conservation system. Section 3 exposes the experimental results obtained. Finally, the conclusions and future perspectives are drawn in Section 4.

2. Material and methods

The proposed HBIM methodology will be based on three interconnected steps (Fig. 1): i) the 3D digitalization of the heritage site by means of WMMS; ii) the monitoring of the main bioclimatic parameters for the preventive conservation of the assets placed within the library and; iii) an HBIM model that manages the information derived from the previous steps and the information related to the assets. Additionally, the HBIM automatically computes and stores different KPI to evaluate the bioclimatic conditions in each asset according to its materials.

Table 1
Zeb-Revo specifications.

WMLS Zeb REVO	
Measuring principle	Time of flight
Operating time	4 h
Field of view	270° (H) x 360° (V)
Wavelength (nm)	905
Scanner resolution (°)	0.625H x 1.8 V
Orientations system	MEMS IMU
Scanner dimensions (mm)	86 × 113 × 287
Total weight (kg)	4.10
Scanner weight (kg)	1.00
Dimensions (mm)	220 × 180 × 470
Working range (m)	0.60–30 m indoors 0.60–15 m outdoors
Measurement rate	40,000 points per second
Accuracy (cm)	1–3

2.1. Digitalization system

The WMMS used for the present work was the ZEB-REVO back-pack mapping system. This device, commercialized by the GeoSLAM company [31], comprises a 2D rotating laser scanner head Hokuyo UTM-30LX-F (Hokuyo Automatic Co., Ltd. Osaka, Japan) rigidly coupled to an IMU on a rotary engine. The data captured by these sensors is stored in a processing unit placed in a small backpack (Fig. 2). The 3D point cloud is generated by combining the information coming from the scanning head with that from the IMU sensor. To this end, the full SLAM approach of the robotic operative system (ROS) library is used [32]. This approach uses an incremental and interactive procedure to register the segments captured by the scanning head one-by-one. Finally, this registration is refined following a similar framework to the well-known Iterative Closest Point algorithm. The error accumulation derived from the incremental procedure is minimized by a global registration on the basis that the starting and ending points are the same (closed-loop solution).

This sensor has a default range of 0.60-30 m for indoors environments and 0.60 to 15 m for outdoor ones, capturing 40,000 points per second (Table 1). Additionally, to the scanning head, the device has a GoPro camera that allows recording a video when the laser is capturing the scene. The manufacturer ensures an accuracy of 1–3 cm for a 10 min scan, with the closing of a single loop [33]. Further detailed specifications of this device are included in Table 1.

2.2. Monitoring system

In parallel to the digitalization of the site, a monitoring network was installed (Fig. 3). The aim was understanding the conservation needs of the indoor assets of the Library. This monitoring network focused on measuring the main bioclimatic parameters by means of the commercial system MHS (Monitoring Heritage System) [34]. This monitoring system has been developed by the Santa Maria La Real Foundation (*https://www.santamarialareal.org/*), highlighting for its minimal visual impact and great autonomy. The number, location and type of node depend on the specific needs, thereby requiring a pre-monitoring stage to define them property. Table 2 shows the general specification of the nodes used by this monitoring network.

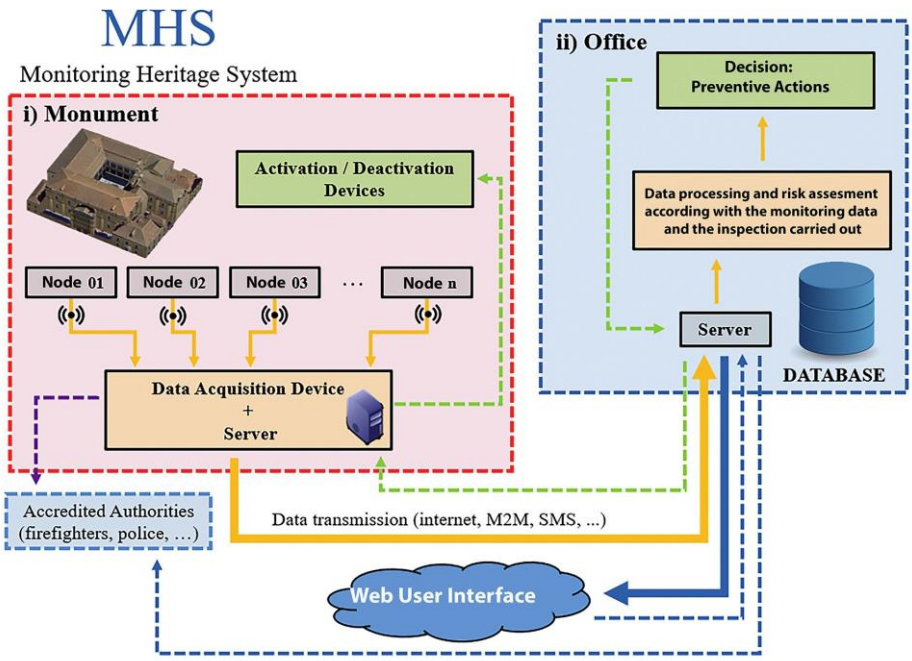

Fig. 3. Scheme of the monitoring network implemented.

The information captured by the local nodes is transmitted to a central node through a Zigbee communication protocol with a bandwidth from 900 MHz to 2.4 GHz. Finally, this information is sent to a dedicated server and can be consulted through a web-based application, as shown in Fig. 3.

2.3. Definition of the HBIM

Even though the relevance of HBIM within the context of historical constructions is assumed, the BIM methodology has been mainly oriented to new buildings, thereby not having a standard consensus for the historic ones yet [35]. This issue makes that some aspects, such as the level of detail (LoD) or the level of information (LoI), should be considered as critical. The LoD determines the graphic aspect of the assets, such as geometry, location in the building, size or orientation; while the LoI stores relevant but non-graphical information of the assets, such as maintenance data, monitoring data, manufacturer information, inspection periods or additional images. In HBIM works objects have so many details difficult to model with unique and non-parametric shapes, specially the ornamental parts, so depending on the purpose of the HBIM it is necessary a higher LoD or a lower LoD. Under this basis, and taking into account that bioclimatic conditions are the main risk for the proper conservation of the assets placed within the Library, the following criteria was adopted: i) a low LoD and; ii) a high LoI. Table 3 shows the different LoD and LoI adopted for each family in accordance with the recommendations exposed by Barmes [36] as well as the international guideline G202TM – 2013 [37] and the Spanish recommendations exposed in the Spanish Chapter of BIM Forum [38].

On the one hand, the geometry of each object (LoD) was based on the data provided by the WMMS, simplifying ornamental elements as well as assuming ideal shapes for the arches and the vault, but defining properly

Table 2
Technical specifications of the nodes used in the monitoring network.

Technical specifications	Values
Communication protocol	ZigBee
Frequency	900 MHz or 2.4 GHz
Programming interface	JTAG/Bootloader
Input/Output	Analogical/Digital
Communication protocols	I2C/ADC/SPI
Energy supply	5 V by means of a converter 3.6 V AA batteries
Signal sensitivity	Up to −110 dBm
Connexion topology	Star / Tree / Mesh
Working temperature	−20 °C/ +70 °C
Limit humidity	80%

Table 3
Level of Detail and Level of Information adopted for each family included in the HBIM model.

Type of object	Level of Detail (LoD)	Level of Information (LoI)
Construction elements	300 Elements properly represented in terms of quantity, size, shape, location and orientation	400 Technical system specification, including components to allow product selection
Assets	300 Elements properly represented in terms of quantity, size, shape, location and orientation	500 Detailed specification of manufacturer's product, testing operation and maintenance
Nodes	200 Generic system, object, or assembly with approximate quantities, size, shape, location, and orientation	500 Detailed specification of manufacturer's product, testing operation and maintenance
Damages	200 Generic system, object, or assembly with approximate quantities, size, shape, location, and orientation	500 Detailed specification of manufacturer's product, testing operation and maintenance

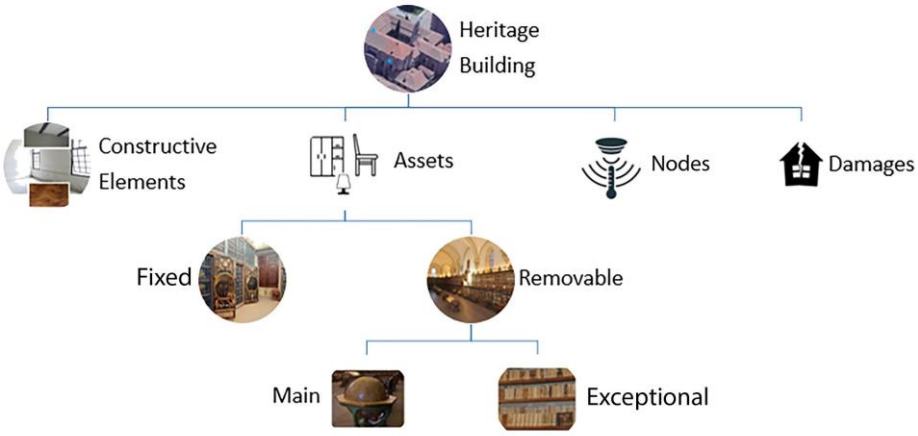

Fig. 4. Object classification proposed.

Name ID Historic Masonry Wall

Category Construction

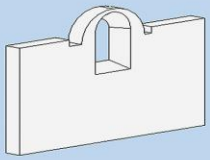

Parameter Name	IFC Type data	Notes
Geometric Data		
Height	IFCReal	Example: 1.20 m
Length	IFCReal	Example: 4.23 m
Thickness	IFCReal	Example: 0.65 m
Material Characterization		
Stone Type	IFCText	Example: Granite
Stone Origin	IFCText	Only if known
Stone Density	IFCReal / IFCMassDensityMeasure	Kg / m3
Other Materials	IFCText	If it is known the presence of other materials
Outdoor Finishing System	IFCText	Finished system of exterior wall
Indoor Finishing System	IFCText	Finished system of interior wall
Facade Composition	IFC Text	Example: 1Leaf / 2Leafs
Conservation Data		
Previous Intervention	IFCText	Type of intervention
Last Intervention Date	IFCText	Date last intervention
Conservation State	IFCText	Good, Medium, Bad
Photographic Survey	IfcRelAssociates	Link to Image

Fig. 5. Construction elements family structure with the IFC parameters added to complete the information.

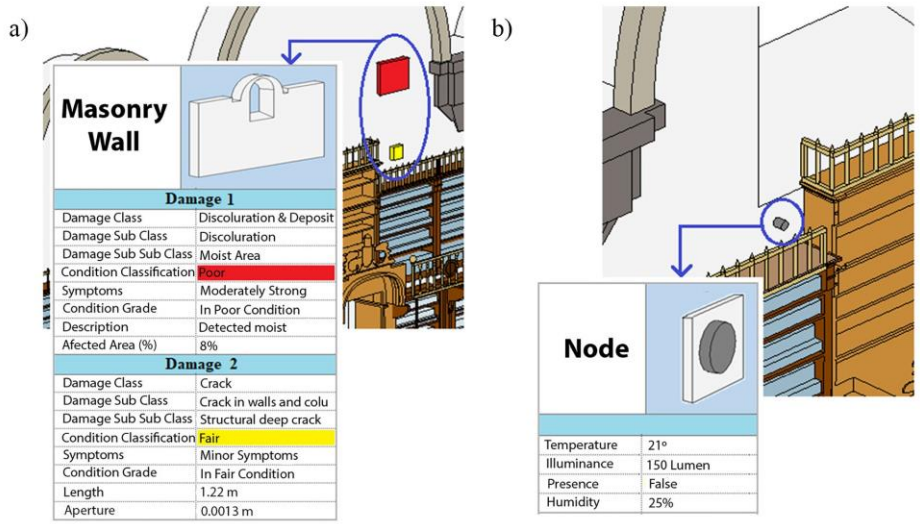

Fig. 6. Damage and node objects within the HBIM model. a) Two damages with different risk attached in a construction element. b) Node patch placed in the library and its parameters.

the materials presented on them. The pass from the point cloud to the CAD model was carried out by means of reverse engineering procedures, similar to those showed by Bautista de Castro et al. [39] or Sánchez-Aparicio et al. [40]. The geometrical information omitted, e.g. the ornamental parts, was included in the LoI of each object.

In contrast to this low LoD, the current methodology introduces an exhaustive LoI to handle the properties of each material, changes suffered, or damages presented. In order to establish this LoI correctly to each object, the elements were classified depending on the information each one needs into 4 main groups (Fig. 4) (Table 3): i) construction elements; ii) assets; iii) nodes; iv) damages.

All this graphical and non-graphical information was translated into the open exchange format IFC4 (Industry Foundation Classes version 4), thereby ensuring the inter-operability between different tools and HBIM scalability. IFC allows to export any kind of information so that all the custom parameters created for the new assets, damages and nodes are well contemplated.

2.3.1. Construction elements

According to the purpose of the HBIM, only the inner envelop of the library was modelled. In this sense it was necessary to take into consideration four different types of families: i) masonry walls; ii) vaults and arches; iii) windows and; iv) slab. The information inserted in the walls and vaults has been defined with the aim of including all the relevant construction parameters, namely (Fig. 5): i) number of leafs; ii) material used in each leaf; iii) finishing material. The main door and the windows, made up by glasses, include the following information labels: i) number of layers; ii) type of glass in each layer and; iii) type of frame. Finally, the timber floor was defined by the following tabs: i) number of joint's sets; ii) type of wood; and iii) finishing material.

Complementarily, these families include all the relevant information with respect to its conservation state. In this sense, the following fields were included: i) previous interventions; ii) last interventions date and iii) conservation state. Due to simplifications during the geometrical modelling, each family includes the possibility of inserting different images that allow complementing the spatial definition of the element defined.

Table 4
Options for the labels condition classification and status risk. The text between brackets is the value assigned to the third information label.

Label	Values
Condition classification	Good
	Fair
	Poor
	Bad
Status risk	Low (long term)
	Moderate (intermediate term)
	High (short term)
	Severe (urgent and immediate)

2.3.2. Damages

Damages are represented by means of custom patch-objects, as proposed Sousa et al. [41]. Path-objects are geometrically simple elements with a low LoD, but with a very complete LoI. In this sense the geometry of each damage is modelled by means of rectangular patches attached to some construction element or asset. Each patch has different size and colour depending on the affected area and relevance of the damage (Fig. 6a). The LoI of this object includes an exhaustive definition of the damage according to the damage atlas developed within the framework of the HeritageCare project [27,28]. This atlas classifies each damage according to a three-level system, i.e. class of damage, sub-class of damage and sub-sub-class of damage. Moreover, these objects include: i) a condition classification; ii) a status risk; iii) urgency to take an action; and iv) affected area. It is worth mentioning that the third information label depends on the values adopted by the status risk (Table 4). The fourth information label refers to the extension of the damage, allowing that the user can introduce the metric values of the damage in two ways: i) by introducing the percentage of the affected area with respect to the constructive element (HeritageCARE approach) [27] or; ii) by introducing the area or volume of this damage. In the case of cracks, this second approach uses two metric parameters: i) the length of the crack and; ii) the aperture of the crack. These parameters allow to monitor the evolution of the damage through time.

Name ID Shelving

Category Removable Asset

Parameter Name	IFC Type data	Notes
Geometric Data		
Height	IFCReal	Example: 1.20 m
Length	IFCReal	Example: 4.23 m
Depth	IFCReal	Example: 0.65 m
Shelves Number	IFCInteger	Example: 1 - 2 - 3
Shelves gap Separation	IFCReal	Example: 0.40 m - 0.50 m
Identification Data		
Asset ID	IFCInteger	Example: 121
Asset Name	IFCText	Example: Shelving with original books
Asset Code	IFCInteger	Example: 111
Asset Category	IFCText	Example: Furniture
Inspection Periods	IFCDate	Date of known inspections
Owner Name	IFCText	Owner's name if known
Owner Contact	IFCTExt	Telephone to contact
Changes / Modifications	IFC Text	Kind of changes suffered for the asset
Short description	IFCTExt	Description of the asset
Material	IFC Text	Main Material
Support Material	IFC Text	If exist any other material
Techniques Manufacture	IFC Text	Types of tools used
Photographic Survey	IfcRelAssociates	Link to the image of the asset
Damages Assesment		
Class of Damage	IFCText	Example: Biological Colonization
Sub-Class of Damage	IFCText	Example: Rot
Sub-Sub-Class of Damage	IFCText	Example: White rot
Condition Classification	IFCText	Example: Good, Fair, Poor, Bad
Symptoms	IFCText	Example: No Symptoms, Minor Symptoms
Condition Grade	IFCText	Example: In good condition, in fair condition
Extent	IFCReal	Example: 10.2 %
Length *	IFCReal	Example: 0.52 m
Aperture *	IFCReal	Example: 0.05 m
Condition Risk	IFCText	Example: Low, Medium, High
Urgency Risk	IFCText	Example: Long Term, Intermediate Term
Status	IFCInteger	Example: 1, 2, 3

Fig. 7. Asset family structure with the IFC parameters for the asset, including conservation and preventive ones, created ad-hoc for the HBIM. In the upper right is the geometric model. * refers to those metric parameters related with the crack damage.

Name ID Node

Category Monitoring Network

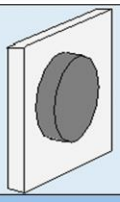

Parameter Name	IFC Type data	Notes
Geometric Data		
Radius	IFCReal	Example: 0.10 m
Identification Data		
Node ID	IFCInteger	Example: 8
Date Installation	IFCDate	Example: 11 / 01/2019
Connection Type	IFCText	Example: Zig-Bee
Monitoring parameter	IFCText	Example: C, S for CO2 and Solar radiation
Inspection Periods	IFCDate	Date of known inspections
Status	IFCInteger	Example: 1, 2, 3 depending of the KPI
Parameters Data (example of tow parameters)		
Temperature	IFCReal	Example: 21º
Humidity	IFCReal	Example: 25%

Fig. 8. Node family structure with the IFC parameters for the monitoring network.

2.3.3. Assets

Both the main and removable assets have been represented by instances of new families, created ad-hoc for this job. The families have their own geometric parameters, which are different for each object type. However, in order to make it reusable and scalable, these families show the same conservation and preventive information parameters. These new set of parameters have been structured in two groups as follows (Fig. 7): i) the data related with the identification and location of the assets and; ii) the data related with the damage presented in the asset.

2.3.4. Monitoring network

The monitoring network is a collection of different instances of a new family, representing each node of the system. This family has also been represented by means of patch-objects (Fig. 6b), which are always attached to a main object, such as construction elements or assets. To represent the nodes, these patches are modelled by cylindrical disks of the same size. The information added to these objects refers to the parameters registered by each node (Fig. 8). The current version of this family integrates 27 parameters including bioclimatic (temperature, CO2, luminosity), structural (e.g. inclination or crack width) and biological (e.g. presence of xylophagous). Each node stores information of the manufacturer, installation date and maintenance protocols, as well.

2.4. Integration of the monitoring data within the HBIM environment

The data acquired by the monitoring network is processed following a workflow specifically designed to make periodic queries to the monitoring server (Fig. 9a). The data of these queries is encapsulated and transmitted through the use of a JSON file, which includes the node description attributes (id, location, description, dimensions, weight, date of installation and custom information provided by the manufacturer) as well as all the parameters showed in Section 2.3.4. (Fig. 9b). The data captured by each node is stored in a MySQL database that allows plotting graphs to analyse the evolution of specific parameters along the time. Moreover, the data can be exported into a tabulated format, i.e. an EXCEL file, to process it by an external software.

It is worth mentioning that each object defined in the HBIM environment includes a label defined as *Status* (Fig. 7 and Fig. 8). This field allows to classify the conservation risk of each object according to its current bioclimatic condition. In this sense, the current version of the API implements the KPI proposed by Corgnati et al. [25] (Eq. (1)). These KPI have been implemented in the previous Service Level of the HeritageCARE method [29].

$$KPI = \frac{N_{in}}{N_{tot}} \tag{1}$$

where N_{in} represents the number of measurements within the defined tolerances and N_{tot} the total number of measurements.

These KPI define the percentage of measurements in which the monitored parameter lies within a required range of tolerances (Eq. (1)). A value of 100 means a perfect match (all the measures are within the limits). Meanwhile a value of 0 represents a total mismatch being all the measures out of tolerance. If the value of the KPI is above 90%, the HBIM

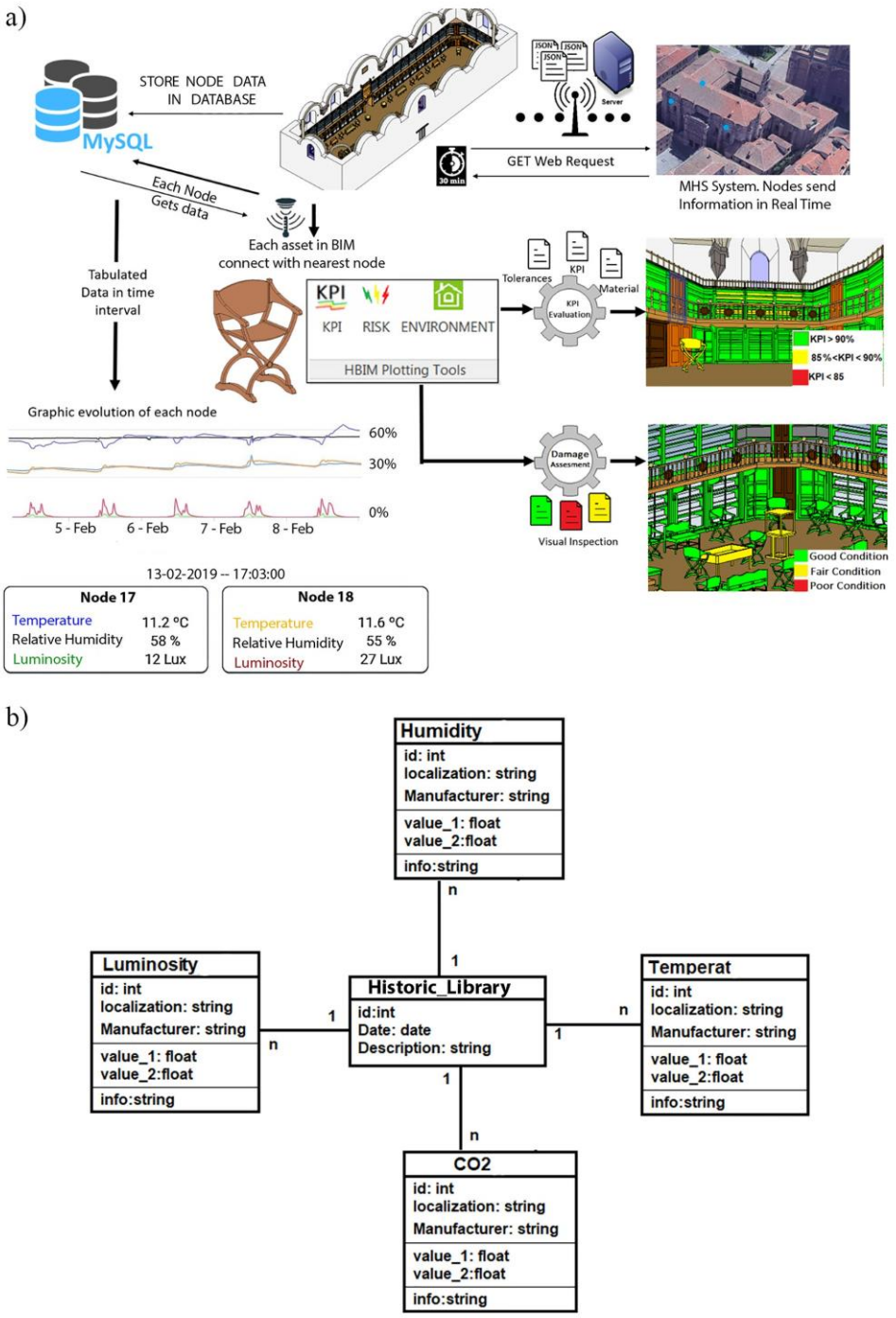

Fig. 9. Connection of the monitoring network with the HBIM environment: a) general workflow; b) Structure of the MySQL database.

Table 5
Admissible tolerances for assets in accordance with its material. Adapted from Adcock [42].

Material	Temperature (°C)	Humidity (%)
Paper	18–22	40–55
Scroll	18–22	45–60
Leather	16–20	45–60
Textile	16–20	30–50
Wood	17–21	45–60
Metal works	18–22	15–55

Table 6
Admissible levels of luminosity for different type of materials. Adapted from Sharif-Askari and Abu-Hijhel [43].

Object Type	Lux lumen/m^2
Very Sensitive[a]	0–50
Sensitive[b]	0–200
Insensitive[c]	0–300

[a] Very sensitive: book, manuscript.
[b] Sensitive: Oil/tempera painting, undyed leather.
[c] Insensitive: Metal, ceramic, stone.

system assigns to the *Status* label a value of 1 (low risk). If the value is below 90% but above 85%, the HBIM system assigns a value of 2 (medium risk). Finally, if the value is below 85% the HBIM system assigns a value of 3 (high risk).

2.5. Tolerances for the bioclimatic monitoring

The preventive conservation of museums and libraries requires a rigorous control of the bioclimatic conditions in order to maintain the assets, e.g. books, manuscripts or painting among others, in optimal conditions. According to Pavlogeorgatos [23], the five main environmental parameters that can promote the degradation of the assets placed in libraries are: i) temperature; ii) relative humidity; iii) illumination; iv) atmospheric pollutant and; v) noise and vibrations. Out of tolerance values in the first four parameters could promote the presence of chemical and physical degradation processes. Meanwhile the last one could promote physical damages.

From this variety of parameters previously shown, the proposed HBIM approach implements the concept of KPI in three of the five fields in accordance with the nodes installed in the monitoring network. In all of these indicators different types of tolerances were taken into consideration according to the materials defined in the HBIM objects (Table 5 and Table 6). These set of tolerances extend those proposed previously by Sánchez-Aparicio et al. [29], including specific tolerances of the different materials presented on the library. Then, this parameter was used to define the label *Status* of each object. Additionally, the system includes a KPI for the xylophagous detector. In this case, only two values were included in the label *Status* [29]: i) 1 if the node does not detect the presence of xylophagous and; ii) 3 if the node detects the presence of xylophagous.

3. Experimental results

3.1. Study case: the Historical Library of the University of Salamanca

The General Historical Library of the University of Salamanca dates back to the XV century and is part of the *Escuelas Mayores*, placed in the historical centre of Salamanca (Castilla y León, Spain). The Library is located on the second floor, behind the main Plateresque style facade (Fig. 10), which is an emblematic symbol of the oldest Spanish University.

The building has been modified several times since its creation in 1254, when the king Alfonso X reorganized the academies. In the reorganization it was created the stationary house. During the XV century, the manuscripts were moved to a specific room in the San Gerónimo chapel, inside the building of *Escuelas Mayores*. The General Historical Library was built between 1509 and 1526. In 1749, it was restructured according to the instructions of Andrés García de Quiñones, and it has maintained its appearance since then (Fig. 11). With respect to the architecture, the Gothic door stands out. It was forged in 1526 with an arch carpanell, archivolts decorated with plant and animal elements

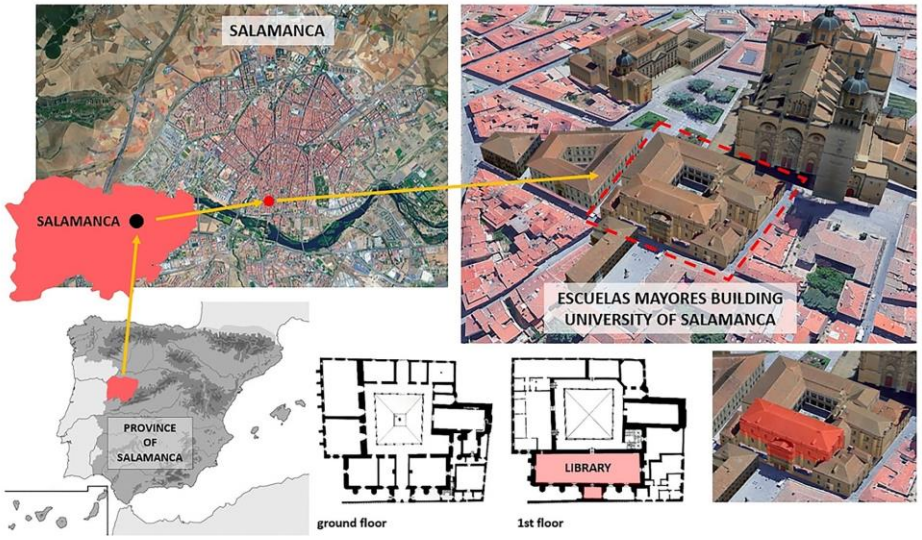

Fig. 10. General Library of the University of Salamanca location.

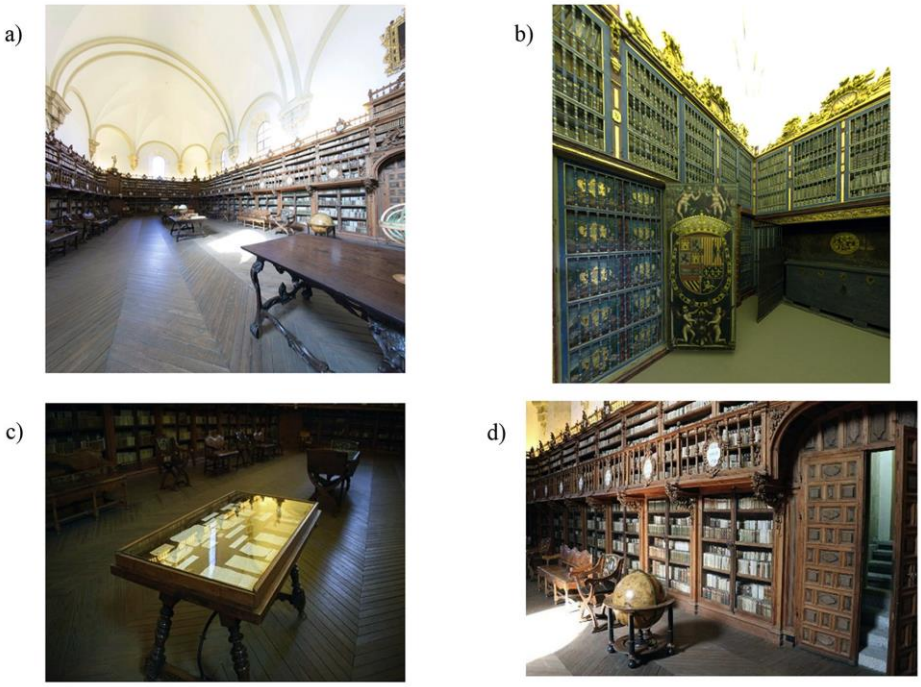

Fig. 11. a) General view of the Library and arrangement of the shelves. b) Manuscript Room. c) Table where several manuscripts are exhibited. d) Books and world globes.

and closed with a Renaissance grille. The gallery is covered with a lunette vault in the centre and a polygonal shape at its ends [44] (Fig. 11a).

The library contains an extensive bibliographic collection formed by 483 incunabula, 2774 manuscripts, and 62,000 printed volumes. All these elements have many different origins so, in order to have them ordered, they are divided in different fields of knowledge. There are eight categories: i) Literature; ii) Maps; iii) Language; iv) Natural; v) History; vi) Religion; vii) Medicine-Science and Technique; viii) Laws and History. The codex *Las Virtuosas y Claras Mujeres,* the incunabulum *Libro de Ajedrez, Libro del Buen Amor* or *the Appian's Cosmography* stand out among the books contained in the library. All of them are stored in wooded Baroque style shelves, designed by Manuel de Lara Churriguera [45]. Apart from the documents and books, there are several celestial and armillary wooden spheres, tables, leather and wood chairs and vitrines (Fig. 11).

Besides the Historical Library, there is a small *incunabulum* room that occupies the interior of the Plateresque façade and holds manuscripts of

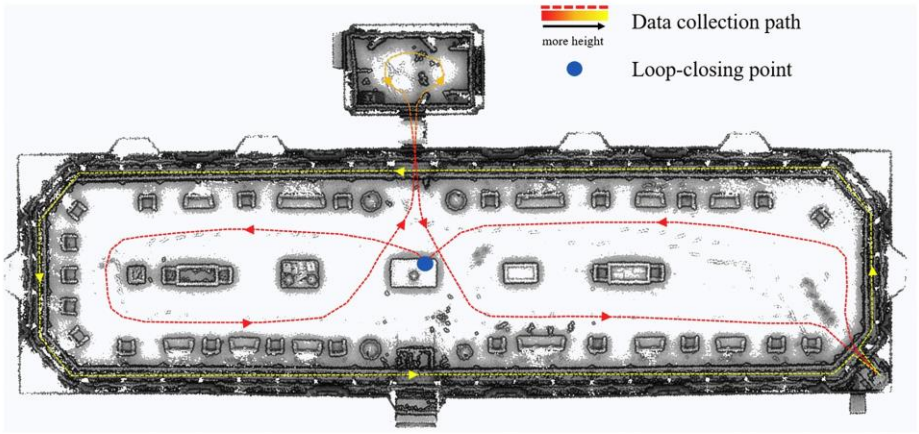

Fig. 12. Data collection path executed for the digitalization of the Library.

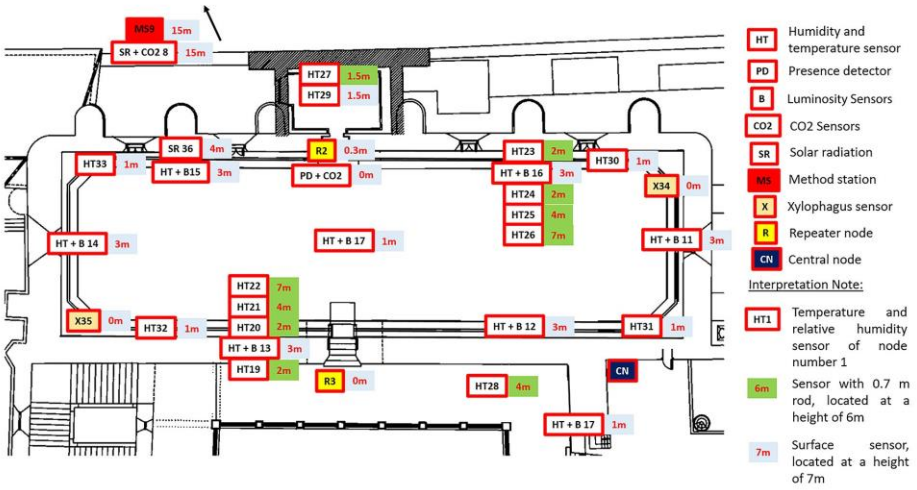

Fig. 13. Nodes distribution in the Library.

the 11th century and the incunabula of the XV century (Fig. 11b). These books are organized in two themes of study: i) Canon Law and; ii) Theology. This room is the old medieval ark of the university, initially used to keep money and, later on, forbidden books.

3.2. *In-field works*

The in-field works were mainly focused on capturing the different type of information required for define the HBIM. Three steps were carried out to this end: i) a visual inspection to improve the knowledge about the conservation state of the Library and its assets; ii) a digitalization of the Library by means of a WMMS and; iii) the installation of a wireless monitoring network.

3.2.1. *Inspection of the library*

The visual inspection of the Library was carried out following the guidelines proposed by the HeritageCare initiative [27,28]. Specifically, the first and second level of inspection protocols were applied. In order to maintaining a common metric during the survey, a mobile app was used, allowing to capture all the necessary data by means of standardized checklists.

On the one hand, the first level of inspection allows to obtain a rapid condition screening of the conservation status of the building. During the inspection, a conservation assessment of each construction element was carried out as well. This assessment included an analysis of the damages presented on the elements following the approach proposed by Masciotta et al. [27]. Each damage is defined by the following variables: i) the class of damage; ii) the condition grade; iii) a short description of the damage; iv) its extension along the construction element and; v) a risk assessment. The result of this inspection allows identifying different types of damage located in the following construction elements: i) structural deep cracks on the bearing wall and on the lunette vault due to the initial accommodation of the structure; ii) moist areas on the vault's keystone coming from the timber roof and iii) some discolorations on the timber floor. Apart from these damages the inspection highlighted the absence of UV filter on the windows, which could promote the photodegradation of some assets as well as inappropriate air ventilation in the *incunabulum* room (Fig. 11b).

The second level of inspection concerned the conservation assessment of the assets presented in the Library by following a similar protocol to the previous one. Due to the huge amount of assets, only the most representative ones were inspected: i) two vitrines; ii) two chairs; iii) one Earth Globe and; iv) twenty-one exceptional books from the different knowledge areas (within its associated shelves). The result of this inspection allowed identifying the different materials presented on the assets as well as the presence of some discolouration and deposits.

Fig. 14. Nodes installation in the Library.

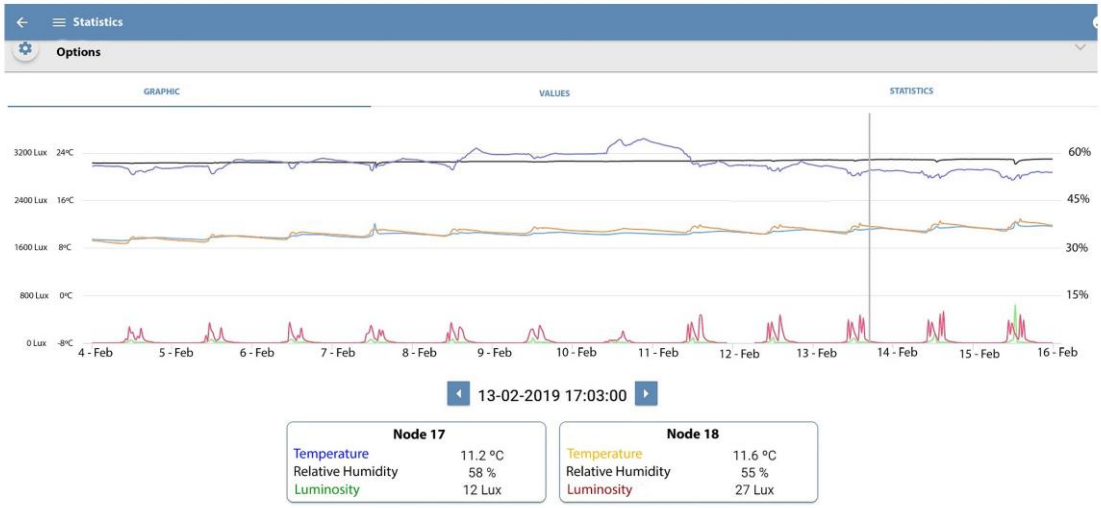

Fig. 15. Real time data captured by the nodes 17 and 18.

3.2.2. Digitalization of the library

The Zeb-Revo Wearable Mobile Mapping System from GeoSlam® [33]. was used for digitalizing the library. The Zeb-Revo system consists of a rotatory head that comprises a 2D laser scan head and an IMU. The head is connected to a processing unit, which is carried by the user in a backpack, allowing the digitalization of large spaces while walking through them. The information captured by the scan head and the IMU are finally integrated to create a 3D point cloud by means of a full-SLAM algorithm [16], providing an accuracy that ranges from 1 to 3 cm.

In order to avoid mistakes and get optimal results, the suggestions of di-Filippo et al. [14] were followed, such as: i) remove any disturbing object; ii) leave doors between different room open to make easy the path; iii) add items to help the algorithm works in those places where the geometry is very similar and with no significant changes and; iv) the designed path should be a loop, starting and finishing in the same point, in order to let the SLAM algorithm adjust errors.

Once the environment was prepared, the digitalization was made in a unique loop with a constant speed to have the same density in all the point cloud and being especially careful in transitions over the doors. For the present case study, 14 min were invested to obtain the 3D point cloud of the whole Library (Fig. 12): eight minutes to capture the data and six to solve the SLAM problem. The point cloud obtained had a total of 15 million of points.

3.2.3. Monitoring system

The final stage of the in-field works involved the installation of a monitoring network. A total of 39 wireless nodes were placed along the Library (Fig. 13 and Fig. 14): i) 23 for monitoring humidity and temperature; ii) 1 for detecting the presence of people; iii) 8 for monitoring luminosity; iv) 2 for monitoring CO_2 in the environment; v) 2 for monitoring solar radiation; vi) 2 for monitoring the presence of xylophagous; vii) and 1 methodological station. In addition to the two local nodes, there was a central node. This node sent the information to the central computer (Fig. 3). The data thrown by each node can be consulted online, providing real time values (Fig. 15). The monitoring system is active since July 2019.

3.3. HBIM environment

The HBIM of the Library was implemented in Revit from Autodesk®. All the features shown in Section 2.3 were included in this framework by means of an in-house plugin named Heritage 5.0 This plugin allows assigning different families to the geometries, with specific LoI, storing and processing the different data captured by the monitoring network as well as calculating the KPI.

The geometrical model of the Library was obtained by using a semi-automatic reverse engineering procedure. This approach starts with the triangulation of the WMMS point cloud, using to this end a 3D Delaunay triangulation. Then the mesh model is processed by applying the stages proposed by Attene [46], which incorporates several automatic and sequential stages: i) a hole filling stage using the radial basis function [47]; ii) a repair stage based on the minimum threshold distance algorithm [48]; iii) a topological and geometric noise removal stage through the use of local re-triangulation methods and anti-aliased Laplacians filters [49]. After this processing stage the mesh is modelled in order to create a suitable solid model for BIM purposes. For basic shapes (e.g. walls or spheres) the RANSAC Shape Detector algorithm was used [50]. For complex shapes a section-based modelling procedure was applied as suggests Sánchez-Aparicio et al. 2019 [40]. All these stages were complemented with standard reverse engineering procedures such as the extrusion for modelling the thickness of different elements (e.g. the walls or the vaults), as well as Boolean operators for creating the windows. Fig. 16 shows a comparative study between several solid models and their corresponding point clouds. As could be observed, the reverse engineering procedure carried out allows to reproduce with an acceptable accuracy the different constructive elements and assets placed within the Library. The largest discrepancies take places on those parts with complex decorative elements which were considered not relevant for the preventive conservation policies of the Library. These decorative elements were included in the information tab of the families (see

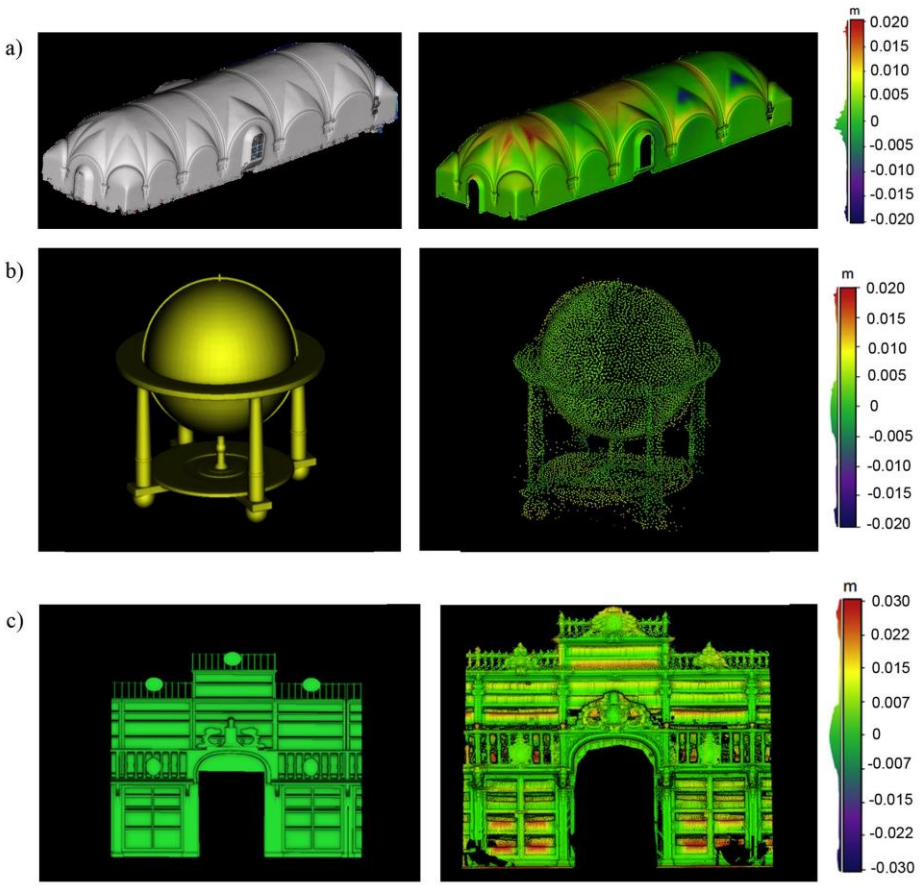

Fig. 16. Discrepancies between the original point cloud and the solid model: a) vault of the Library; b) an armillary wooden sphere and; c) a shelve at the entrance of the Library.

Section 2.3).

The different solid models generated (Fig. 17) were introduced within the BIM environment, using the Heritage 5.0 Plugin to assign the same information attributes to each specific family. The LoI of each asset, node or damage include several common parameters between them (i.e. Condition grade, Inspection Periods, Short Description, Asset ID or Status), which have different values in each particular family. The Heritage 5.0 Plugin allows to add all the common attributes to the desired family in an automatic way, making this task easier and faster (Fig. 18). The data introduced of each family was obtained from the technical inspection (see Section 3.2.1). Additionally, the damages and nodes from the monitoring network were imported by means of path-based families (Fig. 19).

3.3.1. *Checking the monitoring data*

The monitoring network was connected to the HBIM by means of node families according to the disposition shown in Fig. 13. The information shown in each node object corresponds with the latest data received form the *JSON* request. Complementarily, the system stores all this information on its own database (Fig. 9). This allows to plot timeline graphs, thereby assessing the temporal evolution of specific parameters. The user can decide which node and interval is plotted. All this information can be exported in. *CSV* format (Fig. 20).

Additionally, the data stored in the database is used to compute the KPI on each asset of the HBIM. In this case the user can decide the range of dates included in the computation of the KPI. It is worth mentioning that the plugin computes different KPI for the same node according to the different materials presented on the assets (see Section 2.4). Finally, the nearest KPI is assigned to each asset. This KPI is introduced within the *Status* label as an integer value which varies from 1 (green) to 3 (red). Each family has a *Status* label per measured parameter (i.e Status for temperature or Status for relative humidity). In those cases on which the family is integrated by different types of materials, and thus by different ranges of admissible tolerances, the system uses the most unfavourable KPIs to colorize the family (Fig. 21).

Under the basis previously shown different KPI evaluations were

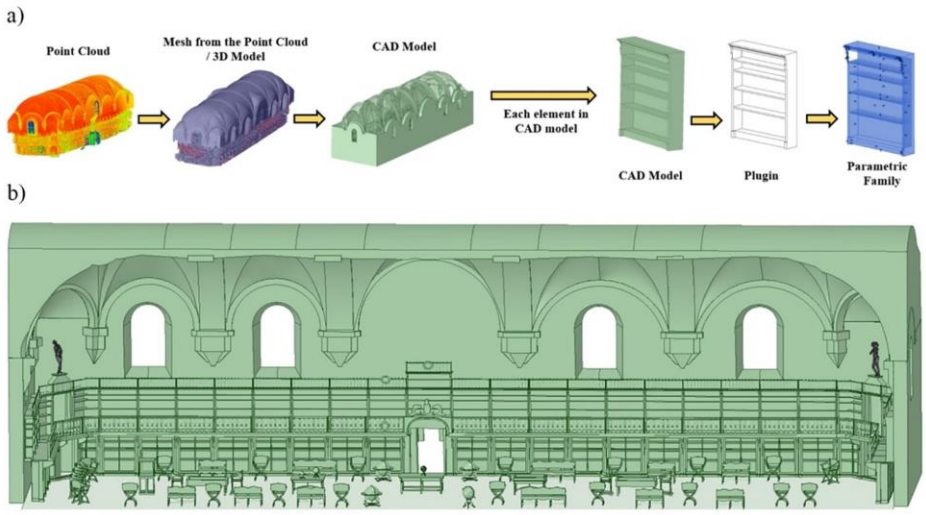

Fig. 17. Geometrical model of the Library: a) workflow; b) detail of the final solid model.

carried out on the Library, considering as the reference period one month. Table 7 and Fig. 22 shows the results of computing the KPI for one cold month such as February. As could be observed, most of the assets are plotted in red which suggest that the bioclimatic conditions could promote some damage on the assets. In all the cases the temperature ranges are not within the acceptable ranges defined in Section 2.5, showing an average value of 12.2 °C with a minimum value of 10.9 °C and a maximum temperature of 16 °C. For this month the relative humidity has an average value of 62% with a minimum value of 58% and a maximum value of 64%, exceeding in most of the cases the admissible ranges (Table 5). Regarding the luminosity, all the nodes of the monitoring network showed optimal values (up to 95%) even for very sensitive assets such as books or manuscripts.

Similar results were obtained for one warm moth (July). In this case the average temperature exceeds the recommended upper bound with an average, maximum and minimum values of 25.4 °C, 27.9 °C and 18.6 °C respectively. These values of temperature could accelerate the degradation of the assets as well as becoming uncomfortable for visitors. The relative humidity during this month was also outside the admissible range, with an average value of 45%. This low value could can cause assets to become dry and brittle.

The results obtained for both months, February and July, corroborates the necessity of a HVAC (Heating, Ventilation and Air Conditioning) control systems for minimizing the possible damage of the assets. This appreciation is in line with the suggestion done during the inspection carried out in Section 3.2.1.

3.3.2. Conservation assessment and damage

Apart from plotting in a graph the KPI of each asset, the plugin allows plotting different parameters of relevance for the preventive conservation of the site, such as the urgency risk. Due to the absence of UV filter in the windows, as well as an adequate ventilation system in the *incunabulum* room, the conservation status of the assets was fixed to fair, implying a mid-term urgency risk (Fig. 23a). Fig. 23b shows the plot in the case of not considering this issue. In this case, some of the assets show a good conservation status (green colour). Complementarily, the plugin highlights the assets with a specific damage (Fig. 23c).

3.4. Discussion of the approaches adopted for the creation of the HBIM model

This section is devoted to discussing the impact of the different approaches adopted in the proposed HBIM methodology.

Regarding the geometrical aspect, the use of a WMMS proves to be a really efficient solution for the digitalization of heritage sites. This device requires just only 14 min to obtain the whole point cloud of the Library, outperforming the time estimated for a terrestrial laser scanner to digitalize the same area, which could be estimated in 225 min. Apart of this, the flexibility of the system allows to obtain data in complex areas such as corridors (Fig. 11d). The density of the data obtained by the WMMS solution allows to create families with a LoD of 300 (Table 3). This LoD could be considered enough for defining the node, damages and assets. In the case of nodes, this threshold is irrelevant in comparison with the LoI since is a family devoted to capturing the monitoring data. However, this threshold has higher impact in the families that define the damages and the assets. On the one hand, the LoD adopted for the damages allows to define it in terms of urgency, position and orientation by means of patch-families with different sizes in accordance with their severity. The extension and other relevant metric values are considered in the LoI. This approach allows not only the integration and monitoring of the evolution of the damages in a simple way, but also having a rapid screening of the impact of each one (Fig. 19). On the other hand, the LoD adopted for the assets families does not include the most detailed ornamental parts which are included in the LoI by means of the historical data as well as a detailed photographic survey. The adoption of this threshold is in line with the current necessities of the Library in terms of preventive conservation.

The use of KPI and operational thresholds in conjunction with the LoI of the families (in special the material definition) allows to synthetize the big data coming from the monitoring network. This combination allows to obtain an easy-reading and robust screening of the climatic conditions of the assets placed within the Library. This combination

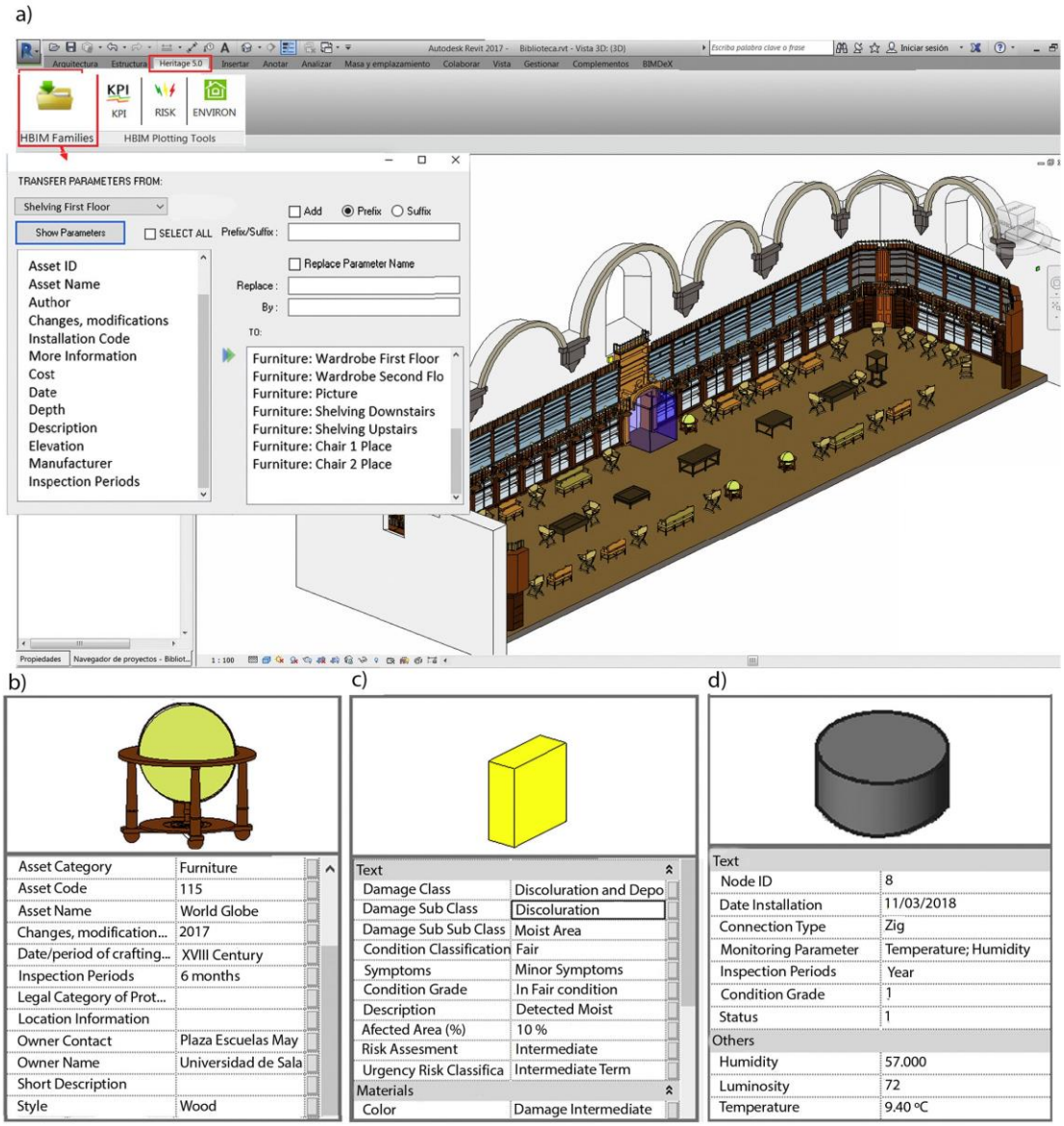

Fig. 18. Application of families to the different solid models created: a) assigning a new family; b) movable asset; c) damage observed in the wall and d) node of the monitoring network.

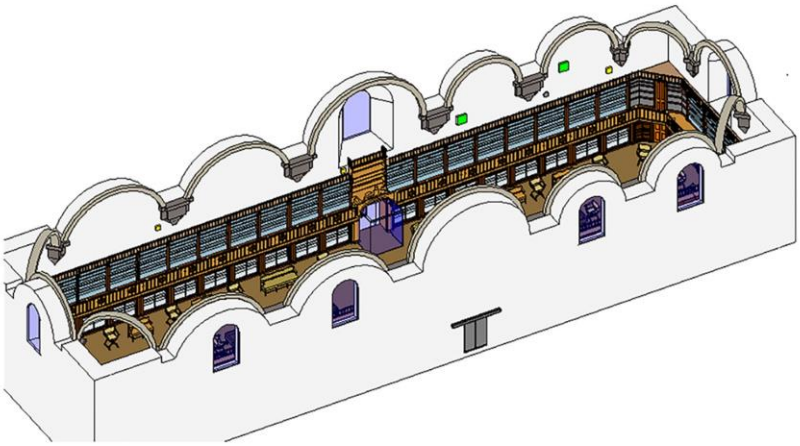

Fig. 19. General view of the HBIM model on which is possible to observe the path-based families used to represent the damages and nodes of the monitoring network.

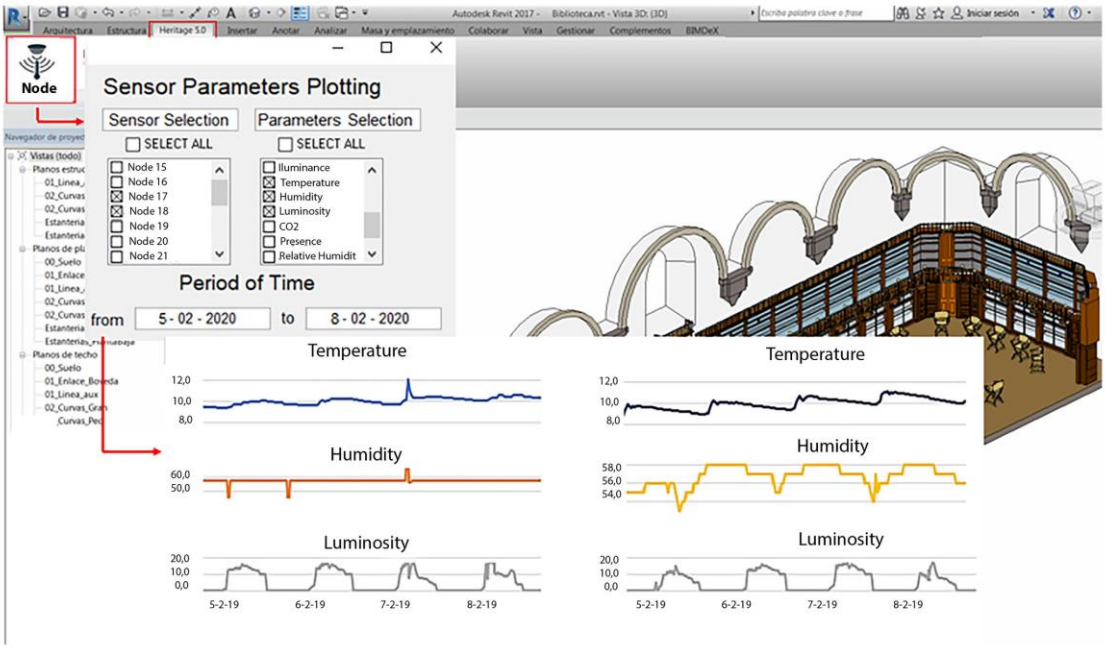

Fig. 20. Appearance of the Heritage 5.0 plugin when the user consults the data of one node.

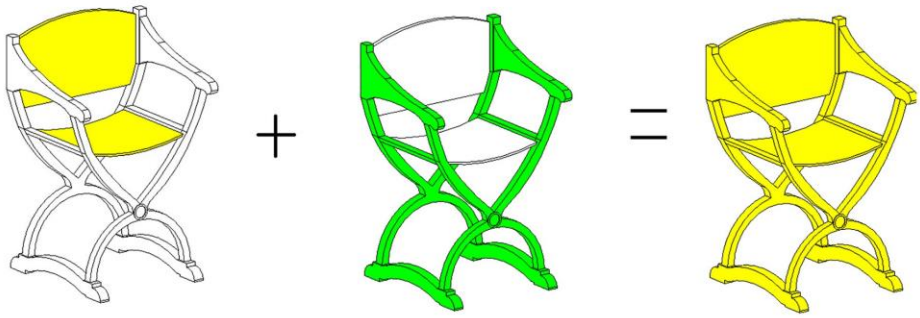

Fig. 21. Computation of the KPI for objects with different materials. Green colour represents a KPI above 90% and Status = 1. Yellow colour represents a KPI between 85% and 90% and Status = 2. (For interpretation of the references to colour in this figure legend, the reader is referred to the web version of this article.)

Table 7
Results of the KPI computation for temperature and humidity during February. Right KPI comes from the temperature evaluation. Left KPI comes from the relative humidity evaluation. Null values refer to situations in which the measured parameters are out of the recommended tolerances.

	Node			
Type of material	07	15	17	18
Paper	0.00 / 1.46	0.00 / 0.00	0.00 / 0.00	21.63 / 0.00
Leather	98.07 / 0.35	0.00 / 0.00	16.38 / 0.00	46.59 / 0.00
Textile	0.00 / 0.35	0.00 / 0.00	0.00 / 0.00	1.41 / 0.00
Wood	98.07 / 0.83	0.00 / 0.00	16.38 / 0.00	46.66 / 0.00
Metal works	0.00 / 1.46	0.00 / 0.00	0.00 / 0.00	21.93 / 0.00

allows to design a deeper preventive conservation plan, enhancing.

4. Conclusions

This paper presents an HBIM approach for the preventive conservation of historical buildings. With this aim, the methodology exploits the latest advances in 3D digitalization, inspection protocols and advanced monitoring networks.

The wearable mobile mapping system pops up due to its lightweight and flexibility compared to traditional approaches, such as photogrammetry and laser scanning. This device just requires to perform a close-loop path to capture the whole scene as well as to compensate a possible error accumulation. The density of the point cloud obtained by this device, within the use of reverse engineering approaches, allows modelling the different elements required to define the HBIM model, such as the assets. To this end, the method applies a post-processing approach for meshing the WMMS point cloud. This mesh is then used as geometrical base for reverse engineering, allowing to obtain a suitable solid model of the construction by means of the use of sections, Loft surfaces, extrusions and Boolean operators.

The low LoD applied in the different families of the HBIM model is complemented by a high LoI. Within this context, the method proposes the use of the standardized inspection protocol proposed by the HeritageCare initiative. This protocol allows the appropriate definition of the different damage presented on the assets as well as the urgency risk. All this information is complemented by images that allow defining different details that are not modelled.

Complementarily to the previously mentioned approaches, the methodology suggests the use of an advance monitoring network that enables capturing different variables of relevance, i.e. environmental variables, used to control the microclimate of the assets. This data can be stored in a database that is directly linked to the HBIM model, allowing to plot graphs as well as to export data in a universal format, i.e. the CSV file.

All the information generated by the different methods is integrated into a unique environment by means of the development of an in-house plugin named Heritage 5.0, thereby generating a multidisciplinary environment that stands out due to its interoperability. This interoperability increases work efficiency between the different agents involved in the preventive conservation of heritage buildings. Apart of fusing this information, the plugin allows exploiting the data contained in each family to compute the so-called KPI in accordance with the different materials presented on the assets. This KPI is plotted in a user-friendly way using a colour-grade scale. Moreover, it could be used to activate any intervention that could facilitate the management of the site. This strategy is also applied for the urgency risk as well as the damage, displaying the conservation status and environmental conditions of the assets as images.

This approach has been applied to one of the most representative Spanish heritage places. It allowed identifying deficiencies that could promote the degradation of the assets, such as the absence of UV filter on the windows or the inappropriate ventilation system in the incunabulum room.

Future works will focus on improving the current version of the tool by adding additional features for the preventive conservation, such as: i) the possibility of plotting technical reports about the conservation state of the site and assets; ii) the integration of structural features that allow evaluating the structural stability of heritage sites by means of HBIM approaches and advanced numerical evaluations; iii) the development of approaches that follow the conservation of heritage sites along time and; iv) the integration of CFD approaches for evaluating the distribution of bioclimatic parameters along the heritage sites. Therefore, new information will be added to the families, such as the transmittance of each layer.

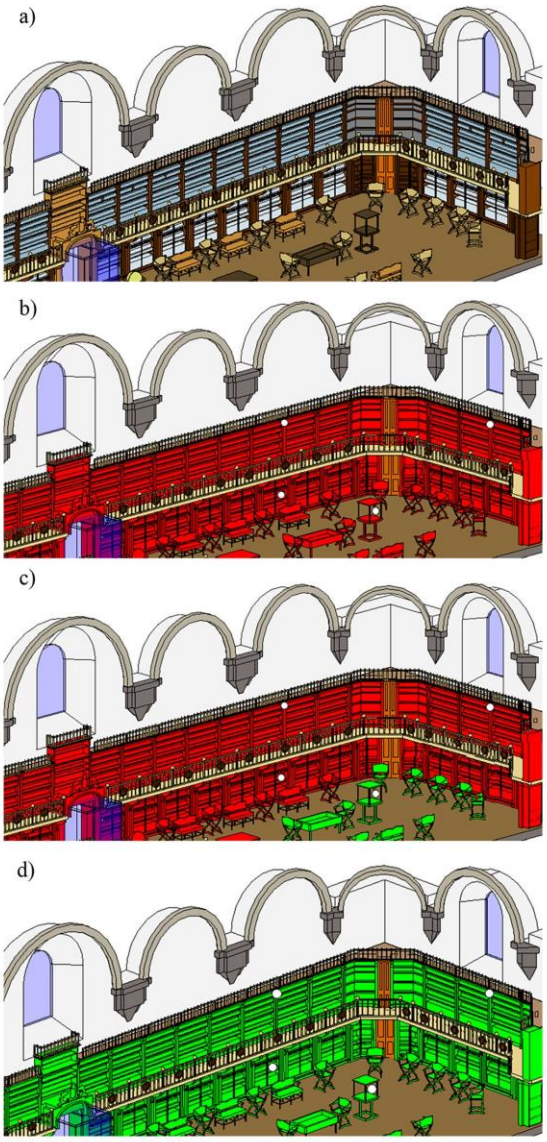

Fig. 22. HBIM model with the KPI plotted: a) general view; b) Computation of the KPI for temperature conditions; c) Computation of the KPI for Humidity conditions And; d) Computation of the KPI for Luminosity conditions. White circles represent the nodes position. The assets plotted in green has a *Status* label of 1, assets in yellow has a *Status* of 2 and assets in yellow a *Status* of 3. (For interpretation of the references to colour in this figure legend, the reader is referred to the web version of this article.)

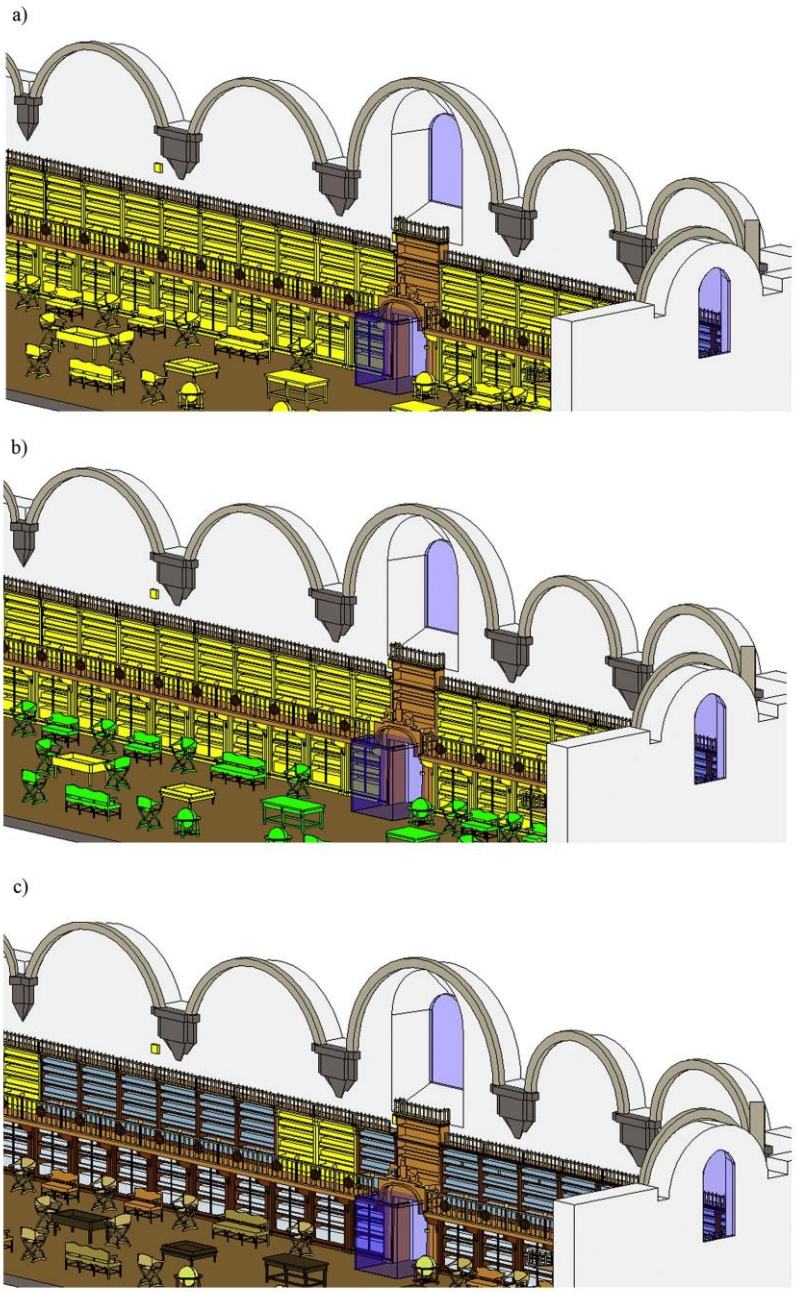

Fig. 23. Graphical plots within the HBIM model: a) Urgency risk considering the absence of ultraviolet (UV) filter and a proper ventilation system; b) urgency risk according with the conservation status of the assets and; c) assets with presence of discolouration.

Declaration of Competing Interest

None.

Acknowledgments

This work was financed by ERDF funds through the V SUDOE INTERREG program within the framework of the HeritageCARE project, Ref. SOE1/P5/P0258 and the research project Patrimonio 5.0 funded by Junta of Castilla y León, Ref. SA075P17.

Authors would like to thank the Department of Cartographic and Land Engineering of the Higher Polytechnic School of Avila and the University of Salamanca, for allowing us to use their facilities and their collaboration during this research. Authors also want to thank the Junta de Castilla y León and the Fondo Social Europeo for the financial support given through programs for human resources (EDU/1100/2017) to the corresponding author of this paper (R.M.), and to the European Union for providing a post-doctoral Grant to another of the authors within the actions Marie Skłodowska-Curie Individual Fellowships, H2020-MSCA-IF-2019 (Grant agreement ID: 894785; AVATAR project) (M.A.M.G.).

References

[1] R.C. Matulionis, J.C. Freitag, Preventive Maintenance of Buildings, Van Nostrand Reinhold, New York, 1991 (ISBN:0-442-31866-9).
[2] P. Jouan, P. Hallot, Digital Twin: A HBIM-based methodology to support preventive conservation of historic assets through heritage significance awareness, in: 27th CIPA International Symposium "Documenting the Past for a Better Future," Ávila, Spain, 2019, pp. 609–615, https://doi.org/10.5194/isprs-archives-XLII-2-W15-609-2019.
[3] M. Murphy, E. Mcgovern, S. Pavia, Historic building information modelling (HBIM), Struct. Surv. 27 (2009) 311–327, https://doi.org/10.1108/02630800910985108.
[4] A. Mol, M. Cabaleiro, H.S. Sousa, J.M. Branco, HBIM for storing life-cycle data regarding decay and damage in existing timber structures, Autom. Constr. 117 (2020) 103262, https://doi.org/10.1016/j.autcon.2020.103262.
[5] R. Brumana, S. Della Torre, D. Oreni, M. Previtali, L. Cantini, L. Barazzetti, A. Franchi, F. Banfi, HBIM challenge among the paradigm of complexity, tools and preservation: the Basilica di Collemaggio 8 years after the earthquake (L'Aquila), in: 26th International CIPA Symposium, Ottawa, Canada, 2017, pp. 97–104, https://doi.org/10.5194/isprs-archives-XLII-2-W5-97-2017.
[6] N. Bruno, R. Roncella, A restoration oriented HBIM system for cultural heritage documentation: the case study of Parma Cathedral, in: ISPRS TC II Mid-Term Symposium "Towards Photogrammetry 2020," Riva del Garda, Italy, 2018, pp. 171–178, https://doi.org/10.5194/isprs-archives-XLII-2-171-2018.
[7] P. Crespi, A. Franchi, P. Ronca, N. Giordano, M. Scamardo, G. Gusmeroli, G. Schiantarelli, From BIM to FEM: the analysis of an historical masonry building, WIT Trans. Built Environ. 149 (2015) 581–592, https://doi.org/10.2495/BIM150471.
[8] A. Calì, Á. Do Valle, P. Dias De Moraes, Building information modeling and structural analysis in the knowledge path of a historical construction, in: Structural Analysis of Historical Constructions, 2018, pp. 2071–2079, https://doi.org/10.1007/978-3-319-99441-3_222.
[9] S. Bruno, M. de Fino, F. Fatiguso, Historic building information modelling: performance assessment for diagnosis-aided information modelling and management, Autom. Constr. 86 (2018) 256–276, https://doi.org/10.1016/j.autcon.2017.11.009.
[10] H.-M. Cheng, W.-B. Yang, Y.-N. Yen, BIM applied in historical building documentation and refurbishing, in: 25th International CIPA Symposium, Taipei, Taiwan, 2015, pp. 85–90, https://doi.org/10.5194/isprsarchives-XL-5-W7-85-2015.
[11] L. Barazzetti, F. Banfi, R. Brumana, D. Oreni, M. Previtali, F. Roncoroni, HBIM and augmented information: Towards a wider user community of image and range-based reconstructions, in: 25th International CIPA Symposium, Taipei, Taiwan, 2015, pp. 35–42. https://re.public.polimi.it/handle/11311/973037 (accessed August 26, 2020).
[12] M. Murphy, E. McGovern, S. Pavia, Historic building information modelling - adding intelligence to laser and image based surveys of European classical architecture, ISPRS J. Photogramm. Remote Sens. 76 (2013) 89–102, https://doi.org/10.1016/j.isprsjprs.2012.11.006.
[13] M. Godinho, R. Machete, M. Ponte, A.P. Falcão, A.B. Gonçalves, R. Bento, BIM as a resource in heritage management: an application for the National Palace of Sintra, Portugal, J. Cult. Herit. 43 (2020) 153–162, https://doi.org/10.1016/j.culher.2019.11.010.
[14] A. di Filippo, L.J. Sánchez-Aparicio, S. Barba, J.A. Martín-Jiménez, R. Mora, D. G. Aguilera, Use of a wearable mobile laser system in seamless indoor 3D mapping of a complex historical site, Remote Sens. 10 (2018) 1–19, https://doi.org/10.3390/rs10121897.
[15] M.Á. Maté-González, L.J. Sánchez-Aparicio, C. Sáez Blázquez, P. Carrasco García, D. Álvarez-Alonso, M. de Andrés-Herrero, J.C. García-Davalillo, D. González-Aguilera, M. Hernández Ruiz, L. Jordá Bordehore, C. López Carnicero, R. Mora, On the combination of remote sensing and geophysical methods for the digitalization of the san Lázaro middle paleolithic rock shelter (Segovia, Central Iberia, Spain), Remote Sens. 11 (2019) 2035, https://doi.org/10.3390/rs11172035.
[16] S. Thrun, Simultaneous localization and mapping, in: Robotics and Cognitive Approaches to Spatial Mapping 38, 2008, pp. 13–41, https://doi.org/10.1007/978-3-540-75388-9_3.
[17] L.J. Sánchez-Aparicio, B. Conde, M.A. Maté-González, R. Mora, M. Sánchez-Aparicio, J. García-Álvarez, D. González-Aguilera, A comparative study between WMMS and TLS for the stability analysis of the San Pedro Church Barrel vault by means of the finite element method, in: 27th CIPA International Symposium "Documenting the Past for a Better Future," Ávila, Spain, 2019, pp. 1047–1054, https://doi.org/10.5194/isprs-archives-XLII-2-W15-1047-2019.
[18] F. Diara, F. Rinaudo, From reality to parametric models of cultural heritage assets for HBIM, in: 27th CIPA International Symposium "Documenting the Past for a Better Future," Ávila, Spain, 2019, pp. 413–419, https://doi.org/10.5194/isprs-archives-XLII-2-W15-413-2019.
[19] R. Brumana, S. Della Torre, M. Previtali, L. Barazzetti, L. Cantini, D. Oreni, F. Banfi, Generative HBIM modelling to embody complexity (LOD, LOG, LOA, LOI): surveying, preservation, site intervention—the Basilica di Collemaggio (L'Aquila), Appl. Geomat. 10 (2018) 545–567, https://doi.org/10.1007/s12518-018-0233-3.
[20] R. Quattrini, R. Pierdicca, C. Morbidoni, Knowledge-based data enrichment for HBIM: exploring high-quality models using the semantic-web, J. Cult. Herit. 28 (2017) 129–139, https://doi.org/10.1016/j.culher.2017.05.004.
[21] M. Azenha, G. Sousa, J. Matos, J. Sena-Cruz, V. Brito, Integrated application of advanced surveying techniques and BIM for inspection and asset management of reinforced concrete bridges, in: International Conference on Interdisciplinary Approaches for Cement-Based Materials and Structural Concrete, 2018. https://repositorium.sdum.uminho.pt/bitstream/1822/58508/1/%5B81%5D.pdf (accessed September 1, 2020).
[22] M.G. Masciotta, L.F. Ramos, P.B. Lourenço, J.A.C. Matos, Development of key performance indicators for the structural assessment of heritage buildings, in: 8th European Workshop on Structural Health Monitoring, EWSHM 2016, 2016, pp. 606–617. https://www.ndt.net/search/docs.php3?showForm=off&id=20121.
[23] G. Pavlogeorgatos, Environmental parameters in museums, Build. Environ. 38 (2003) 1457–1462, https://doi.org/10.1016/S0360-1323(03)00113-6.
[24] M. Bacci, C. Cucci, A.A. Mencaglia, A.G. Mignani, Innovative sensors for environmental monitoring in museums, Sensors 8 (2008) 1984–2005, https://doi.org/10.3390/s8031984.
[25] S.P. Corgnati, V. Fabi, M. Filippi, A methodology for microclimatic quality evaluation in museums: application to a temporary exhibit, Build. Environ. 44 (2009) 1253–1260, https://doi.org/10.1016/j.buildenv.2008.09.012.
[26] De La M.P. Diulio, P. Mercader-Moyano, A.F. Gómez, The influence of the envelope in the preventive conservation of books and paper records. Case study: libraries and archives in La Plata, Argentina, Energy Build. 183 (2019) 727–738, https://doi.org/10.1016/j.enbuild.2018.11.048.
[27] M.G. Masciotta, M.J. Morais, L.F. Ramos, D.V. Oliveira, L.J. Sánchez-Aparicio, D. González-Aguilera, A digital-based integrated methodology for the preventive conservation of cultural heritage: the experience of heritagecare project, Int. J. Archit. Herit. (2019) 1–20, https://doi.org/10.1080/15583058.2019.1668985.
[28] L.F. Ramos, M.G. Masciotta, M.J. Morais, M. Azenha, T. Ferreira, E.B. Pereira, P. B. Lourenço, HeritageCARE: Preventive conservation of built cultural heritage in the South-West Europe, in: K. van Balen, A. Vandesande (Eds.), Innovative Built Heritage Models, CRC Press, London, United Kingdom, 2018, pp. 135–142.
[29] L.J. Sánchez-Aparicio, M.G. Masciotta, J. García-Alvarez, L.F. Ramos, D. V. Oliveira, J.A. Martín-Jiménez, D. González-Aguilera, P. Monteiro, Web-GIS approach to preventive conservation of heritage buildings, Autom. Constr. 118 (2020) 103304, https://doi.org/10.1016/j.autcon.2020.103304.
[30] The British Standards Institution, PAS 198: 2012 Specification for Managing Environmental Conditions for Cultural Collections, 2012 (ISBN: 9780580713156).
[31] GeoSLAM, ZEB Go - GeoSLAM. https://geoslam.com/solutions/zeb-go/, 2020 (accessed September 1, 2020).
[32] M. Quigley, B. Gerkey, K. Conley, J. Faust, T. Foote, J. Leibs, E. Berger, R. Wheeler, A. Ng, ROS: An Open-Source Robot Operating System, ICRA Workshop on Open Source Software 3, 2009, p. 5. Available at, https://www.willowgarage.com/sites/default/files/icraoss09-ROS.pdf (accessed September 1, 2020).
[33] Survey REVOlution, Introducing the ZEB-REVO Mobile Indoor Mapping System, Available at, https://surveyequipment.com/assets/index/download/id/532/, 2017 (accessed September 1, 2020).
[34] M. Chiriac, D. Basulto, E. López, J.C. Prieto, J. Castillo, A. Collado, The MHS System as an Active Tool for the Preventive Conservation of Cultural Heritage, Available at, http://www.arscivilis.org/wp-content/uploads/2013/09/T1P7_MHS_3.pdf, 2013.
[35] M. Azenha, M.G. Masciotta, G. Sousa, C. Alarcon, M.J.C. Morais, J. Sena-Cruz, D. V. Oliveira, Building Information Modelling (BIM) no contexto dos edificios antigos, in: Universidade Nova de Lisboa. Faculdade de Ciências e Tecnologia (Ed.), Conferência Internacional Sobre Reabilitação de Estruturas Antigas de Alvenaria, 2018. http://hdl.handle.net/1822/58488.
[36] P. Barnes, N. Davies, BIM in Principle and in Practice, Ice Publishing, 2015 (ISBN 9780727760920).
[37] American Institute of Architects, AIA Document G202-2013: Project Building Information Modeling Protocol Form, Available at, https://www.aiacontracts.org/contract-documents/19016-project-bim-protocol, 2020 (accessed September 1, 2020).

[38] BuildingSMART Spain, Guía de usuarios BIM. Documento 14- BIM aplicado al Patrimonio Cultura, 2018, pp. 1–46. Available at, https://www.buildingsmart.es/recursos/guías-ubim (accessed September 1, 2020).
[39] Á. Bautista-De Castro, L.J. Sánchez-Aparicio, P. Carrasco-García, L.F. Ramos, D. González-Aguilera, A multidisciplinary approach to calibrating advanced numerical simulations of masonry arch bridges, Mech. Syst. Signal Process. 129 (2019) 337–365, https://doi.org/10.1016/j.ymssp.2019.04.043.
[40] L.J. Sánchez-Aparicio, Á. Bautista-De Castro, B. Conde, P. Carrasco, L.F. Ramos, Non-destructive means and methods for structural diagnosis of masonry arch bridges, Autom. Constr. 104 (2019) 360–382, https://doi.org/10.1016/j.autcon.2019.04.021.
[41] G. Sousa, M. Azenha, J. Matos, V. Brito, Implementação BIM no contexto de inspeção e gestão da manutenção de obras de arte em betão armado: proposta de metodologia e aplicação piloto, in: 2º Congresso Português de Building Information Modelling, 2018, pp. 519–528. Available at, https://repositorium.sdum.uminho.pt/bitstream/1822/58486/1/%5B62%5D.pdf.
[42] E.P. Adcock, M.-T. Varlamoff, V. Kremp, IFLA: Principles for the Care and Handling of Library Material, United States; France, 1998 (ISBN: 2912743001).
[43] H. Sharif-Askari, B. Abu-Hijleh, Review of museums' indoor environment conditions studies and guidelines and their impact on the museums' artifacts and energy consumption, Build. Environ. 143 (2018) 186–195, https://doi.org/10.1016/j.buildenv.2018.07.012.
[44] A. Rodríguez G. De Ceballos, Guía artística de Salamanca, Ediciones Lancia, 2005 (ISBN:9788481771039).
[45] J.L. Díaz Segovia, M.T. Paliza Monduate, Salamanca, Patrimonio de la Humanidad, 1ª Edición, Turimagen Ediciones, 1997 (ISBN: 9788492239702).
[46] M. Attene, A lightweight approach to repairing digitized polygon meshes, Vis. Comput. 26 (2010) 1393–1406, https://doi.org/10.1007/s00371-010-0416-3.
[47] J.W. Branch, F. Prieto, P. Boulanger, Automatic hole-filling of triangular meshes using local radial basis function, in: Third International Symposium on 3D Data Processing, Visualization, and Transmission (3DPVT'06), IEEE Computer Society, Chapel Hill, NC, 2006, pp. 727–734, https://doi.org/10.1109/3DPVT.2006.33.
[48] M. Attene, B. Falcidieno, ReMESH: An interactive environment to edit and repair triangle meshes, in: IEEE International Conference on Shape Modeling and Applications 2006 (SMI 2006), Matsushima, Japan, 2006, p. 41, https://doi.org/10.1109/SMI.2006.29.
[49] I. Guskov, Z.J. Wood, Topological Noise Removal, in: Graphics Interface Proceedings, Ottawa, Canada, 2001, p. 19. Available at, https://digitalcommons.calpoly.edu/cgi/viewcontent.cgi?article=1214&context=csse_fac (accessed September 17, 2020).
[50] R. Schnabel, R. Wahl, R. Klein, Efficient RANSAC for point-cloud shape detection, in: Computer Graphics Forum, Oxford, UK, 2007, pp. 214–226, https://doi.org/10.1111/j.1467-8659.2007.01016.x.

Capítulo V.

Conclusiones y líneas futuras

5. Conclusiones y trabajos futuros

La presente Tesis Doctoral, titulada "*Técnicas de escaneado móvil aplicadas a la digitalización y gestión en edificación",* aborda un análisis detallado sobre el uso de las diferentes metodologías de escaneado móvil aplicadas a la gestión y conservación de edificios, tanto de nueva construcción como edificios históricos. El procedimiento seguido durante la investigación, así como los resultados y conclusiones, se recogen en un total de cuatro artículos científicos de investigación publicados en revistas científicas internacionales de impacto. Los resultados alcanzados por dichos trabajos científicos han derivado en un conjunto de conclusiones y perspectivas futuras que se pasan a exponer a continuación, dividiéndose el primero de estos bloques en un total de tres grupos en función de las diferentes temáticas abordadas y detalladas en la Introducción.

5.1. Conclusiones

5.1.1. Conclusiones Generales

- Las técnicas de escaneado móvil destacan por su flexibilidad, pudiendo ser estas aplicables a una gran diversidad de aplicaciones y plataformas (drones terrestres). La portabilidad de los sistemas de escaneado móvil ha quedado testeada con el uso de dos enfoques totalmente diferentes: por un lado, el empleo de un sistema híbrido formado por la integración de un TLS estático, un dron terrestre y la aplicación de la técnica Stop & Go; y por otro lado mediante el empleo de un sistema de escaneado móvil portable del tipo WMLS junto con la técnica SLAM. En términos de precisión el primer enfoque ofrece precisiones milimétricas mientras que el segundo enfoque tiene precisiones de 1 a 3 centímetros. No obstante, los WMLS son sistemas portables y fáciles de manejar, que disminuyen considerablemente el tiempo de digitalización, permitiendo documentar espacios muy complejos a través de un "paseo" del usuario. Esto los convierte en herramientas muy útiles y versátiles.

- Existe una elevada cantidad de algoritmias que permiten el tratamiento de la nube de puntos resultante y donde encontramos métodos de filtrado o segmentación. El método de procesado básico implementado en esta Tesis Doctoral consta de un filtrado de ruido, una homogeneización de la densidad de los puntos y un alineamiento automático de las diferentes nubes de puntos.

- Las digitalizaciones obtenidas con las diferentes técnicas de escaneado móvil ofrecen precisiones aceptables para sus aplicaciones, habiendo sido validadas en casos de estudio reales con tres fines fundamentales: i) la creación de cartografías 2D y 3D en forma de planos y secciones resultantes; ii) el seguimiento de obras de edificación a través de la comparación de los modelos BIM vs. as-built; y iii) la creación de modelos FEM y HBIM para asistir en el diagnóstico y conservación preventiva de edificios

históricos. Todas estas aplicaciones pueden verse en mayor detalle en los Capítulos II, III y IV.

Resumidas las conclusiones generales, las próximas secciones expondrán, en mayor grado de detalle, las **conclusiones específicas** derivadas de los tres bloques fundamentales tratados en la Tesis Doctoral: i) las técnicas de escaneado móvil; ii) el procesado básico de la nube de puntos; y iii) la aplicación de las nubes de puntos.

5.1.2. Técnicas de escaneado móvil

- Los sistemas de escaneado móvil portables del tipo WMLS son soluciones aptas para la digitalización de edificios, ahorrando gran cantidad de tiempo en la captura de datos y permitiendo la digitalización de escenarios complejos con zonas angostas, o de difícil acceso. Gracias al uso de enfoques SLAM dichas metodologías pueden obtener digitalizaciones con errores comprendidos entre 1-3 cm. En comparación con sistemas de escaneado estático, estas digitalizaciones se obtienen en la décima parte del tiempo.

- Los sistemas de escaneado móvil híbridos del tipo dron terrestre con TLS son sistemas aptos para la digitalización automática de escenarios de forma desasistida. Esta hibridación permite explotar todo el potencial de los sistemas TLS (gran precisión y velocidad de captura de datos) haciéndolos autónomos gracias al uso de plataformas robotizadas y una planificación automática para la toma de los datos. Como resultado de ello, es posible obtener digitalizaciones 3D sin necesidad de disponer de un usuario en el lugar físico, ofreciendo unos resultados de gran calidad, con errores milimétricos y gran densidad de puntos. La mayor limitación del sistema robotizado estudiado reside en los cambios de nivel y la imposibilidad de ser transitados de forma autónoma por parte de este dron terrestre.

- La planificación de la toma de datos es un paso necesario para asegurar una adquisición adecuada a través de sistemas de escaneado móvil. Para el caso del WMLS, dicha planificación ha de tener en consideración la presencia de obstáculos, zonas de paso o zonas con ausencia de características geométricas que pudieran dificultar la toma de datos. Por su parte, los sistemas de escaneado móvil híbridos del tipo dron terrestre y TLS deben disponer de un planificador de rutas integrado que se encargará de calcular la ruta óptima para poder funcionar de manera autónoma. La planificación en este caso debe considerar tres parámetros: i) el porcentaje de solapamiento mínimo requerido entre diferentes tomas, que permita el posterior registro automático; ii) la densidad de cada nube de puntos capturada, que determina la calidad de los datos y; iii) el porcentaje máximo de oclusiones que se admite a fin de asegurar una captura completa y exhaustiva de todo el escenario.

5.1.3. Procesado básico de nubes de puntos

- Las digitalizaciones procedentes de ambos sistemas de escaneo móviles (WMLS y dron terrestre-TLS) requieren del uso de filtros de reducción de ruido para obtener unos resultados óptimos. Para el primero de ellos, el uso del filtro anisotrópico basado en el filtro de aproximación local polinomial (LPA) y la intersección de intervalos de confianza (ICI) aporta muy buenos resultados, mejorando la nube de puntos desde un punto de vista cuantitativo y cualitativo y sin que esto conlleve pérdida de información en el proceso ni la necesidad de introducir inputs para su configuración. En el caso de los sistemas híbridos dron terrestre-TLS, la técnica preferente para eliminar el ruido es el filtro FSOR, que elimina los outliers y puntos claramente erróneos con un coste computacional moderado.

- La densidad y distribución de los puntos de las digitalizaciones realizadas con TLS están condicionadas por la distancia al objeto. Se ha recurrido a técnicas de homogeneización adaptativas de las nubes de puntos mediante técnicas de voxelizado lo que permite tener una densidad homogénea en toda la nube, mejorando los resultados de los procesos posteriores, sin pérdida de calidad o información.

- Los métodos de alineamiento aplicados apoyados en detectores y descriptores 3D han permitido registrar en un mismo sistema de coordenadas una única nube de puntos a partir de diferentes nubes de puntos individuales de manera automática y eficiente. El detector Harris 3D ha resultado de gran utilidad en escenarios de edificación tanto exterior como interior, al detectar esquinas y bordes con gran eficacia. Por su parte el descriptor PFH ha analizado de forma exitosa los puntos, clasificándolos según sean esquinas o bordes.

5.1.4. Aplicaciones de las nubes de puntos

- Las nubes de puntos generadas con sistemas de escaneado móvil pueden utilizarse para realizar modelos CAD as-built a través del uso de métodos de modelado paramétrico y no paramétrico. Dichos modelos pueden ser empleados en fases de diagnóstico y conservación preventiva de edificios históricos.

- Las nubes de puntos procedentes de ambos enfoques, WMLS y dron terrestre-TLS, pueden ser empleadas para obtener cartografías básicas, así como para el seguimiento de obras comparando modelos BIM con modelos as-built a lo largo del tiempo de avance de la obra.

- El análisis estructural de edificios mediante el método FEM puede ejecutarse con los modelos CAD generados. Gracias al uso de métodos no paramétricos tipo NURBS es posible capturar y analizar deformaciones estructurales que comprometen la estabilidad de los edificios.

- Las nubes de puntos capturadas con WMLS pueden ser utilizadas para generar modelos HBIM de los edificios históricos. Para ello es importante determinar el nivel de detalle (LoD) y el nivel de información (LoI) de los elementos. Un LoD bajo con un LoI alto es una configuración adecuada para tareas de conservación y gestión de edificios históricos.

- La gestión y conservación preventiva de edificios históricos se realiza de manera exitosa gracias a la conexión del modelo HBIM (generado con datos geométricos de sistemas láser móvil) con el modelo físico mediante una red de sensores y el uso de la tecnología IoT. Asimismo, el uso de los parámetros tipo KPI permite sintetizar de una manera efectiva el Big-Data procedente de las redes de monitoreo.

5.2. Líneas Futuras

Gracias al desarrollo de la Tesis Doctoral ha sido posible vislumbrar un conjunto de líneas de avance del conocimiento en materia de sistemas de escaneado móvil aplicado a edificación. Dichas líneas se encaminan en el uso de estos métodos para digitalizar y monitorizar escenarios complejos o desasistidos en los que la seguridad de los operarios puede verse comprometida. En concreto se prevé trabajar en los siguientes aspectos:

- Estudiar la viabilidad de los sistemas de escaneado móvil para la digitalización de infraestructuras peligrosas y desatendidas, tales como las subestaciones eléctricas o plantas fotovoltaicas, para las cuales el uso de drones supone una necesidad.
- Investigar y mejorar los procesos de alineamiento automáticos entre diferentes nubes de puntos de manera que sean totalmente automáticos, robustos y eficientes.
- Aplicar técnicas de inteligencia artificial para la segmentación de nubes de puntos y la categorización semántica de los elementos constructivos.
- Contribuir en la automatización del paso de la nube de puntos a los modelos CAD/FEM/BIM a través de modelizaciones basadas en acercamientos paramétricos y no paramétricos.
- Avanzar en la integración de nubes de puntos y/o sistemas CAD de las infraestructuras complejas dentro de gemelos digitales, para los cuales se requiere el uso de sistemas de escaneado móvil a partir de las nubes capturadas

Referencias

Referencias

1. Kim, C., Son, H., Kim, C. **(2013)**. *Automated construction progress measurement using a 4D building information model and 3D data*. Automation in Construction, 31, 75-82. https://doi.org/10.1016/j.autcon.2012.11.041

2. *Australia ICOMOS **(2013)**. Burra Charter: the Australia Charter for Places of Cultural Significance. Australia*. https://australia.icomos.org/wp-content/uploads/The-Burra-Charter-2013-Adopted-31.10.2013.pdf

3. *Athens ICOMOS **(1931)**. Athens Charter: The Athens Charter for the restoration of historic monuments*. In 1st International Congress of Architects and Technicians of Historic Monuments. Athens. https://www.icomos.org/en/charters-and-texts/179-articles-en-francais/ressources/charters-and-standards/167-the-athens-charter-for-the-restoration-of-historic-monuments

4. *Venice ICOMOS **(1964)**. Venice Charter: International charter for the conservation and restoration of monuments and sites*. In 2nd International Congress of Architects and Technicians of Historic Monuments, 25-31. https://www.icomos.org/charters/venice_e.pdf

5. De Naeyer, André, Arroyo, S., & Blanco, J. **(2000)**. *Krakow Charter 2000: principles for conservation and restoration of built heritage*. Krakow, Poland: Bureau Krakow 2000. http://smartheritage.com/wp-content/uploads/2015/03/KRAKOV-CHARTER-2000.pdf

6. Garcia-Gago, J.; Gomez-Lahoz, J.; Rodríguez-Méndez, J.; González-Aguilera, D. **(2014)**. *Historical single image-based modelling: The case of Gobierna Tower, Zamora (Spain).* Remote Sensing, 6(2), 1085–1101. https://doi.org/10.3390/rs6021085

7. Sánchez-Aparicio, L. J., Bautista-De Castro, Á., Conde, B., Carrasco, P., & Ramos, L. F. **(2019)**. *Non-destructive means and methods for structural diagnosis of masonry arch bridges.* Automation in Construction, 104, 360-382. https://doi.org/10.1016/j.autcon.2019.04.021

8. Sánchez-Aparicio, L.J.; Riveiro, B.; Gonzalez-Aguilera, D.; Ramos, L.F. **(2014)**. *The combination of geomatic approaches and operational modal analysis to improve calibration of finite element models: A case of study in Saint Torcato Church (Guimarães, Portugal).* Construction and Building Materials, 70, 118–129. https://doi.org/10.1016/j.conbuildmat.2014.07.106

9. Sánchez-Aparicio, L.J.; Del Pozo, S.; Ramos, L.F.; Arce, A.; Fernandes, F.M. **(2018)**. *Heritage site preservation with combined radiometric and geometric analysis of TLS data.* Automation in Construction, 85, 24–39. https://doi.org/10.1016/j.autcon.2017.09.023

10. Alidoost, F., & Arefi, H. **(2015)**. *An image-based technique for 3D building reconstruction using multi-view UAV images.* The International Archives of Photogrammetry, Remote Sensing and Spatial Information Sciences, 40(1), 43. https://doi.org/10.5194/isprsarchives-XL-1-W5-43-2015

11. Barber, D., Mills, J. **(2007)**. *3D laser scanning for heritage: Advice and guidance to users on laser scanning in archaeology and architecture*. English Heritage. https://historicengland.org.uk/images-books/publications/3d-laser-scanning-heritage/heag155-3d-laser-scanning/

12. Kraus, K.; Waldhäusl, P. **(1993)**. *Photogrammetry: Fundamentals and Standard Processes*. Dümmler Köln, 1, 397. Munich, Germany.

13. Remondino, F.; El-Hakim, S.; Gruen, A.; Zhang, L. **(2008)**. *Turning images into 3D models—Development and performance analysis of image matching for detailed surface reconstruction of heritage objects*. Institute of Electrical and Electronics Engineers. Signal Processing Magazine. 25(4), 55–65. https://doi.org/10.1109/MSP.2008.923093

14. Grün, A.; Remondino, F.; Zhang, L. **(2004)**. *Photogrammetric reconstruction of the Great Buddha of Bamiyan, Afghanistan*. The Photogrammetric Record, 19(107), 177–199. https://doi.org/10.1111/j.0031-868X.2004.00278.x

15. Bayrak, T., & Kaka, A. **(2004)**. *Evaluation of digital photogrammetry and 3D CAD modelling applications in construction management*. In 20th Annual Association of Researchers in Construction Management Conference, 1, 613-621. https://www.arcom.ac.uk/-docs/proceedings/ar2004-0613-0619_Bayrak_and_Kaka.pdf

16. Mongelli, M., de Canio, G., Roselli, I., Malena, M., Nacuzi, A., & de Felice, G. **(2017)**. 3D *Photogrammetric Reconstruction by Drone Scanning for FE Analysis and Crack Pattern Mapping of the "Bridge of the Towers", Spoleto*. Key Engineering Materials, 747, 423–430. https://doi.org/10.4028/www.scientific.net/KEM.747.423

17. Ahmed, M., Haas, C. T., & Haas, R. **(2012)**. *Using digital photogrammetry for pipe-works progress tracking*. Canadian Journal of Civil Engineering, 39(9), 1062-1071. https://doi.org/10.1139/l2012-055

18. Scaioni, M., Barazzetti, L., Giussani, A., Previtali, M., Roncoroni, F., & Alba, M. I. **(2014)**. *Photogrammetric techniques for monitoring tunnel deformation*. Earth Science Informatics, 7(2), 83-95. https://doi.org/10.1007/s12145-014-0152-8

19. Roncella, R., Re, C., & Forlani, G. **(2011)**. *Performance evaluation of a structure and motion strategy in architecture and cultural heritage*. ISPRS International Archives of Photogrammetry, Remote Sensing and Spatial Information Sciences, 38(5/W16), 285-292. https://doi.org/10.5194/isprsarchives-XXXVIII-5-W16-285-2011

20. Gonzalez-Aguilera, D., López-Fernández, L., Rodriguez-Gonzalvez, P., Hernandez-Lopez, D., Guerrero, D., Remondino, F., & Gaiani, M. **(2018)**. *GRAPHOS – open-source software for photogrammetric applications*. The Photogrammetric Record, 33(161), 11-29. https://doi.org/10.1111/phor.12231

21. Guidi, G., Beraldin, J. A., Ciofi, S., & Atzeni, C. **(2003)**. *Fusion of range camera and photogrammetry: a systematic procedure for improving 3-D models metric accuracy.* Institute of Electrical and Electronics Engineers. Transactions on Systems, Man, and Cybernetics, Part B (Cybernetics), 33(4), 667-676. https://doi.org/10.1109/TSMCB.2003.814282

22. Blais, F. **(2004)**. *Review of 20 years of range sensor development*. Journal of electronic imaging, 13(1), 231-243. https://doi.org/10.1117/1.1631921

23. Guidi, G.; Russo, M.; Beraldin, J.-A. **(2010)**. *Acquisizione 3D e Modellazione Poligonale*. McGraw-Hill: New York, NY, USA, ISBN 978-8838665318

24. Nocerino, E., Menna, F., Remondino, F., Toschi, I., & Rodríguez-Gonzálvez, P. **(2017)**. *Investigation of indoor and outdoor performance of two portable mobile mapping systems*. Videometrics, Range Imaging, and Applications XIV, 10332, 103320I_1 - 103320I_15. International Society for Optics and Photonics. https://doi.org/10.1117/12.2270761

25. Kalay, Y.; Kvan, T.; Affleck, J. **(2007)**. *New Heritage: New Media and Cultural Heritage*. *1st Edition*. Routledge: London, UK, ISBN 978-0415773560. https://doi.org/10.4324/9780203937884

26. Del Pozo, S.; Herrero-Pascual, J.; Felipe-García, B.; Hernández-López, D.; Rodríguez-Gonzálvez, P.; González-Aguilera, D. **(2016)**. *Multispectral radiometric analysis of façades to detect pathologies from active and passive remote sensing*. Remote Sensing, 8(1), 80. https://doi.org/10.3390/rs8010080

27. Paparoditis, N.; Papelard, J.-P.; Cannelle, B.; Devaux, A.; Soheilian, B.; David, N.; Houzay, E. **(2012)**. *Stereopolis II: A multi-purpose and multi-sensor 3D mobile mapping system for street visualisation and 3D metrology*. Revue Française de Photogrammétrie et de Télédétection, 200(1), 69–79. http://recherche.ign.fr/labos/matis/pdf/articles_conf/2012/RFPT200_stereopolis.pdf

28. Remondino, F.; Toschi, I.; Orlandini **(2015)**. S. *Mobile Mapping Systems: Recenti sviluppi e caso applicativo*. GEOmedia, 19(4), 6–10. https://doi.org/10.48258/geo.v19i4.1231

29. Rosser, N. J., Petley, D. N., Lim, M., Dunning, S. A., & Allison, R. J. **(2005)**. *Terrestrial laser scanning for monitoring the process of hard rock coastal cliff erosion*. Quarterly Journal of Engineering Geology and Hydrogeology, 38(4), 363-375. https://doi.org/10.1144/1470-9236/05-008

30. Lim, M., Petley, D. N., Rosser, N. J., Allison, R. J., Long, A. J., & Pybus, D. **(2005)**. *Combined digital photogrammetry and time-of-flight laser scanning for monitoring cliff evolution*. The Photogrammetric Record, 20(110), 109-129. https://doi.org/10.1111/j.1477-9730.2005.00315.x

31. Bauer, A.; Paar, G.; Kaufmann, V. **(2003)**. *Terrestrial laser scanning for rock glacier monitoring*. In Proceedings of the 8th International Conference on Permafrost, Zurich, Switzerland, 55–60. https://www.staff.tugraz.at/viktor.kaufmann/Chapter_011.pdf

32. González-Aguilera, D., Gómez-Lahoz, J., & Sánchez, J. **(2008)**. *A new approach for structural monitoring of large dams with a three-dimensional laser scanner*. Sensors, 8(9), 5866-5883. https://doi.org/10.3390/s8095866

33. Alba, M., Fregonese, L., Prandi, F., Scaioni, M., & Valgoi, P. **(2006)**. *Structural monitoring of a large dam by terrestrial laser scanning*. International Archives of Photogrammetry, Remote Sensing and Spatial Information Sciences, 36(5), 6. http://hdl.handle.net/11311/517252

34. Riveiro, B., Morer, P., Arias, P., & De Arteaga, I. **(2011)**. *Terrestrial laser scanning and limit analysis of masonry arch bridges*. Construction and building materials, 25(4), 1726-1735. https://doi.org/10.1016/j.conbuildmat.2010.11.094

35. Lõhmus, H., Ellmann, A., Märdla, S., & Idnurm, S. **(2017)**. *Terrestrial laser scanning for the monitoring of bridge load tests – two case studies*. Survey Review, 50(360), 270–284. https://doi.org/10.1080/00396265.2016.1266117

36. Shanoer, M. M., & Abed, F. M. **(2018)**. *Evaluate 3D laser point clouds registration for cultural heritage documentation*. The Egyptian Journal of Remote Sensing and Space Science, 21(3), 295-304. https://doi.org/10.1016/j.ejrs.2017.11.007

37. Liang, X., Hyyppä, J., Kaartinen, H., Lehtomäki, M., Pyörälä, J., Pfeifer, N., ... & Wang, Y. **(2018)**. *International benchmarking of terrestrial laser scanning approaches for forest inventories*. ISPRS Journal of Photogrammetry and Remote Sensing, 144, 137-179. https://doi.org/10.1016/j.isprsjprs.2018.06.021

38. Cabo, C., Del Pozo, S., Rodríguez-Gonzálvez, P., Ordóñez, C., & Gonzalez-Aguilera, D. **(2018)**. *Comparing terrestrial laser scanning (TLS) and wearable laser scanning (WLS) for individual tree modelling at plot level*. Remote Sensing, 10(4), 540. https://doi.org/10.3390/rs10040540

39. Puente, I., Lindenbergh, R., Van Natijne, A., Esposito, R., & Schipper, R. **(2018)**. *Monitoring of progressive damage in buildings using laser scan data*. International Archives of the Photogrammetry, Remote Sensing and Spatial Information Sciences, 42, 923-929. https://doi.org/10.5194/isprs-archives-XLII-2-923-2018

40. Huber, D., Akinci, B., Tang, P., Adan, A., Okorn, B., & Xiong, X. **(2010)**. *Using laser scanners for modeling and analysis in architecture, engineering, and construction*. Institute of Electrical and Electronics Engineers, 44th Annual Conference on Information Sciences and Systems, 1-6. https://doi.org/10.1109/CISS.2010.5464818

41. Dembski, F., Wössner, U., Letzgus, M., Ruddat, M., & Yamu, C. **(2020)**. *Urban digital twins for smart cities and citizens: the case study of Herrenberg, Germany*. Sustainability, 12(6), 2307. https://doi.org/10.3390/su12062307

42. Gupta, T., & Li, H. **(2017).** *Indoor mapping for smart cities—An affordable approach: Using Kinect Sensor and ZED stereo camera*. Institute of Electrical and Electronics Engineers, International Conference on Indoor Positioning and Indoor Navigation, 1-8. https://doi.org/10.1109/IPIN.2017.8115909

43. Lercari, N. **(2019)**. *Monitoring earthen archaeological heritage using multi-temporal terrestrial laser scanning and surface change detection*. Journal of Cultural Heritage, 39, 152-165. https://doi.org/10.1016/j.culher.2019.04.005

44. Heritage, G. L., & Large, A. R. **(2009)**. *Laser scanning for the environmental sciences.* John Wiley & Sons, Ltd 1(2), 21-34. https://doi.org/10.1002/9781444311952.ch2

45. Pfeifer, N., & Briese, C. **(2007)**. *Laser scanning–principles and applications*. In GeoSiberia International Exhibition and Scientific Congress. European Association of Geoscientists & Engineers. https://doi.org/10.3997/2214-4609.201403279

46. Suchocki, C. **(2020)**. *Comparison of time-of-flight and phase-shift TLS intensity data for the diagnostics measurements of buildings*. Materials, 13(2), 353. https://doi.org/10.3390/ma13020353

47. Previtali, M., Banfi, F., & Brumana, R. **(2019)**. *Handheld 3D Mobile Scanner (SLAM): Data Simulation and Acquisition for BIM Modelling*. In International Workshop on R3 in Geomatics: Research, Results and Review (pp. 256-266). Springer International Publishing. https://doi.org/10.1007/978-3-030-62800-0_20

48. Salgues, H., Macher, H., & Landes, T. **(2020)**. *Evaluation of Mobile Mapping Systems for Indoor Surveys*. The International Archives of Photogrammetry, Remote Sensing and Spatial Information Sciences, 44, 119-125. https://doi.org/10.5194/isprs-archives-XLIV-4-W1-2020-119-2020

49. Kelly, M., & Di Tommaso, S. **(2015)**. *Mapping forests with Lidar provides flexible, accurate data with many uses*. California Agriculture, 69(1), 14-20. https://doi.org/10.3733/ca.v069n01p14

50. Verma, V., Kumar, R., & Hsu, S. **(2006)**. *3d building detection and modeling from aerial lidar data*. Society Conference on Computer Vision and Pattern Recognition, 2, 2213-2220. Institute of Electrical and Electronics Engineers Computer. https://doi.org/10.1109/CVPR.2006.12

51. Haala, N., Petera, M., Kremer, J., & Hunter, G. **(2008)**. *Mobile LiDAR mapping for 3D point cloud collection in urban areas—A performance test*. International Society for Photogrammetry and Remote Sensing. Spat. Inf. Sci, 37(B5), 1119-1124. https://www.isprs.org/proceedings/XXXVII/congress/5_pdf/191.pdf

52. Ortega, S., Santana, J. M., Wendel, J., Trujillo, A., & Murshed, S. M. **(2021)**. *Generating 3D City Models from Open LiDAR Point Clouds: Advancing Towards Smart City Applications*. In: Mobasheri A. (eds). Open-Source Geospatial Science for Urban Studies. Lecture Notes in Intelligent Transportation and Infrastructure. Springer, Cham. https://doi.org/10.1007/978-3-030-58232-6_6

53. Vaaja, M., Kukko, A., et al., **(2013)**. *Data processing and quality evaluation of a boat-based mobile laser scanning system*. Sensors, 13(9), 12497-12515. https://doi.org/10.3390/s130912497

54. Puente, I., González-Jorge, H., Martínez-Sánchez, J., & Arias, P. **(2013)**. *Review of mobile mapping and surveying technologies*. Measurement, 46(7), 2127-2145. https://doi.org/10.1016/j.measurement.2013.03.006

55. Nocerino, E., Rodríguez-Gonzálvez, P., Menna, F, **(2019)**. *Introduction to mobile mapping with portable systems*. ISPRS Book Series, R. Lindenbergh & R. Belen (Eds.). CRC Press. http://doi.org/10.1201/9781351018869-4

56. Williams, K., Olsen, M. J., Roe, G. V., & Glennie, C. **(2013)**. *Synthesis of transportation applications of mobile LiDAR*. Remote Sensing, 5(9), 4652-4692. https://doi.org/10.3390/rs5094652

57. Dong, P., & Chen, Q. **(2017)**. *LiDAR remote sensing and applications*. CRC Press. https://doi.org/10.4324/9781351233354

58. Bartels, M., Wei, H., & Mason, D. C. **(2006)**. *DTM generation from LIDAR data using skewness balancing*. In 18th International Conference on Pattern Recognition. Institute of Electrical and Electronics Engineers, 1, 566-569. https://doi.org/10.1109/ICPR.2006.463

59. Maderal, E. N., Valcarcel, N., Delgado, J., Sevilla, C., & Ojeda, J. C. **(2016)**. *Automatic river network extraction from Lidar Data*. International Archives of the Photogrammetry, Remote Sensing & Spatial Information Sciences, 41, 365-372. https://doi.org/10.5194/isprsarchives-XLI-B8-365-2016

60. Gomez, A., Serrano, J., & Casalprim, D. **(2005)**. *Generation of a DTM based on LiDAR data for the definition of hydraulic models*. In XXII International Cartographic Conference, A Coruña, Spain. The International Cartographic Association. ISBN: 0-958-46093-0. https://www.cartesia.org/geodoc/icc2005/pdf/oral/TEMA24/Session%202/LIDAR.Gomez.pdf

61. Martín-Jiménez, J., Del Pozo, S., Sánchez-Aparicio, M., & Lagüela, S. **(2020)**. *Multi-scale roof characterization from LiDAR data and aerial orthoimagery: Automatic computation of building photovoltaic capacity*. Automation in Construction, 109(102965), 1-14. https://doi.org/10.1016/j.autcon.2019.102965

62. Holgado-Barco, A., Gonzalez-Aguilera, D., Arias-Sanchez, P., & Martinez-Sanchez, J. **(2014)**. *An automated approach to vertical road characterisation using mobile LiDAR systems: Longitudinal profiles and cross-sections*. ISPRS Journal of Photogrammetry and Remote Sensing, 96, 28-37. https://doi.org/10.1016/j.isprsjprs.2014.06.017

63. Zhang, W. **(2010)**. *Lidar-based road and road-edge detection*. Institute of Electrical and Electronics Engineers. Intelligent Vehicles Symposium, 845-848. https://doi.org/10.1109/IVS.2010.5548134

64. Zampa, F.; Conforti, D. **(2009)**. *Mapping with mobile lidar*. GIM International, 23(4), 35–37

65. Durrant-Whyte, H., & Bailey, T. **(2006)**. *Simultaneous localization and mapping: Part I.* Institute of Electrical and Electronics Engineers. Robotics & Automation magazine, 13(2), 99-110. https://doi.org/10.1109/MRA.2006.1638022

66. Lin, Y., Hyyppä, J., & Kukko, A. **(2013)**. *Stop-and-go mode: Sensor manipulation as essential as sensor development in terrestrial laser scanning*. Sensors, 13(7), 8140-8154. https://doi.org/10.3390/s130708140

67. Cadena, C., Carlone, L., Carrillo, H., Latif, Y., Scaramuzza, D., Neira, J. & Leonard, J. J. **(2016)**. *Past, present, and future of simultaneous localization and mapping: Toward the robust-perception age*. Institute of Electrical and Electronics Engineers Transactions on Robotics, 32(6), 1309-1332. https://doi.org/10.1109/TRO.2016.2624754

68. Riisgaard, S., & Blas, M. R. **(2003)**. *SLAM for Dummies. A Tutorial Approach to Simultaneous Localization and Mapping*, 22, 1-127. https://dspace.mit.edu/bitstream/handle/1721.1/119149/16-412j-spring-2005/contents/projects/1aslam_blas_repo.pdf

69. Bresson, G., Alsayed, Z., Yu, L., & Glaser, S. **(2017)**. *Simultaneous localization and mapping: A survey of current trends in autonomous driving*. Institute of Electrical and Electronics Engineers. Transactions on Intelligent Vehicles, 2(3), 194-220. https://doi.org/10.1109/TIV.2017.2749181

70. Kalman, R. E. **(1960)**. *A new approach to linear filtering and prediction problems*. Journal of Basic Engineering, 82(1), 35-45. https://doi.org/10.1115/1.3662552

71. Kalman, R. E., & Bucy, R. S. **(1961)**. *New results in linear filtering and prediction theory*. Journal of Basic Engineering, 83(1), 95-108. https://doi.org/10.1115/1.3658902

72. Julier, S. J., & Uhlmann, J. K. **(1997)**. *New extension of the Kalman filter to nonlinear systems. In Signal processing, sensor fusion, and target recognition.* Society of Photo-Optical Instrumentation Engineers, Signal Processing, Sensor Fusion, and Target Recognition VI 3068, 182-193. https://doi.org/10.1117/12.280797

73. Montemerlo, M., Thrun, S., Koller, D., & Wegbreit, B. **(2002)**. *FastSLAM: A factored solution to the simultaneous localization and mapping problem*. American Association for Artificial Intelligence, 2, 593-598. https://www.aaai.org/Papers/AAAI/2002/AAAI02-089.pdf

74. Newman, P., & Ho, K. **(2005)**. *SLAM-loop closing with visually salient features.* Institute of Electrical and Electronics Engineers. International Conference on Robotics and Automation, 635-642. https://doi.org/10.1109/ROBOT.2005.1570189

75. Ziparo, V. A., Zaratti, M., Grisetti, G., Bonanni, T. M., Serafin, J., Di Cicco, M., & Stachniss, C. **(2013)**. *Exploration and mapping of catacombs with mobile robots*. In 2013 Institute of Electrical and Electronics Engineers, International Symposium on Safety, Security, and Rescue Robotics, 1-2. https://doi.org/10.1109/SSRR.2013.6719380

76. Surmann, H., Nchter, A., Lingemann, K., & Hertzberg, J. **(2003)**. *Kurt3D-an autonomous mobile robot for modelling the world in 3D*. European Research Consortium for Informatics and Mathematics News, 55, 24-25. https://www.ercim.eu/publication/Ercim_News/enw55/nuechter.html

77. Nüchter, A., Elseberg, J., & Borrmann, D. **(2013)**. *Irma3 - An intelligent robot for mapping applications*. International Federation of Automatic Control Proceedings Volumes, 46(29), 119-124. https://doi.org/10.3182/20131111-3-KR-2043.00011

78. Lehtola, V. V., Kaartinen, H., Nüchter, A., Kaijaluoto, R., Kukko, A., Litkey, P. & Hyyppä, J. **(2017*)**. *Comparison of the selected state-of-the-art 3D indoor scanning and point cloud generation methods*. Remote sensing, 9(8), 796. https://doi.org/10.3390/rs9080796

79. Aryan, A., Bosché, F., & Tang, P. **(2021).** *Planning for terrestrial laser scanning in construction: A review*. Automation in Construction, 125, 103551. https://doi.org/10.1016/j.autcon.2021.103551

80. Rodríguez-Gonzálvez, P., Garcia-Gago, J., Gomez-Lahoz, J., & González-Aguilera, D. **(2014)**. *Confronting passive and active sensors with non-Gaussian statistics*. Sensors, 14(8), 13759-13777. https://doi.org/10.3390/s140813759

81. Landa J., Procházka D., Šťastný J. **(2013).** *Point cloud processing for smart systems*. Acta Universitatis Agriculturae et Silviculturae Mendelianae Brunensis, 61 (7), 2415-2421. http://dx.doi.org/10.11118/actaun201361072415

82. Xie H., McDonnell K.T., Qin H. **(2004)**. *Surface Reconstruction of Noisy and Defective Data Sets*. Institute of Electrical and Electronics Engineers, Visualization. 259-266. https://doi.org/10.1109/VISUAL.2004.101

83. Narváez, E. A. L., & Narváez, N. E. L. **(2006)**. *Point cloud denoising using robust principal component analysis*. In Proceedings of the First International Conference on Computer Graphics Theory and Applications, 1, 51-58. https://doi.org/10.5220/0001358900510058

84. Balta, H., Velagic, J., Bosschaerts, W., De Cubber, G., & Siciliano, B. **(2018)**. *Fast statistical outlier removal-based method for large 3D point clouds of outdoor environments*. International Federation of Automatic Control – Papers On Line, 51(22), 348-353. https://doi.org/10.1016/j.ifacol.2018.11.566

85. Han, X. F., Jin, J. S., Wang, M. J., Jiang, W., Gao, L., & Xiao, L. **(2017)**. *A review of algorithms for filtering the 3D point cloud*. Signal Processing: Image Communication, 57, 103-112. https://doi.org/10.1016/j.image.2017.05.009

86. Zhang, Z. **(1994)**. *Iterative point matching for registration of free-form curves and surfaces*. International journal of computer vision, 13(2), 119-152. https://link.springer.com/content/pdf/10.1007/BF01427149.pdf

87. Rusu, R. B., Blodow, N., Marton, Z., Soos, A., & Beetz, M. **(2007)**. *Towards 3D object maps for autonomous household robots*. Institute of Electrical and Electronics Engineers, International Conference on Intelligent Robots and Systems 3191-3198. https://doi.org/10.1109/IROS.2007.4399309

88. Carrilho, A. C., Galo, M., & Santos, R. C. **(2018)**. *Statistical Outlier Detection Method for airborne LIDAR data*. International Archives of the Photogrammetry, Remote Sensing & Spatial Information Sciences, 42(1), 87-92. https://doi.org/10.5194/isprs-archives-XLII-1-87-2018

89. Balta, H., Bedkowski, J., Govindaraj, S., Majek, K., Musialik, P., Serrano, D. & De Cubber, G. **(2017)**. *Integrated data management for a fleet of search-and-rescue robots*. Journal of Field Robotics, 34(3), 539-582. https://doi.org/10.1002/rob.21651

90. Rusu, R. B., & Cousins, S. **(2011)**. *3d is here: Point cloud library (PCL)*. Institute of Electrical and Electronics Engineers, International Conference on Robotics and Automation, 1-4. https://doi.org/10.1109/ICRA.2011.5980567

91. Xu, Z.; Foi, A. **(2019)**. *Anisotropic Denoising of 3D Point Clouds by Aggregation of Multiple Surface-Adaptive Estimates*. Institute of Electrical and Electronics Engineers, Transactions on Visualization and Computer Graphics, 1. https://doi.ieeecomputersociety.org/10.1109/TVCG.2019.2959761

92. Cheng, L., Chen, S., Liu, X., Xu, H., Wu, Y., Li, M., & Chen, Y. **(2018)**. *Registration of laser scanning point clouds: A review*. Sensors, 18(5), 1641. https://doi.org/10.3390/s18051641

93. Bellekens, B., Spruyt, V., Berkvens, R., Penne, R., & Weyn, M. **(2015)**. *A benchmark survey of rigid 3D point cloud registration algorithms*. International Journal on Advances in Intelligent Systems, 8, 118-127. https://www.researchgate.net/publication/280040097_A_

94. Bueno, M., González-Jorge, H., Martínez-Sánchez, J., & Lorenzo, H. **(2017)**. *Automatic point cloud coarse registration using geometric keypoint descriptors for indoor scenes*. Automation in Construction, 81, 134-148. https://doi.org/10.1016/j.autcon.2017.06.016

95. Chen, H., & Bhanu, B. **(2007)**. *3D free-form object recognition in range images using local surface patches*. Pattern Recognition Letters, 28(10), 1252-1262. https://doi.org/10.1016/j.patrec.2007.02.009

96. Zhong, Y. **(2009)**. *Intrinsic shape signatures: A shape descriptor for 3d object recognition*. Institute of Electrical and Electronics Engineers, 12th International Conference on Computer Vision Workshops, 689-696. https://doi.org/10.1109/ICCVW.2009.5457637

97. Lindeberg, T. **(2012)**. *Scale Invariant Feature Transform*. Scholarpedia, 7 (5), 10491. https://doi.org/10.4249/scholarpedia.10491

98. Salti, S., Tombari, F., & Di Stefano, L. **(2011)**. *A performance evaluation of 3d keypoint detectors*. Institute of Electrical and Electronics Engineers, International Conference on 3D Imaging, Modelling, Processing, Visualization and Transmission 236-243. https://doi.org/10.1109/3DIMPVT.2011.37

99. Rusu, R. B., Marton, Z. C., Blodow, N., & Beetz, M. **(2008)**. *Persistent point feature histograms for 3D point clouds*. In Proceedings of 10th International Conference on Intelligent Autonomous Systems, 10, 119-128. https://doi.org/10.3233/978-1-58603-887-8-119

100. Tombari, F., Salti, S., & Di Stefano, L. **(2010)**. *Unique signatures of histograms for local surface description*. Springer, European Conference on computer vision, 356-369 https://doi.org/10.1007/978-3-642-15558-1_26

101. Hana, X. F., Jin, J. S., Xie, J., Wang, M. J., & Jiang, W. **(2018)**. *A comprehensive review of 3d point cloud descriptors*. ArXiv. https://arxiv.org/pdf/1802.02297v1.pdf

102. R. B. Rusu, G. Bradski, R. Thibaux, J. Hsu, **(2014).** *Fast 3d recognition and pose using the viewpoint feature histogram*. Institute of Electrical and Electronics Engineers, International Conference on Intelligent Robots and Systems, 2155–2162. https://doi.org/10.1109/IROS.2010.5651280

103. M. Madry, C. H. Ek, R. Detry, K. Hang., **(2012).** *Improving generalization for 3d object categorization with global structure histograms*. Institute of Electrical and Electronics Engineers, International Conference on Intelligent Robots and Systems, 1379–1386. https://doi.org/10.1109/IROS.2012.6385874

104. Hadji, I., & DeSouza, G. N. **(2014)**. *Local-to-Global signature descriptor for 3D object recognition*. Computer Vision, Asian Conference on Computer Vision, 570-584. https://doi.org/10.1007/978-3-319-16628-5_41

105.K. Alhamzi, M. Elmogy, S. Barakat. **(2015)**. *3d object recognition based on local and global features using Point Cloud Library*. International Journal of Advancements in Computing Technology, 7(3), 43–54. https://www.researchgate.net/publication/277328662

106.Li, P., Wang, R., Wang, Y., & Tao, W. **(2020)**. *Evaluation of the ICP Algorithm in 3D Point Cloud Registration*. Institute of Electrical and Electronics Engineers Access, 8, 68030-68048. https://doi.org/10.1109/ACCESS.2020.2986470

107.Sánchez Aparicio, L. J. **(2016)**. *Damage evaluation in constructions based on geomatic and dynamic approaches*. (Tesis Doctoral). Universidad de Salamanca. http://hdl.handle.net/10366/132986

108.Stubbs, N. **(1987).** *A general theory of non-destructive damage detection in structures*. Structural control, 694-713. Springer, Dordrecht. https://doi.org/10.1007/978-94-009-3525-9_44

109.Paiho, S., Seppä, I. P., & Jimenez, C. **(2015)**. *An energetic analysis of a multifunctional façade system for energy efficient retrofitting of residential buildings in cold climates of Finland and Russia*. Sustainable cities and society, 15, 75-85. https://doi.org/10.1016/j.scs.2014.12.005

110.Cardinale, N., & Ruggiero, F. **(2000)**. *Energetic aspects of bioclimatic buildings in the Mediterranean area: a comparison between two different computation methods*. Energy and Buildings, 31(1), 55-63. https://doi.org/10.1016/S0378-7788(99)00005-5

111.Clarke, J. A., & Clarke, J. A. **(2001)**. *Building Simulation. Energy simulation in building design, 2nd Edition*. Butterworth-Heinemann, 64-98. https://doi.org/10.1016/B978-075065082-3/50003-6

112.Rey-Hernández, J. M., Velasco-Gómez, E., José-Alonso, S., Julio, F., Tejero-González, A., & Rey-Martínez, F. J. **(2018)**. *Energy analysis at a near zero energy building. A case-study in Spain*. Energies, 11(4), 857. https://doi.org/10.3390/en11040857

113.Coelho, G. B., Silva, H. E., & Henriques, F. M. **(2018)**. *Calibrated hygrothermal simulation models for historical buildings*. Building and Environment, 142, 439-450. https://doi.org/10.1016/j.buildenv.2018.06.034

114.Künzel, H. M., Holm, A., Zirkelbach, D., & Karagiozis, A. N. **(2005)**. *Simulation of indoor temperature and humidity conditions including hygrothermal interactions with the building envelope*. Solar Energy, 78(4), 554-561. https://doi.org/10.1016/j.solener.2004.03.002

115.Vertaľ, M., Zozulák, M., Vašková, A., & Korjenic, A. **(2018)**. *Hygrothermal initial condition for simulation process of green building construction*. Energy and Buildings, 167, 166-176. https://doi.org/10.1016/j.enbuild.2018.02.004

116.Barazzetti, L., Banfi, F., Brumana, R., Gusmeroli, G., Previtali, M., & Schiantarelli, G. **(2015)**. *Cloud-to-BIM-to-FEM: Structural simulation with accurate historic BIM from laser scans*. Simulation Modelling Practice and Theory, 57, 71-87. https://doi.org/10.1016/j.simpat.2015.06.004

117.Song, S., Yang, J., & Kim, N. **(2012)**. *Development of a BIM-based structural framework optimization and simulation system for building construction*. Computers in Industry, 63(9), 895-912. https://doi.org/10.1016/j.compind.2012.08.013

118.Guarnieri, A., Pirotti, F., Pontin, M., & Vettore, A. **(2006)**. *3D Surveying for structural analysis applications*. In 12th FIG symposium on Deformation Measurements. https://www.fig.net/resources/proceedings/2006/baden_2006_comm6/PDF/LS1/Guarnieri.pdf

119.Ramos, L. F., Marques, L., Lourenço, P. B., De Roeck, G., Campos-Costa, A., & Roque, J. **(2010)**. *Monitoring historical masonry structures with operational modal analysis: Two case studies*. Mechanical Systems and Signal Processing, 24(5), 1291-1305. https://doi.org/10.1016/j.ymssp.2010.01.011

120.Milani, G., & Valente, M. **(2015)**. *Comparative pushover and limit analyses on seven masonry churches damaged by the 2012 Emilia-Romagna (Italy) seismic events: Possibilities of non-linear finite elements compared with pre-assigned failure mechanisms*. Engineering Failure Analysis, 47, Part A, 129-161. https://doi.org/10.1016/j.engfailanal.2014.09.016

121.Gonilha, J. A., Barros, J., Correia, J. R., Sena-Cruz, J., Branco, F. A., Ramos, L. F., Santos, T. **(2014)**. *Static, dynamic and creep behaviour of a full-scale GFRP-SFRSCC hybrid footbridge*. Composite Structures, 118, 496-509. https://doi.org/10.1016/j.compstruct.2014.08.009

122.Bautista-De Castro, A., Sánchez-Aparicio, L. J., Ramos, L. F., Sena-Cruz, J., & González-Aguilera, D. **(2018)**. *Integrating geomatic approaches, Operational Modal Analysis, advanced numerical and updating methods to evaluate the current safety conditions of the historical Bôco Bridge*. Construction and Building Materials, 158, 961-984. https://doi.org/10.1016/j.conbuildmat.2017.10.084

123.Yang, H., Xu, X., & Neumann, I. **(2014)**. *The benefit of 3D laser scanning technology in the generation and calibration of FEM models for health assessment of concrete structures*. Sensors, 14(11), 21889-21904. https://doi.org/10.3390/s141121889

124.Gonizzi Barsanti, S., Guidi, G., & Rodríguez-Navarro, P. **(2017)**. *Geometrical processing of real data for Finite Element Analysis of historical fortified structures*. International Conference on Modern Age Fortifications of the Mediterranean Coast - Proceedings - Vol. II, 377-384. Universidad de Alicante. http://hdl.handle.net/10045/70531

125.Castellazzi, G., D'Altri, A. M., Bitelli, G., Selvaggi, I., & Lambertini, A. **(2015)**. *From laser scanning to finite element analysis of complex buildings by using a semi-automatic procedure*. Sensors, 15(8), 18360-18380. https://doi.org/10.3390/s150818360

126.Cabaleiro, M., Riveiro, B., Arias, P., Caamaño, J. C., & Vilán, J. A. **(2014)**. *Automatic 3D modelling of metal frame connections from LiDAR data for structural engineering purposes*. ISPRS Journal of Photogrammetry and Remote Sensing, 96, 47-56. https://doi.org/10.1016/j.isprsjprs.2014.07.006

127.Piegl, L., & Tiller, W. **(1996)**. *The NURBS book, 2nd Edition*. Springer Science & Business Media, 646 pp. https://doi.org/10.1007/978-3-642-59223-2

128.Sacks, R., Eastman, C., Lee, G., & Teicholz, P. **(2018)**. *BIM handbook: A guide to building information modeling for owners, designers, engineers, contractors, and facility managers*. John Wiley & Sons. https://doi.org/10.1002/9781119287568

129.Bryde, D., Broquetas, M., & Volm, J. M. **(2013)**. *The project benefits of building information modelling (BIM)*. International journal of project management, 31(7), 971-980. https://doi.org/10.1016/j.ijproman.2012.12.001

130.Volk, R., Stengel, J., & Schultmann, F. **(2014)**. *Building Information Modeling (BIM) for existing buildings—Literature review and future needs*. Automation in construction, 38, 109-127. https://doi.org/10.1016/j.autcon.2013.10.023

131.R. Brumana, S. Della Torre, M. Previtali, L. Barazzetti, L. Cantini, D. Oreni, F. Banfi. **(2018)**. *Generative HBIM modelling to embody complexity (LOD, LOG, LOA, LOI): surveying, preservation, site intervention—the Basilica di Collemaggio (L'Aquila)*, Applied Geomatics 10. 545–567. https://doi.org/10.1007/s12518-018-0233-3

132.Matulionis, R. C., & Freitag, J. C. **(1991)**. *Preventive maintenance of buildings*. Van Nost.Reinhold. ISBN: 9780442318666

133.GeoSLAM, ZEB Go - GeoSLAM. https://geoslam.com/solutions/zeb-go/, 2020 (accessed April 1, 2021).

134.Rodríguez-Gonzálvez, P., Jimenez Fernandez-Palacios, B., Muñoz-Nieto, Á. L., Arias-Sanchez, P., & Gonzalez-Aguilera, D. **(2017)**. *Mobile LiDAR system: New possibilities for the documentation and dissemination of large cultural heritage sites*. Remote Sensing, 9(3), 189. https://doi.org/10.3390/rs9030189

135.Masciotta, M. G., Morais, M. J., Ramos, L. F., Oliveira, D. V., Sanchez-Aparicio, L. J., & González-Aguilera, D. **(2019)**. *A digital-based integrated methodology for the preventive conservation of cultural heritage: the experience of HeritageCare project*. International Journal of Architectural Heritage, 1-20. https://doi.org/10.1080/15583058.2019.1668985

136.Ramos, L., Masciotta, M., Morais, M., Azenha, M., Ferreira, T., Pereira, E., & Lourenco, P. **(2018)**. *HeritageCARE: Preventive conservation of built cultural heritage in the South-West Europe*. Reflections on Cultural Heritage Theories and Practices. https://doi.org/10.1201/9781351014793-16

137.Corgnati, S. P., Fabi, V., & Filippi, M. **(2009)**. *A methodology for microclimatic quality evaluation in museums: Application to a temporary exhibit*. Building and environment, 44(6), 1253-1260. https://doi.org/10.1016/j.buildenv.2008.09.012

Anexo I.

Indexación y factor de impacto de las revistas

Anexo I. Indexación y factor de impacto de las revistas

Artículos I y III:

- ✓ Use of a Wearable Mobile Laser System in Seamless Indoor 3D Mapping of a Complex Historical Site
- ✓ Integration of a wearable mobile mapping solution and advance numerical simulations for the structural analysis of historical constructions: A case of study in San Pedro church (Palencia, Spain)

Revista	Remote Sensing
Editorial	MDPI AG
ISSN	2072-4292
Factor de impacto (2021)	4.509
Ranking	9/30
Cuartil	Q1

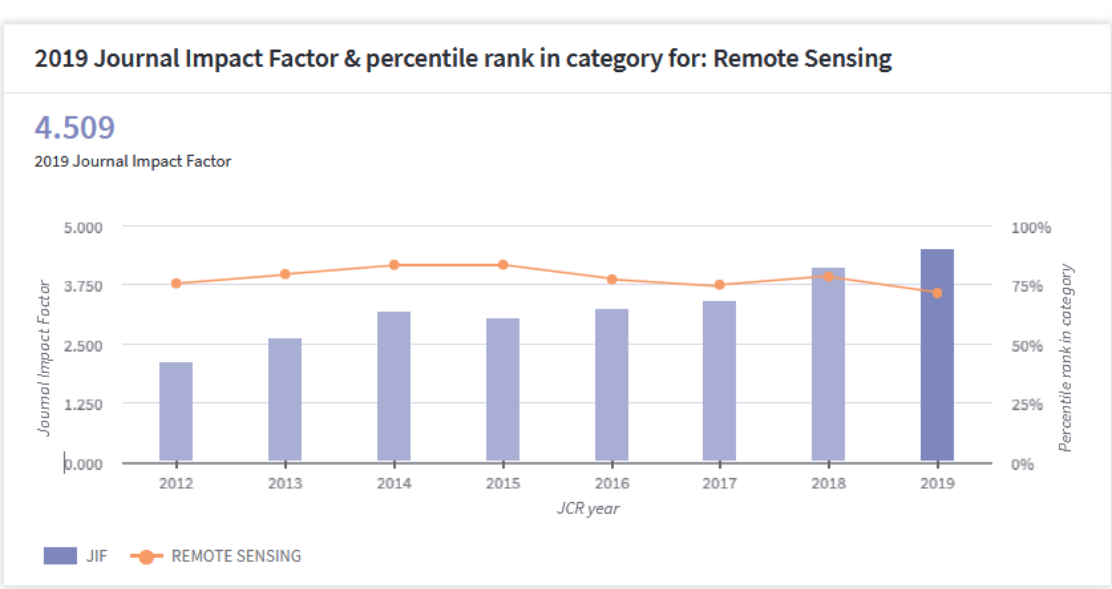

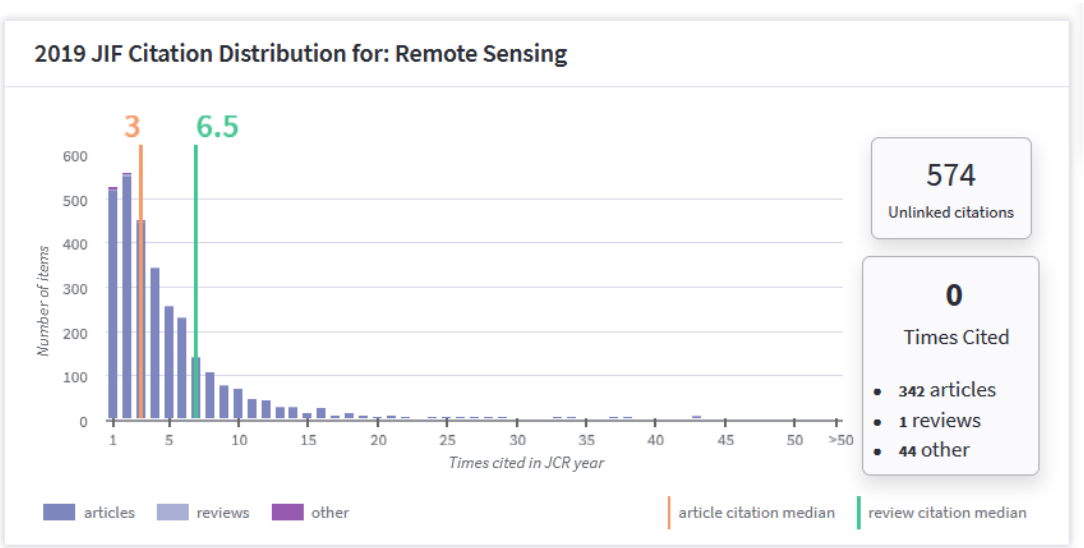

JCR Impact Factor

JCR Year	REMOTE SENSING		
	Rank	Quartile	JIF Percentile
2019	9/30	Q2	71.667
2018	7/30	Q1	78.333
2017	8/30	Q2	75.000
2016	7/29	Q1	77.586
2015	5/28	Q1	83.929
2014	5/28	Q1	83.929
2013	6/27	Q1	79.630
2012	7/27	Q2	75.926

ESI Total Citations

Rank

JCR Year	GEOSCIENCES
2019	14/435-Q1
2018	21/421-Q1
2017	41/419-Q1
2016	60/417-Q1
2015	89/408-Q1
2014	116/393-Q2
2013	154/388-Q2

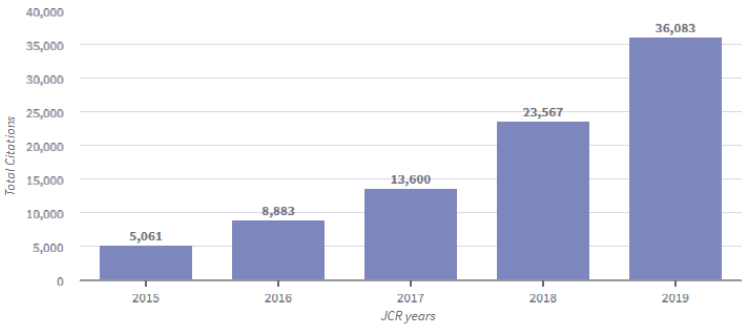

Artículo II:

✓ Automatic Point-Cloud Registration for Quality control in Building Works

Revista	Applied Sciences
Editorial	MDPI AG
ISSN	2076-3417
Factor de impacto (2021)	2.217
Ranking	32/91
Cuartil	Q1

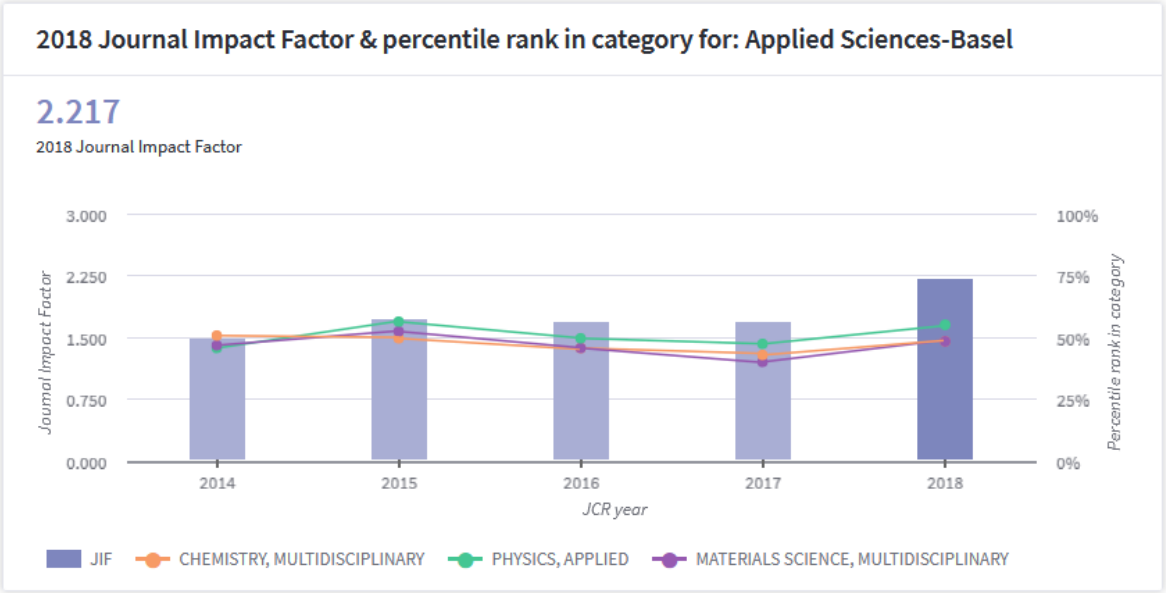

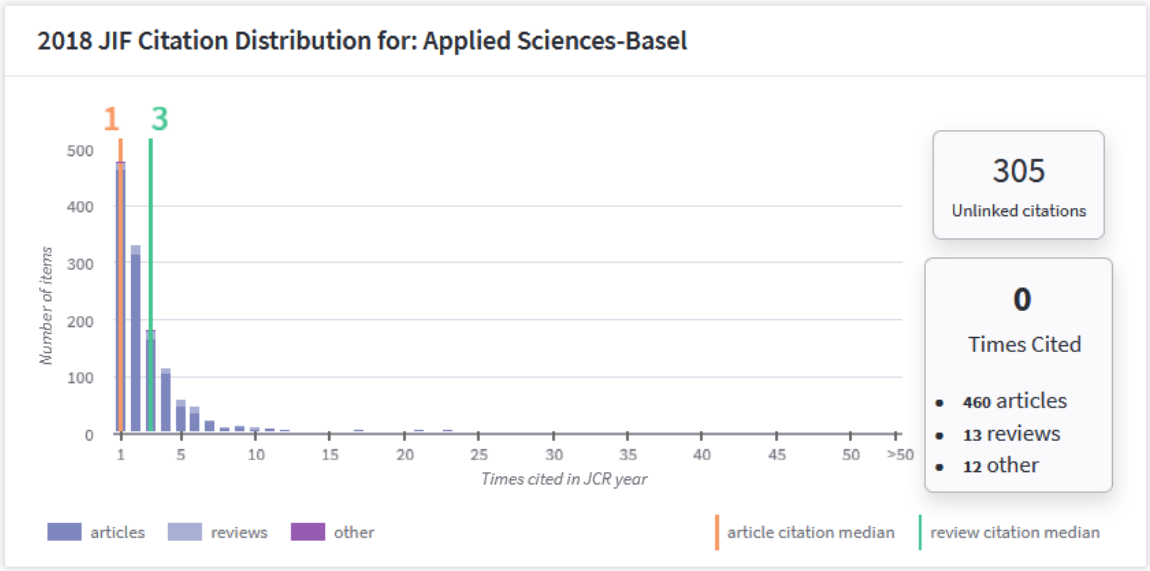

JCR Impact Factor

JCR Year	CHEMISTRY, MULTIDISCIPLINARY			ENGINEERING, MULTIDISCIPLINARY		
	Rank	Quartile	JIF Percentile	Rank	Quartile	JIF Percentile
2019	88/177	Q2	50.565	32/91	Q2	65.385
2018	89/172	Q3	48.547	n/a	n/a	n/a
2017	98/171	Q3	42.982	n/a	n/a	n/a
2016	91/166	Q3	45.482	n/a	n/a	n/a
2015	83/163	Q3	49.387	n/a	n/a	n/a
2014	78/157	Q2	50.637	n/a	n/a	n/a

ESI Total Citations

Rank

JCR Year	ENGINEERING
2019	82/909-Q1
2018	211/893-Q1
2017	367/867-Q2
2016	579/861-Q3
2015	695/850-Q4

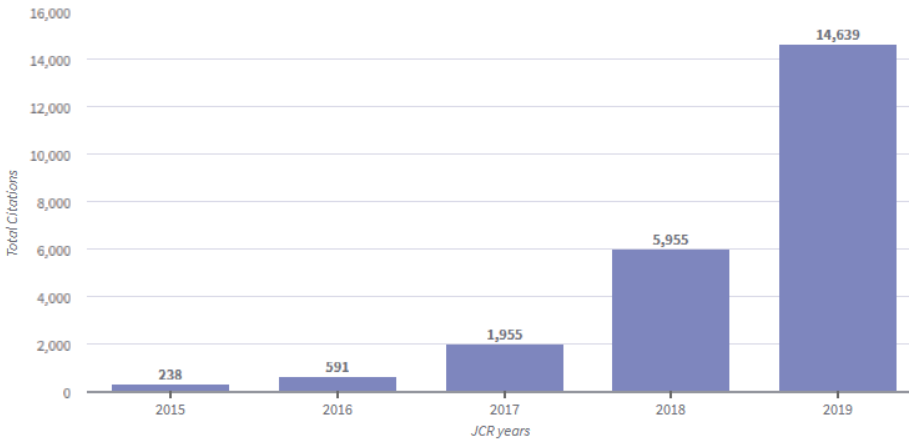

Artículo IV:

- ✓ An historical building information modelling approach for the preventive conservation of historical constructions: Application to the Historical Library of Salamanca

Revista	Automation in Construction
Editorial	ELSEVIER
ISSN	0926-5805
Factor de impacto (2021)	5.5669
Ranking	4/63
Cuartil	Q1

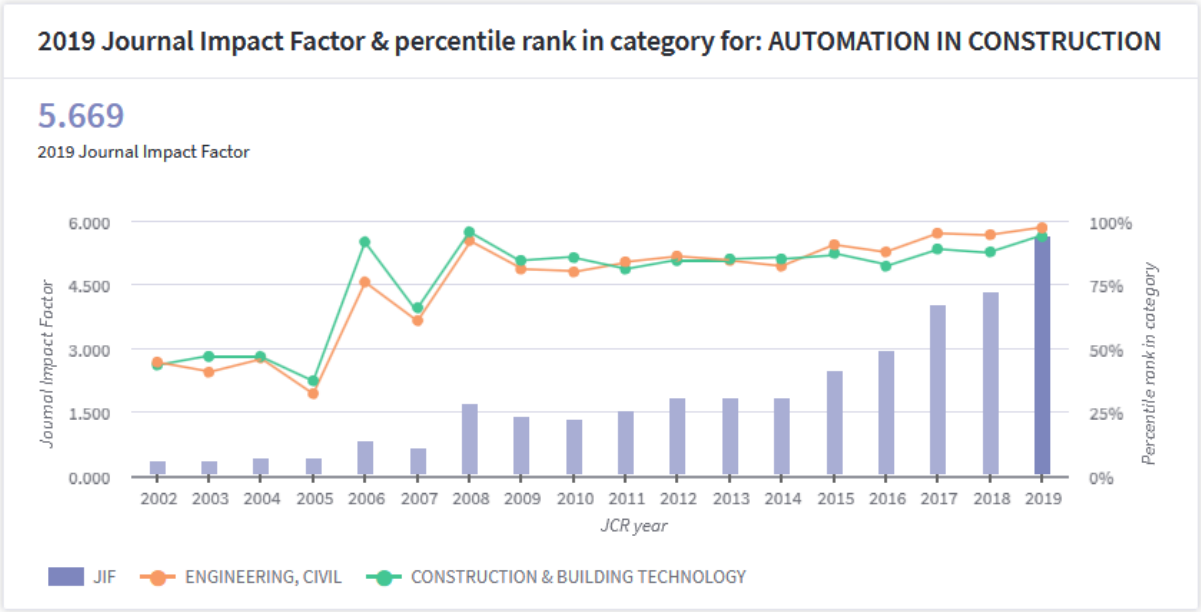

2019 JIF Citation Distribution for: AUTOMATION IN CONSTRUCTION

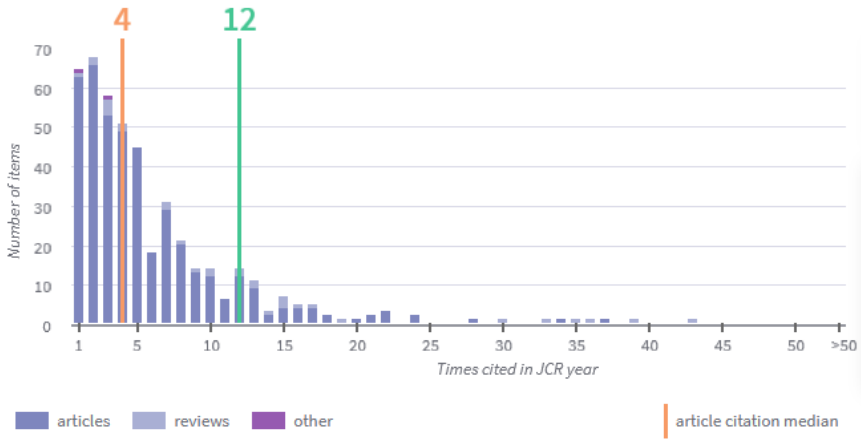

14
Unlinked citations

0
Times Cited

- 41 articles
- 1 reviews
- 3 other

JCR Impact Factor

JCR Year	CONSTRUCTION & BUILDING TECHNOLOGY		
	Rank	Quartile	JIF Percentile
2019	4/63	Q1	94.444
2018	8/63	Q1	88.095
2017	7/62	Q1	89.516
2016	11/61	Q1	82.787
2015	8/61	Q1	87.705
2014	9/59	Q1	85.593

ESI Total Citations

Rank

JCR Year	ENGINEERING
2019	124/909-Q1
2018	139/893-Q1
2017	165/867-Q1
2016	196/861-Q1
2015	203/850-Q1
2014	224/838-Q2
2013	240/837-Q2